THE CRUSTAL EVOLUTION OF NEMEGT AND ALTAN UUL, SOUTHERN MONGOLIA

Thesis submitted for the degree of
Doctor of Philosophy
at the University of Leicester

by

Stephen James Rippington (M.Geol)
Department of Geology
University of Leicester

December 2007

Abstract

This thesis concerns the crustal evolution of Nemegt and Altan Uul in the Gobi Altai mountains of southern Mongolia. Nemegt and Altan Uul consist of polydeformed Palaeozoic rocks uplifted in the Cenozoic at a restraining bend along the active left-lateral Gobi-Tien Shan intra-continental fault system, one of several east-west trending left-lateral intra-continental transpressional fault systems associated with eastward continental extrusion tectonics in Central Asia. The tectonic evolution of southern Mongolia is of particular interest as it forms part of the Central Asian Orogenic Belt, which is the largest area of Phanerozoic continental growth on Earth, and is a natural laboratory for studying processes of continental growth and deformation including terrane accretion, ophiolite obduction, terrane amalgamation, terrane dispersal and crustal reactivation. The uplifted Palaeozoic rocks exposed in Nemegt and Altan Uul offer an opportunity to understand multiple phases of the crustal evolution of southern Mongolia.

A series of cross-strike transects of Nemegt and Altan Uul were carried out to document the lithologies and structure of the ranges. Samples were taken along the transects and at several important localities, to constrain the metamorphic petrography of the rocks in the ranges. This data is used to define several distinct east-west trending litho-tectonic sequences in Nemegt and Altan Uul. The ranges have a systematic south to north litho-tectonic variation from greenschist grade meta-volcanic and volcaniclastic rocks, thrust north over a discontinuous ophiolite belt, which is thrust north over greenschist to epidote-amphibolite grade arkosic to mature meta-sedimentary rocks. Four phases of deformation are identified from cross-cutting field relationships and constrained by existing regional data: east-west trending south-dipping cleavage (D1), and north-vergent folds of cleavage and north-directed ductile thrust shear zones (D2) formed during late Carboniferous south to north arc-terrane accretion and ophiolite obduction. East-west and northeast-southwest trending D3 normal faults formed during Cretaceous basin extension. East-west and northwest-southeast trending D4 left-lateral oblique-slip and dip-slip thrust faults formed during Cenozoic transpressional deformation and define the modern mountain ranges. The structures identified are conservatively extrapolated to depth to suggest Nemegt and Altan Uul have a positive flower structure in cross-section. An evolutionary model of Nemegt and Altan Uul suggests that D1 and D2 structures and the ophiolitic rocks in the area may represent south-dipping east-west trending fabrics and rheological weaknesses that have been reactivated in a left-lateral transpressional sense in the Cenozoic.

Acknowledgements

I'd like to begin by thanking my parents, Jacqueline and David Rippington. Without their love, encouragement, advice and more than generous sponsorship over many years, I wouldn't even have been in a position to start a PhD, let alone finish one. Thanks are also due to my brother John for his support and humour over the years.

I owe a great debt to my supervisors, Dr Dickson Cunningham and Dr Richard England. Their guidance, criticism and timely kicks to the rear end have propelled me forward and made me a better geologist.

Like most PhD projects, mine has seemed like a set of constantly mobile goalposts, but I'd like to thank Dickson for conjuring the original concept for the project out of the ether. I'd also like to thank him for his supervision and encouragement, in the UK and Mongolia, and for his exemplary editorial skills.

Richard England has been a constant source of support regardless of his busy schedule. I thank him for all the ideas and discussions, in and out of the pub, and for his thorough and constructive reviews of this thesis.

I'd also like to thank Dr Sarah Davies. She accompanied me and Dickson to Mongolia in 2004 and 2005. Her organisation of the logistics for the trips was awesome to behold, and our joint miscalculation of how much beer one man can consume kept me happily entertained on the long Gobi Desert evenings for 3 months in 2004.

I've only known Jessica Card for a short time, but her love and patience have been a huge support to me in the crucial final months of the project. Thanks for making me sandwiches, giving me lifts, and most of all for keeping me smiling.

I've always thought the key to sticking at anything is to laugh when things aren't going so well and to have as much fun as possible when they are: I count myself extremely lucky to have some really great friends who have definitely kept the fun going through my formative years at school, through university and right upto the present day. I'd especially like to thank Toby Bellman, Andy Jones and Jim Fursedon who I've been privileged to know for many years, and hope to know for many more.

I have also made some fantastic friends in Leicester over the years. I should start with a special mention of my housemates at 44 Cromer Street. All three of them are sterling chaps who supported me, entertained me, and when I most needed it, bought beer (and champagne) for me.

First up is Tom 'Gimpson' Salter, who I have known since 2000, when we first had the misfortune of living together in Mary Gee houses. If I had known then that we would still be living together in 2007, I probably would have asked to move. Thanks for all the gooning

about and rum. Second is Alex ‘Maximus’ Parker, who I met for the first time in 2004 when we arranged to move into 44 Cromer Street. His lovely long locks were a constant source of joy to me, wherever I found them. Thanks for all the dragon-slaying and hair. Last but not least, is James ‘Jamesor’ Blight, who I knew as the crazy, scary, skateboarding kid in the year above me as an undergraduate. I was soon to learn that he is a thoroughly good chap whose constant internal struggle between fear and rage has repeatedly entertained all who know him. Thanks for all the CorelDraw help, PhD advice, Halo and beer.

Thanks to Pete Fitch, who gave me somewhere to live in the last 6 months of the project, and for all the late-night sessions on the rum back in 2006.

I’d like to thank all my colleagues for their support and friendship over the years. Special mention is due to certain individuals; Rowan Whittle (for the office paper tennis in F32, and all the fun and nights out in our first year and since); Alex Page (for reintroducing me to cricket and for that trip to Vienna); Dave Cornwell (for the excellent Halloween parties, discussions about tectonics, and music exchanges); Dan Smith (for the command and conquer and Halo sessions, music, whisky and beers); Simon ‘The Jow’ Jowitt (for the extensive geochemistry advice, for the nights in the Lansdowne and Shampoo, and for the many, many beers); Pablo Davila Harris (for the jamming); Ben Ellis (for the Bad Attitude…what else?!); Jo Tudge (for cunningly arranging to be out of the office while I wrote up – the desk is all yours!); Andy ‘Tiger’ Shore (for captaining us to glory in the summer of 2007, and for being ever eager to join me in the pub); Becky Williams (for her general championing of the pub and for dancing the robot with me).

Thanks to all the staff in the department for all the guidance, ideas and support over the years. Special thanks to Mike Branney (for all the advice as an undergraduate), the late Tim Brewer (for the geochemistry help and wicked one liners), Mike Norry (for all the undergraduate field trips and constant humour), Andy Saunders (for being a great lecturer, and getting me interested in hard-rock geology in the first place), Jan Zalasiewicz (for all the help as my undergraduate tutor), Andy Myers (for all the computer help and letting me be thoroughly useless in goal for the last few years) and all the technicians that have made my project a relatively painless process. To the people I’ve inevitably omitted to mention personally, many thanks.

Leicester has been very good to me. I’m looking forward to the next step now, but I’ll always look on Leicester, and more importantly the people I first met here, with great fondness. It’s been awesome.

Steve Rippington
14 December 2007

List of figures

Chapter 1
Introduction

The relative buoyancy and weakness of the continental lithosphere compared to oceanic lithosphere, ensures it is long-lived and undergoes repeated tectonic deformation, reactivation and reworking (Holdsworth et al. 2001). Areas of polydeformed continental crust provide an opportunity to study the strains resulting from multiple phases of deformation and how pre-existing structure affects the geometry and kinematics of subsequent deformation events (Storti et al. 2003).

This thesis is concerned with the tectonic evolution of rocks deformed and uplifted within the left-lateral Gobi-Tien Shan transpressional fault system in the Gobi Altai of southern Mongolia. The region consists of Palaeozoic terranes that amalgamated in the late Palaeozoic and were repeatedly deformed in the Mesozoic and late Cenozoic (Tapponier & Molnar 1979, Traynor & Sladen 1995, Badarch et al. 2002, Meng, 2003). Left-lateral intraplate transpressional fault systems, thought to have formed in response to the ongoing northward indentation of India into Eurasia, extend from north of the Himalayan collision zone in Tibet to the Gobi Altai in southern Mongolia (Fig. 1.1 inset; Tapponier & Molnar 1979, Baljinnyam et al. 1993).

Continental intraplate deformation zones can be of considerable economic significance: First, intraplate strike-slip faults often control the location, architecture and evolution of sedimentary basins which may contain hydrocarbon bearing sediments (Storti et al. 2003). For example, transtensional faults in Thailand may have controlled the formation and evolution of Tertiary hydrocarbon bearing basins (Morley, 2002). Second, intraplate strike-slip faults may act as a conduit for the flow of magma and hydrothermal fluids, potentially leading to the accumulation of economic ore deposits, as in the Eastern Goldfields Province in western Australia (Cox, 1999). Finally, there are many regions of frequent high magnitude, and potentially damaging earthquakes focussed along intraplate strike-slip faults in continental intraplate settings, like the Denali Fault in Alaska and the Kunlun Fault in Tibet (Ozacar & Beck, 2004) and the Bogd fault in southern Mongolia (Florensov et al. 1967).

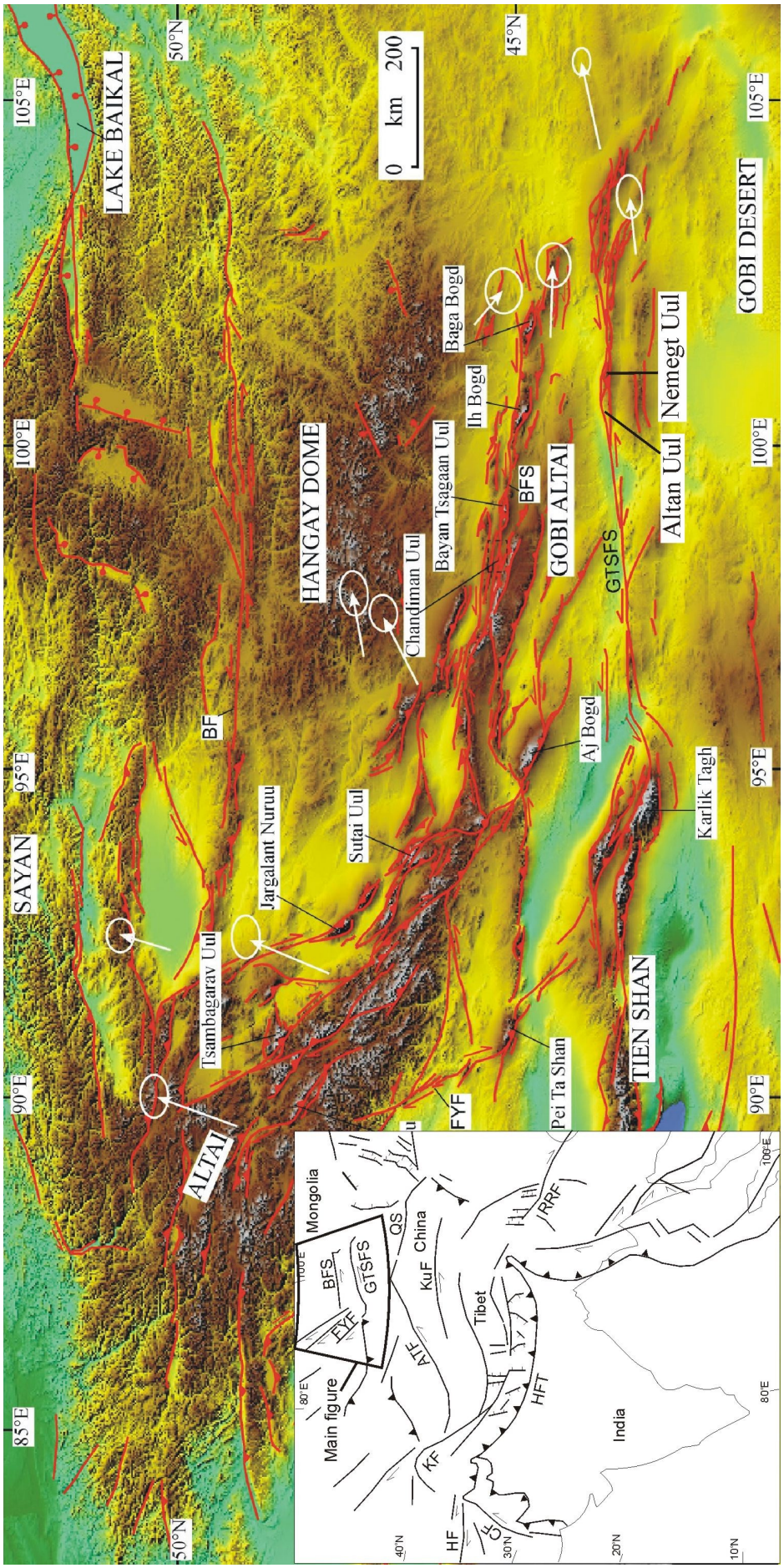

Fig.1.1. Digital topographic map showing active fault systems in Altai, Gobi Altai, easternmost Tien Shan, and Hangay Dome regions, Central Asia (after Cunningham, 2007). Nemegt and Altan Uul are located along the east-west trending left-lateral Gobi-Tien Shan fault system in southern Mongolia. GPS vectors with error ellipses taken from Calais et al. (2003). Inset shows the major fault systems between the Himalayan collision front and southern Mongolia.
ATF = Altyn Tagh fault, BFS = Bogd fault, CF = Chaman fault, GTSFS = Gobi Tien Shan fault system, HF = Herat fault, HFT = Himalayan frontal thrust, KF = Karakorum fault, KuF = Kunlun fault, QS = Qilan Shan fault, RRF = Red River fault, FYF = Fu-Yun Fault (redrawn from Tapponier et al. 1982).

Intraplate strike-slip deformation zones, like the Gobi –Tien Shan fault system (Fig. 1.1), commonly form zones of interlinked faults (Storti et al. 2003). The fault linkages may occur by interaction of local stress fields at fault tips (Westaway, 1995) resulting in fault orientations that define alternating areas of localised convergence and divergence along the 'principal deformation zone' (Cunningham & Mann, 2007). Typically convergent (restraining) and divergent (releasing) bends are defined as zones between continuously linked and curved bounding faults that cross an offset area between strike-slip faults, forming sigmoidal restraining bend mountain ranges or releasing basins, whereas restraining and releasing stepovers are defined as zones of slip transfer between distinct offset parallel master faults, resulting in more rhomboidally shaped mountain ranges and basins (Wilcox 1973, Crowell 1974, Aydin & Nur, 1985). Fault stepovers may evolve with progressive fault movements, leading to linkage between the master faults across the deformation zone, and the stepover may develop into a restraining bend (Westaway, 1985, McClay & Bonora, 2001). Restraining bends localise uplift along intraplate strike-slip faults, commonly producing topographically isolated and elongate mountain ranges like the Tsost Uul range in southern Monglia (Cunningham et al. 1997) and the Denali range in Alaska (Fitzgerald et al. 1993). However, restraining bends are one of the least understood types of mountain range and their 3D architecture is rarely documented. Restraining bends have important socio-economic significance. They can act as seismic propagation barriers (Sibson, 1985) but may also act as nucleation sites for earthquakes (Shaw, 2006), making them an important consideration for seismic hazard assessment. They also exhume basement rocks that contain important mineral resources (e.g. Muir, 2002), host hydrocarbons in their interiors and flanking basins (Christie-Blick & Biddle, 1985), and form major topographic highs that may provide a locally significant rain catchment area and potential groundwater resources (Cunningham et al. 1996, Cunningham, 2005, 2007).

This thesis concentrates on the polyphase evolution of Nemegt and Altan Uul, two Cenozoic mountain ranges in the Gobi Altai, southern Mongolia (Fig. 1.1; Fig. 1.2). Previous reconnaissance studies suggested Nemegt Uul has a positive flower structure in cross-section, and speculated that it was uplifted at a restraining bend along the Gobi-Tien Shan fault system (Cunningham et al, 1996, Owen et al, 1999b). Nemegt and Altan Uul consist of greenschist to epidote-amphibolite grade meta-volcanic and volcaniclastic meta -sedimentary rocks, mafic-ultramafic rocks, and arkosic-mature meta-sedimentary rocks

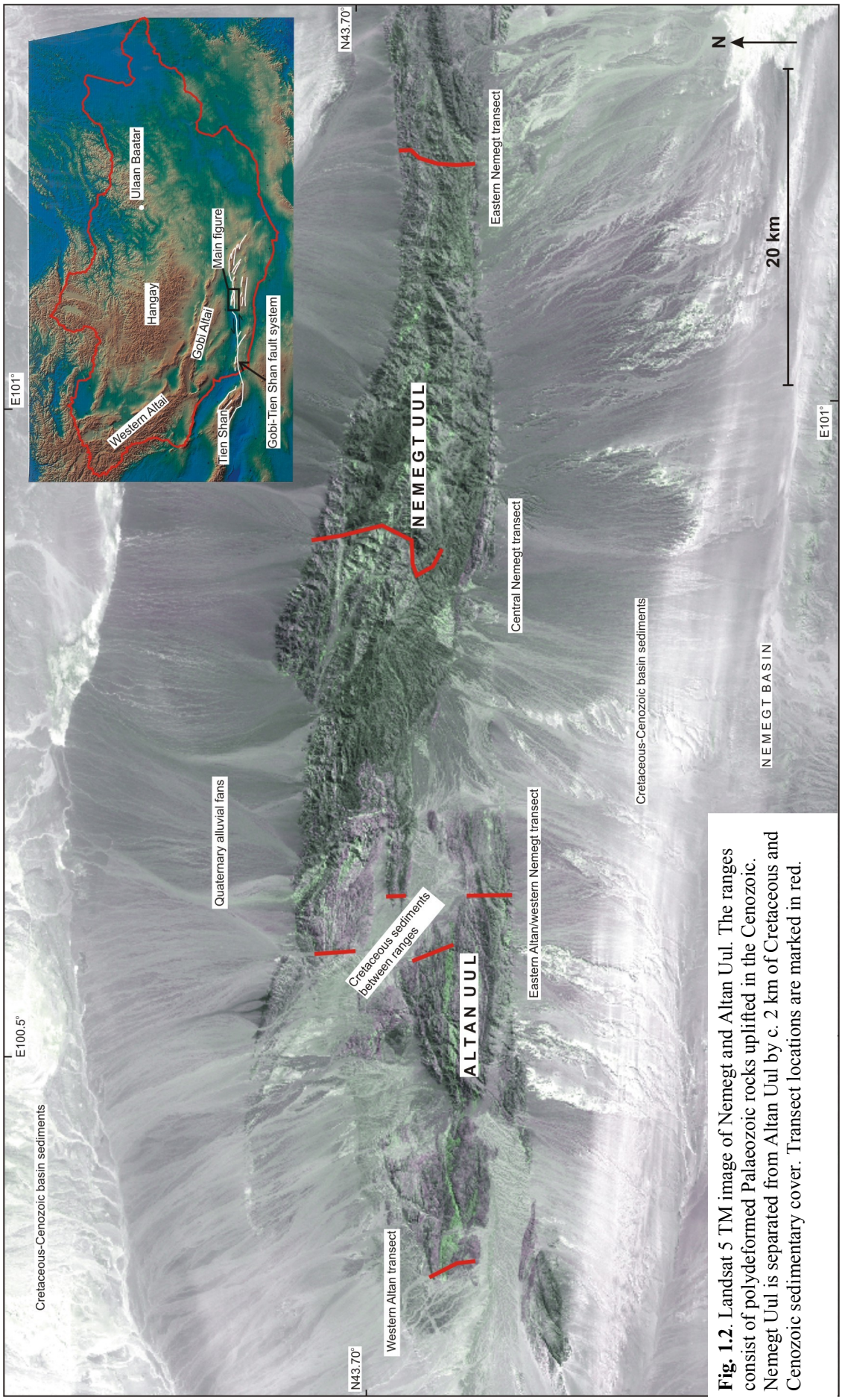

Fig. 1.2. Landsat 5 TM image of Nemegt and Altan Uul. The ranges consist of polydeformed Palaeozoic rocks uplifted in the Cenozoic. Nemegt Uul is separated from Altan Uul by c. 2 km of Cretaceous and Cenozoic sedimentary cover. Transect locations are marked in red.

intruded by various granitic and dioritic rocks. The area is of particular interest because the rocks are the deepest exhumed rocks in the region and have been polydeformed by contractional, extensional and transpressional deformation that occurred during Palaeozoic continental amalgamation and subsequent Mesozoic extensional and Cenozoic transpressional deformation events. Consequently, the rocks of Nemegt and Altan Uul offer a unique opportunity to investigate whether faults and cleavage developed during early deformation events have affected the geometry and kinematics of structures formed during subsequent deformation events, as well as providing essential data to constrain and modify current models for terrane amalgamation, restraining bend evolution and uplift along intraplate strike-slip systems, and the crustal evolution of southern Mongolia.

Specific objectives of this study include: 1) documenting the lithologies, variation in metamorphic grade, and structures of Nemegt and Altan Uul; 2) differentiating between structures of different ages based on cross-cutting field relationships; 3) characterising each of the structures that deformed the rocks of Nemegt Uul in order to understand the polyphase evolution of the area; 4) ascertaining the origin of mafic-ultramafic rocks in Nemegt and Altan Uul in order to determine if they represent an ophiolitic sequence; 5) conservatively extrapolating surface geology to depth to construct a 3D model of the architecture of the ranges; 6) testing current Palaeozoic terrane and terrane accretion models for the formation and evolution of the Palaeozoic rocks in the ranges and the surrounding area against new field data collected during this study; and 7) proposing an evolutionary model of the region including the formation of the rocks and their subsequent deformation, uplift and exhumation.

Fieldwork was carried out over two 3-month field seasons in 2004 and 2005. Four south to north cross-strike transects were carried out in Nemegt and Altan Uul to document the lithologies and structures within the ranges. More detailed mapping was carried out in structurally complex areas in eastern Nemegt Uul, and some major faults were traced between transects to document their continuity and slip vector variations. Samples were taken along all the transects and in other key areas for petrographic analysis at the University of Leicester, to better constrain lithological, metamorphic and strain variations in the ranges. Samples of mafic-ultramafic rocks in Altan Uul were taken for petrological analysis of major and trace elements using standard X-ray fluorescence techniques at the University of Leicester, to determine if the rocks represent a partial ophiolite sequence. Photo-geological interpretation of Landsat 5 Thematic Mapper

(Landsat TM), Shuttle Radar Topography Mission 90 Digital Elevation Model (SRTM-90 DEM), and limited high resolution GoogleEarth imagery was carried out to gain information about the geology and geomorphology of areas that were not visited in the field, and to determine the along-strike continuity of lithologies and structures within Nemegt and Altan Uul.

This project connects with longstanding geological research in Mongolia carried out by members of the Crustal Processes Research Group at the University of Leicester, UK. This project builds on previous work into the Palaeozoic amalgamation of the Central Asian Orogenic Belt (Windley et al. 1994, 2007, Buchan et al. 2002, Blight, 2008), Cretaceous rifting in southern Mongolia (Cunningham et al. submitted), and transpressional deformation in the Gobi Altai region (Cunningham et al. 1996, 1997), including restraining bend mountain building (Cunningham, 2005, 2007). This thesis also incorporates data recently accepted for publication in a paper concerning the Altan Uul ophiolite (Rippington et al. 2008). This study represents the first in depth study of the formation, metamorphic grade and polyphase deformation, of the rocks in Nemegt and Altan Uul.

Chapter synopsis

This thesis contains four chapters. Chapter 2 focuses on the Palaeozoic evolution of Nemegt and Altan Uul. Four south to north transects across the ranges are presented (Fig. 1.2). Each transect is divided into distinct litho-tectonic sequences[1] and the lithologies, structure and metamorphic petrography of the rocks in each sequence are discussed. The petrology of meta-gabbros in an east-west trending mafic-ultramafic belt transected in western Altan Uul is documented and the rocks are interpreted as a partial ophiolite sequence. The lithologies, structure and metamorphic petrography of the litho-tectonic sequences defined along each transect are discussed and compared in the context of other limited studies of the region (Lamb & Badarch, 2001, Helo et al. 2006) to suggest that there is a systematic south to north variation in the rocks of Nemegt and Altan Uul. In the south, meta-volcanic and volcaniclastic rocks with arc affinities are exposed. Moving

[1]For the purpose of this study, the term "sequence" is not used in a stratigraphic context, as the relative ages of the pre-dominantly fault bound rock units in the region are often unknown. "Sequence" is taken to mean an assemblage of rocks with a distinct lithological and/or structural style. "Unit" refers to a single rock type found within a lithotectonic sequence. The term "belt" is used where the outcrop of a sequence is narrow across-strike and elongate along-strike.

north through a partial ophiolite sequence, arkosic and mature meta-sedimentary rocks are exposed and sit unconformably above a discontinuous east-west trending belt of orthogneiss along the north front of Nemegt Uul. Cross-cutting relationships between structures and lithologies in the ranges are used to identify four phases of deformation: Two phases of south to north Palaeozoic contractional deformation (D1 and D2) that are likely to have occurred in succession under similar stress conditions during Palaeozoic terrane accretion, a phase of approximately north-south Cretaceous extensional deformation (D3) that likely also formed the range flanking Cretaceous sediment filled basins to the north and south of the ranges (Fig. 1.2), and a phase of Cenozoic left-lateral transpressional deformation (D4) that uplifted the Palaeozoic rocks in the area to form Nemegt and Altan Uul.

Chapter 3 focuses on the Mesozoic and Cenozoic post-accretionary evolution of Nemegt and Altan Uul. Cretaceous extensional structures (D3) are discussed. Cenozoic transpressional faults (D4) and the geomorphology of the area are discussed and along-strike variations in the geometry and kinematics of some major Cenozoic faults are documented. Evidence for the architecture and Cenozoic evolution of the Nemegt Uul restraining bend and the connections between Nemegt and Altan Uul are reviewed. Finally, the first model of the 3D architecture of the Nemegt and Altan Uul ranges is presented.

Chapter 4 is a synthesis of the evidence for the Palaeozoic to Cenozoic evolution of Nemegt and Altan Uul. Current models for Palaeozoic terrane amalgamation of the Central Asian Orogenic Belt are discussed. A brief review of the ophiolite belts of Mongolia and the Palaeozoic rocks surrounding Nemegt and Altan Uul is presented, before the evidence and conclusions presented in chapters 2 and 3 are amalgamated and placed in a regional context to propose the first Palaeozoic to Cenozoic evolutionary model for the rocks in Nemegt and Altan Uul. Evidence for the Cenozoic evolution of the Gobi-Tien Shan fault system is discussed.

Chapter 5 presents the main conclusions of this study and considers the direction that should be taken with future work in the region.

Chapter 2

The Palaeozoic evolution of Nemegt Uul and Altan Uul

2.1. Introduction

The Central Asian Orogenic Belt is a complex collage of Neoproterozoic-Palaeozoic terranes extending from the Urals in the west, to the Pacific in the east, and from the Angaran craton in the north, to the Tarim basin and North China craton in the south (Fig. 2.1A). This region is the largest area of Phanerozoic continental growth on Earth and is a natural laboratory for studying processes of continental growth and deformation including terrane accretion, ophiolite obduction, terrane amalgamation, terrane dispersal and crustal reactivation (Lamb & Badarch 2001, Badarch et al. 2002, Windley et al. 2007).

Southern Mongolia is situated within the Central Asian Orogenic Belt (Fig. 2.1A,B). The region is a large, sparsely populated area that has been difficult to access until recently. Consequently, the geology of large areas of southern Mongolia is poorly understood and new data about the nature of the lithologies, geochemistry, structure and age of the rocks in the region are needed to better constrain models for the evolution of the region. Detailed local studies allow the geology of geographically disparate areas to be compared, making it possible to define tectonic terranes and to test current models for the tectonic amalgamation of the Central Asian Orogenic Belt (Sengor et al. 1993, Badarch et al. 2002).

This chapter describes Palaeozoic arc rocks, marine sedimentary rocks and a previously unreported ophiolite complex in southern Mongolia. The work is based on new field, petrographical and petrological data from the Altan Uul and Nemegt Uul mountain ranges in the Gobi Altai of southern Mongolia (Fig. 2.1C). Altan Uul and Nemegt Uul are isolated mountain ranges that are sites of Late Cenozoic uplift at a possible restraining bend along the left-lateral Gobi-Tien Shan Fault Zone (Fig. 2.2; Cunningham et al. 1996, Owen et al. 1999). The ranges are bound to the north and south by extensive Cretaceous basins, which are dated by dinosaur fossils and plant spores found in the sediments (Jerzykiewicz & Russell 1991, Krassilov & Makulbekov 1996, Benton et al. 2000).

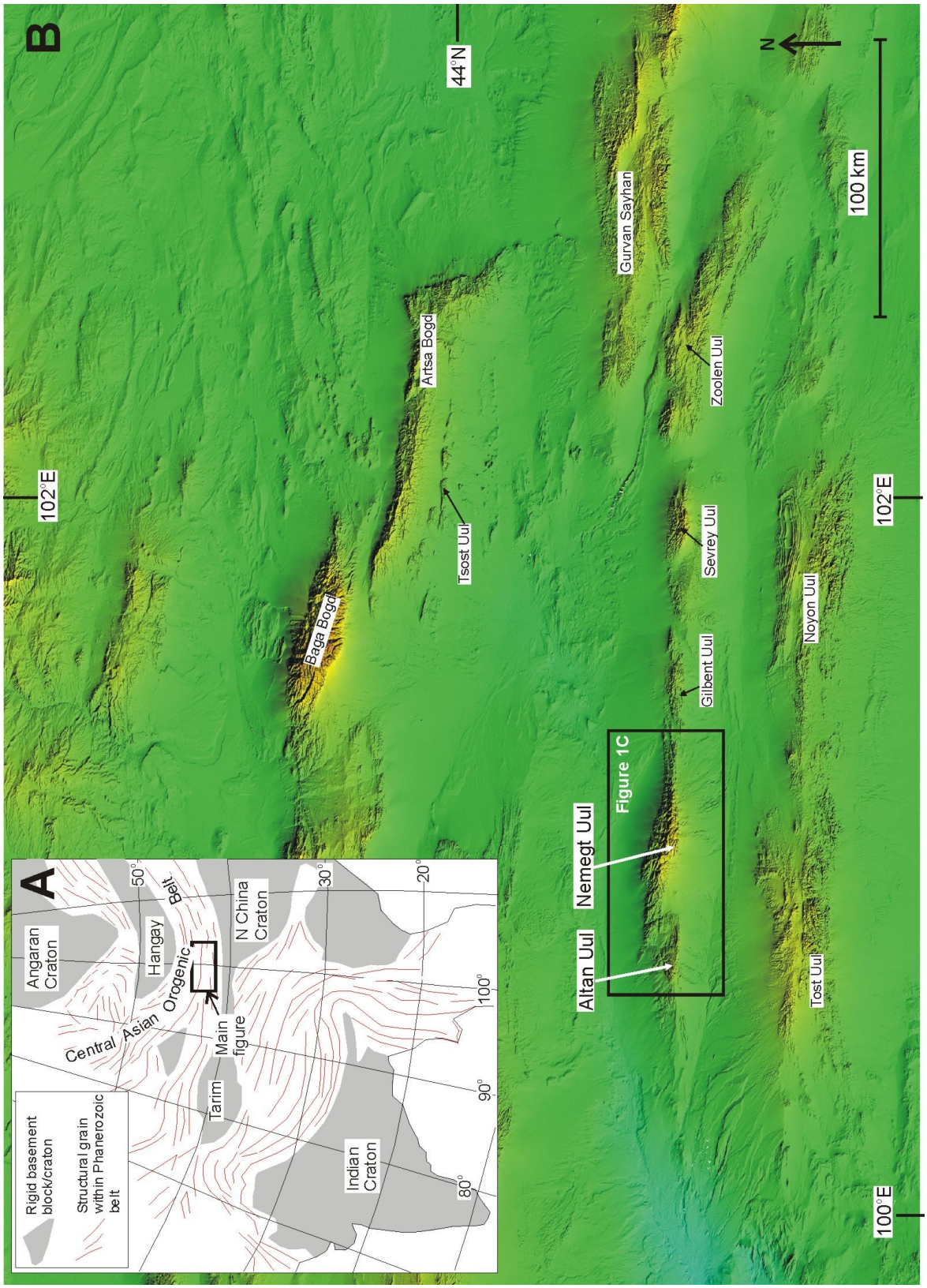

Fig. 2.1. Nemegt Uul and Altan Uul are Cenozoic uplifted mountain ranges in southern Mongolia (A and B), which forms a large part of the Central Asian Orogenic Belt. (Part C overleaf).

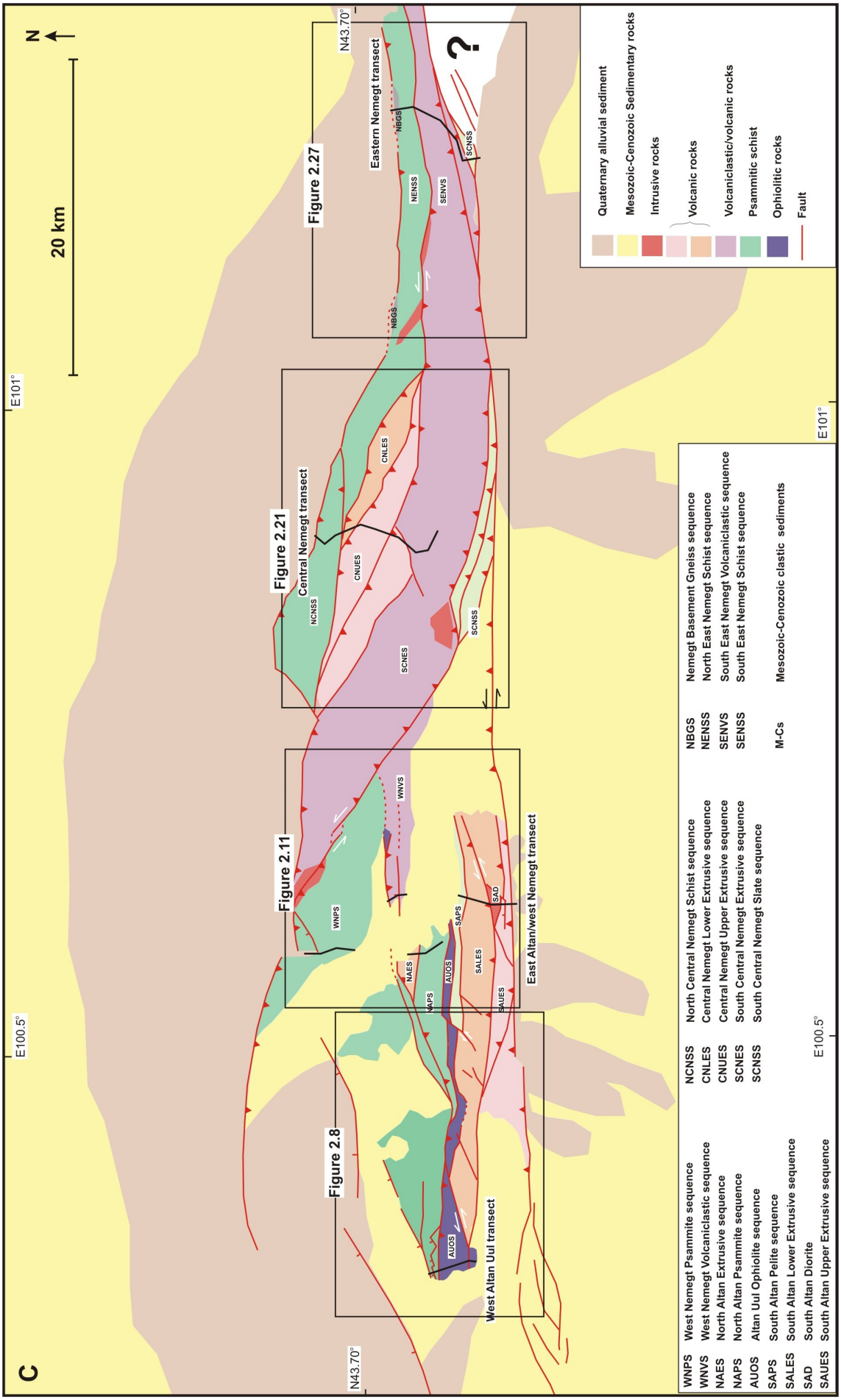
C
N
20 km
E101°
E100.5°
N43.70°
Figure 2.27
Eastern Nemegt transect
Figure 2.21
Central Nemegt transect
Figure 2.11
East Altan/west Nemegt transect
Figure 2.8
West Altan Uul transect
?
Quaternary alluvial sediment
Mesozoic-Cenozoic Sedimentary rocks
Intrusive rocks
Volcanic rocks
Volcaniclastic/volcanic rocks
Psammitic schist
Ophiolitic rocks
Fault
WNPS West Nemegt Psammite sequence
WNVS West Nemegt Volcaniclastic sequence
NAES North Altan Extrusive sequence
NAPS North Altan Psammite sequence
AUOS Altan Uul Ophiolite sequence
SAPS South Altan Pelite sequence
SALES South Altan Lower Extrusive sequence
SAD South Altan Diorite
SAUES South Altan Upper Extrusive sequence
NCNSS North Central Nemegt Schist sequence
CNLES Central Nemegt Lower Extrusive sequence
CNUES Central Nemegt Upper Extrusive sequence
SCNES South Central Nemegt Extrusive sequence
SCNSS South Central Nemegt Slate sequence
NBGS Nemegt Basement Gneiss sequence
NENSS North East Nemegt Schist sequence
SENVS South East Nemegt Volcaniclastic sequence
SENSS South East Nemegt Schist sequence
M-Cs Mesozoic-Cenozoic clastic sediments

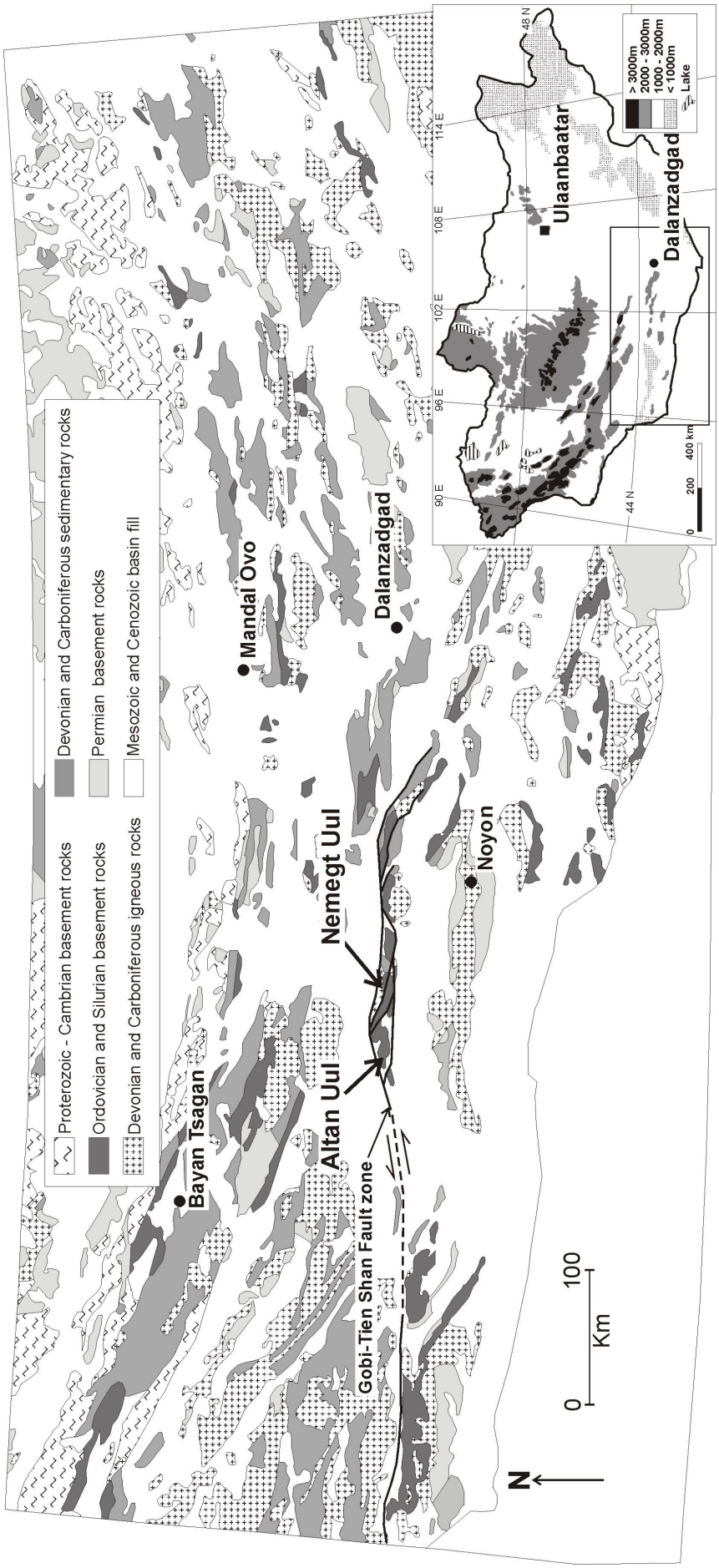

Fig. 2.2. Geological map of southern Mongolia (after Lamb & Badarch 2001). Nemegt and Altan Uul are Cenozoic mountain ranges consisting of Palaeozoic rocks situated along the Gobi-Tien Shan fault system.

Nemegt and Altan Uul are also flanked by alluvial fans, which form an extensive array to the north of Nemegt Uul, and a smaller discontinuous array to the south (Fig. 2.1C). Detailed sedimentological analysis of alluvial fans associated with Late Cenozoic uplifted mountain ranges in the Gobi Altai, suggest that the majority of alluvial fan sedimentation in the region is Quaternary (Owen et al. 1997).

Previous workers have placed the Palaeozoic rocks uplifted in Nemegt and Altan Uul within the Zoolen terrane (Fig. 2.3) which is characterised by dominantly Ordovician -Carboniferous volcanic rocks, melange sequences and variably metamorphosed marine sediments that are polyphase deformed (Badarch et al. 2002). Specifically, Altan Uul consists of fault-bound Silurian-Devonian greenschist-grade psammites, meta-pelites, volcaniclastic schists, andesitic lavas, arkosic and volcaniclastic sandstones, mudstones and cherts, and a sequence of greenschist-grade meta-gabbros, serpentinites, and altered basaltic lavas. Nemegt Uul consists of fault-bound units of dominantly Silurian-Carboniferous greenschist-grade meta-psammitic and meta-pelitic schists, phyllites, slates, volcaniclastic meta-psammites, meta-pelites, conglomerates and breccias, meta-andesitic lavas and meta-rhyolitic tuffs, and unmetamorphosed arkosic and volcaniclastic sandstones. Western Nemegt Uul also contains a small fault bound sliver of serpentinite,

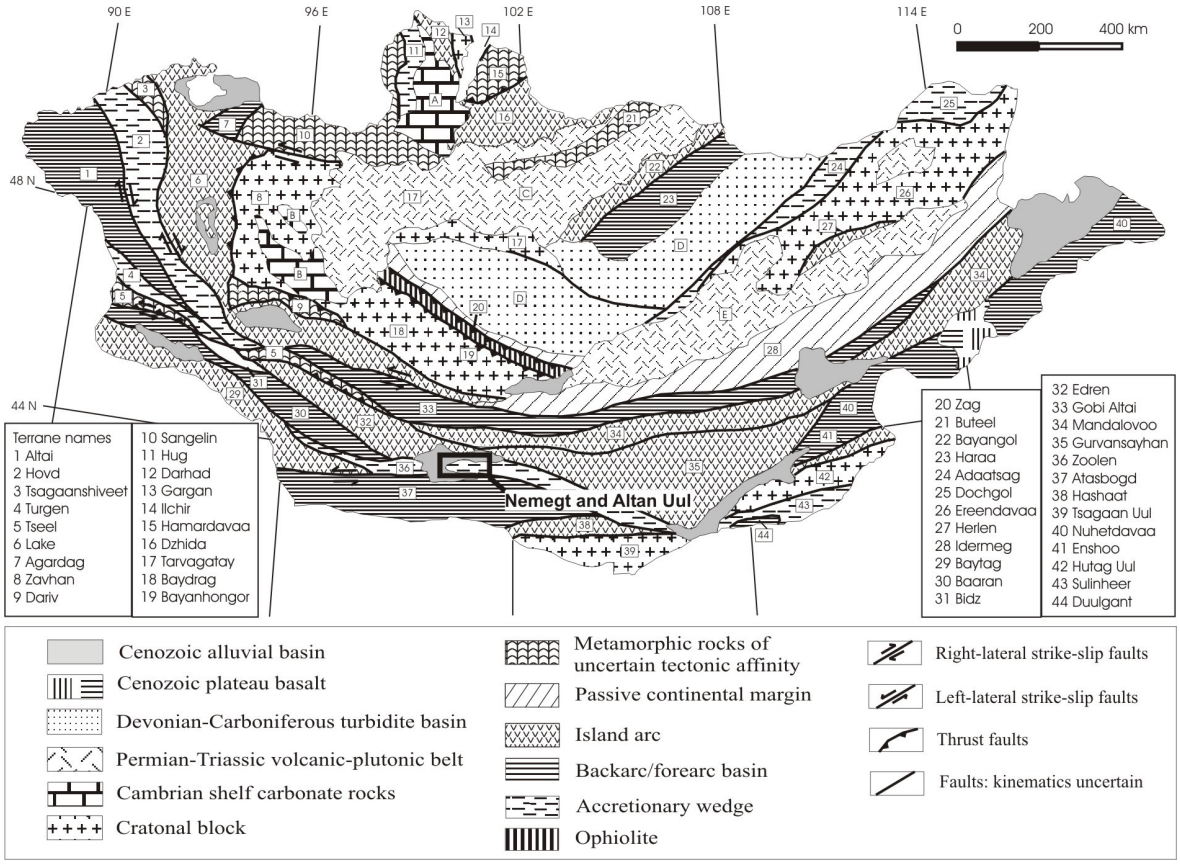

Fig. 2.3. Map of Mongolian terranes (after Badarch et al. 2002).

gabbro, extrusive volcanic rocks and marine sediments. At the northern front of the range in eastern Nemegt Uul, meta-pelites sit unconformably on orthogneiss. Altan and Nemegt Uul are intruded by small granite plutons. The ages for the rocks in Nemegt and Altan Uul given here are based on Russian-Mongolian maps (Mongolian National Atlas, 1990), and the work of Badarch et al. (2002). However, the ages of the Palaeozoic rocks in Nemegt and Altan Uul are actually poorly constrained by geochronological and palaeontological evidence. The quality of the age determinations for Palaeozoic rocks in southern Mongolia is discussed further in section 2.2.

During fieldwork in 2004 and 2005, four structural and lithological transects through Nemegt and Altan Uul were carried out. Data from these transects were used to define a mixed assemblage of east-west trending fault bound lithotectonic sequences and a suite of mafic and ultramafic rocks in western Altan Uul and Nemegt Uul (Fig. 2.1C). Samples were taken for petrographical analysis to more accurately document lithological and metamorphic grade variations across both ranges. The mafic-ultramafic rocks in western and central Altan Uul were also sampled for petrographic and XRF analysis to determine whether they have geochemical characteristics of oceanic crust. The Palaeozoic rocks of Nemegt and Altan Uul appear to represent accreted fragments of a late Palaeozoic arc and dismembered parts of an ophiolite, although a complete ophiolite stratigraphy is not exposed. Volcanic, meta-sedimentary rocks and possible ophiolitic rocks in Nemegt Uul were previously reported by Owen et al. (1999b) and Helo et al. (2006).

Detailed structural analysis of faults and folds in the ranges was also undertaken to further constrain the structural evolution of the area. Analysis of Landsat TM imagery was used to determine the along-strike continuity of faults and lithotectonic sequences, including ophiolitic rocks, and to gain geological information about areas not visited in the field.

2.2. Regional Geology

Badarch et al. (2002) described and identified 44 terranes in Mongolia, providing the most recent and comprehensive synthesis of the rocks in Mongolia at this time (Fig. 2.3). However, the quality of the data on which the Badarch et al. (2002) terrane synthesis is based must be addressed. Many of the Palaeozoic rocks in Mongolia, especially in the

Gobi Desert in the south, are covered by Mesozoic and Cenozoic sedimentary sequences so the correlations made between Palaeozoic litho-tectonic sequences and terrane boundaries over large distances are uncertain. There are also many areas in Mongolia containing exposed Palaeozoic rocks that have not been studied, or have poor data coverage. Age constraints on the rocks are often based on rare geochronological data and uncited palaeontological data, so it is not possible to assess the quality of the data. It is not always clear if interpretations based on geochemical data are constrained by thorough field work. Nevertheless, the terrane synthesis of Badarch et al. (2002) is a useful working model for the Palaeozoic evolution of southern Mongolia, against which to test new data and interpretations.

Nemegt Uul and Altan Uul have previously been placed in the Zoolen terrane (Fig. 2.3; Badarch et al. 2002). Badarch et al. (2002) describe it as a narrow belt of thrust sheets, tectonic slivers and melanges containing Ordovician-Silurian greenschist grade metamorphosed volcano-sedimentary sequences including tholeiitic pillow basalt, andesite, tuff, meta-psammite, meta-pelite, chert, limestone and olistostromes, Lower Carboniferous marine conglomerate, sandstone and siltstone, and numerous fragments of peridotite, serpentinite, gabbro, diorite and diabase.

The chronostratigraphy of Palaeozoic rocks in Nemegt and Altan Uul is poorly constrained. Radiometric data are restricted to two Silurian detrital zircon ^{206}Pb-^{238}Ur SHRIMP ages of 421 ± 3.0 Ma and 417 ± 2.2 Ma from volcano-sedimentary sequences in Nemegt Uul (Helo et al. 2006), which are in agreement with palaeontological evidence for Silurian to Devonian deposition of the Zoolen terrane sedimentary assemblages (Eenzhin 1983, Ruzhentsev 1985, Badarch et al. 2002). Badarch et al. (2002) also use uncited palaeontological evidence for Devonian to Carboniferous deposition of volcaniclastic and shallow-marine argillaceous sediments in the Zoolen terrane. Russian-Mongolian maps (1990) show Silurian to Devonian rocks in Altan Uul and Silurian to Carboniferous rocks in Nemegt Uul, but it is not clear how these designations have been derived.

Helo et al. (2006) compared major and trace element geochemistry of meta-basaltic and meta-andesitic rocks in Nemegt Uul and Altan Uul in the Zoolen terrane with volcanic rocks in the Gurvansayhan range in the Gurvansayhan terrane to the northeast (Fig. 2.3), and concluded that they have indistinguishable, mutual geochemical characteristics which suggests that Nemegt and Altan Uul, and Gurvansayhan range

contain elements of a single intra-oceanic island arc/fore-arc, and that they may belong to the same terrane. They suggest that the Zoolen terrane has a more complex lithological make-up than proposed by Badarch et al. (2002), and that rocks within it may not belong to a single discrete terrane. Post-accretionary assemblages in the Zoolen terrane include Upper Carboniferous to Permian non-marine volcanic, sedimentary and plutonic rocks, and Jurassic molasse (Badarch et al. 2002).

Timing of accretion can be further constrained in the Zoolen terrane. Lamb & Badarch (1997, 2001) presented sandstone petrographic data from southern Mongolia. Lamb & Badarch (1997, 2001) assigned the rocks ages based on their assessment of the quality of the palaeontological or geochronological ages the rocks are given by other workers (Kozakov 1986, Voznesenskaya 1989, Gibsher et al. 1991, Ruzhentsov & Pospelov 1992, Dorjnamjaa et al. 1993, Zorin et al. 1993, Kotov et al. 1995, Kovach et al. 2005). Unfortunately, in the original papers it is not always clear how these workers produced age determinations for specific rocks or what criteria Lamb & Badarch (1997, 2001) used to assess the quality of the data. Based on the observations of Lamb & Badarch (1997, 2001), the sandstones in the southern Gobi Altai region of southern Mongolia have mature continental type signatures shifting to lithic-rich arc type signatures in the Devonian, which suggests that arc activity in the region had initiated by this time. Devonian – Carboniferous sandstone at Nemegt Uul has a transitional arc-arc provenance signature. Helo et al. (2006) describe lower Carboniferous marine sediments in the Zoolen terrane, which suggests that an ocean may have persisted in the area until this time. Permian strata in the region are primarily non-marine (Hendrix et al. 1996) and Permian volcanic rocks plot as intra-plate alkali basalts (Lamb & Badarch 2001). This suggests that terrane amalgamation had finished and the Palaeozoic basement rocks in the Zoolen terrane had been uplifted by the Permian.

2.3 Geology of Nemegt and Altan Uul

In the following sections the lithologies, metamorphic grade and structure of the rocks in Nemegt Uul and Altan Uul are discussed[1]. Four transects (Fig. 2.4-2.7. N.B. Transect figures 2.5-2.7 are duplicated at the beginning of sections 2.5-2.7.) are presented through the combined ranges from west to east. For each transect, the lithologies,

1Coordinates for all localities shown on photos and photomicrographs are given in Appendix A.

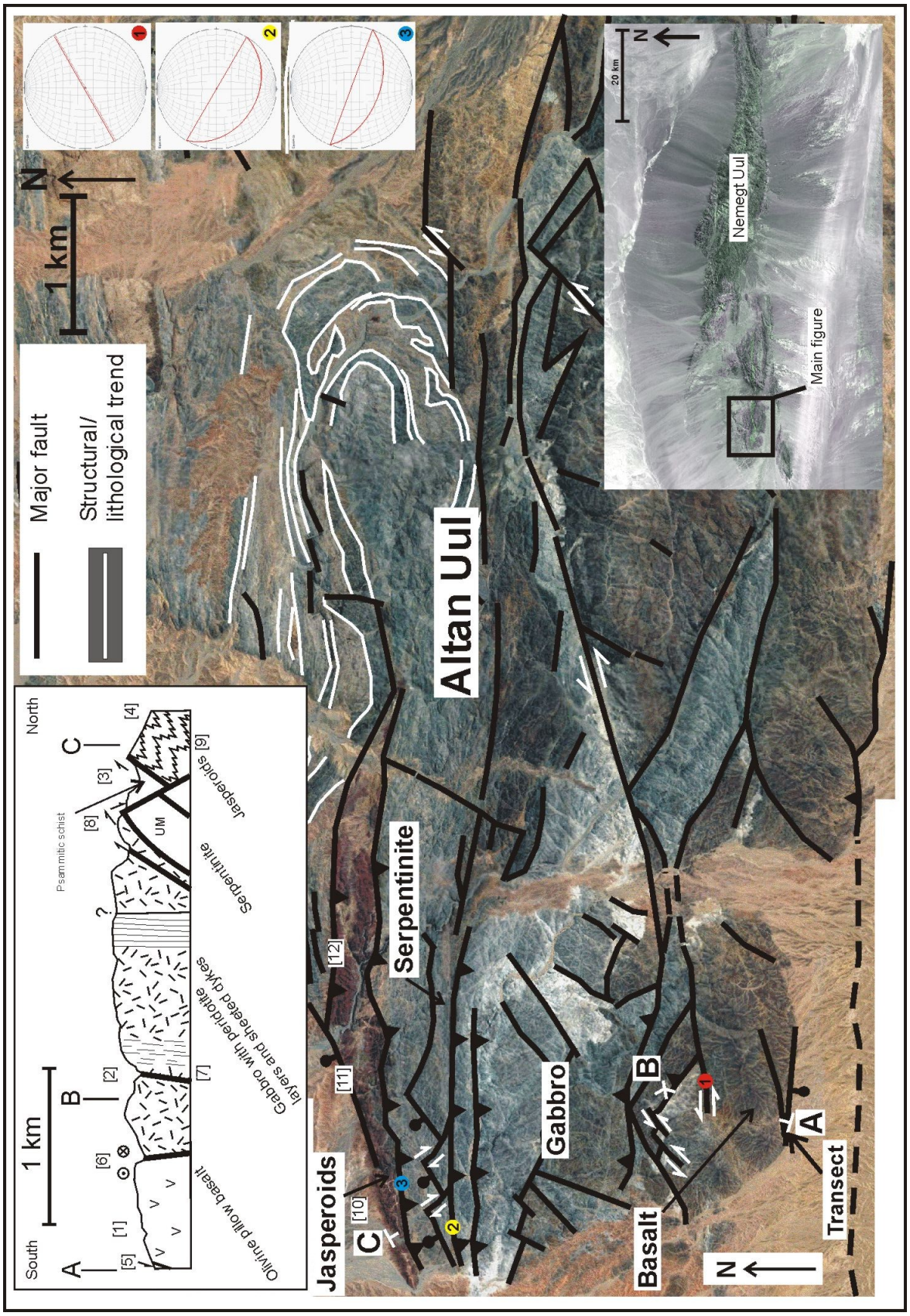

Fig. 2.4. Photo-geological interpretation of satellite image from GoogleEarth, showing the trace of faults and folded fabrics of west Altan Uul. The Western Altan transect through the western extent of the range is also shown. Stereonets show the geometry of key faults documented along the transect. Numbers in square brackets [#] are locations referred to in the main text. UM = Ultramafic.

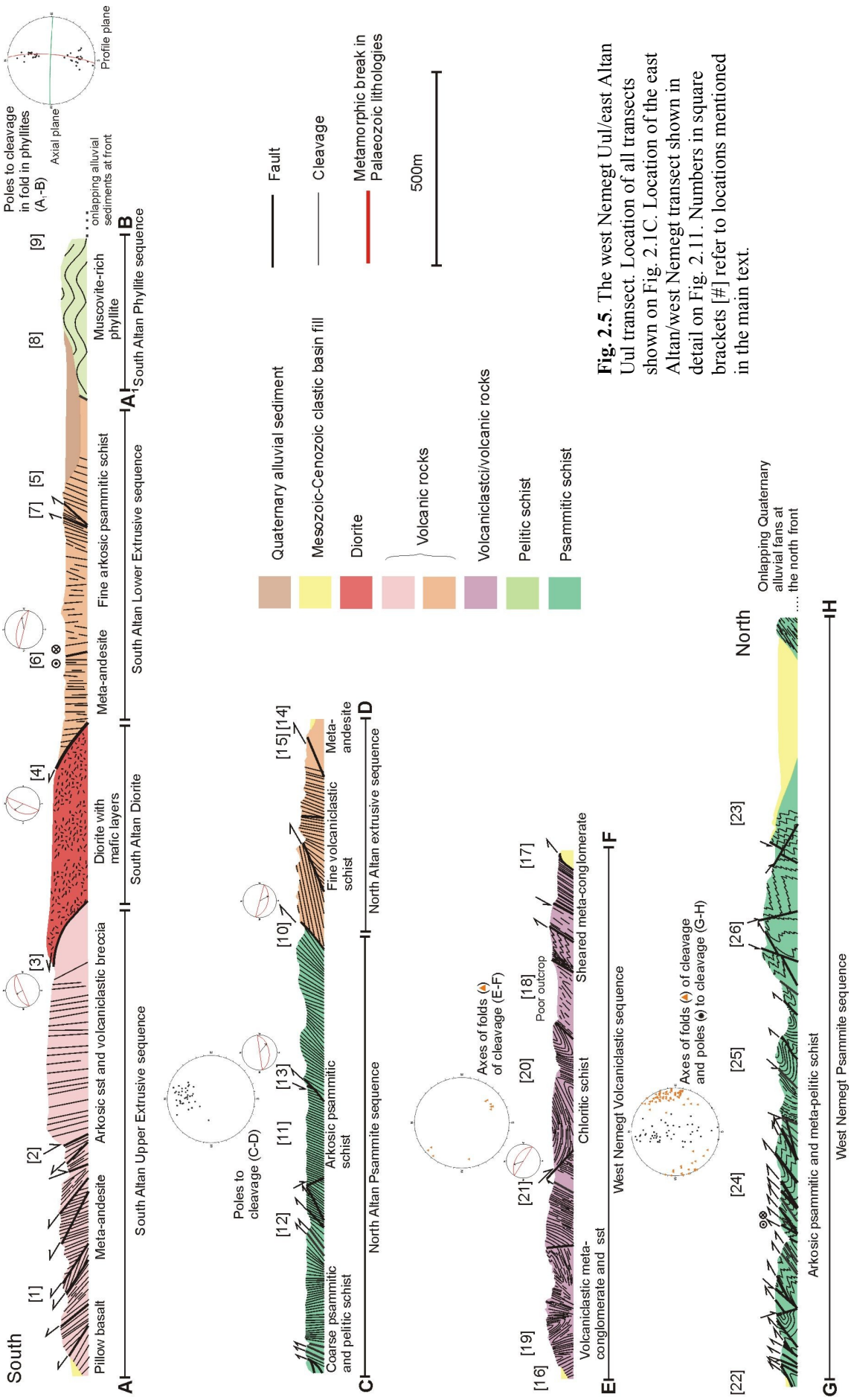

Fig. 2.5. The west Nemegt Uul/east Altan Uul transect. Location of all transects shown on Fig. 2.1C. Location of the east Altan/west Nemegt transect shown in detail on Fig. 2.11. Numbers in square brackets [#] refer to locations mentioned in the main text.

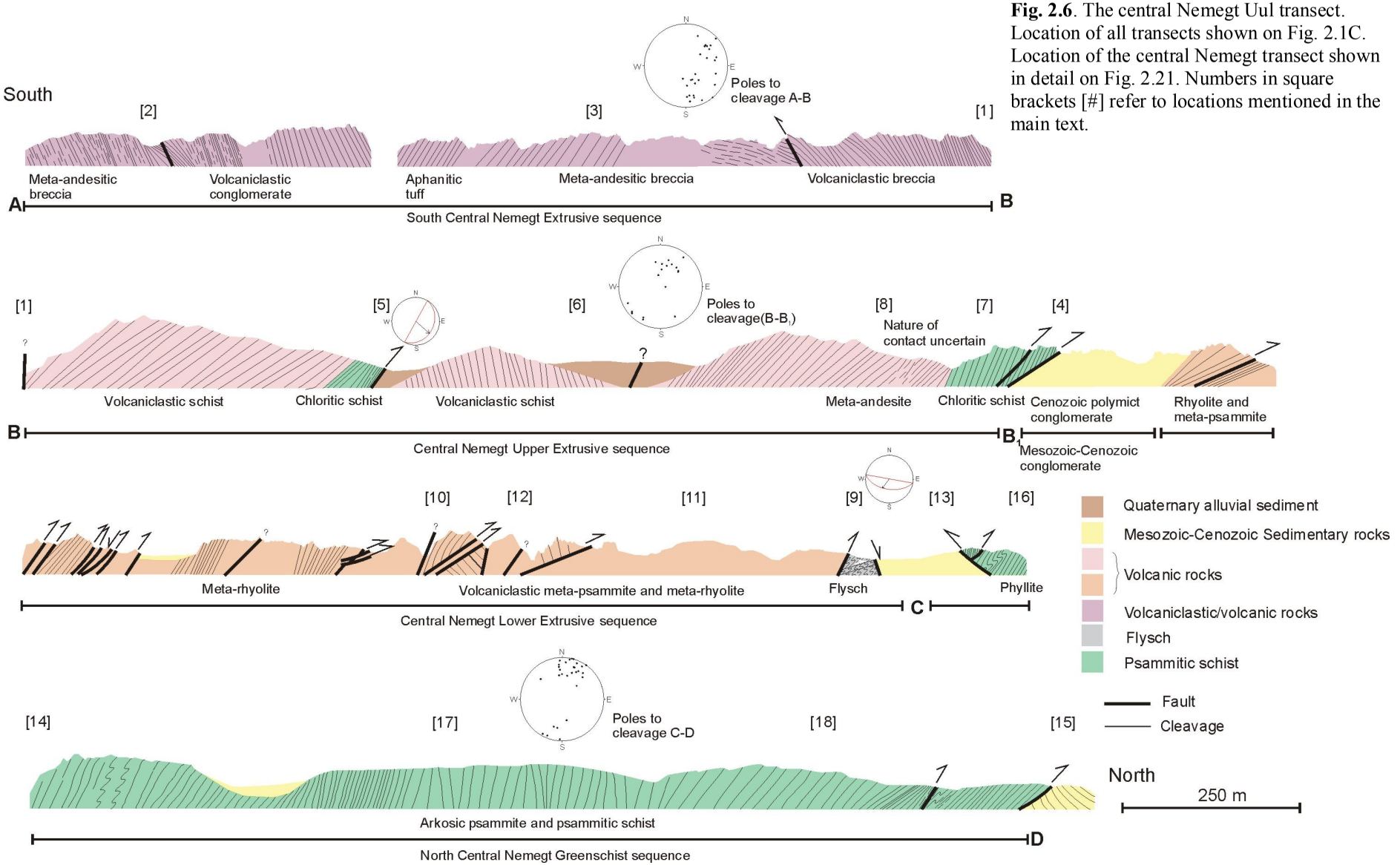

Fig. 2.6. The central Nemegt Uul transect. Location of all transects shown on Fig. 2.1C. Location of the central Nemegt transect shown in detail on Fig. 2.21. Numbers in square brackets [#] refer to locations mentioned in the main text.

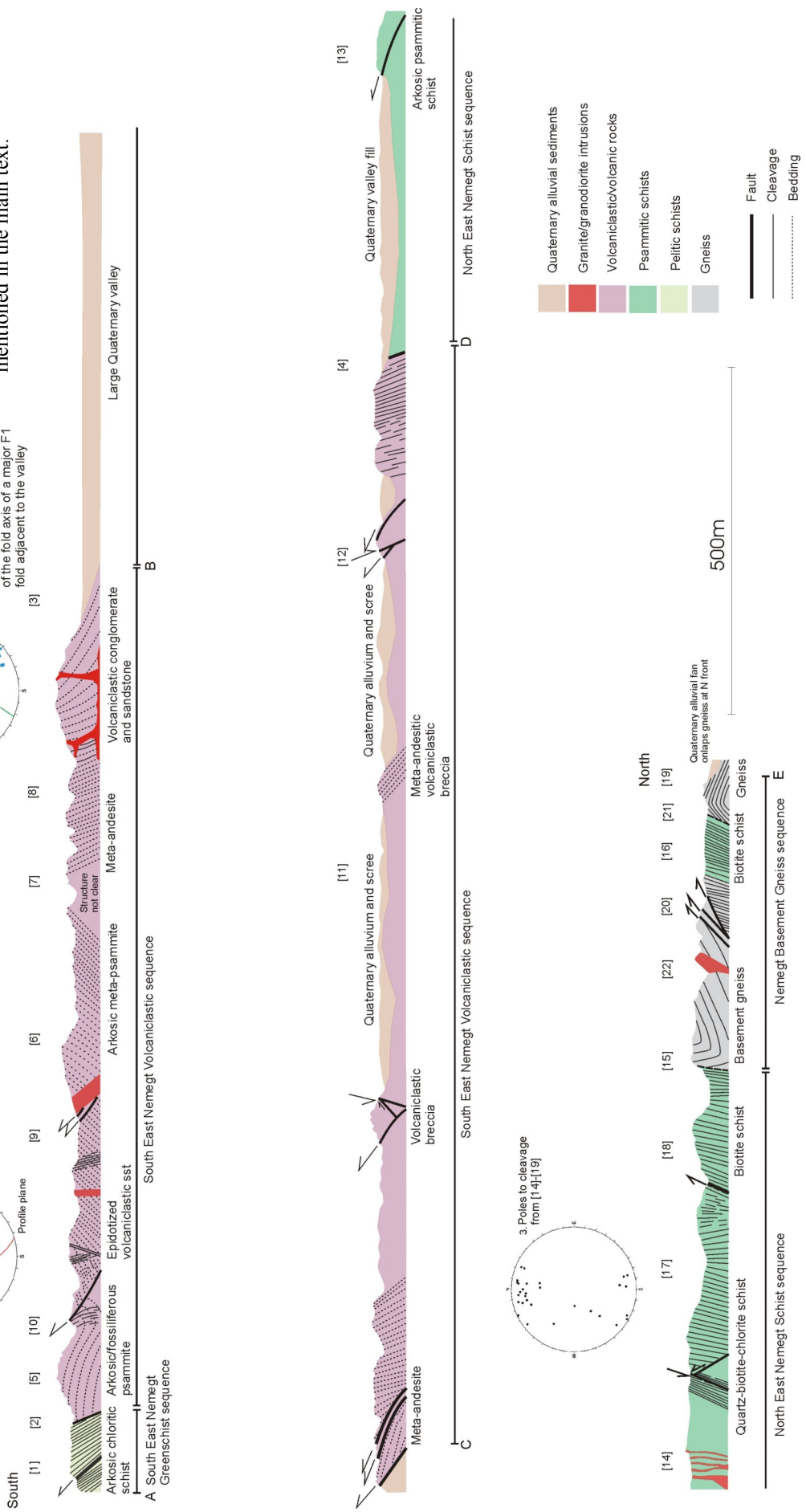

Fig. 2.7. The east Nemegt Uul transect. Location of all transects shown on Fig. 2.1C. Location of the central Nemegt transect shown in detail on Fig. 2.27. Numbers in square brackets [#] refer to locations mentioned in the main text.

metamorphic grade and structure are systematically documented from south to north. Lithotectonic sequences have been defined along each transect, grouping rocks of similar lithological, metamorphic and structural affinity, giving an overview of the geology of the area. For each lithotectonic sequence, the outcrop appearance is described, followed by a description of the petrography of each lithology. Mineral percentages are given as approximate average ranges and values of modal abundance based on visual estimation in thin section over several samples, and consequently do not add up to 100 % for each rock type. The modal abundance of primary mineral phases in volcanic and igneous rocks was compared to the descriminations on an extrusive or plutonic Quartz Alkali Plagioclase Feldspathoid (QAPF) diagram to determine the rock type (e.g. basaltic, andesitic, rhyolitic, gabbroic, dioritic, granitic). Primary textures were observed in thin section to determine volcaniclastic rocks from extrusive or intrusive volcanic rocks. Next, the structure and metamorphic grade of each lithotectonic sequence is described. The metamorphic mineral assemblages observed are used to identify the facies of peak metamorphism.

In the absence of a published stratigraphy or currently agreed names for units in this area, the author uses their own names for the lithotectonic sequences, based on the geographic location in which the rocks have been best documented. The Palaeozoic rocks in Nemegt and Altan Uul have been polyphase deformed and are exposed in fault-bound sequences. Consequently, the relative ages of the rocks are not always certain. In the absence of quality age constraints it is not possible to construct a general vertical section for the Palaeozoic rocks in Nemegt and Altan Uul at this time. However, the distribution of Palaeozoic lithologies and strain, and the variation in metamorphic grade, is summarised in section 2.10.

2.4 West Altan Uul Transect

2.4.1 The Altan Uul Ophiolite sequence

The Southwest Altan Ophiolite sequence is a collage of tectonically dismembered meta-basalts, pillow meta-basalts, cumulate meta-gabbros, serpentinites, sheeted dykes and cherts. It is the only sequence to crop out at the furthest west extent of Altan Uul (Fig. 2.8), and is dominantly blocky and fractured throughout the transect area. In the south, the

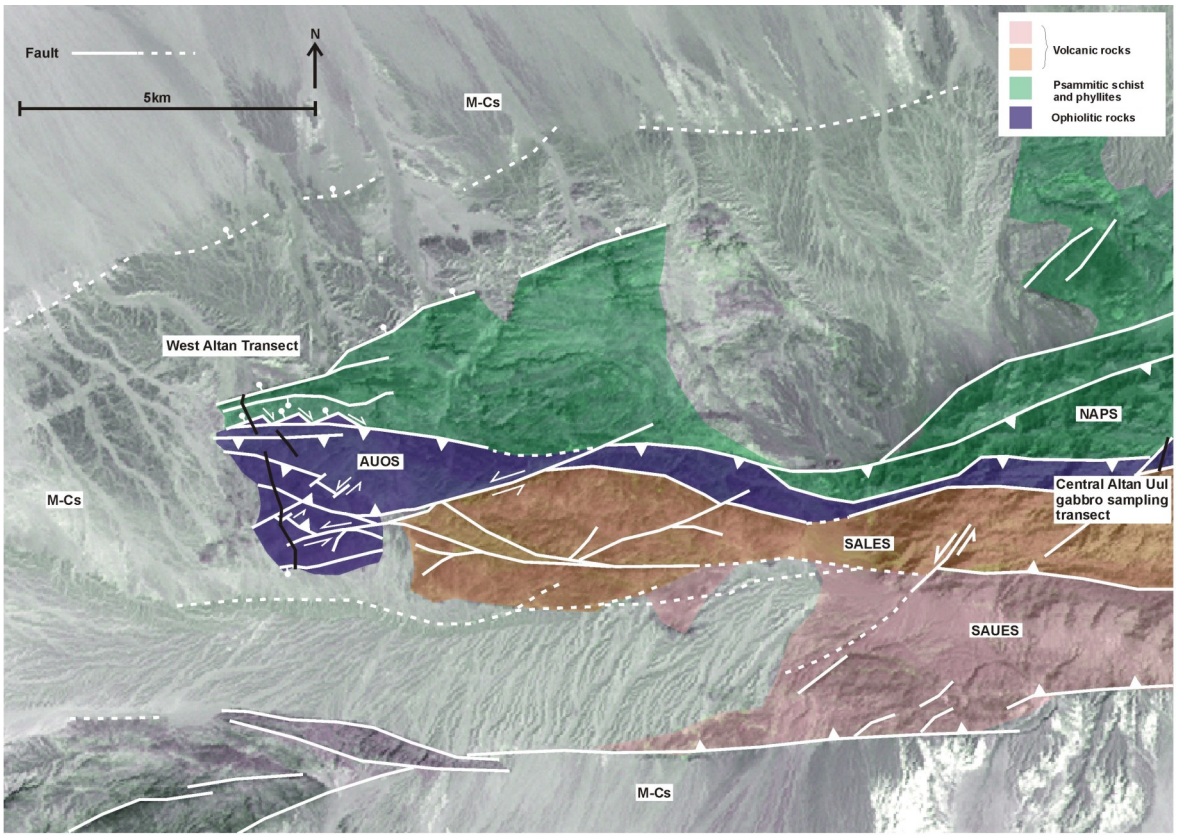

Fig. 2.8. West Altan Uul location map with litho-tectonic sequences. Ophiolitic rocks in central Altan Uul are also labelled. SAUES = South Altan Upper Extrusive sequence. SALES = South Altan Lower Extrusive sequence. AUOS = Altan Uul Ophiolite sequence. NAPS = North Altan Psammite sequence. M-Cs = Mesozoic-Cenozoic sediments.

sequence is onlapped by Cretaceous sediments. In the north, the sequence is bound by a steep northeast-southwest trending brittle normal fault, but is also locally onlapped by Quaternary alluvial fans. The Southwest Altan Ophiolite sequence can be traced east on Landsat TM imagery to a fault-bound sequence of gabbro and serpentinite exposed in central Altan Uul (Fig. 2.8).

Lithologies and petrography

At the southern end of the transect, blocky exposures of meta-basalt, occasionally containing pillows (Fig. 2.9A), can be seen in a series of anastamosing low-lying valleys (Fig. 2.4 [1]). To the north, topography increases and extrusive meta-volcanics give way to cliff faces made from blocky and highly fractured meta-gabbros, sometimes containing near vertical cumulate layering (Fig. 2.9B; Fig. 2.4 [2]). The meta-gabbro is interbedded with slivers of serpentinite and a zone of sheeted dykes (Fig. 2.9C). North of the meta-gabbro and serpentinite, a c.450 m wide unit of meta-psammite crops out in low-lying

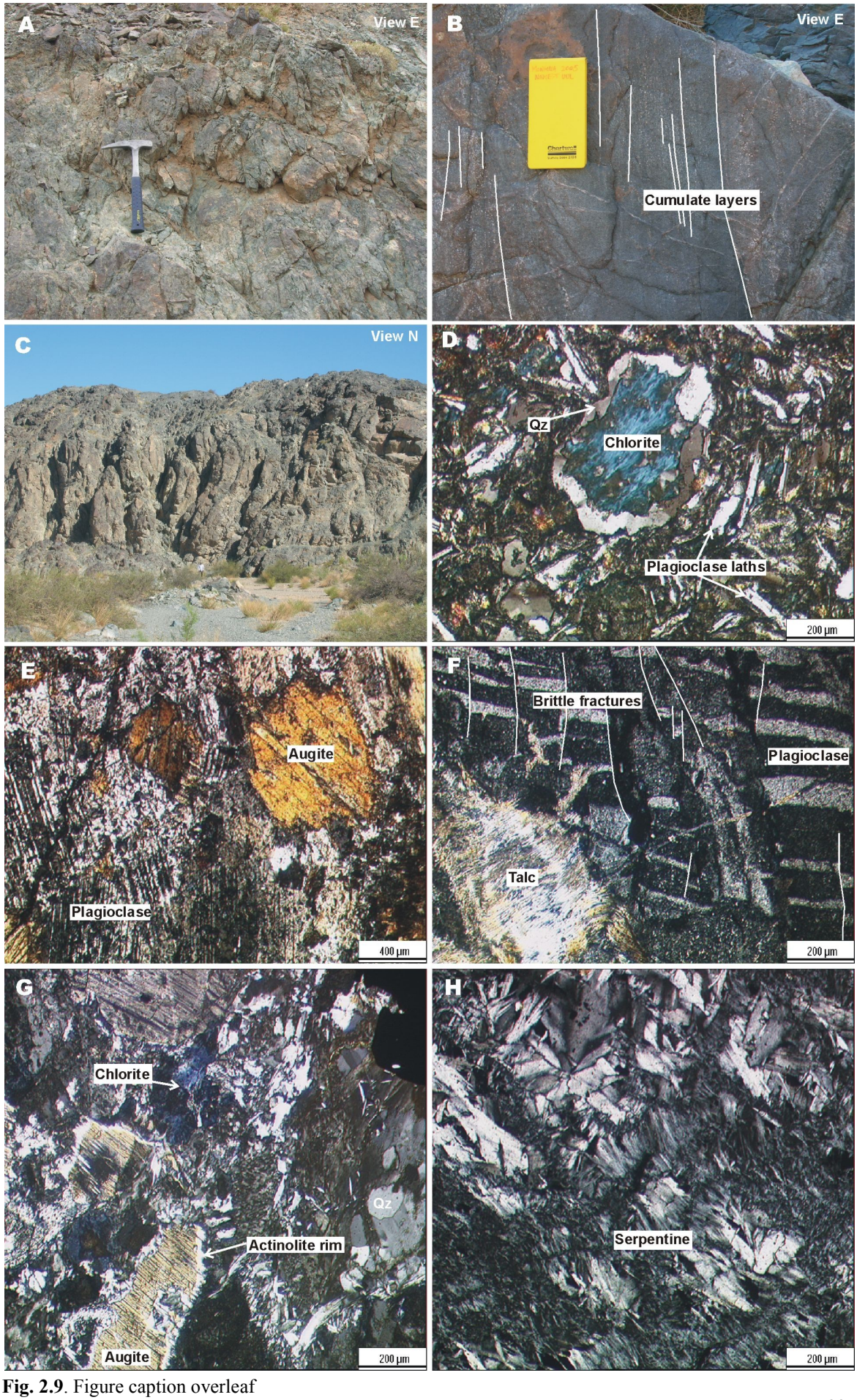

Fig. 2.9. Figure caption overleaf

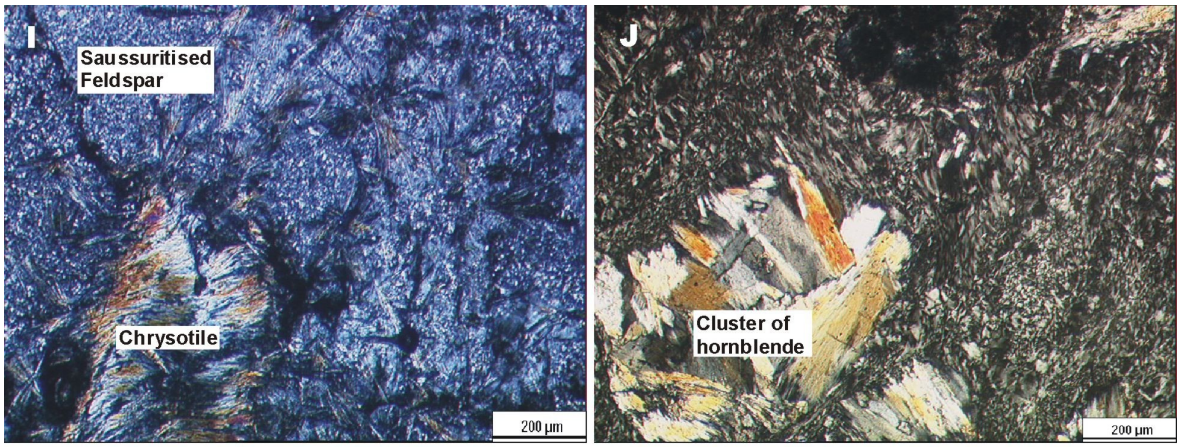

Fig. 2.9. Ophiolite transect lithologies. A) Pillow basalt at loc. 194. B) Cumulate layers in gabbro at loc. 215. C) Sheeted dykes at loc. 216. D) Unstrained sub-speherical chlorite-filled vesicle in basalt at loc. 226. E) Gabbro with plagioclase and augite at loc. 219. F) Gabbro with brittle fractures in plagioclase at loc. 202. G) Chlorite and actinolite rim around augite in gabbro at loc. 236. H) Serpentine-rich layer in gabbro at loc. 220. I) Chrysotile and altered feldspar in gabbro at loc. 214. J) Hornblende overgrowths in gabbro at loc. 233.

hills either side of a wide east-west valley in northwest Altan Uul (Fig. 2.4 [3]). North of the valley and the meta-psammites, bedded and folded jasperoids outcrop in a c.500 m wide ridge before the northern front of Altan Uul (Fig. 2.4 [4]).

The meta-basalts in the southern part of the area contain subhedral 0.2 mm albitized plagioclase feldspar crystals (60-80 %) and 0.2 mm subhedral augite crystals (5-10%), and euhedral 0.2 mm olivine crystals (c.5 %). Olivine has often been altered to calcite (c.5 %) and serpentine (5-15 %), which is often widely distributed throughout the groundmass, and feldspars are often altered to epidote (5-15 %), giving them a speckled and sometimes cloudy appearance. Round, unstrained amygdales of quartz are dotted throughout the rock. Quartz also forms small veins cutting everything. Some of the basalts to the north contain chlorite-filled vesicles and fractures (Fig. 2.9D).

The meta-gabbros consist of small (0.1 mm) subhedral olivine crystals (c.5 %), 0.25-8 mm subhedral plagioclase feldspar (20-50 %), and 1-6 mm subhedral, interstitial, augite (20%; Fig. 2.9E). Plagioclase feldspar crystals are altered to epidote (15-25 %) and sometimes brittly deformed (Fig. 2.9F), making it difficult to identify their anorthite content, although some retain lamellar twinning. 0.5 mm anhedral calcite crystals (c.5 %) cut the epidote and plagioclase crystals. Chlorite (10 %) occurs as streaky patches in feldspar crystals and in fractures. Augite crystals typically have a rim of actinolite (Fig. 2.9G). In some samples, there is a groundmass composed of very fine serpentine (10-30 %; Fig. 2.9H) and brucite (c.5 %). Where serpentine is present, 0.2-2 mm fibrous chrysotile (10 %) and 1-2 mm streaky talc (5-10 %) can sometimes be seen overgrowing

the groundmass (Fig 2.9I). 0.5 mm clusters of subhedral hornblende (c.5 %) are often present (Fig 2.9J), cutting the remains of augite, actinolite, calcite, chlorite, talc, chrysotile and the serpentine groundmass. All the samples have thin (0.5-1mm) veins of epidote and sometimes quartz cutting all other minerals. The petrography and petrology of the cumulate gabbros are discussed in more detail in section 2.9.

The meta-psammites contain rounded 0.1-2mm plagioclase crystals (35 %), variably altered to clusters of small tabular epidote (15 %), and sometimes surrounded by small amounts of muscovite (5 %) and chlorite (10 %). 0.001-0.1mm grains of recrystallised quartz (20 %) is ubiquitous, often formed with a preferred orientation in veins that cut the feldspar. Calcite veins cut everything.

There are no thin sections of the jasperoids available. In hand specimen they are very fine grained and homogenous.

Structure and Metamorphism

Throughout the Southwest Altan Ophiolite sequence, intense fracturing and jointing (Fig. 2.10A) makes identification of fault planes difficult. The meta-basalts in the very south of the area are downthrown on a northwest-southeast trending moderately steep south dipping brittle normal fault with a c.5 cm wide zone of fault breccia (Fig. 2.10B; Fig. 2.4 [5]). To the north, joints cut meta-basalts in all directions, giving them a blocky appearance. Sub-spherical vesicles in some of the meta-basalts suggest the rocks have not been flattened (Fig. 2.9D). Approximately 850 m from the southern front, there is a 10 m wide near-vertical zone of cohesive fault breccia trending 240^{o} (Figure 2.4 stereonet 1). Approximately east-west trending vertical foliation shows sinistral sense fault drag where it passes through the fault zone (Fig. 2.10C). The brittle sinistral strike-slip fault zone separates the basalts to the south from the fractured cumulate gabbros to the north (Fig. 2.4 [6]).

Approximately 350 m to the north, both sides of a major east-west valley contain scattered exposures of cohesive fault breccia (Fig. 2.4 [7]). One outcrop displays thrust and normal sense kinematics. At the northern boundary of the gabbros, a cohesive fault breccia striking 300^{o} and dipping 32^{o} to the southwest marks a shallow dipping fault thrusting the gabbros north over serpentinite (Fig. 2.4 stereonet 2). Thrust sense was determined by fault-dragged foliation in the serpentinites above the fault zone. The thrust

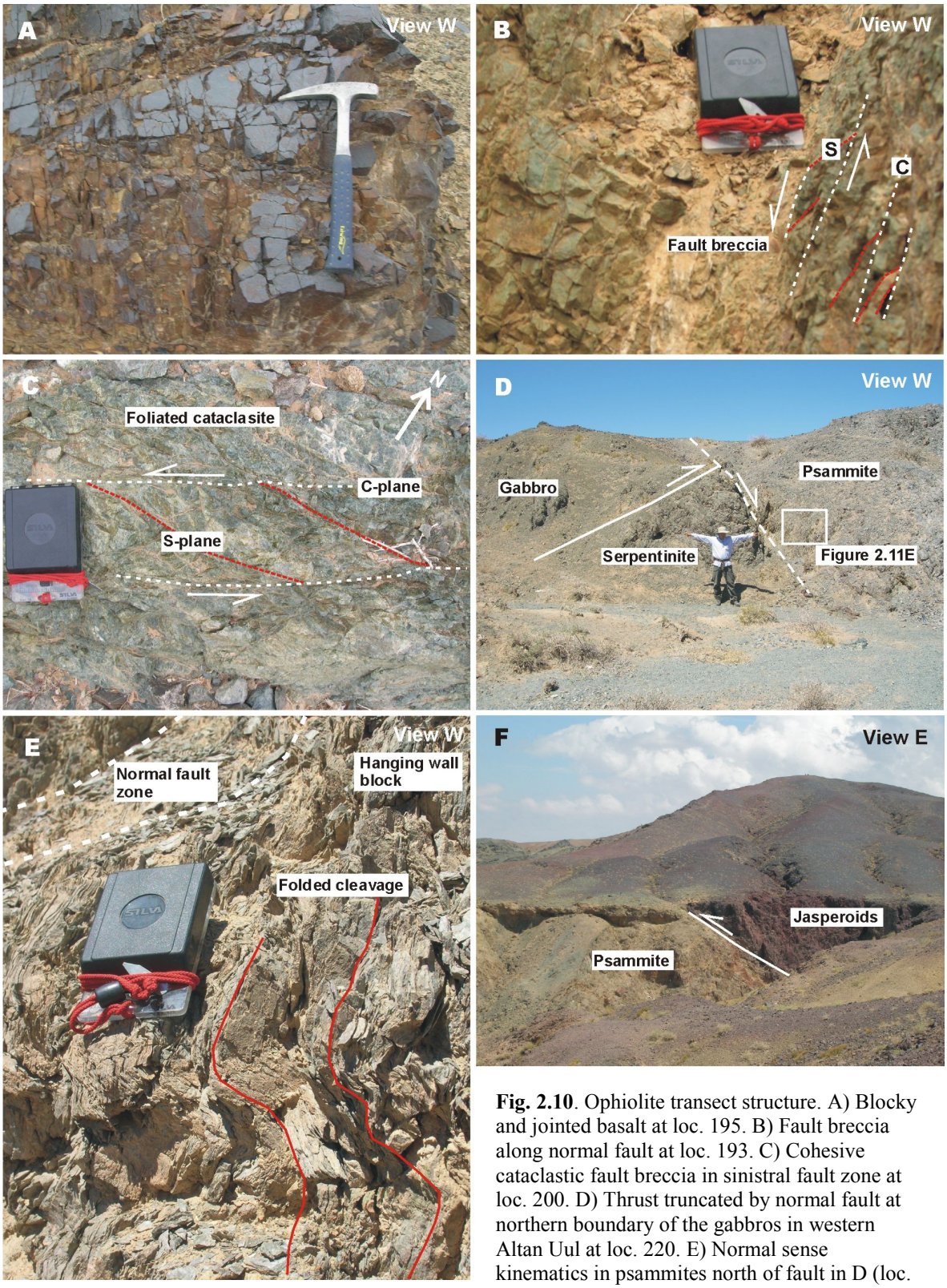

Fig. 2.10. Ophiolite transect structure. A) Blocky and jointed basalt at loc. 195. B) Fault breccia along normal fault at loc. 193. C) Cohesive cataclastic fault breccia in sinistral fault zone at loc. 200. D) Thrust truncated by normal fault at northern boundary of the gabbros in western Altan Uul at loc. 220. E) Normal sense kinematics in psammites north of fault in D (loc. 220). F) Jasperoids thrust north over psammites to the east of the West Altan Uul transect.

fault is truncated by a 1-2 m wide steep northwest-southeast trending canyon (Fig. 2.10D; Fig. 2.4 [8]). Small <1 m scale folds of cleavage in meta-psammites on the north side of the canyon, are localised adjacent to the fault zone suggesting they have been formed by fault drag (Fig. 2.10E). This suggests that the canyon may mark a normal fault, trending c.105^{o} and dipping c.75^{o} to the north, downthrowing the meta-psammites to the north.

The meta-psammites outcrop in a c.450 m wide east-west trending valley. To the north of the valley, a 10 m wide ductile shear zone striking 280^{o} and dipping 52^{o} to the southwest, marks the northern boundary of the psammites (Fig. 2.4 [9], stereonet 3). Fault -dragged foliation in the shear zone suggests the fault is a thrust. Immediately to the north, jasperoids in a c.500 m wide east-west belt are bedded and folded into moderate-tight north-vergent folds. In the transect location, scree and Quaternary alluvial fans onlap the jasperoids (Fig. 2.4 [10]), obscuring the structure at the mountain front. To the east, a normal fault dipping 20-40^{o} to the northwest marks the front of the range and the northern boundary of the Southwest Altan Ophiolite sequence (Fig. 2.4 [11]). Further to the east, a moderate south-dipping brittle thrust fault carries the jasperoids north over meta-psammites (Fig. 2.4 [12]), which crop out along the mountain front (Fig. 2.10F).

The proximity of the basalts and gabbros in the area suggests they probably underwent a similar set of initial prograde metamorphic reactions. The mineral assemblages outlined above are consistent with greenschist to epidote amphibolite facies metamorphism which may have occurred in an ocean-floor setting or during regional metamorphism (Manning et al. 1996, Nicolas & Mainprice 2005). The metamorphic reactions, setting and P-T conditions of peak metamorphism are discussed in more detail in section 2.9.1. The psammites to the north of the gabbros have a chlorite-muscovite-epidote-albite assemblage, typical of greenschist grade metamorphism (Deer et al. 1966).

2.5 West Nemegt Uul/East Altan Uul Transect

The West Nemegt Uul/East Altan Uul transect (Fig. 2.11) starts in at the south front of Altan Uul. To the north, there is a small gap in the transect between southern Altan Uul and northern Altan Uul (Fig. 2.11 [1]), where access was not possible during the study. The Cretaceous-Cenozoic sediments in the basin north of Altan Uul (Fig. 2.11 [2]) were not investigated. The transect continues to the northeast across a narrow ridge in western Nemegt Uul (Fig. 2.11 [3]). Again, the Cretaceous-Cenozoic sediments in the

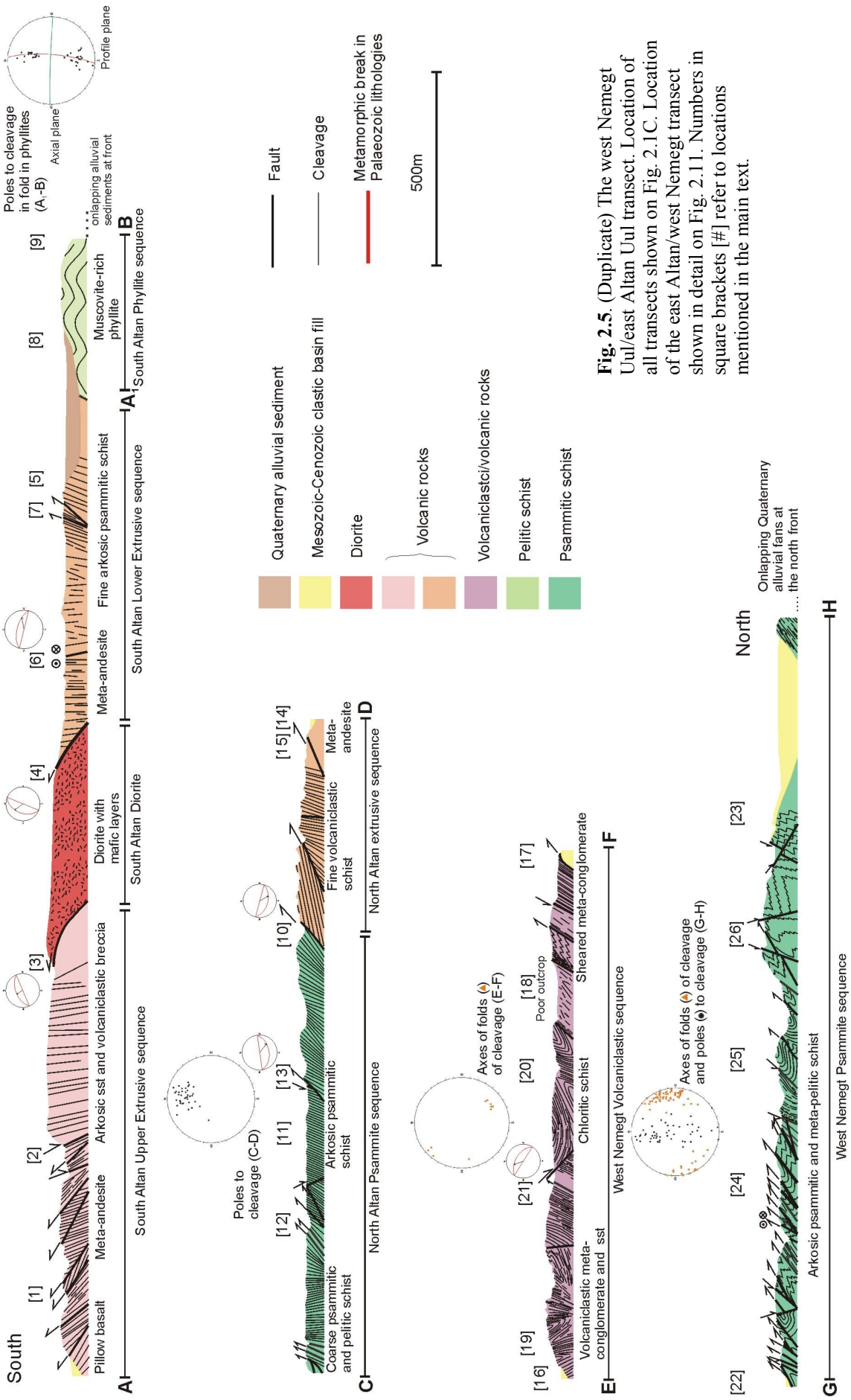

Fig. 2.5. (Duplicate) The west Nemegt Uul/east Altan Uul transect. Location of all transects shown on Fig. 2.1C. Location of the east Altan/west Nemegt transect shown in detail on Fig. 2.11. Numbers in square brackets [#] refer to locations mentioned in the main text.

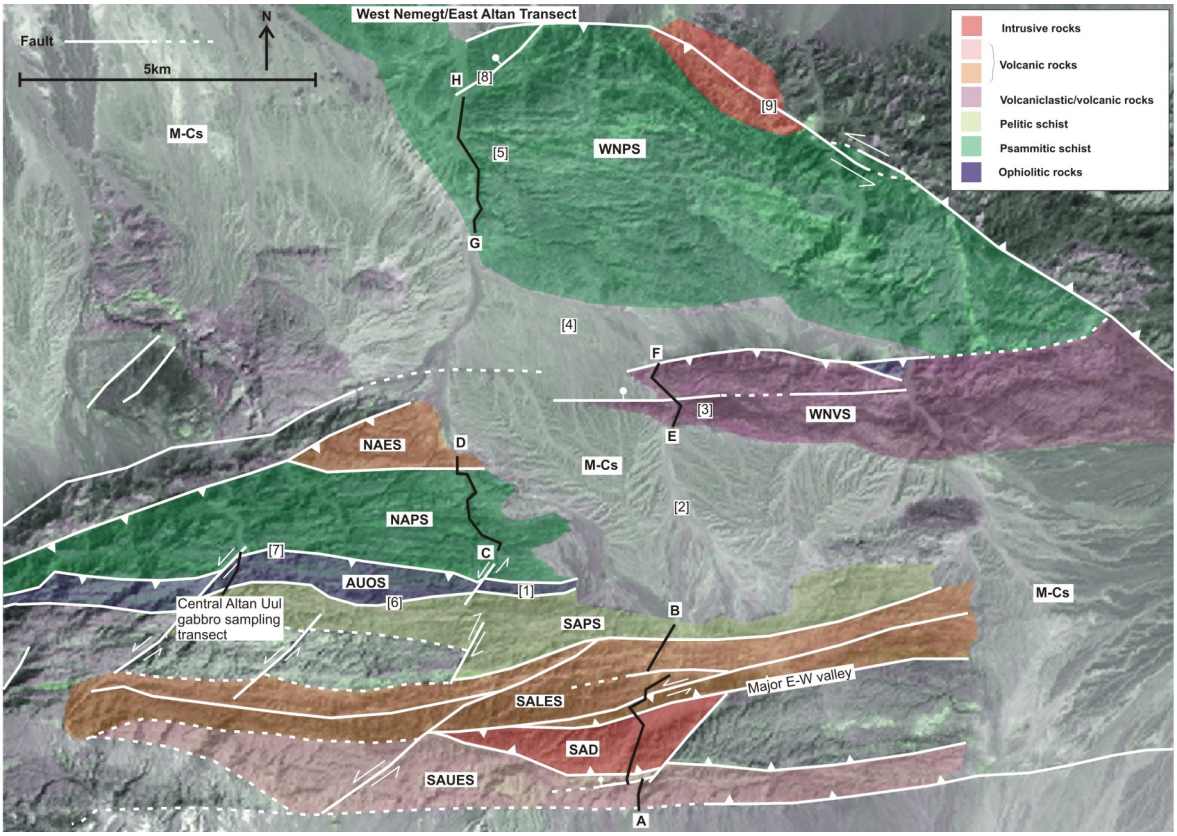

Fig. 2.11. Western Nemegt Uul transect location map with litho-tectonic sequences. Numbers in square brackets [#] refer to locations mentioned in the main text. SAUES = South Altan Upper Extrusive sequence. SAD = South Altan Diorite. SALES = South Altan Lower Extrusive sequence. AUOS = Altan Uul Ophiolite sequence. NAPS = North Altan Psammite sequence. NAES = North Altan Extrusive sequence. WNVS = West Nemegt Volcaniclastic sequence. WNPS = West Nemegt Psammite sequence. M-Cs = Mesozoic-Cenozoic sediments.

basin (Fig. 2.11 [4]) between the West Nemegt Volcaniclastic sequence and the West Nemegt Psammite sequence were not investigated. The transect continues and ends to the northwest in westernmost Nemegt Uul (Fig. 2.11 [5]), where Palaeozoic rocks are onlapped by Cretaceous and Quaternary cover.

2.5.1 The South Altan Upper Extrusive sequence

The South Altan Upper Extrusive sequence is a mixed assemblage of extrusive volcanic rocks and arkosic and volcaniclastic sedimentary rocks cropping out in southern Altan Uul (Fig. 2.11). Quaternary alluvial fan sediments onlap meta-basalts on the southern front of Altan Uul in the transect area. To the east, the meta-basalts are thrust south over Cretaceous basin sediments. In the north, the South Altan Upper Extrusive sequence is overthrust by the South Altan Diorite.

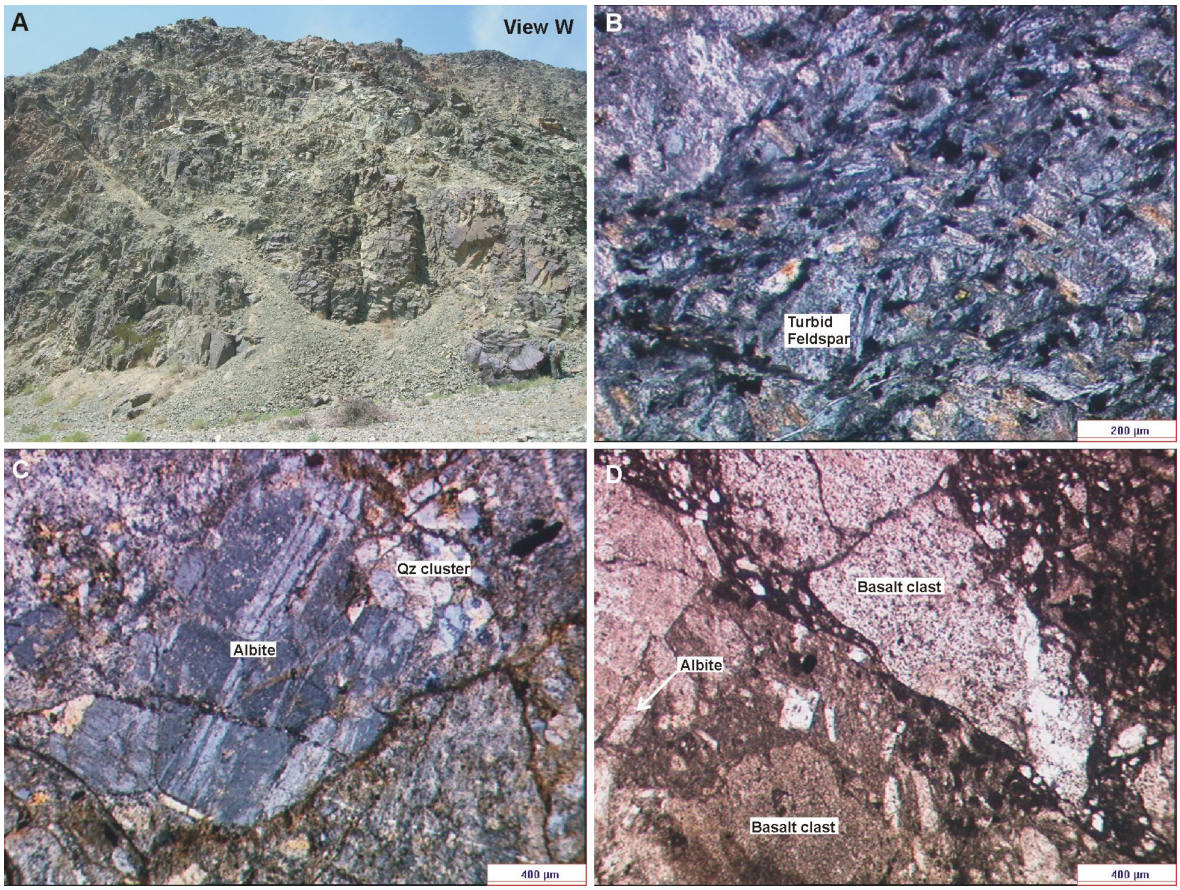

Fig. 2.12. South Altan Upper Extrusive sequence lithologies. A) Blocky basalt at loc. 240. B) Turbid interlocking feldspars in andesite at loc. 241. C) Albite and quartz in arkosic sandstone layer at loc. 248. D) Angular andesite clasts with interlocking feldspar crystals in volcaniclastic breccias at loc. 249.

Lithologies and petrography

Meta-basalts (Fig. 2.12A) form block outcrop in a c.470 m wide east-west trending belt of deeply incised valleys at the southern front of Altan Uul (Fig. 2.5 [1]), and is the southernmost unit in the South Altan Extrusive sequence. To the north, volcaniclastic sandstones crop out in a 200-300 m wide east-west belt forming a major topographic escarpment (Fig. 2.5 [2]), consisting of interbedded layers of flaggy arkosic sandstone and blocky volcaniclastic breccia.

The meta-basalts consist of small (0.2-0.5 mm) interlocking subhedral epidote-altered feldspar crystals (80-90 %; Fig. 2.12B), and small (0.1-0.2 mm) anhedral opaque minerals (5-10 %). Small amounts of chlorite (c. 5 %) surround and fill fractures in the albite.

The arkosic sandstones consist of 0.5-3 mm sub-rounded albite crystals (10-15 %)

in a clast-supported matrix of 0.1-0.25 mm rounded saussuritised feldspar grains (60-70 %) and 0.2 mm anhedral quartz grains (10-15 %; Fig. 2.12C). Small (0.1 mm) opaque mineral grains (c. 5 %) are scattered throughout the sandstones. The volcaniclastic breccia contains 1-3 mm subrounded and brecciated clasts of basalt (20-50 %; Fig. 2.12D). The clasts are surrounded by a very fine matrix of <0.001 mm recrystallised quartz grains (40 %) with occasional small (0.15 mm) subhedral albite crystals (c.5 %). Small (0.01 %) epidote grains (c.5 %) are scattered throughout the quartz matrix.

Structure and Metamorphism

The volcaniclastic sandstones and localised areas of the meta-basalts have a strong moderate to steep north dipping spaced cleavage (Fig. 2.13A), distinguishing the sequence from the rocks immediately to the north. In the meta-basalt, cleavage is localised around high strain zones associated with faults.

The meta-basalts at the south front of Altan Uul contain some layers with pillow structures (Fig. 2.13B), persisting for c. 50 m into the range from the mountain front. The meta-basalts are cut by several c. 20 cm wide brittle fault zones striking 085-112^{o} and dipping 35-52^{o} to the northeast, all containing cohesive fault breccia (Fig. 2.13C). Thrust sense movement was determined from fault-dragged foliation cut by the fault zones.

Moving north, fault zones become less obvious. However, north dipping shear planes striking 074^{o} and dipping 23^{o} to the northwest cut obliquely across cleavage striking 100^{o} and dipping 66^{o} to the northeast. The cleavage is dragged by the shear planes, giving an approximately south-directed thrust sense of movement (Fig. 2.13D). Approximately 100 m to the north, there is a major east-west valley marking the base of a major topographic escarpment (Fig. 2.5 [2]). Outcrop in the valley is poor, but a steep north-dipping fault zone can be seen along-strike to the east (Fig. 2.13E). Slickenlines plunging 58^{o} towards 009^{o} on fault parallel surfaces striking 097^{o} and dip 60^{o} to the northeast in the valley indicate the faults movement was dip-slip (Fig. 2.13F). Exposure is poor on the major escarpment north of the valley. At the top of the escarpment, exposures are dominated by the volcaniclastic sandstone unit, consisting of flaggy and cleaved arkosic sandstone with occasional interbedded layers of blocky volcaniclastic breccia. Approximately 400 m from the top of the escarpment, a steepening north dipping fault thrusts the South Altan Diorite to the south, marking the end of outcrop of the South

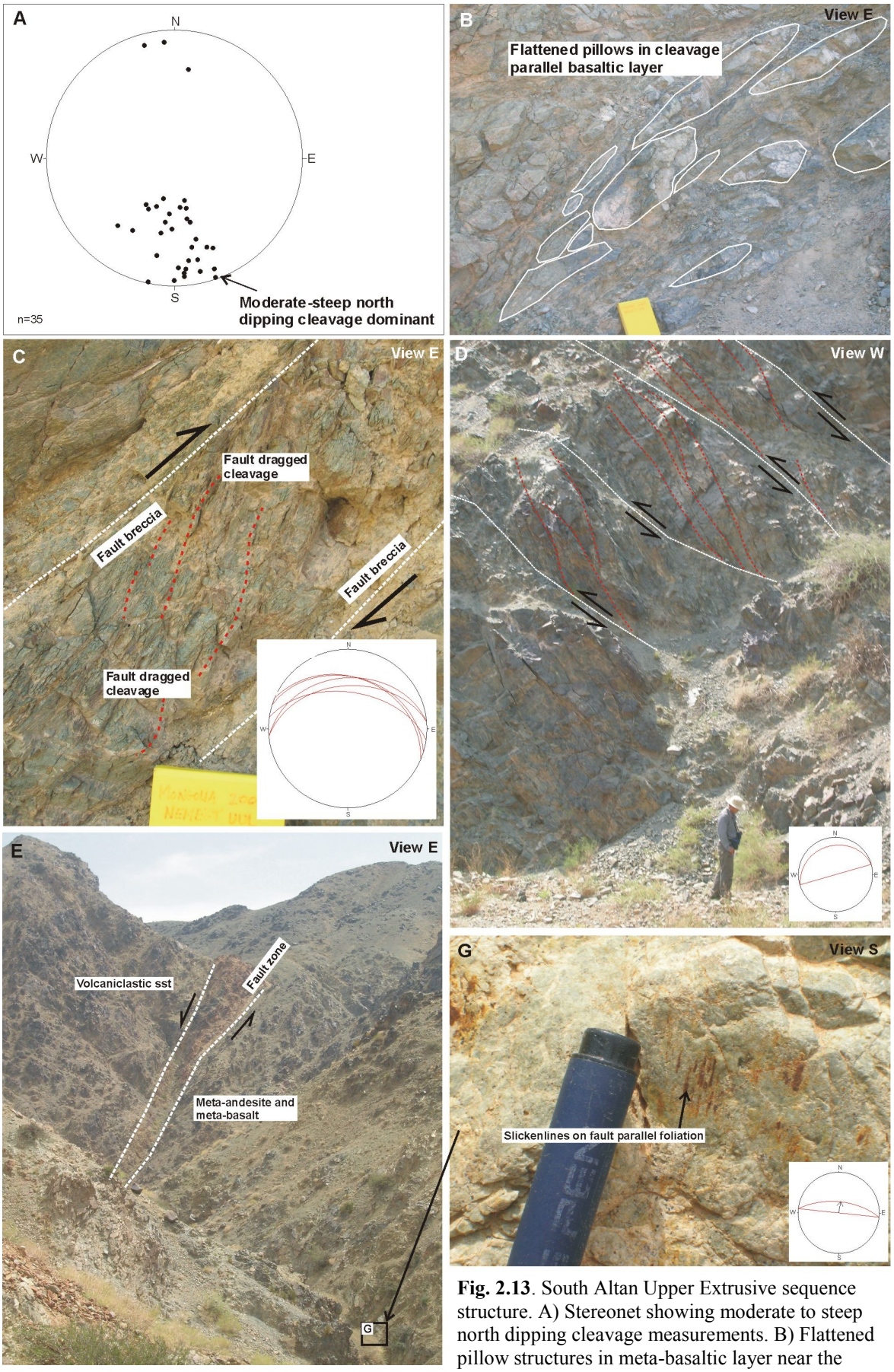

Fig. 2.13. South Altan Upper Extrusive sequence structure. A) Stereonet showing moderate to steep north dipping cleavage measurements. B) Flattened pillow structures in meta-basaltic layer near the southern front of Altan Uul (loc. 239). C) Fault breccia in typical south-vergent (continued…)

(continued from previous page) thrust fault and stereonet showing thrust fault orientations (loc. 239). D) Parallel shear zones with south-vergent thrust sense kinematics with stereonet showing typical shear zone geometry at loc. 242. E) Large normal fault zone marking a metamorphic break from greenschist grade meta-basalts to unmetamorphosed volcaniclastic and arkosic sediments at loc. 244. G) Slickenlines from outcrop in the E-W valley along strike from the large normal fault in F (loc. 244).

Altan Upper Extrusive sequence along the transect Fig. 2.5 [3]).

There is an obvious metamorphic break in the South Altan Upper Extrusive sequence. In the meta-basalts the presence of epidote altered albite surrounded by chlorite suggests greenschist metamorphism (Bucher & Frey 1994). North of the major escarpment, the volcaniclastic breccias and arkosic sandstones contain saussuritised feldspar and are brecciated and fractured in places, suggesting they may have been subjected to hydrothermal alteration. However, there is no evidence they have been regionally metamorphosed to the same degree as the meta-basalts to the south. This metamorphic break coincides with a large fault (Fig. 2.5 [2]). The sense of movement on the fault was not clear in the field. However, the hanging wall of the fault consists of volcaniclastic sandstones with little or no evidence of regional metamorphism compared to the footwall where greenschist grade meta-basalts suggest the fault has moved in a normal sense.

2.5.2 The South Altan Diorite

The South Altan Diorite crops out in a wide (c.500 m) E-W trending fault-bound belt (Fig. 2.11). In the south, it is thrust south over the South Altan Upper Extrusive sequence. In the north, it is overthrust by the South Altan Lower Extrusive sequence.

Lithology and petrography

The South Altan Diorite crops out to form part of an east-west trending ridge through southern Altan Uul. Outcrop is generally blocky, and the composition is generally homogenous. In places, there are near vertical dipping mafic layers within the diorite. It consists of 1-3 mm interlocking euhedral albitised plagioclase crystals (35-40 %), often partially broken down to epidote, and 1 mm subhedral augite crystals (c.5 %) with actinolite rims. Chlorite (20-30 %) forms rims and fills fractures in albite and augite. Small 0.005-1 mm quartz grains (5 %) are scattered throughout the diorite. Hornblende (20-35 %) can be seen overgrowing all the mineral phases (Fig. 2.14A).

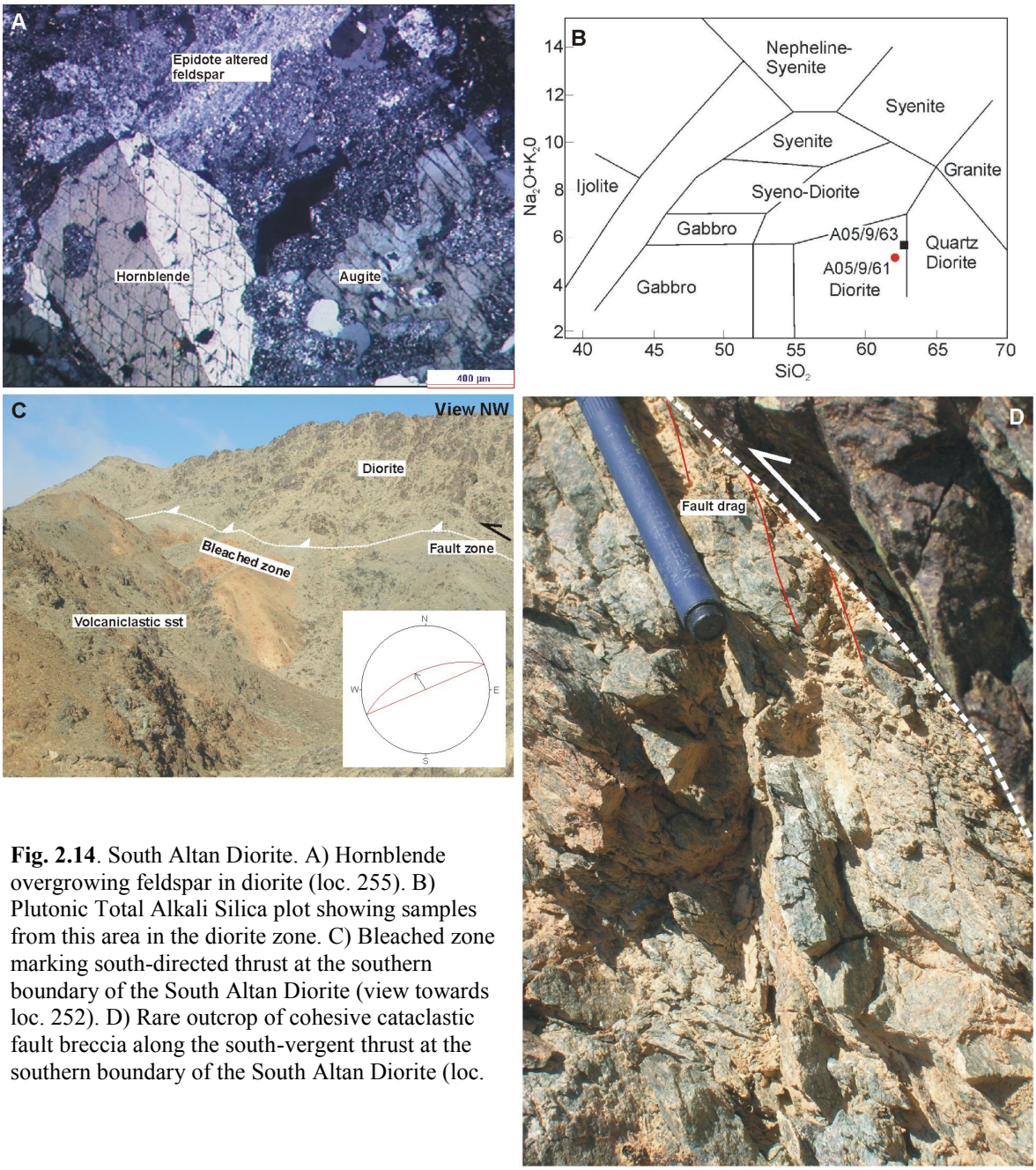

Fig. 2.14. South Altan Diorite. A) Hornblende overgrowing feldspar in diorite (loc. 255). B) Plutonic Total Alkali Silica plot showing samples from this area in the diorite zone. C) Bleached zone marking south-directed thrust at the southern boundary of the South Altan Diorite (view towards loc. 252). D) Rare outcrop of cohesive cataclastic fault breccia along the south-vergent thrust at the southern boundary of the South Altan Diorite (loc.

Petrology of the diorite

In the field, the diorite looks similar to the cumulate gabbros seen in western Altan Uul (section 2.4.1; 2.9.1). Samples were taken to compare the South Altan Diorite with gabbros in western Altan Uul. Two Samples of diorite were prepared for analysis using standard x-ray fluorescence spectroscopy (XRF) techniques at the University of Leicester, UK (Tarney & Marsh 1991). The samples were taken from the least visibly altered outcrops along the western transect. The samples plot in the diorite field of a plutonic

total-alkali silica (TAS) diagram (Fig. 2.14B), which is consistent with hand specimen and petrographic characteristics of these rocks.

Structure and metamorphism

A 10-20 m wide bleached zone marks the southern boundary of the Southern Altan Diorite (Fig. 2.14C; Fig. 2.5 [3]). Most of the fault plane is buried by scree, but where exposed it consists of a 1m wide zone of foliated cataclasite striking 067^{o} and dipping 66^{o} to the northwest. Slickenlines on foliation within the fault zone plunge 46^{o} towards 328^{o} (Fig. 2.14C). Fault-dragged foliation within the fault zone suggests the fault has moved in a thrust sense (Fig. 2.14D). The diorite is fractured in all orientations, but otherwise appears undeformed.

The mineralogy of the South Altan Diorite is uniform, implying a uniform metamorphic grade. The presence of epidote altered albite surrounded by chlorite is indicative of greenschist grade metamorphism. The presence of hornblende overgrowing all other mineral phases, and chlorite in the diorite suggests the transition from greenschist to amphibolite grade metamorphism was reached (Bucher & Frey 1994, Moody et al. 1983).

2.5.3 The South Altan Lower Extrusive sequence

The South Altan Lower Extrusive sequence is an assemblage of extrusive meta-volcanic rocks and greenschist meta-sedimentary rocks (Fig. 2.11). The sequence is divided into two units; meta-andesite and meta-psammitic schist. It is thrust south over the South Altan Diorite (Fig. 2.5 [4]). To the north, it is onlapped by Quaternary alluvial sediments (Fig. 2.5 [5]).

Lithologies and petrography

The meta-andesite crops out in a c. 200 m wide northeast-southwest trending belt in southern Altan Uul. It is fairly blocky in outcrop. Directly to the north, the psammitic schist crops out in a c. 200 m wide northeast-southwest trending belt, widening to c.400 m to the west.

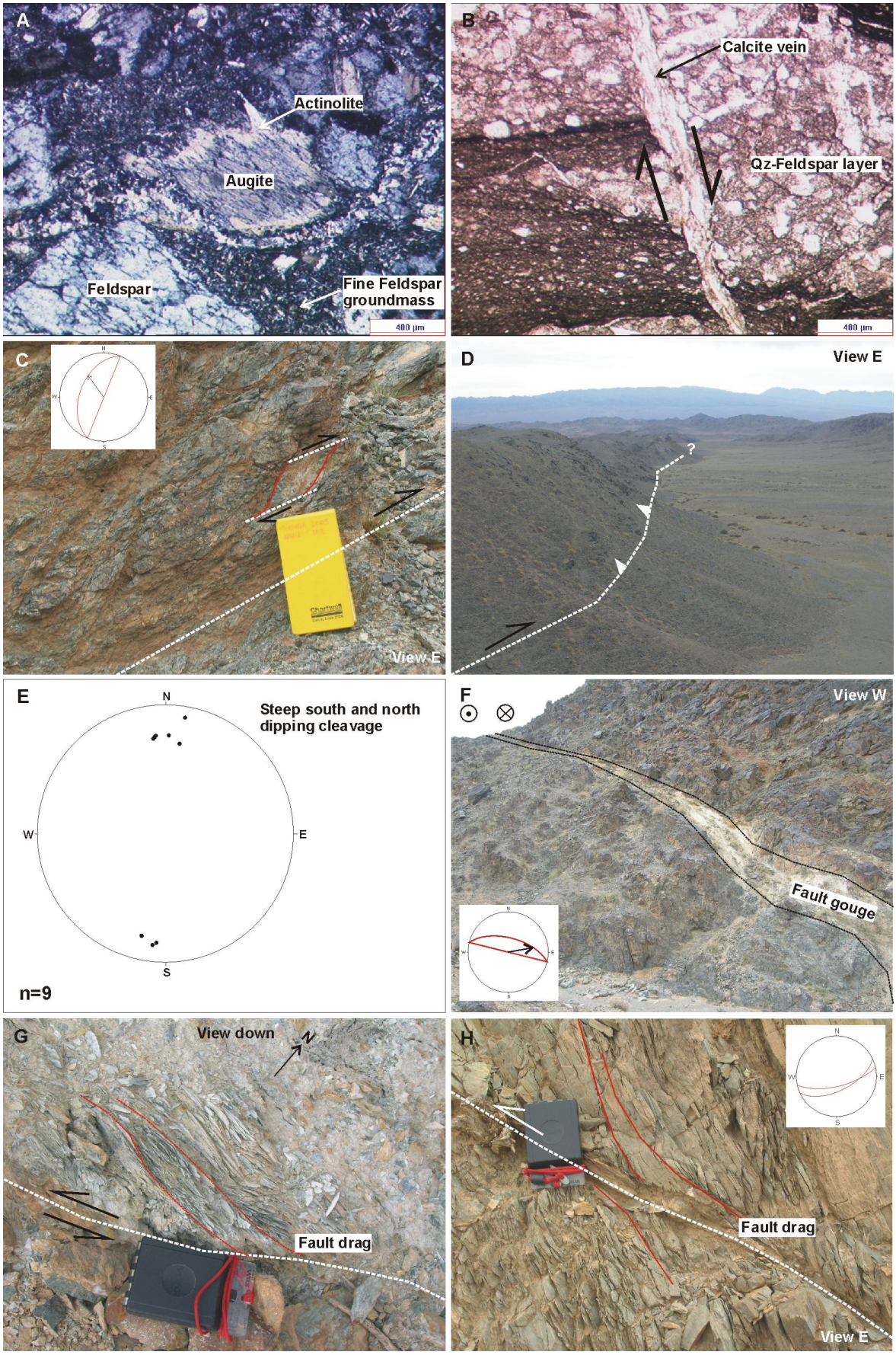

Fig. 2.15. Photos and photomicrographs showing the major lithologies and structures of the South Altan Lower Extrusive sequence. A) Actinolite rim about augite crystal in meta-andesite (loc. 259). B) Calcite-filled fracture offsetting quartz-feldspar layer in psammitic schist (loc. 259). (continued...)

(...continued from previous page) C) Cohesive cataclastic fault breccia in thrust zone at southern boundary of the South Altan Lower Extrusive Group (loc. 258). D) Thrust-fault bound major E-W valley east of loc. 258 (see Fig. 2.11). E) Stereonet showing scarce steep south and north dipping cleavage measurements. F) Sinistral oblique-thrust fault between meta-andesites and meta-psammitic schists (loc. 260). G) Sinistral thrust sense kinematic indicators in sinistral oblique-thrust fault (loc. 260). H) North-directed brittle thrust fault with fault drag kinematic indicators (loc. 261). Stereonet shows orientation of the north-directed reverse faults cutting this part of the sequence.

The meta-andesite consists of 1-3 mm subhedral feldspar crystals (15-20 %) often partially altered to epidote, and 1 mm anhedral augite crystals (10 %), which often have actinolite rims (Fig. 2.15A), in a matrix of 0.5 mm interlocking feldspar laths (30-50 %). Chlorite surrounds some augite and surrounds and fills fractures in some of the feldspars. Small (0.01 mm) recrystallised quartz grains (5-10 %) are scattered throughout the meta-andesites. Epidote alteration of the feldspars makes it difficult to determine their anorthite content. However, relict albite twinning can be made out in approximately 80 % of feldspar crystals in the rock.

The meta-psammitic schist is compositionally layered, with layers consisting of small 0.1-0.2 mm rounded albite grains (10-30 %) with occasional 0.01 mm recrystallised quartz grains, alternating with layers of recrystallised quartz (60-80 %). Muscovite (c. 5 %) and chlorite (c. 5 %) form the cleavage. Quartz and calcite veins cut everything at a high angle to the cleavage (Fig. 2.15B).

Structure and metamorphism

In the south, between the South Altan Lower Extrusive sequence and the South Altan Diorite (Fig. 2.5 [4]), there is a 2 m wide bleached white fault zone striking 022^{o} and dipping 44^{o} to the northwest. Slickenlines on the fault plunge 41^{o} towards 321^{o} (Fig. 2.15C). The fault consists of foliated cataclasite and smaller cm-scale zones of friable cataclasite. Fault-dragged foliation within the fault zone suggests it moved in a southeast-directed thrust sense (Fig. 2.15C). To the east, the fault bounds a major northeast-southwest trending valley (Fig. 2.15D).

There is a moderate-steep south to north dipping cleavage in the area (Fig. 2.15E), which is most dominant in the psammitic schist. The meta-andesite in the south of the area is heavily jointed in all directions, giving the outcrop a blocky appearance.

Moving north, the boundary between the meta-andesites and the psammitic schists is marked by a 10 m wide zone of intense fracturing (Fig. 2.15F) and friable fault breccia

(Fig. 2.15G; Fig. 2.5 [6]) striking 105^{o} and dipping 62^{o} to the northeast. Slickenlines on the footwall plunge 38^{o} towards 080^{o} (Fig. 2.15F). The central 2 m of the fault zone consists of foliated cataclasite and gouge. Fault-dragged foliation on the edge of the cataclasite zone suggests the fault zone moved in a left-lateral oblique-slip sense with an element of southwest-directed thrust movement. The psammitic schists north of the left-lateral strike-slip fault are cut by two c.20 cm wide brittle faults striking 245-257^{o} and dipping 60-70^{o} (Fig. 2.15H; Fig. 2.5 [7]). Fault-dragged foliation is cut by these faults and suggests they moved with a north-directed thrust sense.

In the meta-andesites, the presence of epidote altered albite surrounded by chlorite, and augite surrounded by actinolite rims, is indicative of greenschist grade metamorphism (Bucher & Frey 1994). In the psammitic schist, the albite, quartz, chlorite, muscovite assemblage suggests the rocks were metamorphosed in the chlorite zone of the greenschist facies (Bucher & Frey 1994).

2.5.4 The South Altan Phyllite sequence

The South Altan Phyllite sequence is a c. 1500 m wide northeast-southwest trending belt of interbedded phyllites and meta-pelites (Fig. 2.11). At its southern boundary, the South Altan Phyllite sequence is onlapped by Quaternary alluvial sediments (Fig. 2.5 [8]). In the north of the transect area, the sequence is onlapped by Cretaceous-Cenozoic basin sediments and Quaternary alluvial sediments (Fig. 2.5 [9]). To the west the phyllites are separated from ophiolitic rocks in central Altan Uul by a shear zone of unknown slip sense (Fig. 2.11 [6]).

Lithologies

The phyllites and meta-pelites of the South Altan Phyllite sequence are weathered and friable in outcrop. They were not sampled, but field observations were made. They consist of fine grained quartz. Muscovite and chlorite are clearly visible and likely form the cleavage. Large (1 cm) euhedral pyrite crystals have grown across the cleavage planes in outcrop (Fig. 2.16A)

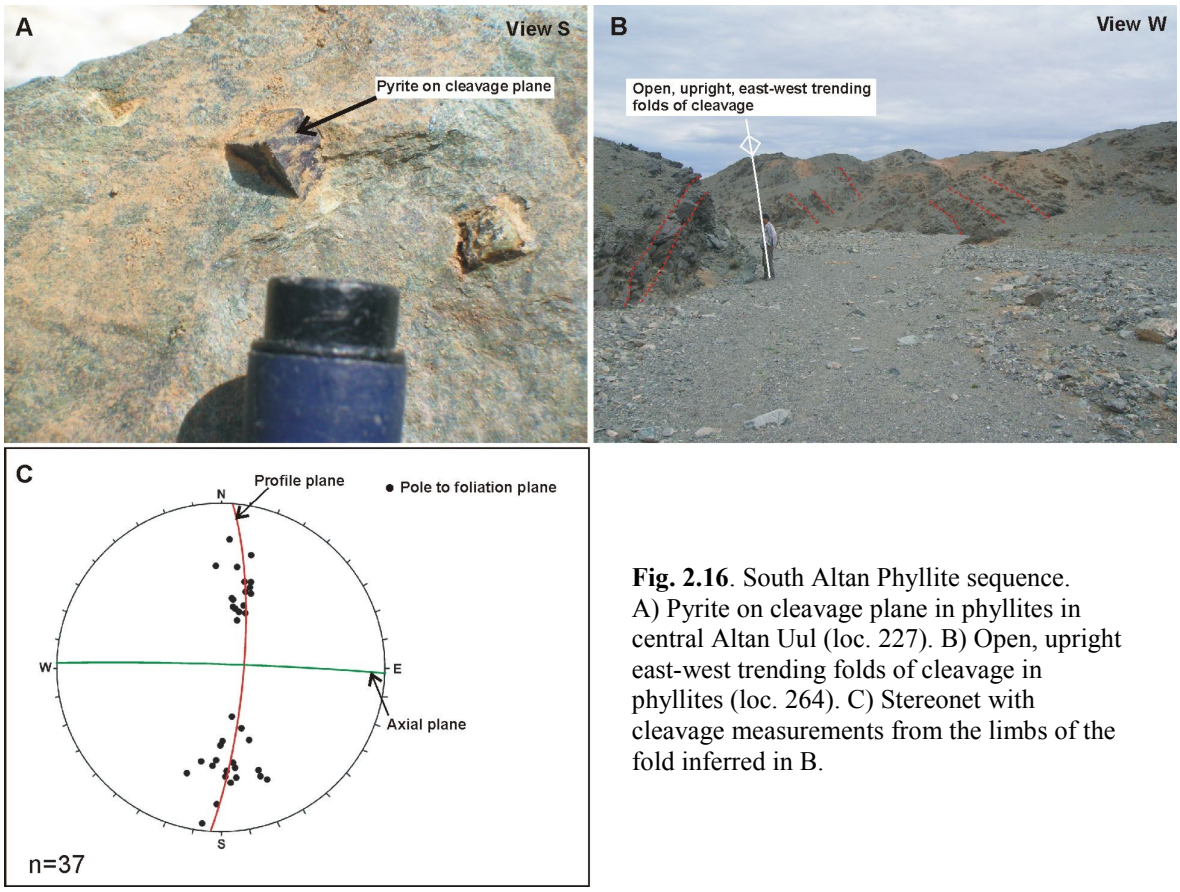

Fig. 2.16. South Altan Phyllite sequence. A) Pyrite on cleavage plane in phyllites in central Altan Uul (loc. 227). B) Open, upright east-west trending folds of cleavage in phyllites (loc. 264). C) Stereonet with cleavage measurements from the limbs of the fold inferred in B.

Structure and metamorphism

The phyllites and meta-pelites are commonly intensely deformed by a pervasive cleavage, which has been folded into upright E-W trending open folds, in clear contrast to the areas surrounding it to the north and south (Fig. 2.16B-C).

Along strike in central Altan Uul (Fig. 2.11 [6]), a c. 20 cm wide ductile shear zone striking 250^{o} and dipping 60^{o} to the south separates phyllites to the south from gabbros in the Altan Uul ophiolite sequence to the north. Kinematic indicators could not be identified.

The mineral composition of the South Altan Phyllite sequence is constant from its southern to its northern boundary. The assemblage of quartz, muscovite and chlorite suggest the rocks were metamorphosed in the chlorite zone of the greenschist facies (Bucher & Frey 1994).

2.5.5 The North Altan Psammite sequence

The North Altan Psammite sequence is an assemblage of interbedded greenschist grade metamorphosed arkosic meta-psammite, meta-pelite and limestone cropping out in a c.1300 m east-west trending belt in northern Altan Uul (Fig. 2.11). It was not possible to reach the southern boundary of the sequence in the transect location. However, to the west of the transect area, it is overthrust by gabbro and serpentinite (Fig. 2.11 [7]). In the north, a 10 cm wide shallow dipping north-directed thrust fault marks the northern extent of the North Altan Psammite sequence and has carried it north over the North Altan Extrusive sequence (Fig. 2.5 [10]).

Lithologies and petrography

The meta-psammites are flaggy, but meta-pelitic layers within the meta-psammites are particularly flaggy and friable. Limestone forms a small part of the North Altan Psammitic sequence. It is interbedded with psammite in the north of the area (Fig. 2.5 [11]).

The arkosic meta-psammites and meta-pelites consist of 0.1-0.6 mm rounded grains of albitised plagioclase feldspar (from 10 % in the meta-pelites to 55 % in the arkosic meta-psammites), often partially altered to epidote (15-20 %) and chlorite (5-10 %), and 0.05 mm rounded grains of quartz (10-25 %). Quartz is also recrystallised into bands defining the cleavage. Kinematic indicators are often visible in thin section where cleavage-forming muscovite (10-20 %) and chlorite wrap around feldspar and quartz porphyroclasts. Small (0.05 mm) calcite veins cut everything at a high angle to the cleavage (Fig. 2.17A).

The limestones consist of small accumulations of very small (0.05-0.2 mm) quartz (5 %) and albitised feldspar grains (5 %), in a matrix of layered calcite (90 %). Very thin layers of unidentified mica (5 %) form a cleavage and are seen wrapping around quartz and albite grains forming distinctive δ-type tails (Fig. 2.17B).

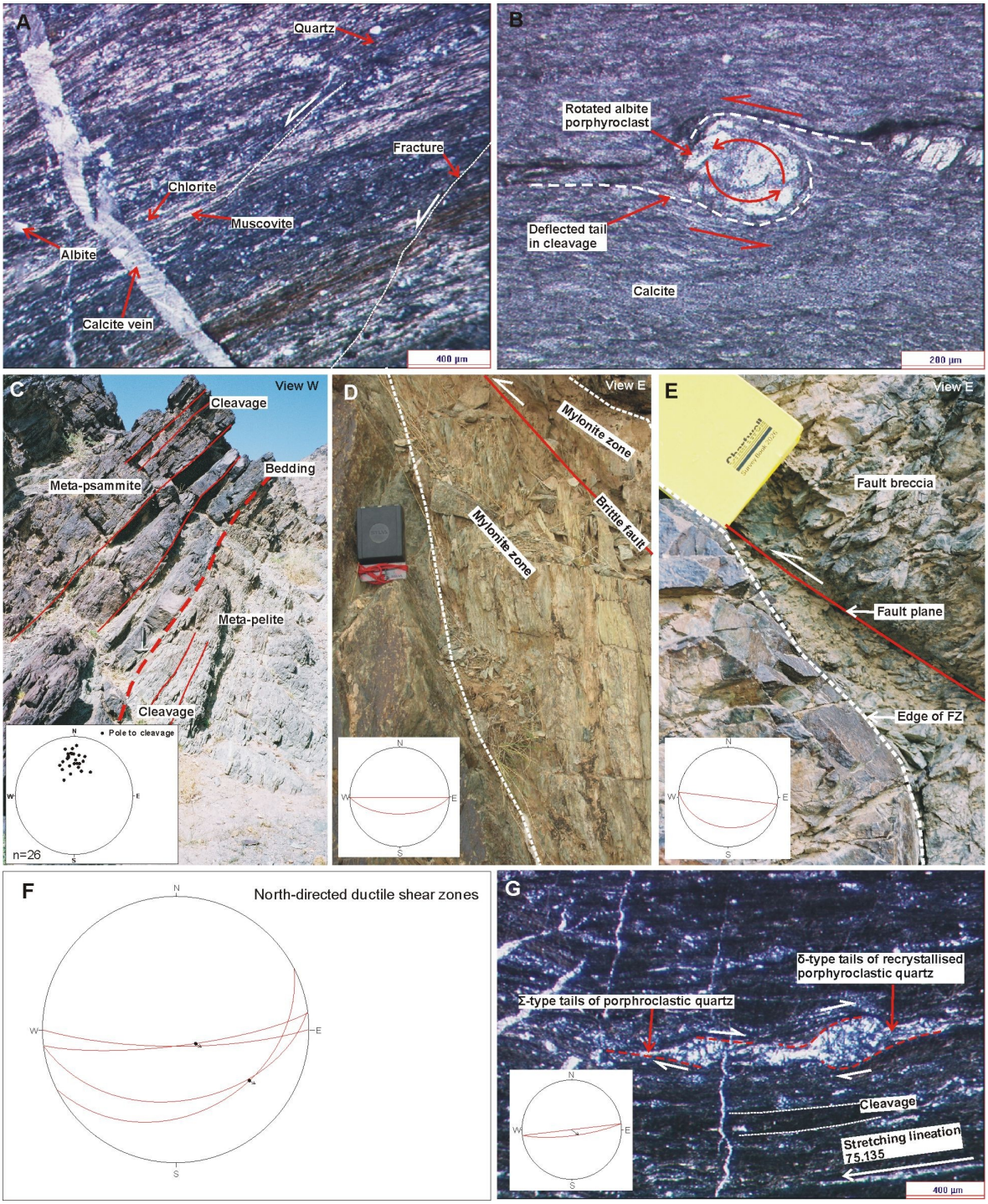

Fig. 2.17. Photos and photomicrographs to show main lithologies and structure of the North Altan Psammite sequence. A) Meta-pelite with chlorite and muscovite forming a cleavage around quartz and albite grains (loc. 57). Quartz is recrystallised into bands which also define the cleavage.
B) Rotated albite porphyroclast in meta-pelite (loc. 55). C) Moderately steep south-dipping cleavage, parallel to bedding. (loc. 62). D) Mylonitic zone and brittle fault plane carrying ophiolitic rocks north over meta-psammite west of the transect area (loc. 237). E) Incohesive fault breccia in thrust zone (loc. 64). F) Stereonet showing orientations and slip vectors for north-directed thrust faults in the area. G) σ- and δ-type tails give northwest-directed thrust sense in meta-pelites (loc. 57).

Structure and metamorphism

The North Altan Psammite sequence is characterised by a pervasive moderate-steep south-dipping cleavage (Fig. 2.17C). Cleavage is parallel to bedding throughout the area.

At the southern boundary of the sequence, to the west of the transect area, a steep south-dipping fault, marked by a 5 m wide zone of mylonite that strikes 270^{o} and dips 62^{o} to the south, carries gabbro and serpentinite north over meta-psammite (Fig. 2.11 [7]). Mineral stretching lineations were not seen, but fault-dragged foliation in the shear zone suggests there was north-directed thrust movement. A single brittle fault plane cuts through the centre of the mylonite zone, parallel to the margins (Fig. 2.17D).

In the transect area, c. 500 m north of the southern boundary of the North Altan Psammite sequence, several brittle thrust faults striking 276^{o} and dipping 39^{o} to the southwest cut meta-psammite (Fig. 2.5 [12]). The faults are marked by 5-10 cm wide zones of incohesive fault breccia (Fig. 2.17E). Quartz veins offset across these faults suggest there has been 10-30 cm of north-directed thrust displacement on each fault. Similar shallow, 10-50 cm north-directed thrust faults are typical throughout the North Altan Psammite sequence.

To the north, localised cleavage intensity increases in finer grained meta-pelitic layers, and in c.5 m wide ductile shear zones striking 243-270^{o} and dipping 80-36^{o} to the south (Fig. 2.17F). Mineral stretching lineations along a ductile shear zone that strikes 263^{o} and dips 80^{o} to the southeast, plunge 75^{o} towards 126^{o}. The ductile shear zones are often heavily weathered and friable, making it difficult to find kinematic indicators. However, recrystallised porphyroclastic quartz tails seen in thin section (Fig. 2.17G) and fault-dragged foliation within the shear zones suggest they underwent north to northwest-directed thrust sense slip. Throughout the area, steep south dipping cleavage is cut by shallow shear planes. Fault-dragged foliation cut by some of these shear planes suggests north-directed thrusting occurred throughout the area.

Approximately 400 m from the northern boundary of the sequence, a 10 cm wide mylonitic fault zone in a cliff face is truncated by a brittle fault plane that strikes 262^{o} and dips 45^{o} to the southeast, with slickenlines that plunge 34^{o} towards 125^{o}. (Fig. 2.5 [13]). The mylonite zone could not be accessed so mineral stretching lineations were not seen.

However, fault-dragged cleavage within and around the mylonite zone suggests the fault moved in a normal sense. Fault-dragged cleavage cut by the brittle fault suggests it moved in a northwest-directed thrust sense.

At the northern boundary of the sequence, a brittle fault plane striking 285^{o} and dipping 50^{o} to the southwest with slickenlines plunging 40^{o} towards 150^{o} cuts cleaved psammitic schist (Fig. 2.5 [10]). Fault-dragged cleavage on both sides of the fault suggest it moved in a northwest-directed thrust sense.

There is little variation in the mineralogy in the meta-psammites and meta-pelites in the North Altan Psammite sequence. The assemblage of albite, quartz, and muscovite and chlorite suggests the rocks were metamorphosed in the chlorite zone of the greenschist facies (Bucher & Frey 1994).

2.5.6 The North Altan Extrusive sequence

The North Altan Extrusive sequence is an assemblage of volcaniclastic rocks and extrusive meta-volcanic rocks in northern Altan Uul (Fig. 2.11). It is dominated by volcaniclastic schists, with some meta-andesites in the north. In the south, it is overthrust by the North Altan Psammite sequence (Fig. 2.5 [10]). In the north, it is onlapped by Mesozoic and Quaternary alluvial sediments (Fig. 2.5 [14]).

Lithologies and petrography

The volcaniclastic schists are intensely cleaved and sometimes flaggy in outcrop whilst the meta-andesites form more blocky exposures.

The volcaniclastic schists consist of 2-6 mm rounded andesite clasts (15-20 %) and rounded feldspar grains (20-50 %), often altered to epidote (10-15 %), in a matrix of recrystallised quartz (5-10 %). The clasts contain small (0.05-0.1 mm) interlocking albitised feldspar laths (c.90 %; Fig. 2.18A). Cleavage forming muscovite (5-10 %) and chlorite (10 %) wrap around clasts and grains. Some albite grains are cut by fractures filled with chlorite. Calcite veins cut everything (Fig. 2.18B).

The meta-andesites are dominated by two phases of feldspar, consisting of 0.5-1 mm euhedral plagioclase crystals (20 %) and small (0.1 mm) interlocking laths of feldspar (10 %), often entirely altered to epidote (10 %) and chlorite (5 %; Fig. 2.18C).

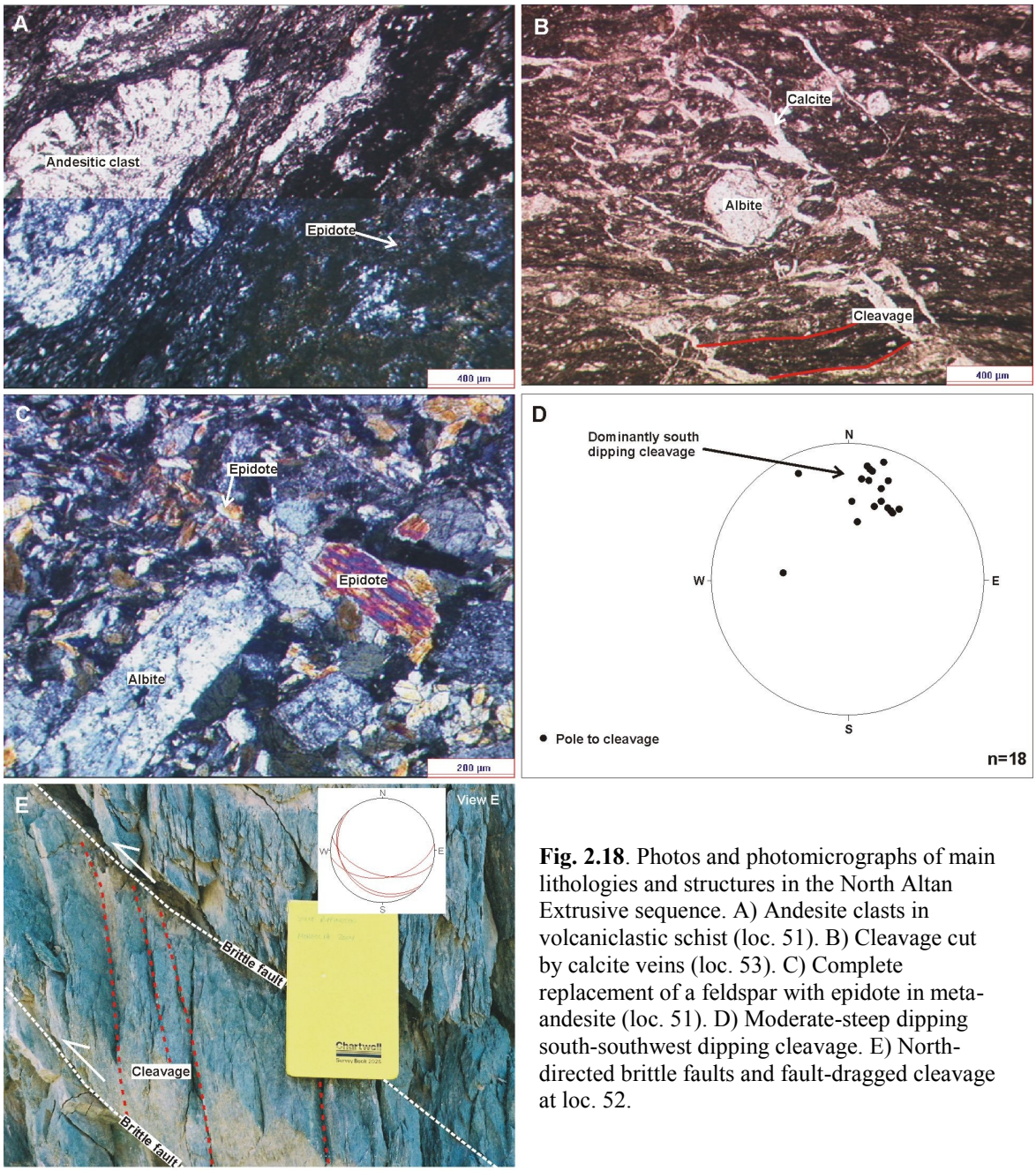

Fig. 2.18. Photos and photomicrographs of main lithologies and structures in the North Altan Extrusive sequence. A) Andesite clasts in volcaniclastic schist (loc. 51). B) Cleavage cut by calcite veins (loc. 53). C) Complete replacement of a feldspar with epidote in meta-andesite (loc. 51). D) Moderate-steep dipping south-southwest dipping cleavage. E) North-directed brittle faults and fault-dragged cleavage at loc. 52.

Augite (15 %) scattered throughout the rocks, are often altered to actinolite (10 %). Subhedral hornblendes c.0.2 mm in size (20 %) overgrow everything, which suggests they are a metamorphic phase.

Structure and metamorphism

Moderate-steep, south-southwest dipping bedding and parallel cleavage occur throughout the area (Fig. 2.18D). The volcaniclastic schists are repeatedly cut by small-scale brittle faults that strike 310-320^{o} and dip 24-20^{o} to the southwest. Kinematic

indicators are hard to identify, but fault-drag in cleavage cut by the brittle fault sometimes suggests that north-directed thrusting occurred (Fig. 2.18E).

Within 20 m of the northern extent of the transect through Altan Uul, volcaniclastic schist is thrust north over meta-andesite by a brittle fault that strikes 284^{o} and dips 56^{o} to the southwest (Fig. 2.5 [15]). Thrust-sense movement was determined from fault-dragged cleavage in the volcaniclastic schists in the hanging wall of the fault. Photo-geological interpretation of Landsat TM imagery suggests the meta-andesites continue to crop out to the northwest (Fig. 2.11).

The mineralogy is uniform throughout the North Altan Extrusive sequence, suggesting the metamorphic grade is also uniform. The mineral assemblage of albite, quartz, muscovite and chlorite suggest the volcaniclastic schists were metamorphosed in the chlorite zone of the greenschist facies (Bucher & Frey 1994). In the meta-andesites, chlorite, actinolite and secondary hornblende is indicative of greenschist grade metamorphism (Bucher & Frey 1994).

North of Altan Uul, there is a large Cretaceous basin (Fig. 2.11 [2]). The transect through the Palaeozoic basement continues north of this basin in Western Nemegt Uul (Fig. 2.11 [3]).

2.5.7 The West Nemegt Volcaniclastic sequence

From south to north, the West Nemegt Volcaniclastic sequence is a mixed assemblage of volcaniclastic meta-conglomerate, chloritic schist and meta-conglomerate cropping out in a c. 1100 m wide east-west trending belt in southwest Nemegt Uul (Fig. 2.11). Generally flaggy exposure makes structural analysis of the area difficult in places. At the southern extent of the seqeunce, along the transect, Cretaceous-Cenozoic sediments onlap volcaniclastic sandstone (Fig. 2.5 [16]). At the northern extent of the sequence, chloritic schist and meta-conglomerate are thrust north over Cretaceous-Cenozoic basin fill (Fig. 2.5 [17]).

Lithologies and petrography

Exposure is variable along this part of the transect. Volcaniclastic meta-conglomerates form excellent cliff outcrops with bedding, cleavage and folded cleavage

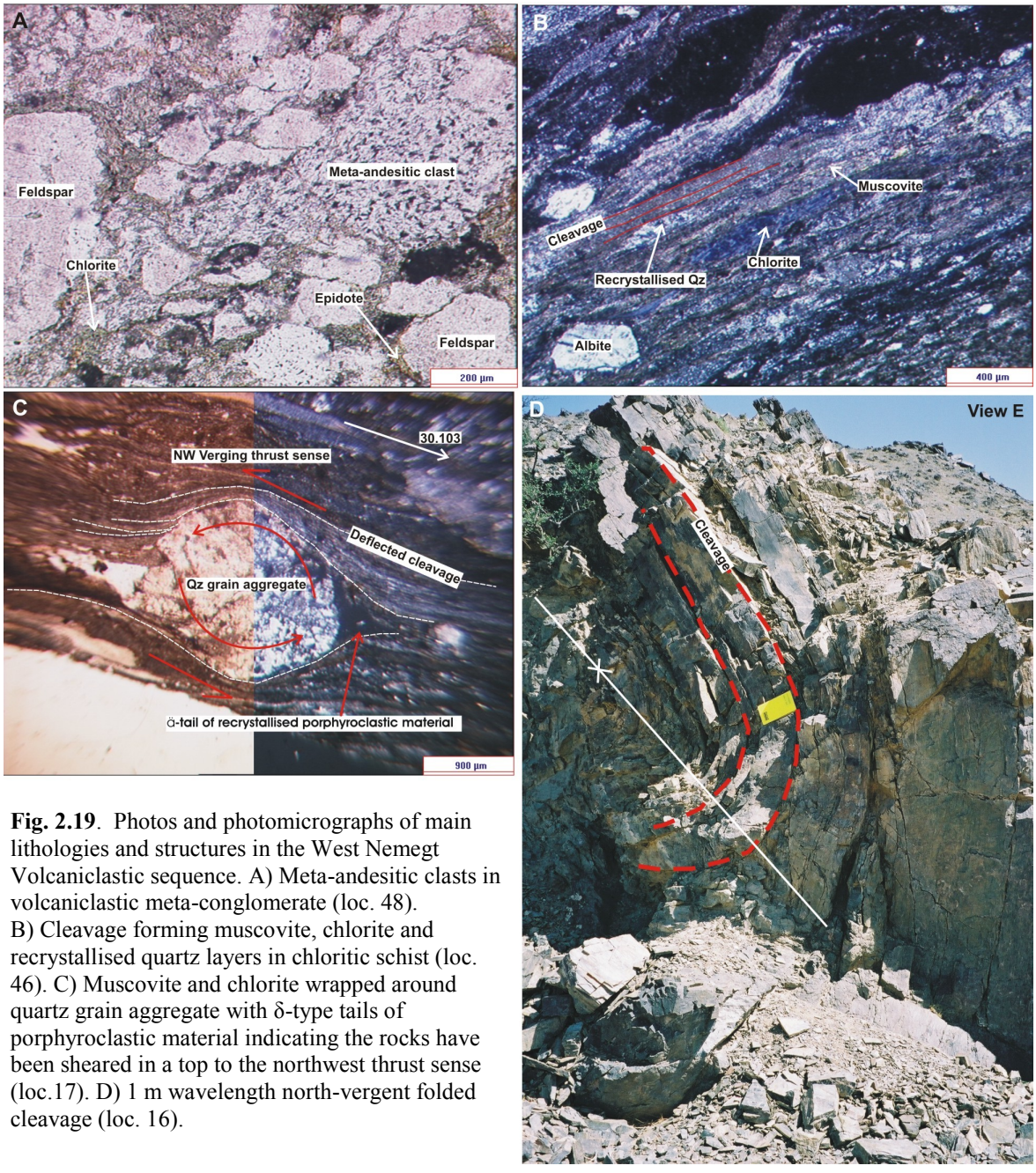

Fig. 2.19. Photos and photomicrographs of main lithologies and structures in the West Nemegt Volcaniclastic sequence. A) Meta-andesitic clasts in volcaniclastic meta-conglomerate (loc. 48). B) Cleavage forming muscovite, chlorite and recrystallised quartz layers in chloritic schist (loc. 46). C) Muscovite and chlorite wrapped around quartz grain aggregate with δ-type tails of porphyroclastic material indicating the rocks have been sheared in a top to the northwest thrust sense (loc.17). D) 1 m wavelength north-vergent folded cleavage (loc. 16).

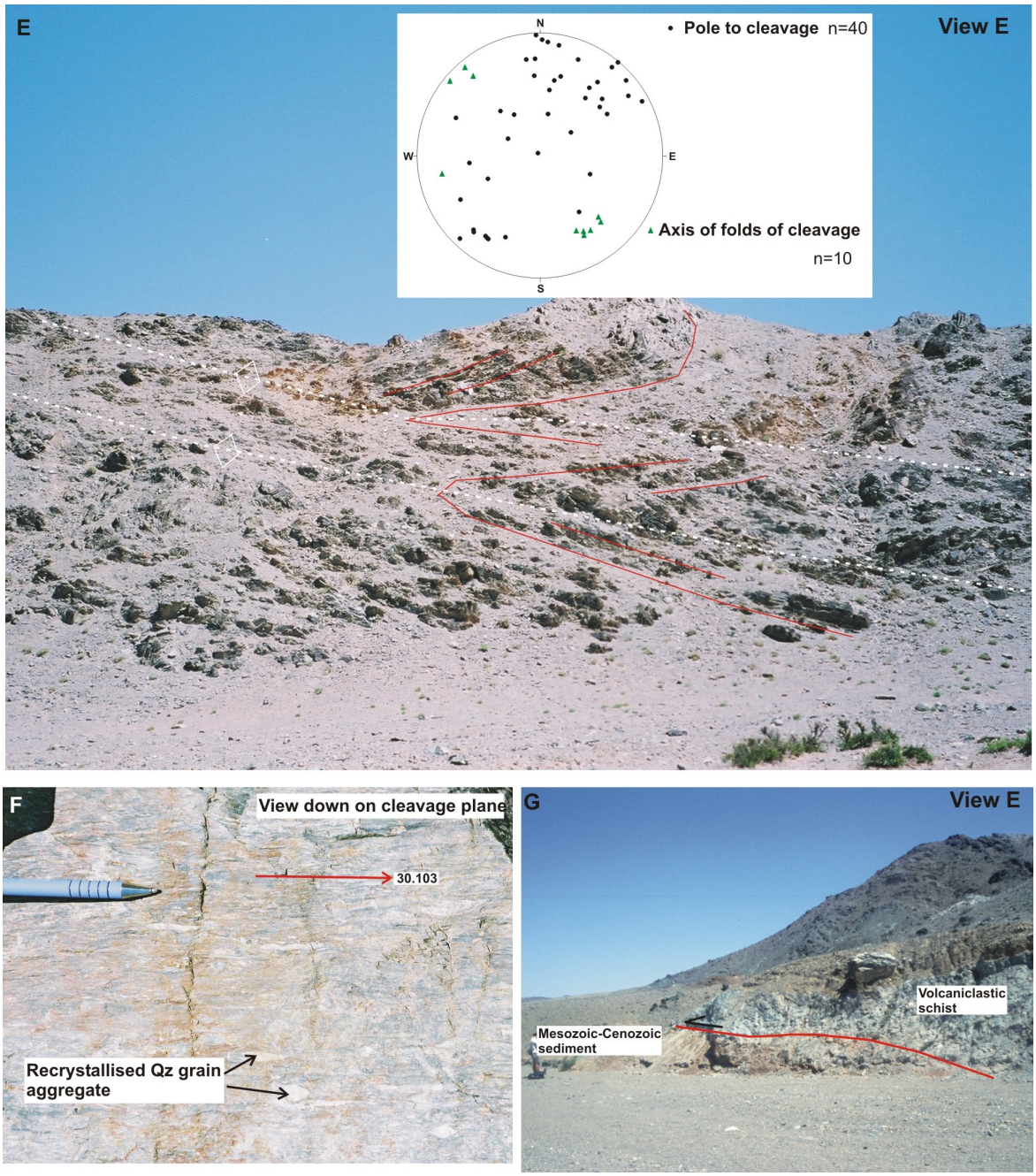

(Fig. 2.19 continued from previous page) E) 10 m wavelength north-vergent folds of cleavage (loc. 46). F) Meta-conglomerate L-S tectonite (loc. 45). G) North-directed Cenozoic thrust fault at the northern boundary of the group (at Fig. 2.5 [17]; loc. 16).

clearly visible. To the north, chloritic schists have a strong pervasive cleavage, but are poorly exposed and flaggy (Fig. 2.5 [18]).

The volcaniclastic meta-conglomerates are polymictic and poorly sorted with clasts (30-40 %) ranging in size from 0.5-2 mm in a recrystallised quartz matrix (30-50 %). The smaller clasts (15-25 %) are grains of albite and quartz. The largest are rounded clasts of andesite (10-15 %; Fig. 2.19A), containing interlocking feldspar laths, often partially broken down to epidote (c. 5 %) and chlorite (c. 5 %), with a preferred orientation. Rounded 0.05-0.2 mm opaque minerals (5 %) are scattered throughout the rocks.

In the chloritic schists, cleavage is defined by c. 0.5 mm wide bands of recrystallised quartz (50 %) surrounded by chlorite (15-20 %) and muscovite (5-15 %; Fig. 2.19B). Roughly rectangular clusters of small (0.01-0.1) epidote crystals (15-30 %) throughout may be the alteration product of feldspar.

To the north of the chloritic schists, meta-conglomerates crop out in a c. 30 m wide east-west trending zone. The meta-conglomerates consist of 0.1-1 mm quartz grain aggregates (60-70 %) with undulose extinction and fragments of albite (c. 5 %), often broken down to epidote (c. 5 %). Cleavage forming muscovite (5-10 %) and biotite (10-15 %) wrap around everything, giving top to the northwest thrust-sense kinematic indicators (Fig. 2.19C).

Structure and metamorphism

The West Nemegt Volcaniclastic sequence is a structural vergence-divide in the transect area. Southeast trending south-vergent folds of cleavage occur in the south (Fig. 2.5 [19]) and north-vergent folds of cleavage occur in the north (Fig. 2.19D; Fig. 2.5 [20]).

In the middle of the belt, outcrop is brown and heavily fractured around a c.1m wide mylonitic shear zone striking 132^{o} and dipping 63^{o} to the northeast. Mineral stretching lineations in the shear zone plunge 43^{o} towards 341^{o} (Fig. 2.5 [21]). The shear zone cuts across the transect into a broadly east-west valley and can be clearly traced on Landsat TM imagery, where it bounds the Cretaceous basin to the west (Fig. 2.11). It is tentatively classified as a normal fault based on its geometry, location and orientation.

The chlorite schists in the hanging wall of the normal fault are strongly cleaved

and often flaggy (Fig. 2.5 [20]. Tight, north-vergent folds of cleavage occur on a 1-10 m scale (Fig. 2.19D-E). Localised areas of intense strain are marked by a meta-conglomerate L-S tectonite (Fig. 2.19F). Thin section analysis of the L-S tectonite suggests the rocks were sheared with a northwest-directed thrust sense (Fig. 2.19C).

At the northern extent of the sequence, chloritic schist is thrust north over Cenozoic-Mesozoic basin fill by a shallow, but southward steepening, zone of white fault gouge and unconsolidated breccia (Fig. 2.19G; Fig. 2.5 [17]). North of the sequence there is a narrow 1 km wide section of Mesozoic basin which onlaps the West Nemegt Psammite sequence to the north (Fig. 2.11 [4]).

The metamorphic grade of the rocks in the West Nemegt Volcaniclastic sequence increases slightly to the north. The volcaniclastic schists and chloritic schists in the south have an albite-quartz-epidote-chlorite mineral assemblage, suggesting the rocks were metamorphosed in the chlorite zone of the greenschist facies (Bucher & Frey 1994). To the north, the meta-conglomerate and chloritic schist also contain muscovite and biotite, suggesting the rocks may have been metamorphosed in the biotite zone of the greenschist facies (Bucher & Frey 1994).

2.5.8 The West Nemegt Psammite sequence

The West Nemegt Psammite sequence is a c. 5 km wide belt of interbedded arkosic meta-pelitic schists, phyllites, arkosic psammitic schists and dolomite cropping out in northwest Nemegt Uul (Fig. 2.11 [5]). In the south, the sequence is onlapped by Cretaceous-Cenozoic basin fill (Fig. 2.5 [22]). In the north, in the transect area, the sequence is also onlapped by Mesozoic-Cenozoic basin fill (Fig. 2.5 [23]). Palaeozoic rocks in the West Nemegt Psammite sequence exposed at the northern front of Nemegt Uul are onlapped by Quaternary alluvial fan sediments. However, further to the east, along the northern front of Nemegt Uul, the West Nemegt Psammite sequence is thrust north over Cretaceous-Cenozoic basin fill.

Lithologies and petrography

The sequence crops out in the walls of a steep-sided canyon. Consequently, exposure is consistently good. Pervasively cleaved and folded fine grained phyllites and

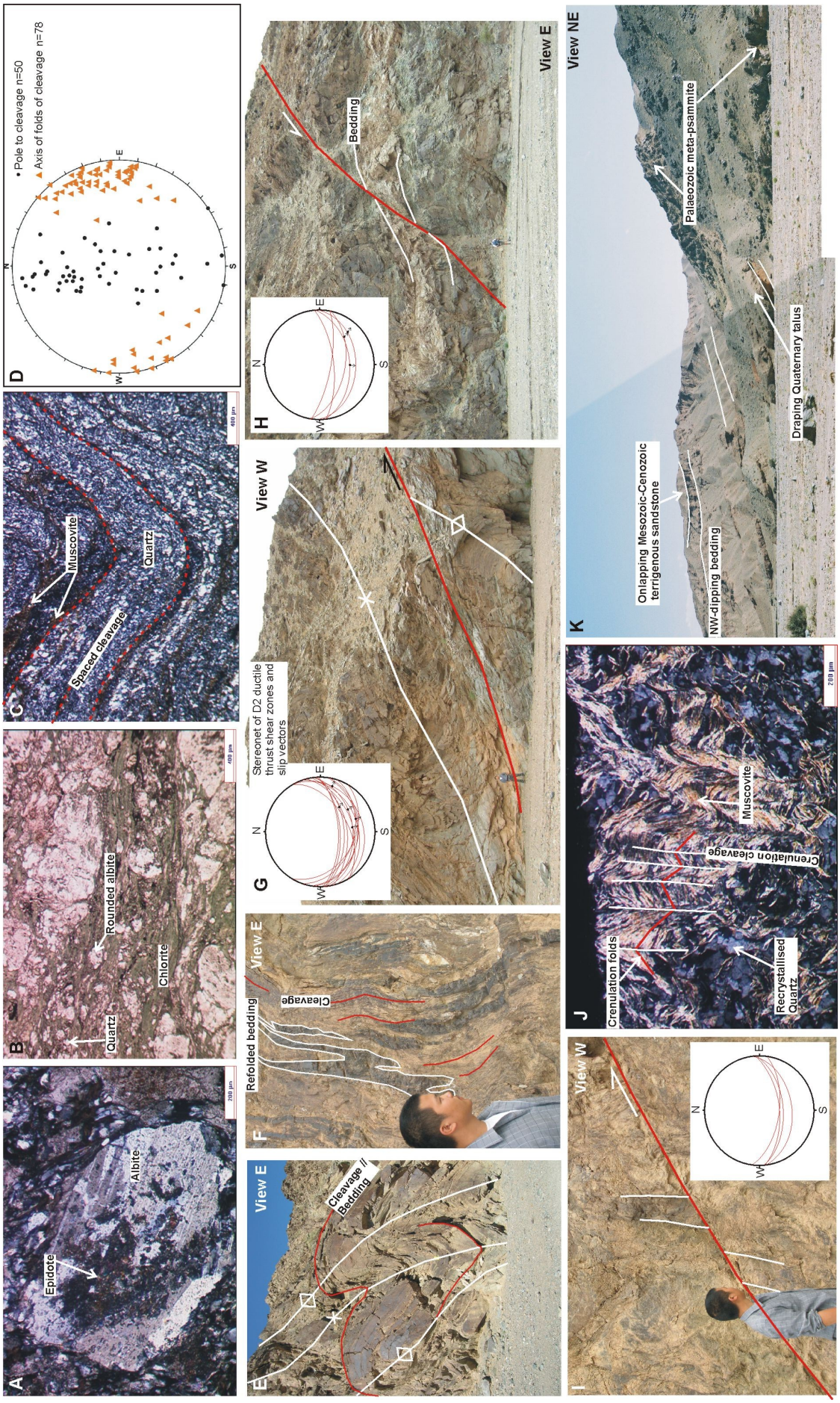

Fig. 2.20. Figure caption overleaf

Fig. 2.20. (Figure on previous page) Photos and photomicrographs of main lithologies and structure of the West Nemegt Psammite sequence. A) Albite partly broken down to epidote (loc. 21). B) Chlorite wrapping around quartz and rounded albite grains (loc. 21). C) Folded cleavage formed by muscovite, chlorite, and bands of recrystallised quartz (loc. 25). D) Stereonet of cleavage and fold axis measurements showing east-west trending folds of cleavage. E) Tight north-vergent folds of cleavage (loc. 21). F) Refolded bedding parallel to cleavage (loc. 25). G) North-directed ductile thrust cutting folds of cleavage and stereonet of ductile thrusts, with slip vectors marked where present, that excise fold limbs in the sequence (loc. 22). H) Brittle normal fault and stereonet of normal faults that cut the sequence (loc. 22). I) North-directed brittle thrust fault (loc. 25). J) Crenulation folds of muscovite in thin section (loc. 22). K) Cretaceous-Cenozoic sediments onlapping Palaeozoic meta-psammite towards the northern front in western Nemegt Uul (loc. 44).

arkosic meta-pelitic schist dominate the outcrop in the south of the sequence. The rocks coarsen to the north, becoming arkosic meta-psammitic schist, with occasional interbedded dolomite layers.

The arkosic meta-pelitic schists and phyllites consist of 0.5-1 mm rounded albite grains (20-40 %), often partially broken down to epidote (5-20 %; Fig. 2.20A), in a quartz matrix (5-30 %). Chlorite (20-40 %) and muscovite (c. 10 %) form the cleavage (Fig. 2.20B).

The arkosic meta-psammites consist of layers of 0.5-1 mm rounded albite grains (<20 %) and layers of recrystallised quartz (40-65 %) with a clear preferred orientation. The muscovite (5-10 %) and chlorite (5-15 %) content of the meta-psammites is less than in the meta-pelites but both minerals form the cleavage (Fig. 2.20C). Some meta-pelitic rocks in the north also contain biotite, defining a cleavage which is wrapped around small (0.1mm) anhedral garnet crystals (c. 5 %).

Structure and metamorphism

A pervasive cleavage, folded into tight north-vergent E-W trending folds is characteristic throughout the transect area (Fig. 2.20D-E). It is consistently parallel to bedding (Fig. 2.20F).

Approximately 10 cm wide mylonitic shear zones, striking 240-287^{o} and dipping 23-60^{o} with mineral stretching lineations plunging 22-52^{o} towards 140-161^{o} respectively (Fig. 2.20G), are ubiquitous throughout the transect area. Fault-dragged cleavage on either side of these shear zones suggests movement in a northwest to northeast-directed thrust sense has excised the long-limb of many of the tight north-vergent folds of cleavage (Fig. 2.20G; Fig. 2.5 [24]). In several places brittle faults, striking 265-280^{o} and dipping 35-74^{o} to the south-southwest, and formed of c.50 cm wide zones of gouge and

incohesive fault breccia, cut the mylonitic thrust shear zones and folds of cleavage (Fig. 2.5 [25]; Fig. 2.20H). Fault-dragged cleavage on both sides of these faults, and in rare instances offset bedding, suggest they have moved in a normal sense. Where bedding is cut by one fault, c.5 m normal offset across the fault can be ascertained (Fig. 2.20H). Several brittle faults striking 264-278^{o} and dipping 40-60^{o} to the south cross the area (Fig. 2.20I), in places cutting brittle normal faults and ductile thrust shear zones. North-directed thrust sense slip on these faults has been determined by observation of fault-dragged cleavage and offset bedding cut by the fault planes.

In some meta-pelitic schists, mm-scale folds of bedding-parallel cleavage are visible in thin section, often in association with sub-mm scale chevron folds highlighted by layers of muscovite. In places, a second crenulation cleavage can be seen associated with these folds in thin section (Fig. 2.20J).

In the north of the area (Fig. 2.11 [8]), a brittle normal detachment fault striking 055^{o} and dipping 52^{o} to the northwest marks the boundary between Palaeozoic cleaved and folded arkosic meta-psammite and an unmetamorphosed Mesozoic sedimentary succession (Cunningham et al. submitted). The Mesozoic sediments onlap isolated psammite outcrops further north (Fig. 2.20K), before Quaternary alluvial fans onlap the mountain front.

There is a variation in the metamorphic grade in the area. In the south, the rocks have a quartz-albite-muscovite-chlorite-epidote mineral assemblage, suggesting the rocks were metamorphosed in the chlorite zone of the greenschist facies (Bucher & Frey 1994). Approximately 2300 m from the northern front of Nemegt Uul, a block of meta-pelitic schist with a quartz-biotite-garnet-epidote-chloritoid mineral assemblage typical of Al-rich meta-pelites metamorphosed in upper greenschist to epidote-amphibolite facies (Bucher & Frey 1994) crops out in a normal fault bound block (Fig. 2.5 [26]).

2.6 Central Nemegt Uul Transect

South of the Central Nemegt Uul transect, there is an east-west trending fault bound sequence of poorly exposed slates along the southern front of Nemegt Uul (Fig. 2.21 [1]). Due to problems with accessibility, there is a gap in the data before the transect through the range begins, just north of the southern front (Fig. 2.21 [2]). Otherwise, the transect is almost continuous through Nemegt Uul to the northern front of the range.

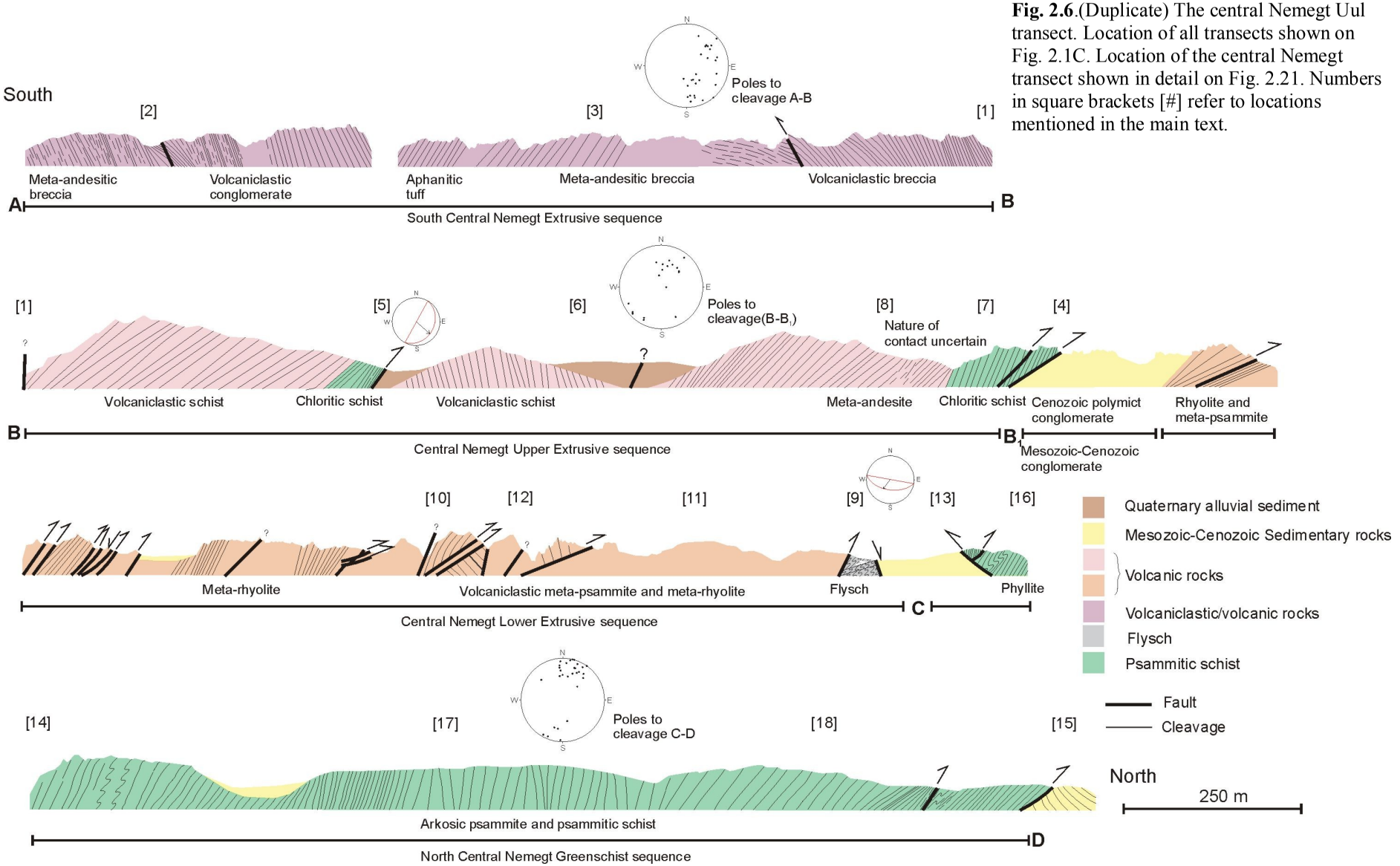

Fig. 2.6.(Duplicate) The central Nemegt Uul transect. Location of all transects shown on Fig. 2.1C. Location of the central Nemegt transect shown in detail on Fig. 2.21. Numbers in square brackets [#] refer to locations mentioned in the main text.

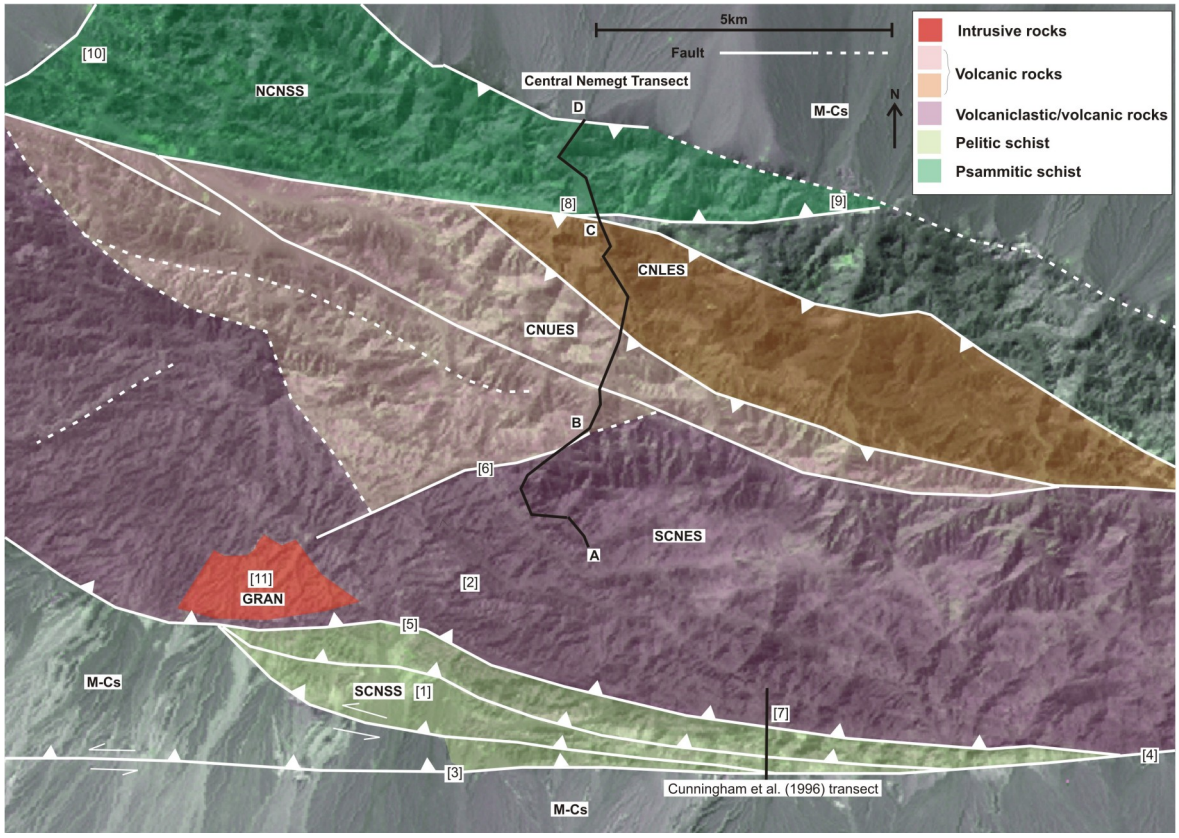

Fig. 2.21. Central transect location map with litho-tectonic sequences. Numbers in square brackets [#] refer to locations mentioned in the main text. SCNSS = South Central Nemegt Slate sequence. GRAN = Granite. SCNES = South Central Nemegt Extrusive sequence. CNUES = Central Nemegt Upper Extrusive sequence. CNLES = Central Nemegt Lower Extrusive sequence. NCNSS = North Central Nemegt Schist sequence. M -Cs = Mesozoic-Cenozoic sediments.

2.6.1 South Central Nemegt Slate sequence

The South Central Nemegt Slate sequence is a mixed assemblage of tectonically dismembered slates and phyllites that crop out in isolated patches along the southern front of Nemegt Uul (Fig. 2.21). In places, the sequence is onlapped by Quaternary alluvial sediments. In the southwest, the sequence is bound by fault cutting through the Cretaceous-Cenozoic sediments between Nemegt and Altan Uul (Fig. 2.21 [3]). The fault plane is not seen between the ranges, but is inferred by an increase in topography across its projected position, southward tilted sediments basinward of the fault, and spring lines marking its trace. This fault is discussed further in section 3.5.2. To the east, the slates probably subcrop beneath the South Central Nemegt Extrusive sequence, which is thrust south over Cretaceous-Cenozoic basin sediments and Quaternary alluvial sediments at the south front of Nemegt Uul (Fig. 2.21 [4]; Fig. 2.22A).

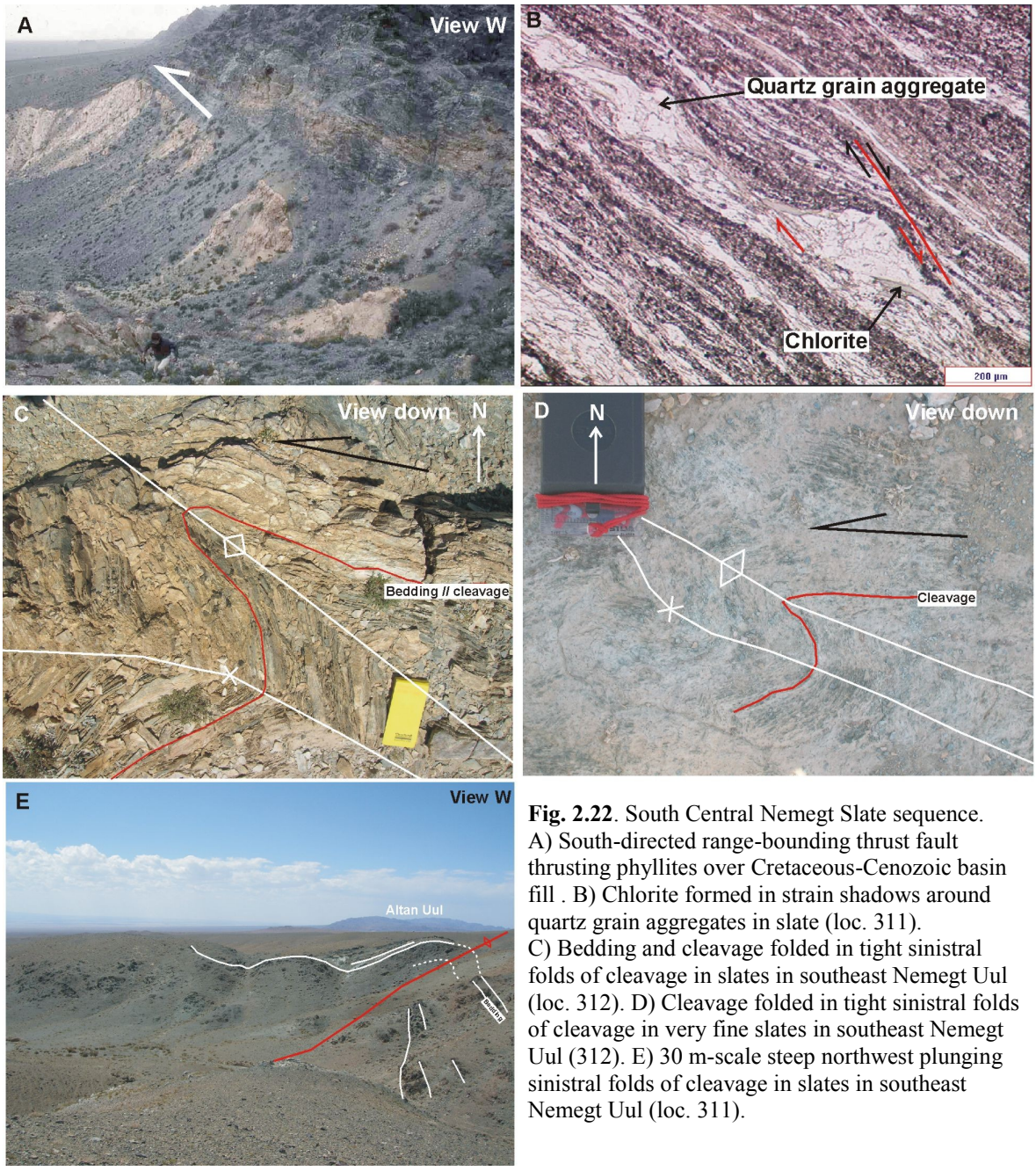

Fig. 2.22. South Central Nemegt Slate sequence. A) South-directed range-bounding thrust fault thrusting phyllites over Cretaceous-Cenozoic basin fill . B) Chlorite formed in strain shadows around quartz grain aggregates in slate (loc. 311). C) Bedding and cleavage folded in tight sinistral folds of cleavage in slates in southeast Nemegt Uul (loc. 312). D) Cleavage folded in tight sinistral folds of cleavage in very fine slates in southeast Nemegt Uul (312). E) 30 m-scale steep northwest plunging sinistral folds of cleavage in slates in southeast Nemegt Uul (loc. 311).

Lithology and petrography

Exposure is poor in southwest Nemegt Uul. The slates form small hills, covered in Quaternary alluvial sediment. However, it is possible to trace the sequence for several kilometres along the south front of Nemegt Uul (Fig. 2.21).

The slates consist of 0.3 mm quartz lenses (10 %) wrapped in cleavage forming chlorite (10 %), muscovite (c. 5 %), recrystallised quartz bands (65 %). Layers of epidote (10 %) can be seen between some quartz layers. Strain shadows around the quartz grain

aggregates are often filled with chlorite, and make clear kinematic indicators (Fig. 2.22B).

Structure and metamorphism

The sequence is characterised by a strong slatey cleavage, which is folded into moderate-tight 20 m scale moderate-steep northeast plunging folds (Fig. 2.22C-E). These folds are found between a series of south-directed oblique-slip brittle thrust faults striking 080^{o} and dipping of 40^{o} to the northwest , to striking 111^{o} and dipping 24^{o} to the northeast. These faults form a strike-slip duplex branching off from the southern frontal thrust of Nemegt Uul, which is discussed further in chapter 3.

The mineralogy of the South Central Nemegt Slate sequence is uniform suggesting the metamorphic grade is uniform. The slates have a quartz-chlorite mineral assemblage, suggesting they were metamorphosed in the chlorite zone of the greenschist facies (Bucher & Frey 1994).

2.6.2 The South Central Nemegt Extrusive sequence

The South Central Nemegt extrusive sequence is a mixed assemblage of interbedded extrusive meta-volcanic rocks and closely associated meta-sedimentary rocks cropping out in a c. 3.5 km wide arcuate belt through southern Nemegt Uul (Fig. 2.21). The sequence consists of volcanic breccia and conglomerate, fine grained tuff, meta-andesite and altered volcaniclastic breccia units.

In the transect area, the sequence is thrust south over the South Central Nemegt Slate sequence (Fig. 2.21 [5]) and, further east, Cretaceous-Cenozoic basin fill (Fig. 2.21 [4]). In the north, a highly linear southwest-northeast valley, probably marking a major fault zone, defines the northern extent of the South Central Nemegt Extrusive sequence (Fig. 2.6 [1]; Fig. 2.21 [6]). Rocks from the southern part of the South Central Nemegt Extrusive sequence and the slate sequence just to the south of it, were first documented to the east of the transect area (Fig. 2.21 [7]) by Cunningham et al. (1996).

Lithologies and petrography

Exposure lacks bedding and cleavage throughout much of the area, so outcrop is generally blocky in appearance. However, bedding and cleavage can sometimes be seen

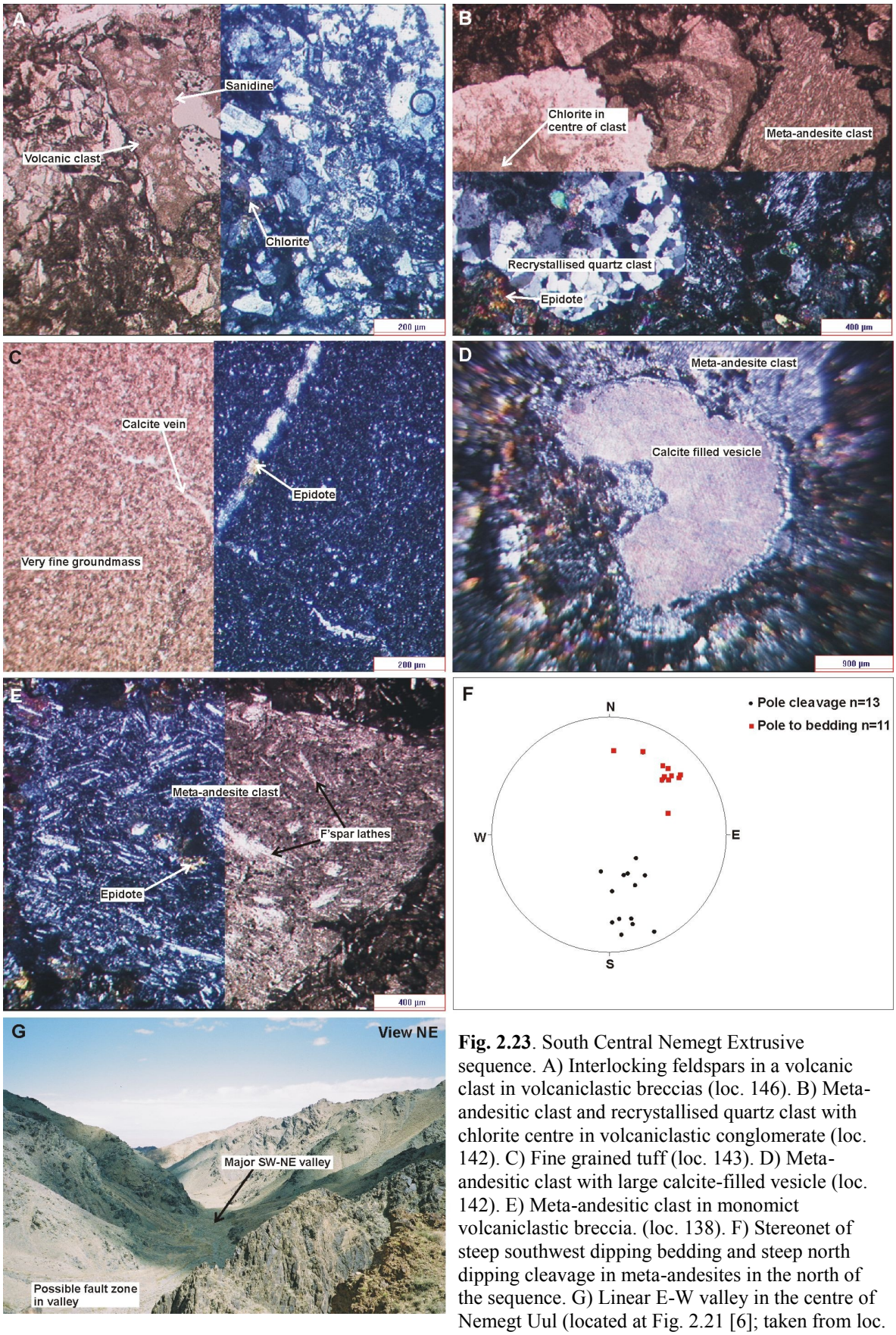

Fig. 2.23. South Central Nemegt Extrusive sequence. A) Interlocking feldspars in a volcanic clast in volcaniclastic breccias (loc. 146). B) Meta-andesitic clast and recrystallised quartz clast with chlorite centre in volcaniclastic conglomerate (loc. 142). C) Fine grained tuff (loc. 143). D) Meta-andesitic clast with large calcite-filled vesicle (loc. 142). E) Meta-andesitic clast in monomict volcaniclastic breccia. (loc. 138). F) Stereonet of steep southwest dipping bedding and steep north dipping cleavage in meta-andesites in the north of the sequence. G) Linear E-W valley in the centre of Nemegt Uul (located at Fig. 2.21 [6]; taken from loc. 137).

in volcaniclastic units. In the south, volcaniclastic breccias and conglomerates crop out (Fig. 2.6 [2]). To the north, blocky fine tuffs and meta-andesites crop out (Fig. 2.6 [3]). At the northern extent of the sequence, meta-andesites give way to another unit of volcaniclastic breccia.

The volcanic breccias in the south consist of 2 mm subhedral albite phenocrysts (10-20 %) and 2-4 mm sub-angular meta-andesitic clasts (40-55 %) consisting of small 0.01-0.1 mm feldspar laths (80 % of clast) and chlorite (20 % of clast), and sub-angular meta-psammitic clasts (10-20 %) consisting of fine recrystallised quartz (60 % of clast) overgrown by anhedral calcite crystals (40 % of clast). The clasts are in a groundmass of 0.15-0.25 mm interlocking feldspar laths (20 %) and 0.05-0.25 mm epidote crystals (10-20 %; Fig. 2.23A).

The volcanic conglomerates consist of c. 5 mm rounded clasts of andesite (60 %), consisting of interlocking feldspar laths (80 % of clast) and round calcite amygdales (20 % of clast), 1.5-3 mm rounded clasts of fine grained pink tuff (10 %), 2 mm rounded clasts of recrystalised quartz with chlorite centres (20 %; Fig. 2.23B), and 2 mm sub-rounded clasts made from small (0.1 mm) albite laths with a clear preferred orientation (c.10 %). All the feldspars are partially altered to epidote (10 %) and chlorite (10 %).

The tuffs have a pale pink groundmass of barely distinguishable feldspar, possibly sanidine (c.65 %) and quartz grains (c.25 %; Fig. 2.23C). Very small (0.01-0.1 mm) zoisite (c.5 %) and calcite crystals (c.5 %) are just distinguishable throughout the rock.

The meta-andesites consist of 1-2 mm subhedral plagioclase phenocrysts (25-40 %), often partially broken down to epidote (c.10 %) and chlorite. The groundmass is dominated by 0.1 mm feldspar laths (45-60 %), which are often completely broken down to chlorite (c. 10%), so only their shape remains. The rock contains numerous chlorite filled, and calcite filled, vesicles (c.10%; Fig. 2.23D).

The monomict volcaniclastic breccias at the northern extent of the sequence, consist of 2.5-3 mm subangular clasts of meta-andesite (20-30 %) identical to the rocks seen directly to the south and described in the paragraph above (Fig. 2.23E). The clasts are contained in a matrix of 0.1 mm subhedral epidote (25 %) and quartz (45 %).

Structure and metamorphism

Rock exposures in the South Central Nemegt Extrusive sequence are generally

blocky although steep southwest dipping bedding is documented in some places. Steep north dipping cleavage at an angle to steep southwest dipping bedding is seen in meta-andesitic rocks in the northern part of the area (Fig. 2.23F). Fault zones are hard to identify and may be represented by valleys between outcrops.

A highly linear southwest-northeast valley, probably marking a major fault zone (Fig. 2.6 [1]; Fig. 2.21 [6]), defines the northern extent of the South Central Nemegt Extrusive sequence in this area (Fig. 2.23G). No fault plane is seen and poor exposure on either side of the valley makes it impossible to determine the slip sense. The fault also defines a thrust fault slip sense watershed in the range, with the thrust faults to the south directed to the south and the majority of thrust faults to the north directed to the north (Fig. 2.6).

The metamorphic grade of the sequence varies little. Regardless of lithology, the sequence has an albite-quartz-chlorite-epidote mineral assemblage suggesting the rocks were metamorphosed in the greenschist facies (Bucher & Frey 1994).

2.6.3 The Central Nemegt Upper Extrusive sequence

The Central Nemegt Upper Extrusive sequence is a mixed assemblage of extrusive volcanic rocks and volcaniclastic meta-sedimentary rocks outcropping in a c.2250 m northwest-southeast trending fault bound belt in central Nemegt Uul (Fig. 2.21). From south to north it consists of volcaniclastic schist and meta-andesite. The sequence is bound to the south by a highly linear southwest-northeast valley (Fig. 2.6 [1]; Fig. 2.21 [6]), probably marking a major fault zone (Fig. 2.23G). At the northern boundary, the Central Nemegt Upper Extrusive sequence is thrust north over unmetamorphosed poorly consolidated matrix supported polymict conglomerate with pebble size clasts (Fig. 2.6 [4]).

Lithologies and metamorphism

The volcaniclastic schists in the south of the sequence are often cleaved and flaggy in outcrop. Outcrops directly south of an east-west valley (Fig. 2.6 [5]) cutting through the sequence, change lithology to muscovite-chlorite schist. Approximately 200 m to the north, in another east-west trending valley, conglomeratic alluvium sits

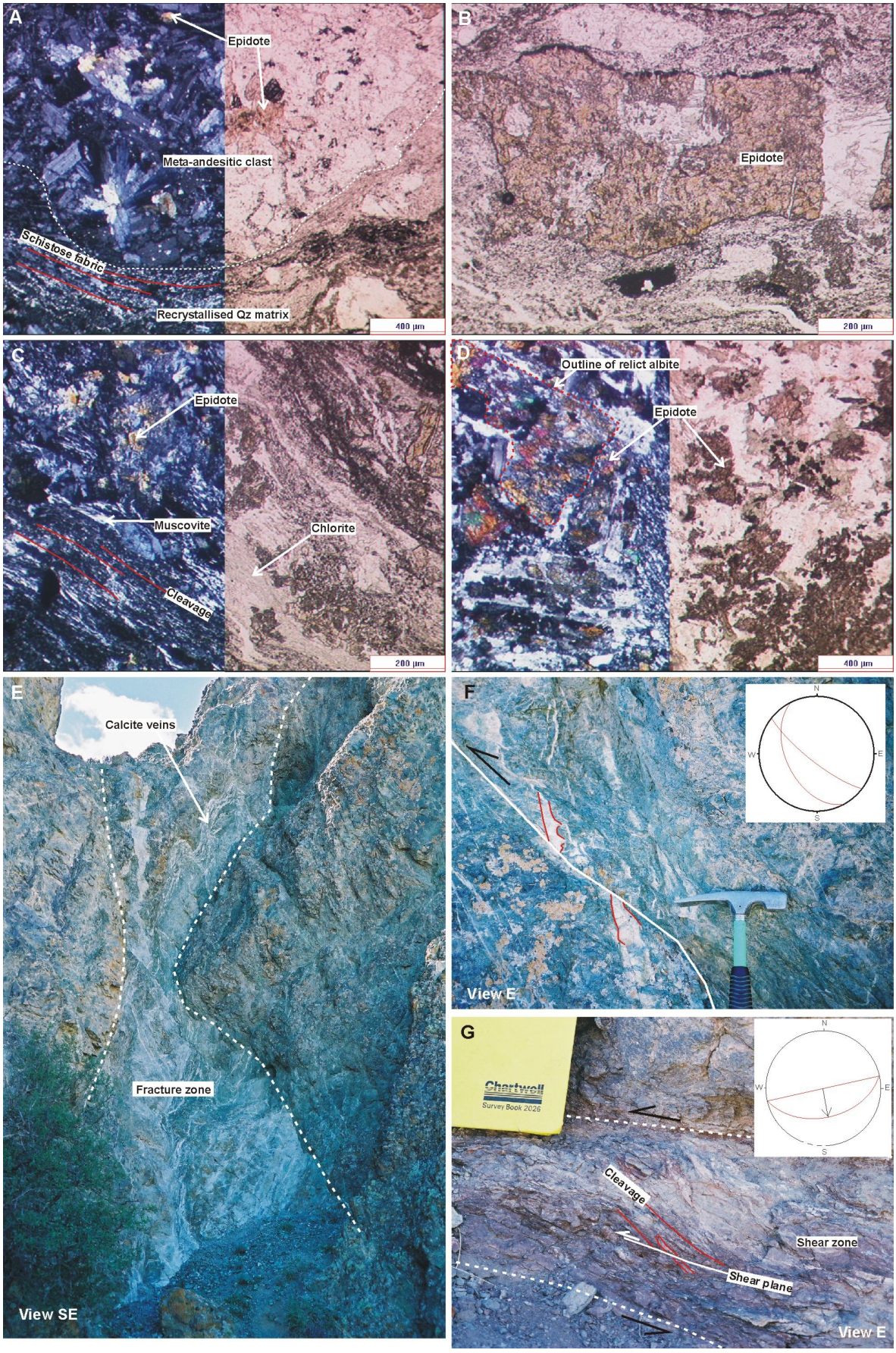

Fig. 2.24. Central Nemegt Upper Extrusive sequence. A) Meta-andesite clast wrapped in recrystallised quartz matrix in volcaniclastic schist (loc. 129). B) Complete replacement of mineral, probably feldspar, by epidote (loc. 310). C) Cleavage forming muscovite and chlorite in chloritic schist (loc. 310). (continued…)

(continued from previous page) D) Epidote from the breakdown of albite in meta-andesite (loc. 128). E) Calcite-veined fracture (loc. 127). F) Typical northeast-directed thrust fault displacing vein (loc. 127). G) Northwest-directed ductile thrust shear zone at the northern boundary of the group (loc. 123).

unconformably above volcaniclastic schists (Fig. 2.6 [6]). Blocky meta-andesites crop out the other side of the valley. The meta-andesites sit above another c. 200 m thick unit of interbedded muscovite-chlorite schist and volcaniclastic schist (Fig. 2.6 [7]). However, scree and alluvium covers much of the exposure and it is not clear if the contact between the meta-andesites and chloritic schist is structural, conformable or unconformable.

The volcaniclastic schists consist of 0.5-2 mm rounded grains of feldspar (40-50 %) with a dominantly albite composition, often partially altered to epidote (5-15 %) and chlorite (5-15 %), and c. 1.5 mm clasts of meta-andesite (30 %), as seen in the South Central Nemegt Extrusive sequence described in the previous section, in a matrix of cleavage forming (0.01 mm) recrystallised quartz bands (20-30 %; Fig. 2.24A), muscovite and chlorite. Small (0.2 mm) calcite (c. 5 %) crystals overprint everything.

The muscovite-chlorite schists consist of c.1 mm anhedral epidote crystals, that have retained the shape of crystals, probably feldspar, from which they were formed (15-20 %; Fig. 2.24B), and occasional remnants of albite (c. 10 %) wrapped in a matrix of 0.01 mm recrystallised quartz (30-70 %), and cleavage forming muscovite (5-10 %) and chlorite (15-30 %; Fig. 2.24C).

The meta-andesites consist of small 0.5-1 mm subhedral albite crystals (c.30%) and 0.05 mm laths of sanidine (c.15%). Epidote (15-20 %) is ubiquitous from the breakdown of feldspar (Fig. 2.24D). Chlorite (5-10 %) and anthophyllite (c. 5 %) surround some feldspar crystals.

Structure and metamorphism

The volcaniclastic rocks in the Central Nemegt Upper Extrusive sequence are cleaved in places, but lack a consistent cleavage orientation. Outcrop of the volcanic rocks is typically blocky in appearance.

The meta-andesites are cut by several metre-wide fracture zones that strike c. 351^{o} and dip 52^{o} to the southwest, some of which contain intense calcite veining (Fig. 2.24E; Fig. 2.6 [8]). The meta-andesites are cut by brittle thrust faults that strike 308-314^{o} and dip78-45^{o} to the southwest (Fig. 2.24F). No slickenlines were seen, but the faults often

displace calcite veins by c.5 cm (Fig. 2.24F) which indicates north-northeast directed thrust sense.

At the northern extent of the sequence, chloritic schist is thrust over an unmetamorphosed poorly consolidated matrix-supported polymict pebble conglomerate. The thrust is marked by a 10 cm wide foliated cataclastic fault zone striking 258^{o} and dipping 47^{o} to the southeast with slickenlines plunging 47^{o} towards 170^{o} (Fig. 2.24G stereonet inset). The juxtaposition of metamorphosed schist in the hanging wall against non-metamorphosed conglomerate in the footwall of the fault, suggests the thrust was north-directed (Fig. 2.24G).

The volcaniclastic schists and muscovite-chlorite schists have a quartz-muscovite-chlorite mineral assemblage, suggesting that the rocks were metamorphosed in the chlorite zone of the greenschist facies (Bucher & Frey 1994). The meta-andesites to the north have an albite-quartz-epidote-chlorite mineral assemblage, suggesting that the rocks have been metamorphosed to greenschist grade (Bucher & Frey 1994).

2.6.4 The Central Nemegt Lower Extrusive sequence

The Central Nemegt Lower Extrusive sequence is an assemblage of extrusive meta-volcanic rocks and closely associated volcaniclastic meta-sedimentary rocks cropping out in a c.1500 m wide northwest-southeast trending belt in central Nemegt Uul (Fig. 2.21). In the south, the sequence is onlapped by unmetamorphosed polymict conglomerate, which has been overthrust by the Central Nemegt Upper Extrusive sequence (Fig. 2.6 [4]). In the north, the sequence is thrust north over the North Central Schist sequence (Fig. 2.6 [9]).

Lithologies and petrography

In the south of the area there are blocky exposures of rhyolite. An east-west trending gully, marking a steep fault of undetermined slip sense cuts the valley and marks the northern boundary of the rhyolites (Fig. 2.6 [10]). Volcaniclastic meta-sandstones, interbedded with occasional rhyolite layers, crop out to the north of the gully. Exposure is consistently blocky throughout the area (Fig. 2.6 [11]), although cleavage is found in finer grained meta-sandstone beds.

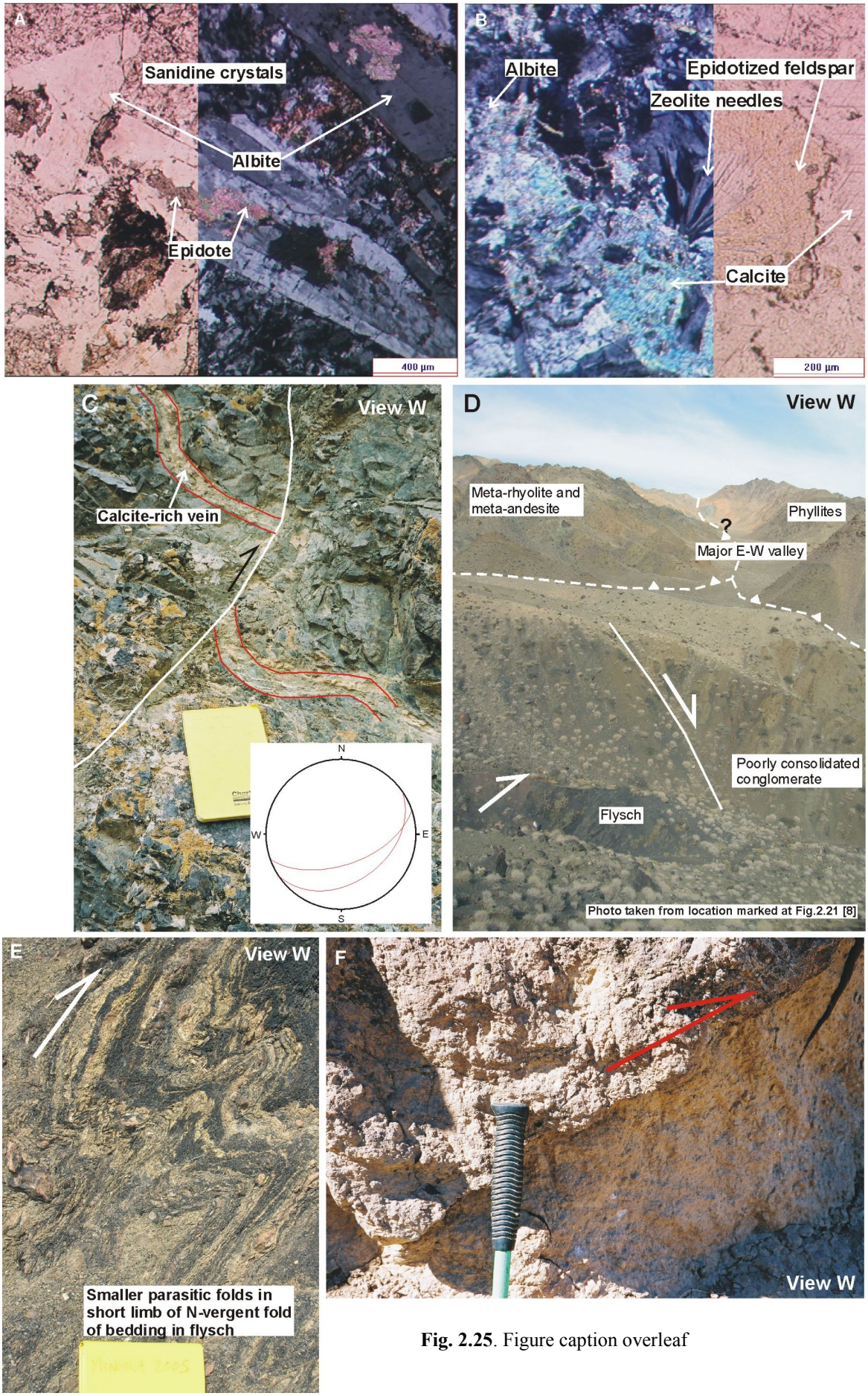

Fig. 2.25. Figure caption overleaf

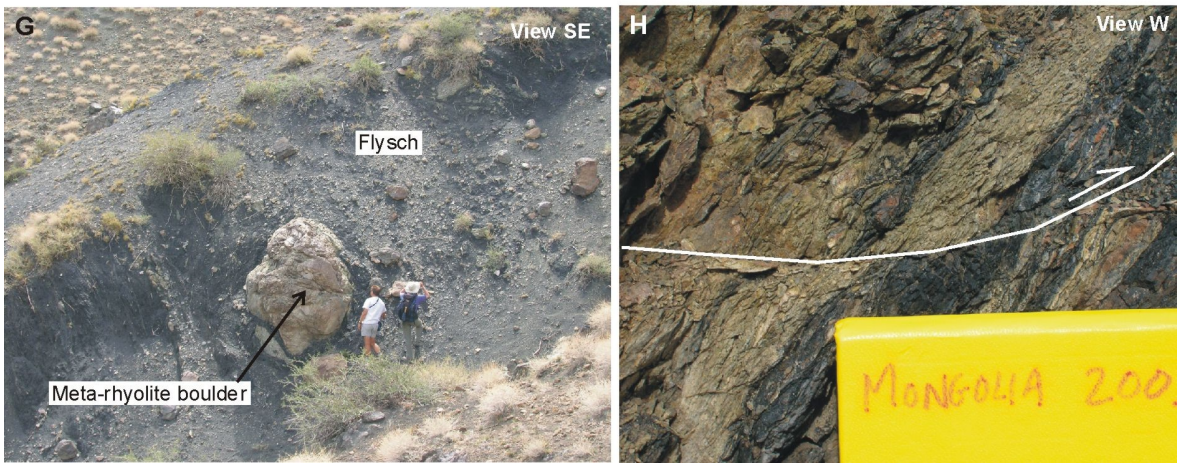

Fig. 2.25. Central Nemegt Lower Extrusive sequence. A) Feldspar phenocryst altered to epidote in rhyolite (loc. 122). B) Radial zeolite crystals in volcaniclastic meta-sandstone (loc. 119). C) Small north-directed brittle faults displacing veins (loc. 120). D) Flysch zone and downthrown conglomerate to the north. To the west a major east-west valley marks a fault between the Central Nemegt Lower Extrusive sequence and the North Central Nemegt Schist sequence (located at Fig. 2.21 [8]; loc. 187)). E) Intense north-directed ductile deformation in the flysch (loc. 187). F) Fault gouge between the meta-rhyolites in the Central Nemegt Lower Extrusive sequence and the flysch (loc. 126). G) Large rounded meta-rhyolitic boulder in the flysch zone (loc. 187). H) North-directed brittle thrust in the flysch (loc. 187).

The rhyolites consist of large 2 mm subhedral albite phenocrysts (30 %) in a groundmass of 0.25-0.5 mm pink and cloudy alkali feldspar laths (50 %). Many of the feldspar phenocrysts have altered to epidote (c.5 %) and chlorite (5-10 %) in the centre (Fig. 2.25A). Small (0.1 mm) recrystallised quartz grains (10-20 %) overgrow sanidine in the groundmass and quartz veins cut everything.

The volcaniclastic meta-sandstones consist of 2 mm diameter, rounded clasts (10-20 %) made from interlocking laths of feldspar. Approximately 10 % of the clasts contain 0.1-0.2 mm zeolite needles (Fig. 2.25B). Some 0.2 mm sub-rounded feldspar grains (20-40 %), often fractured and partially altered to epidote (5 %) and chlorite (5 %), also exist outside the clasts. The matrix consists of fine recrystallised quartz (10-15 %) with no preferred orientation. Large (0.2-2 mm) calcite crystals (15 %) that overgrow everything and c.0.5 mm wide calcite veins that cut everything are ubiquitous throughout the transect area.

At the northern boundary of the sequence, a crumbly dark flysch crops out. No sample was taken. The flysch contains thin layers of meta-rhyolite sourced from the meta-volcanic rocks to the south interbedded with a fine organic-rich matrix. The meta-rhyolite was entrained before the flysch was ductiley deformed, but large boulders of the meta-rhyolite were also incorporated during north-directed thrusting within the flysch zone.

Structure and metamorphism

The rocks in the Central Nemegt Upper Lower Extrusive sequence are cleaved in places, but do not have a consistent cleavage orientation. The rocks are dominantly blocky in outcrop.

The area is dominated by small steep and shallow south-dipping brittle thrust faults that strike 235-251^{o} and dip 35-56^{o} to the southeast, often displacing calcite veins by c.10 cm (Fig. 2.25C). No major fault planes are evident. Several east-west trending gullies off the transect valley, commonly mark slight changes in lithology and may be weathered out bedding or fault planes (Fig. 2.6 [10,12]).

At the northern boundary of the sequence, a 100 m wide belt of deformed flysch marks a zone of intense north-directed ductile shearing (Fig. 2.6 [9]; Fig. 2.25D, E). The flysch is overthrust by meta-rhyolites in the Central Nemegt Lower Extrusive sequence. The thrust fault is marked by a c.30 cm wide zone of fault gouge striking 280^{o} and dipping 54^{o} to the southwest (Fig. 2.25F). Several large boulders of meta-rhyolite are entrained in the flysch (Fig. 2.25G). Slickenlines in calcite veins cutting the earlier ductile fabrics in the flysch, plunge 28^{o} towards 215^{o}. Fault drag of cleavage along localised brittle shear planes that cut all earlier fabrics suggest there may have been a later left-lateral oblique-slip thrust sense brittle movement that has overprinted north-directed ductile thrust movements along the flysch shear zone (Fig. 2.25H).

A normal fault, striking 123^{o} and dipping 72^{o} northeast, downthrows unmetamorphosed polymict conglomerate, which is similar to Cretaceous conglomerate on the north front of the range, and cuts the ductile fabrics in the flysch (Fig. 2.25D). To the west, both the flysch and the conglomerate pinch out beneath the brittle thrust placing the Central Nemegt Lower Extrusive sequence over phyllites in the North Central Nemegt Schist sequence (Fig. 2.25D). No fault plane is seen (Fig. 2.21 [8]), but there is a major east-west trending valley which may be a fault. Along the transect, a south-directed brittle thrust striking 083^{o} and dipping 47^{o} to the northwest places phyllites in the North Central Nemegt Schist sequence over the conglomerate (Fig. 2.6 [13])

There is little variation in the metamorphic grade of the Central Nemegt Lower Extrusive sequence. The rhyolite has an albite-chlorite-epidote mineral assemblage, and the volcaniclastic schists have a quartz-chlorite-epidote mineral assemblage, suggesting

that the rocks were metamorphosed in the greenschist facies (Bucher & Frey 1994).

2.6.5 The North Central Nemegt Schist sequence

The North Central Nemegt Schist sequence is a c. 1500 m wide east-west trending belt of phyllite and meta-pelite cropping out in the north of Nemegt Uul. The sequence pinches out c. 5 km east of the central transect (Fig. 2.21 [9]), but thickens to c. 2.5 km in the west (Fig. 2.21 [10]). The phyllites in the south of the sequence (Fig. 2.4 [14]) are to the north of a c. 15 km long, 100-200 m wide highly linear east-west valley (Fig. 2.26A). North of the valley, the phyllites grade into arkosic psammitic schist. The central transect reaches the northern front of Nemegt Uul, where the North Central Schist sequence is thrust north over Mesozoic-Cenozoic basin sediments (Fig. 2.6 [15]).

Lithologies and petrography

Intensely cleaved phyllites crop out in the south of the seqeunce (Fig. 2.6 [16]). To the north, the phyllites grade into cleaved arkosic psammites (Fig. 2.6 [17]), which become progressively more flaggy and weathered approaching the northern front of Nemegt Uul (Fig. 2.6 [18]).

Field observations suggest the phyllites consist of layers of fine quartz, and cleavage forming muscovite and chlorite. The arkosic psammitic schists to the north of the phyllites are clearly cleaved and often flaggy in outcrop. They contain small (0.01-0.5 mm) rounded cloudy feldspar crystals (25-30 %), suggesting that they are alkali feldspars, but they are often almost completely altered to epidote (10 %) and chlorite (15-20 %; Fig. 2.26 B), making it impossible to fully identify their composition. Fractured 0.25-0.5 mm hornblende porphyroblasts (c.5 %) are scattered throughout. The matrix consists of very fine grained recrystallised quartz (40-50 %; c.0.001mm) and cleavage forming chlorite.

Structure and metamorphism

The North Central Nemegt Schist sequence is characterised by dominantly steep south-southeast dipping slatey cleavage in the transect area (Fig. 2.26C), distinguishing it from areas to the south.

The phyllites to the west of the transect in the south of the sequence are cut by a

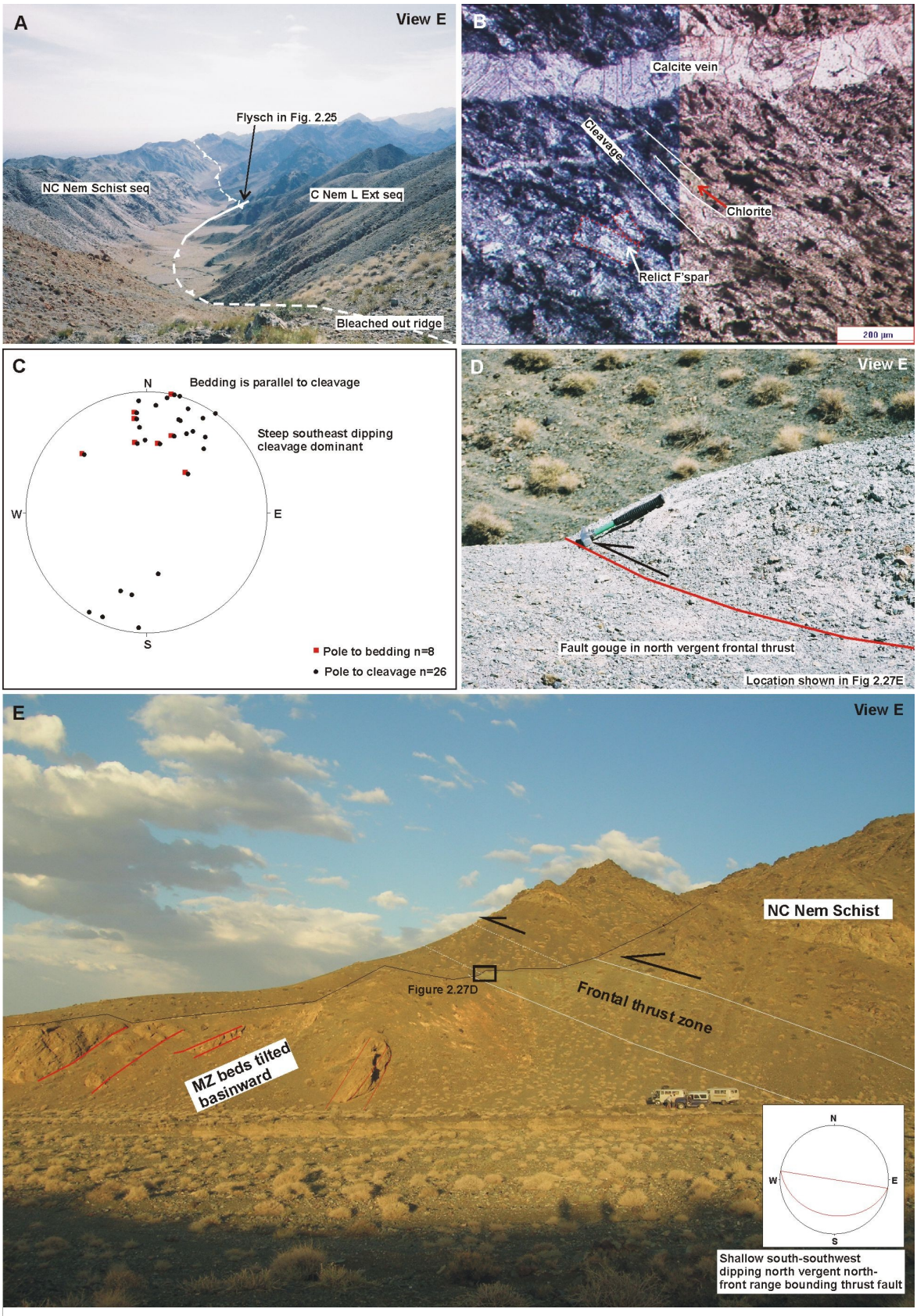

Fig. 2.26. North Central Nemegt Schist sequence (NC Nem Schist). A) Linear E-W valley cutting phyllites in the south of the group located at Fig. 2.21 [8]. The photo is taken from a bleached out ridge crossing the valley, suggesting a fault passes through the area. The flysch shown in figure 2.25 is at the eastern end of the valley and appears to pinch out under the thrust fault placing the Central Nemegt Lower Extrusive sequencen (C Nem L Ext seq) over rocks to the north. A south-directed thrust fault places phyllites and psammites in the North Central Nemegt Schist sequence south over conglomerate at the (continued...)

(...continued from previous page) eastern end of the valley. B) Turbid relict feldspars and chlorite in arkosic psammite (loc. 131). C) Dominantly steep-moderate south dipping cleavage parallel to bedding. D) Fault gouge in the north-directed frontal thrust (loc. 133). E) Cretaceous sediments tilted basinward by the north-directed frontal thrust (loc. 133).

c.15 km long, 100-200 m wide highly linear east-west valley (Fig. 2.21 [8]; Fig. 2.26A). However, Quaternary valley fill obscures the rocks directly adjacent to the valley, so it is not possible to identify a fault plane or ascertain the slip sense at this location. Along the transect, phyllites are thrust south over unmetamorphosed polymict conglomerate (section 2.6.4).

The north frontal thrust of Nemegt Uul is marked by a 10 m wide bleached zone of gouge and incohesive fault breccia dipping c.35^{o} to the south (Fig. 2.26D; Fig. 2.6 [15]). Cretaceous sediments to the north strike 081^{o} and dip 60^{o} to the north where they have been tilted basinward by the overriding frontal thrust (Fig. 2.26E).

There is little variation in the metamorphic grade through the North Central Nemegt Schist sequence. The quartz-albite-epidote-chlorite mineral assemblage suggests the rocks were metamorphosed in the chlorite zone of the greenschist facies (Bucher & Frey 1994).

2.7 Eastern Nemegt Uul Transect

The Eastern Nemegt Uul transect (Fig. 2.27) begins at the southern front of eastern Nemegt Uul. Exposure is often poor along the line of the transect. In less well exposed areas, little data could be collected. The transect is otherwise continuous through Nemegt Uul to the northern front.

2.7.1 The South East Nemegt Schist sequence

The South East Nemegt Schist sequence is c.100 m wide east-west trending belt of arkosic chloritic schist cropping out on the southern front of Nemegt Uul in the east (Fig. 2.27; Fig. 2.7 [1]). At the southern front, chloritic schist is unconformably overlain by Quaternary alluvial fans. However, to the west, greenschist grade meta-sediments are thrust south over Cenozoic-Cretaceous basin fill (Fig. 2.21 [3]). The northern boundary of the sequence is marked by a steep north-dipping fault zone of unknown slip sense (Fig. 2.7 [2]).

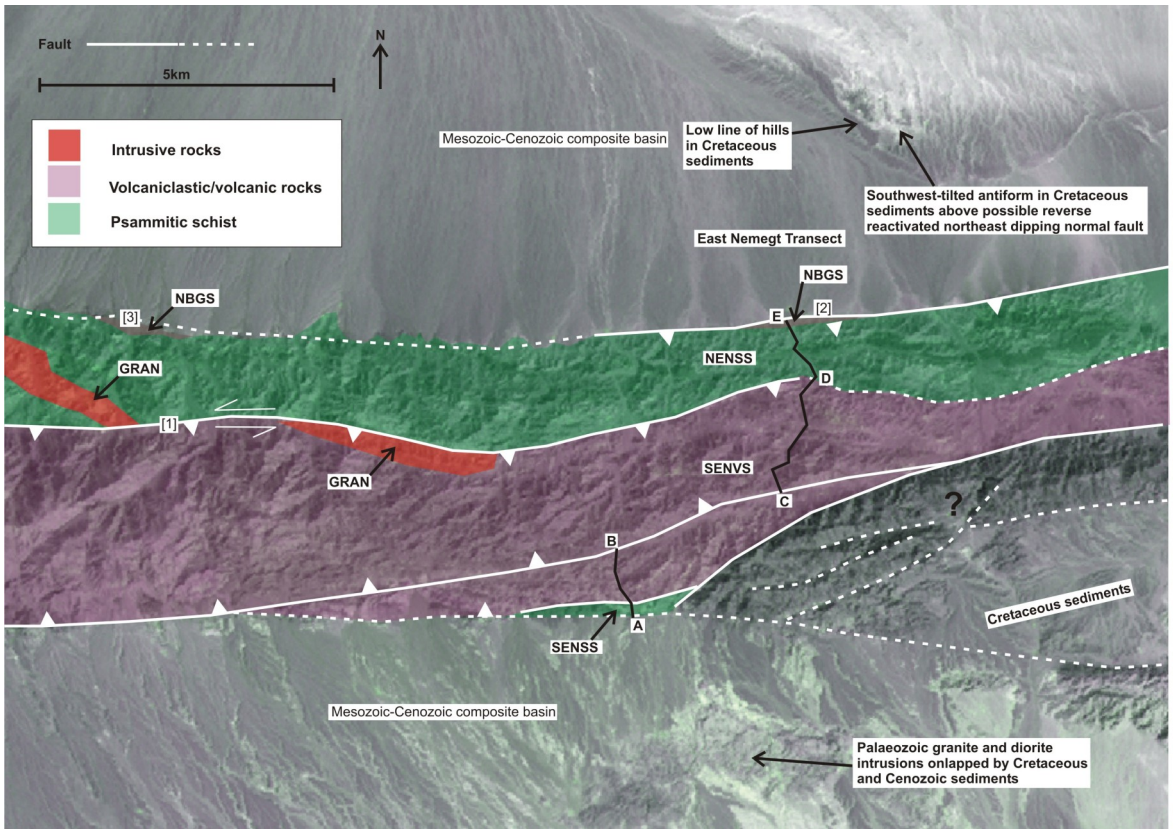

Fig. 2.27. Eastern transect location map with litho-tectonic sequences. Low line of hills and southwest-tilted antiform labelled in the northeast corner of the map are referred to in more detail in chapter 3. Numbers in square brackets [#] refer to locations mentioned in the main text. SENSS = South East Nemegt Schist sequence. SENVS = South East Nemegt Volcaniclastic sequence. NENSS = North East Nemegt Schist sequence. NBGS = Nemegt Basement Gneiss sequence. GRAN = Granite.

Lithologies and petrography

Arkosic chloritic schists crop out close to a major fault zone, and are friable, flaggy and bleached. In thin section, they consist of 0.1-0.5 mm rounded albite grains (10-20 %), internally altered to epidote (5-10 %), in a matrix of 0.1-0.2 mm recrystalised quartz grains (40-60 %) and cleavage forming chlorite (10-20 %; Fig. 2.28A).

Structure and metamorphism

The South East Nemegt Schist sequence is characterised by a penetrative intensely developed cleavage (Fig. 2.28A). Although no fault is seen at the southern front in this area, evidence for the presence of a south-directed shear zone buried beneath the Quaternary alluvial fans at the front is supported by an increase in the intensity of

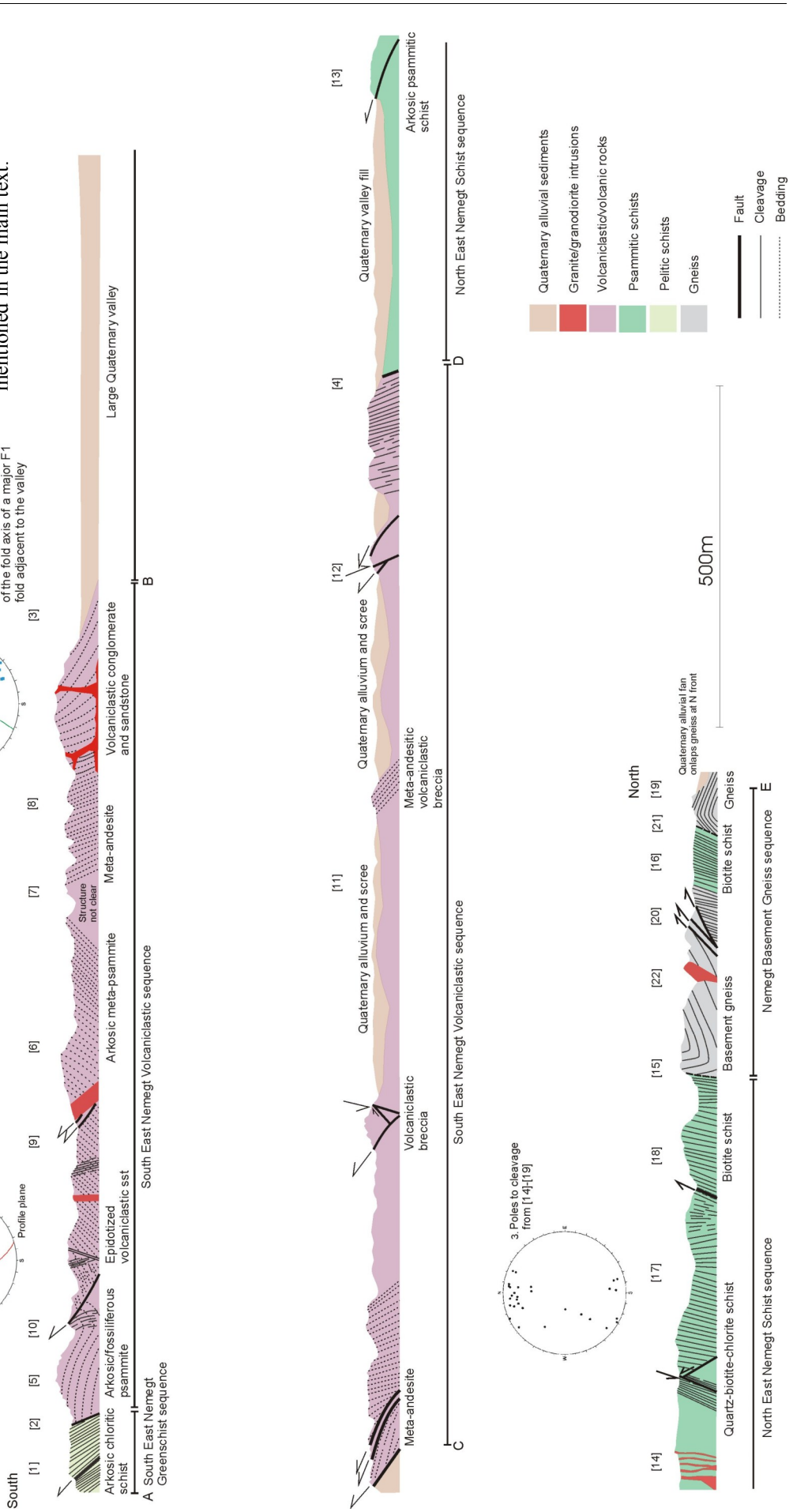

Fig. 2.7. (Duplicate) The east Nemegt Uul transect. Location of all transects shown on Fig. 2.1C. Location of the central Nemegt transect shown in detail on Fig. 2.27. Numbers in square brackets [#] refer to locations mentioned in the main text.

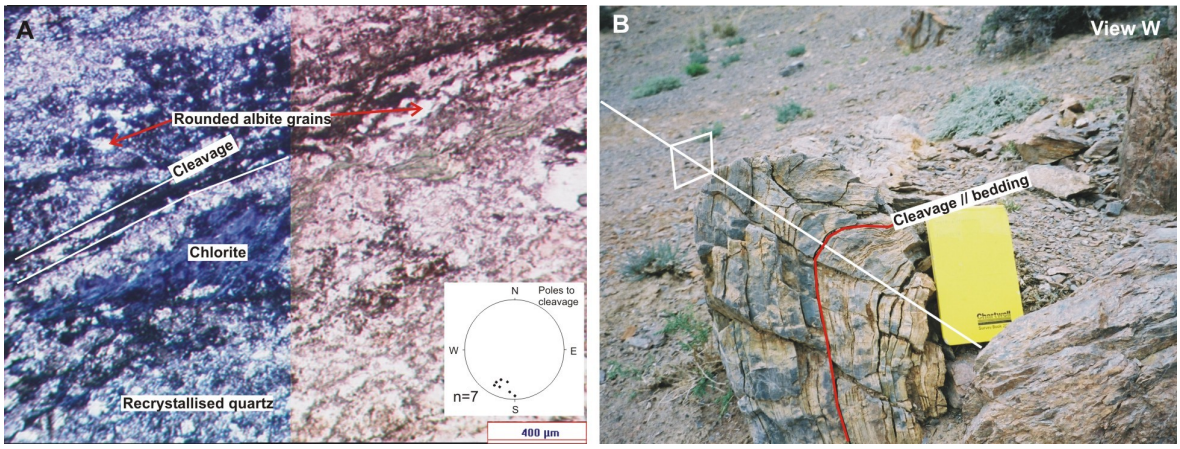

Fig. 2.28. South East Nemegt Schist sequence. A) Albite grains in a matrix of recrystallised quartz and chlorite in arkosic chloritic schist (loc. 153). B) Tight south-vergent folds of cleavage adjacent to the south front of eastern Nemegt Uul (loc. 153).

cleavage towards the front and localised fault-related folding in response to south-directed thrusting adjacent to the southern front (Fig. 2.28B). Along the southern front c.10 km to the west, there is a well documented south-directed brittle thrust zone thrusting meta-psammites and meta-pelites over Cretaceous-Neogene sediments (Fig. 2.22A; Cunningham et al. 1996, Owen et al. 1999). The linear mountain front can be traced to the east on Landsat TM imagery (Fig. 2.27), to the southern extent of the South East Nemegt Schist sequence, suggesting the fault may also exist in this area.

The South East Nemegt Schist sequence has a uniform metamorphic grade. The quartz-albite-epidote-chlorite mineral assemblage suggests the rocks were metamorphosed in the chlorite zone of the greenschist facies (Bucher & Frey 1994).

2.7.2 The South East Nemegt Volcaniclastic sequence

Where it is cut by the eastern transect, the South East Nemegt Volcaniclastic sequence (Fig. 2.27) forms a c. 1 km wide east-west trending belt consisting of arkosic volcaniclastic meta-sandstones interbedded with brachiopod-rich meta-sandstones, arkosic meta-psammites, meta-andesites and arkosic volcaniclastic breccias. The southern boundary of the sequence is marked by a steep north-dipping fault zone of unknown slip sense (Fig. 2.7 [2]). The sequence is cut by two major linear valleys (Fig. 2.7 [3,4]). The northernmost of these valleys (Fig. 2.7 [4]) is broadly east-west trending and marks the northern boundary of the sequence.

Lithologies and petrography

In the south of the area, arkosic volcaniclastic meta-sandstones are exposed in isolated outcrops in hillsides which are often draped by scree (Fig. 2.7 [5]). They are interbedded with brachiopod-rich meta-sandstones that are often weathered and crumbly. To the north, lower hills draped in scree and poor flaggy outcrops mark a change in lithology to arkosic meta-psammite (Fig. 2.7 [6]).

To the north (Fig. 2.7 [7]), a c.10 m wide east-west valley marks a contact between the arkosic meta-psammites to the south and the meta-andesites to the north (Fig. 2.29A). The actual contact is not exposed. To the north, arkosic volcaniclastic conglomerates lie conformably on top of the meta-andesite (Fig. 2.7 [8]). A number of granodiorite dykes cut through the south of the area. In places, they cut early south-directed brittle faults (Fig. 2.7 [9])

The arkosic volcaniclastic meta-sandstones are clast supported. They consist of small (0.5 mm) rounded clasts of meta-andesite (30-35 %), containing 0.05-0.1 mm interlocking albite laths, often completely altered to epidote (10 %) and chlorite (c.5 %), 0.2-0.6 mm sub-angular feldspar grains (20-30 %) and 0.05 mm recrystallised quartz grains (40 %; Fig. 2.29B).

The fossiliferous meta-sandstone beds have a similar mineralogy, but also contain fragments of unidentified brachiopods (Fig. 2.29C). In thin section, there are several 0.2 mm anhedral calcite grains (10-15 %) with rib-like structures representing shell fragments, but were too fragmented to identify.

The arkosic meta-psammites are clast supported and consist of 0.1 mm rounded alkali feldspar grains (30-40 %), often altered to epidote (10-30 %; Fig. 2.29D), in a matrix of 0.05-0.1 mm rounded quartz grains (30-40%) and chlorite (5-10 %). Brown staining suggests iron oxide is present in the matrix.

The meta-andesites consist of 1-2 mm subhedral albite phenocrysts (5-10 %) in a groundmass of interlocking 0.2-0.4 mm subhedral feldspar laths (60-70 %). Feldspar is variably altered to chlorite (10-15 %; Fig. 2.29E) and epidote (5-10 %), some leaving only relict outlines. Small (0.1 mm) anhedral opaque crystals (c. 5 %) overgrow everything.

The arkosic volcaniclastic conglomerates contain brecciated 5-15 mm sub-angular

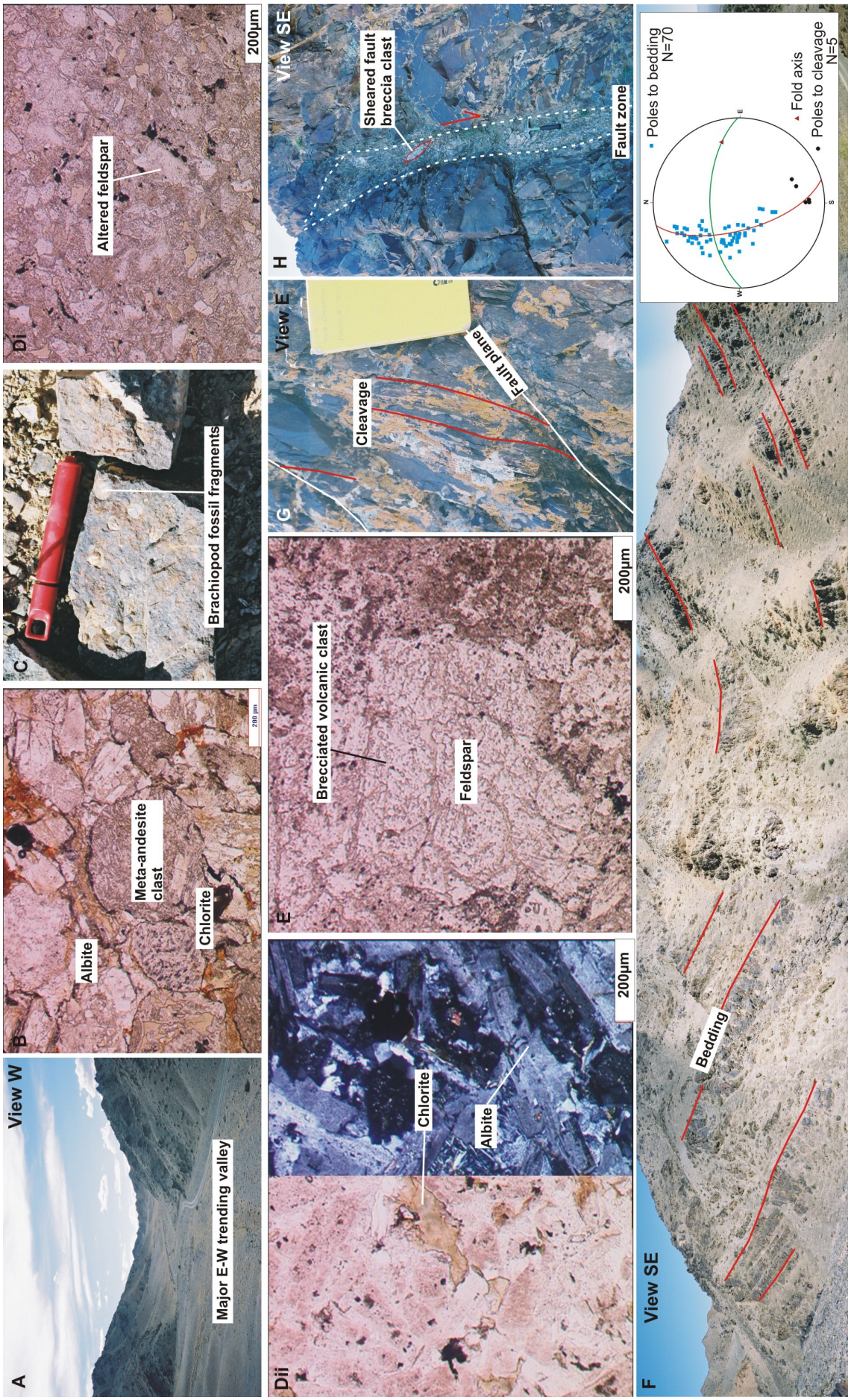

Fig. 2.29. South East Nemegt Volcaniclastic sequence. A) Major east-west valley cutting through the range (passes through B and C on Fig. 2.27) marks the trace of a major fault (loc. 170). B) Small rounded clasts of meta-andesite, albite and recrystallised quartz in arkosic meta-sandstone (loc. 154). C) Unidentified brachiopod (continued...)

(continued from previous page) remains in fossiliferous sandstone (loc. 154). Di) Altered feldspars in arkosic meta-psammite (loc. 158). Dii) Albite and chlorite in meta-andesite found interbedded with volcaniclastic meta-psammites (loc. 168). E) Brecciated volcanic clast (loc. 183). F) Open east west trending folds of bedding in fossiliferous and volcaniclastic sandstone with stereonet showing poles to bedding and poles to cleavage (loc. 154). G) Typical south-directed brittle thrust planes (loc. 155). H) Incohesive fault breccia along normal fault (loc. 158).

clasts of meta-andesite (5-10 %) and rounded 0.25-1 mm albite grains (20 %). Albite is often altered to epidote (10-15 %) and chlorite (c.5 %). A fine groundmass of quartz (50-75) surrounds the clasts and albite grains.

Structure and metamorphism

The area is characterised by moderately inclined northeast plunging open folds of bedding (Fig. 2.7 stereonet 1), which transition to steeply inclined open steeply north plunging folds of bedding in the north (Fig. 2.7 stereonet 2) adjacent to a northeast-southwest valley that cuts through the range. The apparent anticlockwise rotation of the fold axis (Fig. 2.7 stereonet 2) adjacent to this valley suggests that the valley may contain a left-lateral fault. Cleavage is rare, but where it was measured in the southern part of the sequence it is axial planar to folds of bedding (Fig. 2.29F).

At (Fig. 2.7 [10]), a series of characteristic cm-wide shear bands that strike 013^{o} and dip 48^{o} to the northwest cut the meta-psammites (Fig. 2.29G). Fault-dragged cleavage adjacent to the shear bands suggests approximately south-directed thrusting (Fig. 2.29H). Approximately 1200 m from the southern front of Nemegt Uul, a c. 500 m wide major linear east-west valley crosses the range and marks the northern boundary of the South East Nemegt Volcaniclastic sequence (Fig. 2.7 [3]; Fig. 2.29A). Quaternary alluvial sediments and scree drape the landscape around the valley, making it impossible to determine if there is a fault zone, and what its slip sense might be.

Moving north into the centre of the range (Fig. 2.7 [11]), the quality of the exposure becomes poorer. Scree covers low-lying hills, making it difficult to document the structure. Approximately 200 m from the northern boundary of the sequence (Fig. 2.7 [12]) a steep gully is filled with foliated cataclasite and gouge that strikes 341^{o} and dips 70^{o} to the southwest. No slickenlines were found but fault-dragged foliation within the fault zone suggests the fault has moved in a normal sense (Fig. 2.29H).

The northern boundary of the sequence is marked by an east-west trending valley (Fig. 2.7 [4]). Quaternary alluvial sediment drapes the valley making it difficult to

establish the presence of a fault zone. However, the valley can be traced to the west on Landsat TM imagery to a major left-lateral fault zone which cuts and offsets a granite pluton in central Nemegt Uul (Fig. 2.27 [1]).

The greenschist metamorphic grade is constant throughout the South East Nemegt Volcaniclastic sequence. The volcaniclastic schists all have a quartz-albite-chlorite-epidote mineral assemblage, and the meta-andesites have an albite-chlorite-actinolite mineral assemblage, suggesting that the rocks were metamorphosed in the chlorite zone of the greenschist facies (Bucher & Frey 1994).

2.7.3 The North East Nemegt Schist sequence

The North East Nemegt Schist sequence crops out in a c.1.5 km wide east-west trending belt in northeastern Nemegt Uul (Fig. 2.27). From south to north, it consists of arkosic psammite, quartz-biotite-chlorite schist and quartz-biotite-schist.

Lithologies and petrography

In the southern part of this sequence, wide stretches of low scree cover isolated outcrops of arkosic psammite in low hills, making it difficult to identify the contacts between lithologies (Fig. 2.7 [13]). Approximately 750 m from the northern front, the quality of the exposure improves, marking a change in lithology to quartz-biotite-chlorite schist which is intruded by small 5 m wide granodiorite dykes and centimetre- to metre-scale granite pegmatite dykes (Fig. 2.7 [14]). Approximately 400 m from the northern front of Nemegt Uul, the quartz-biotite-chlorite schists rest on an east-west trending angular unconformity that dips 50-70^{o} to the south along the top of a c. 300 m wide east-west trending belt of gneiss (Fig. 2.7 [15]). A 70-100 m east-west trending belt of biotite-schist has been dismembered from the main sequence and is overthrust by the gneiss (Fig. 2.7 [16]). However, 30-50 m from the northern front the biotite-schist rests unconformably upon another sliver of basement gneiss. Repetition of the lithological sequence either side of both unconformities suggests they represent the same erosion surface that has been tectonically duplicated.

The arkosic psammite consists of 0.1 mm interlocking sub-rounded quartz grains (50 %) and 0.1-0.5 mm sub-rounded fractured albite grains (25 %), mostly surrounded by

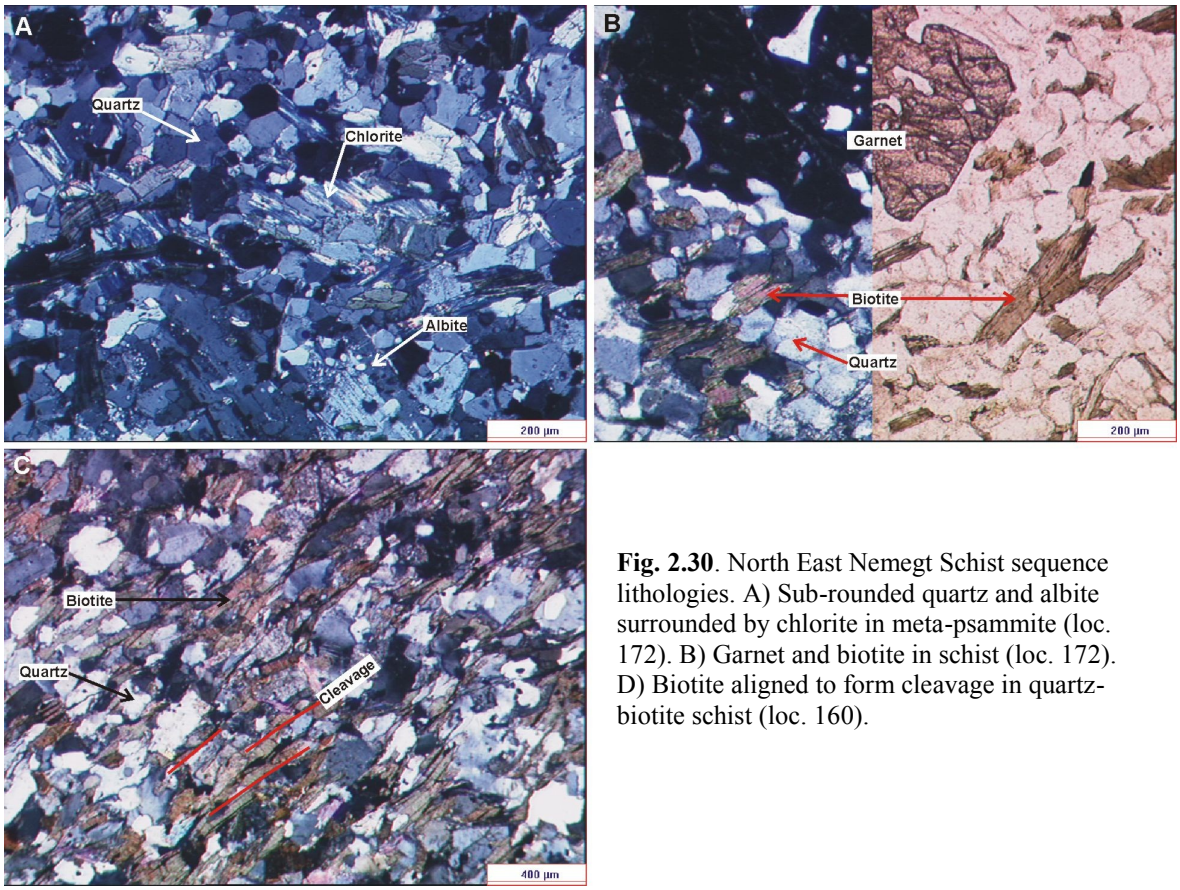

Fig. 2.30. North East Nemegt Schist sequence lithologies. A) Sub-rounded quartz and albite surrounded by chlorite in meta-psammite (loc. 172). B) Garnet and biotite in schist (loc. 172). D) Biotite aligned to form cleavage in quartz-biotite schist (loc. 160).

muscovite (5 %) and chlorite (10 %; Fig. 2.30A). In some places there are bands of fine (<0.001 mm) recrystallised quartz (10 %).

The quartz-biotite-chlorite schists consist of layers of 0.1 mm sub-angular quartz grains (70 %) and layers of cleavage forming chlorite (5 %). In places there are c.0.5 mm rounded relict garnets (10 %) overgrowing the cleavage forming minerals. The garnets are often included by quartz and heavily embayed around the edges. Small 0.4 mm subhedral biotite laths (10 %) overgrow the quartz matrix but are aligned parallel to the aligned chlorite (Fig. 2.30B).

The biotite-schists consist of 0.2-0.5 mm rounded quartz grains (65 %) and occasional 0.2-0.5 mm albite grains (10 %) wrapped in 0.5-1 mm laths of biotite (20 %; Fig. 2.30C). Small (0.1-0.2 mm) anhedral garnets (5 %) overgrow the quartz.

Structure and metamorphism

The North East Nemegt Schist sequence is characterised by pervasive near-vertical dominantly south-dipping cleavage in the eastern transect area (Fig. 2.31A). The south and centre of the area is cut by brittle thrust faults and shear bands (Fig. 2.31B-H;

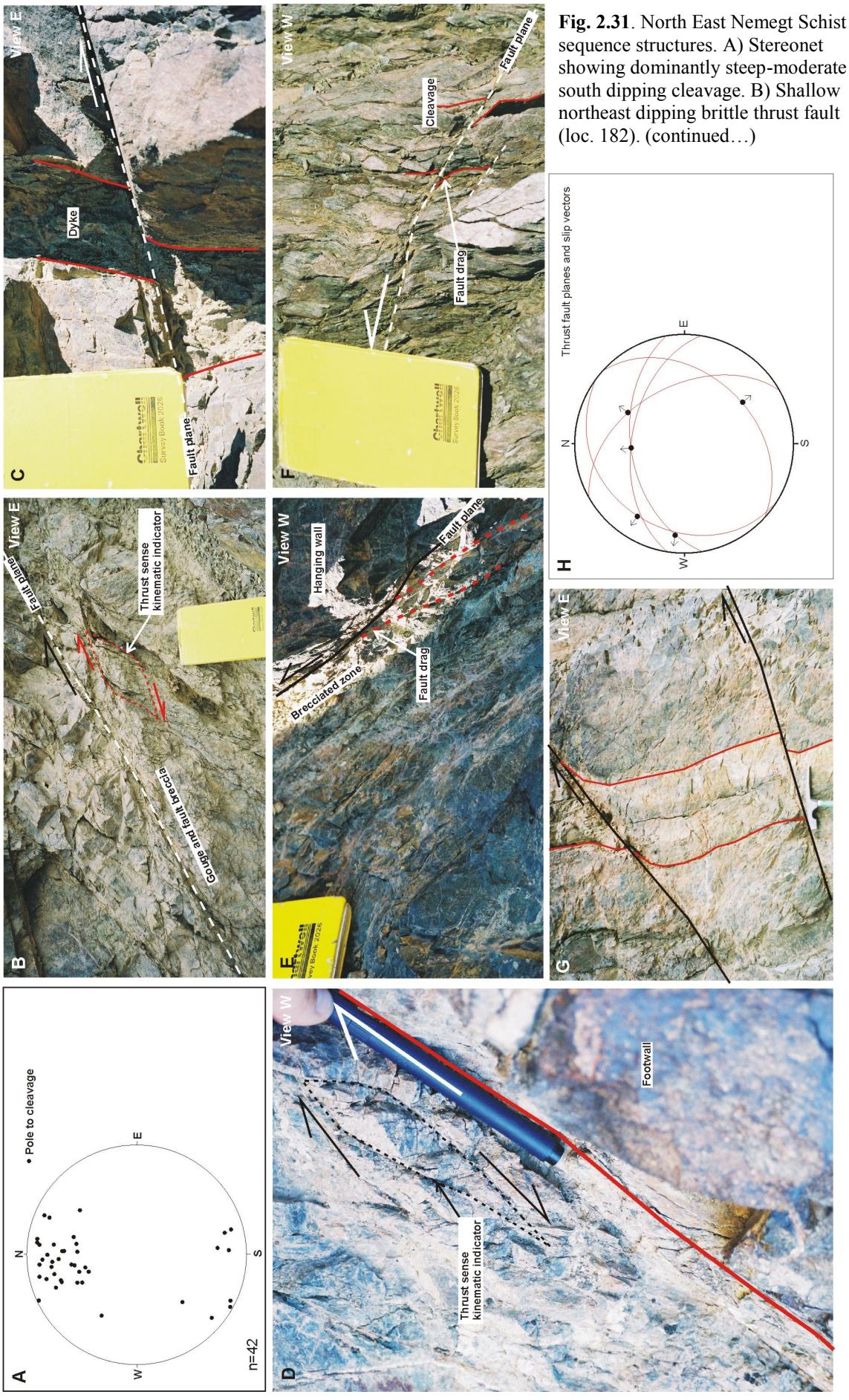

Fig. 2.31. North East Nemegt Schist sequence structures. A) Stereonet showing dominantly steep-moderate south dipping cleavage. B) Shallow northeast dipping brittle thrust fault (loc. 182). (continued…)

(continued from previous page) C) South-directed brittle thrust fault displacing granodiorite dyke (loc. 179). D) Steep south-dipping zone of fault breccia with north-directed reverse sense kinematic indicators (loc. 178). E) Shallow-moderate southwest dipping zone of cohesive fault breccia with north-directed thrust sense kinematic indicators (loc. 177). F) Typical shallow south dipping shear plane with fault drag suggesting north-directed thrust sense movement has occurred (loc. 174). G) Typical small brittle fractures with fault-dragged bedding suggesting thrust sense movement has occurred (loc. 174). H) Stereonet showing the range of orientations and slip vectors of thrust faults cutting the rocks in the sequence.

Fig. 2.7 [13-17]) that range in size from single fault planes, some of which displace granodiorite dykes by c. 10cm (Fig. 2.31C), to 30 cm wide zones of cohesive fault breccia (Fig. 2.31E).

Approximately 500 m from the northern front, the quality of the exposure improves. Flattened schists crop out with a dominant steep south dipping cleavage (Fig. 2.31A; Fig. 2.7 [18]).

Approximately 250 m from the north front, biotite-schist and gneiss are intruded by two granites: the older granite is cut by the younger granite. Geological mapping revealed a structural and unconformable relationship between the schists, gneiss and intrusions (Fig. 2.32). No basal conglomerate was identified in the schists that sit unconformably above the gneiss. However, pegmatite dykes that intrude the gneiss are truncated by the contact (Fig. 2.32), suggesting that it is an unconformity, not the edge of an intrusion.

The metamorphic grade through much of the North East Nemegt Schist sequence increased to the north. In the south, the arkosic psammitic schists have an albite-quartz-muscovite-chlorite mineral assemblage, suggesting that they were metamorphosed in the chlorite zone of the greenschist facies, but cleavage-parallel laths of biotite in the schists in the north of the sequence suggest the rocks were metamorphosed in the biotite zone of the greenschist facies (Bucher & Frey 1994). In the north, garnet overgrowths (Fig. 2.30B) cut metamorphic fabrics in thin section and the presence of large flakes of muscovite, with no preferred orientation, in the rocks directly adjacent to granite intrusions, suggest that the quartz-biotite-chlorite schists and biotite schists were metamorphosed by the granites after the regional metamorphism.

2.7.4 The Nemegt Basement Gneiss

The Nemegt Basement Gneiss sequence is a discontinuous belt of basement orthogneiss cropping out on the northern front of Nemegt Uul (Fig. 2.27, Fig. 2.32). It is

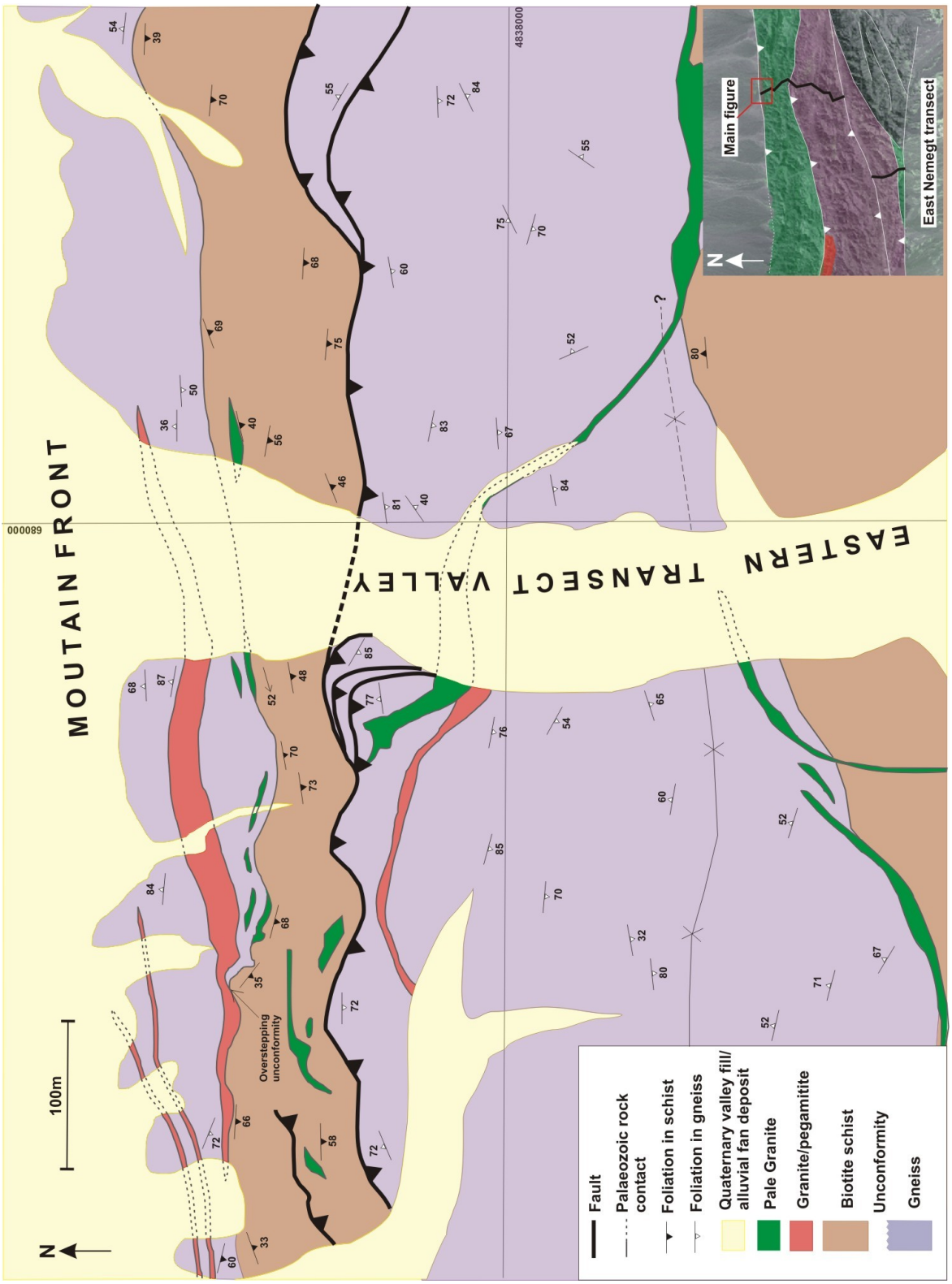

Fig. 2.32. Detailed geological map of the northern front along the East Nemegt transect. Coordinates system is UTM WGS84 sector 47T. The red granite/pegmatite is truncated by the angular contact between the gneiss and the schist suggesting it is an unconformity.

described here where it is exposed along the eastern Nemegt Uul transect (Fig. 2.27 [2]), but it also crops out in a narrow (100 m wide by 500 m long) belt along the northern front approximately 10 km to the west of the eastern transect (Fig. 2.27 [3]). In the south, the North East Nemegt Schist sequence unconformably oversteps the gneiss and the oldest phase of granite intrusion in the area (Fig. 2.7 [15]; Fig. 2.32). In the north, the gneiss is onlapped by Quaternary alluvial fan sediments (Fig. 2.7 [19]).

Lithologies and petrography

The orthogneiss consists of 0.5-1 mm anhedral feldspar crystals (40-50 %), some of which are microcline (c.5 %; Fig. 2.33A), between 0.5-4 mm wide layers of 0.25 mm recrystallised quartz grains (20-30 %), chlorite (10-15 %) and biotite (5-10 %; Fig. 2.33B). Stubby 0.1-0.2mm subhedral epidote crystals (5-10 %) overgrow the microcline and chlorite. A foliation in the orthogneiss, and its feldspathic composition suggest it is a foliated migmatite.

Structure and metamorphism

The northern front of Nemegt Uul in the east, has a complex structure of unconformities, thrusts and intrusions (Fig. 2.32). The gneiss has a clear fabric (Fig. 2.33C), which is folded into open east-west trending folds on a 10 m scale . However, on a smaller scale, it is often deformed into north-vergent folds on the scale of 10 cm (Fig. 2.33D) to 1 m. This contrasts with the schists that unconformably overlie the gneiss-schist unconformity and which have a pervasive cleavage but are not obviously folded like the gneiss. The gneiss must have been affected by the same contractional deformation event which formed the cleavage in the schists. This suggests the orthogneiss already had a fabric to be folded when the schist-cleavage forming deformation event took place. The gneiss is cut by several steep south dipping north-directed brittle thrusts striking 270-317^{o} and dipping 32-44^{o} to the south-southwest (Fig. 2.7 [16]) and south vergent back-thrusts striking c.091^{o} and dipping 64^{o} to the north (Fig. 2.33E-F). Offset pegmatite dykes indicate 1-5 m slip on some of the smaller faults. The northernmost north-directed thrust fault strikes 302^{o} and dips 36^{o} to the southwest (Fig. 2.33E) and can be traced as a bleached white zone of gouge and fault breccia for at least 500 m to the east and west

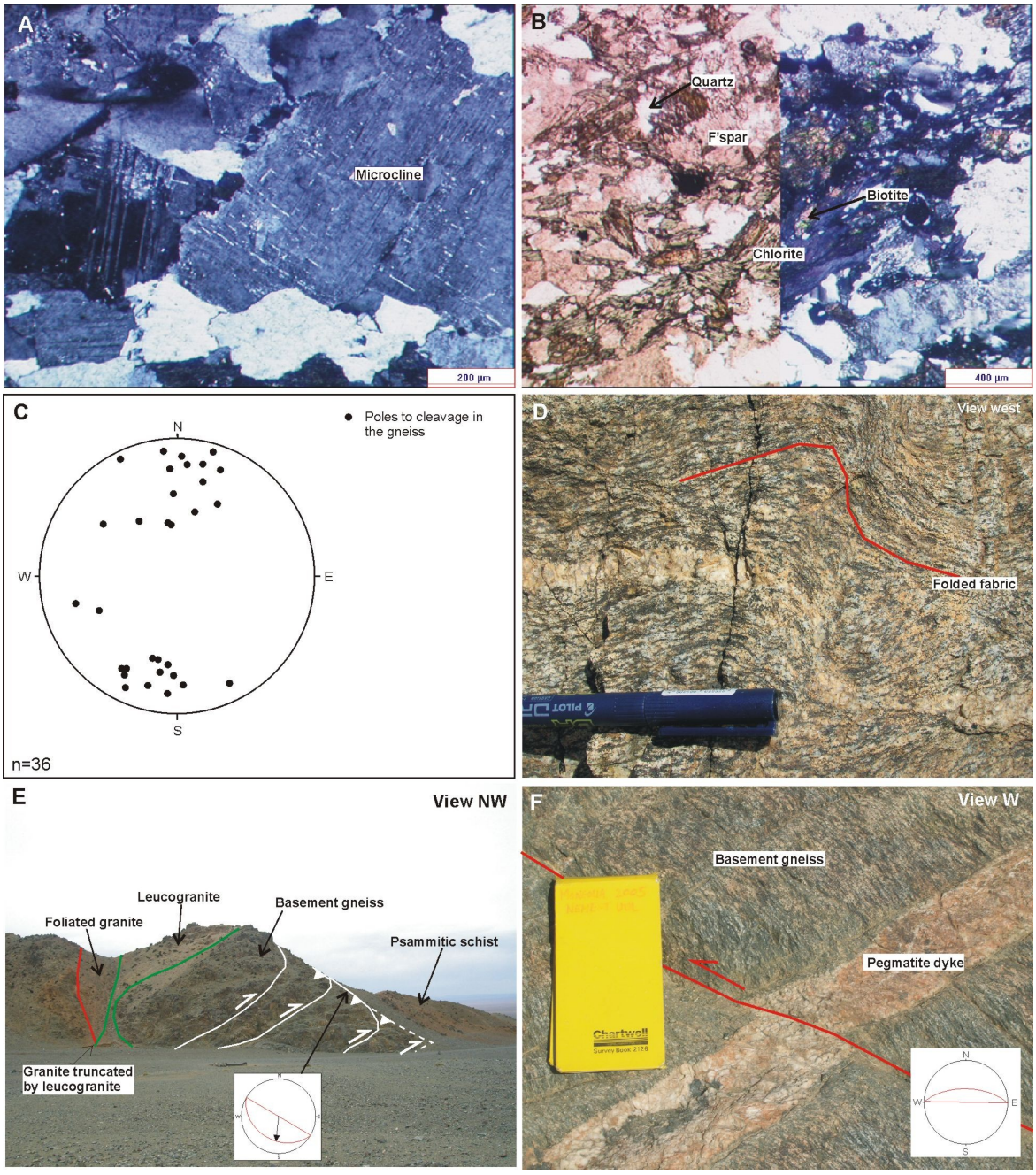

Fig. 2.33. Nemegt Basement Gneiss sequence. A) Interlocking feldspar crystals in gneiss (Loc. 159). B) Finer layer of recrystallised quartz and feldspar surrounded by chlorite and biotite (Loc. 159). C) Stereonet of poles to cleavage in the gneiss. D) Small scale north-vergent folds of fabric in gneiss (Loc. 337). E) Series of three faults thrusting the gneiss north over psammitic schist (Loc. 392). F) Small south-directed back-thrust fault offsetting a pegmatite dyke that has intruded the gneiss (Loc. 325).

(Fig. 2.32). Slickenlines on the fault plane plunge 36° towards 186° (Fig. 2.33E). The thrust fault carries the orthogneiss north over a belt of biotite-schist belonging to the North East Nemegt Schist sequence. The biotite-schist sits unconformably above another narrow c. 50 m wide east west trending belt of orthogneiss (Fig. 2.7 [21]). The angular unconformity trends east-west and dips between 50-70° to the south. The gneiss is

onlapped by Quaternary alluvial fans at the northern front (Fig. 2.7 [19]). Several of the faults in the area are cut by leucogranite intrusions (Fig. 2.7 [22]).

The orthogneiss has a chlorite-biotite-hornblende mineral assemblage, indicating greenschist grade metamorphism (Bucher and Frey, 1994). However, it may have undergone recrystallisation, overprinting evidence of earlier metamorphic events.

2.8 Granites

Palaeozoic meta-sedimentary and meta-volcanic rocks in Nemegt Uul are cut by several granitic intrusions. In the northwest of Nemegt Uul, a 2 km long, by 1 km wide granite pluton in the West Nemegt Psammite sequence is cut and left-laterally offset by a major range-traversing fault (Fig. 2.11 [9]). In the south, the South Central Nemegt Extrusive sequence is cut by another large granite intrusion (Fig. 2.21 [11]). In the east, another granite is cut by a left-lateral south-vergent oblique-slip thrust fault (Fig. 2.27 [1]). The fault can be traced east on Landsat TM imagery, to the boundary between the Northeast Nemegt Schist sequence and the Southeast Nemegt Vocaniclastic sequence (Fig. 2.27).

The granites described above have similar mineralogies of interlocking subhedral albite (10-20 %) and microcline crystals (20-30 %; Fig. 2.34A), 0.2 mm anhedral quartz crystals (40-50 %), feldspars showing microperthitic texture (c.15 %), and 0.4 mm anhedral hornblende crystals (5-10 %). These are overprinted by 0.3 mm patches of chlorite (5-10 %) and biotite (c.5 % ;Fig. 2.34B). Chlorite and epidote (c.5 %) are often seen within and around the edges of plagioclase crystals and obscuring them. In some instances, intergrown quartz and alkali feldspar have produced a graphic texture (Fig. 2.34C). Overgrowths of chlorite and biotite and the breakdown of feldspars in the granites to epidote suggests these granites have been in greenschist facies conditions (Bucher and Frey, 1994).

In the east, two generations of granite intrusion are seen at the northern front (Fig. 2.32). An older foliated meta-granite is cut by the younger leucogranite (Fig. 2.32). The North East Nemegt Schist sequence oversteps the contact between the foliated meta-granite and the Nemegt Basement Gneiss (Fig. 2.32). The foliated meta-granite is very fine grained, and sometimes has a clear folded fabric in outcrop (Fig. 2.34D). In thin section it consists of small (0.01 mm) interlocking alkali feldspar crystals (c. 70 %) and

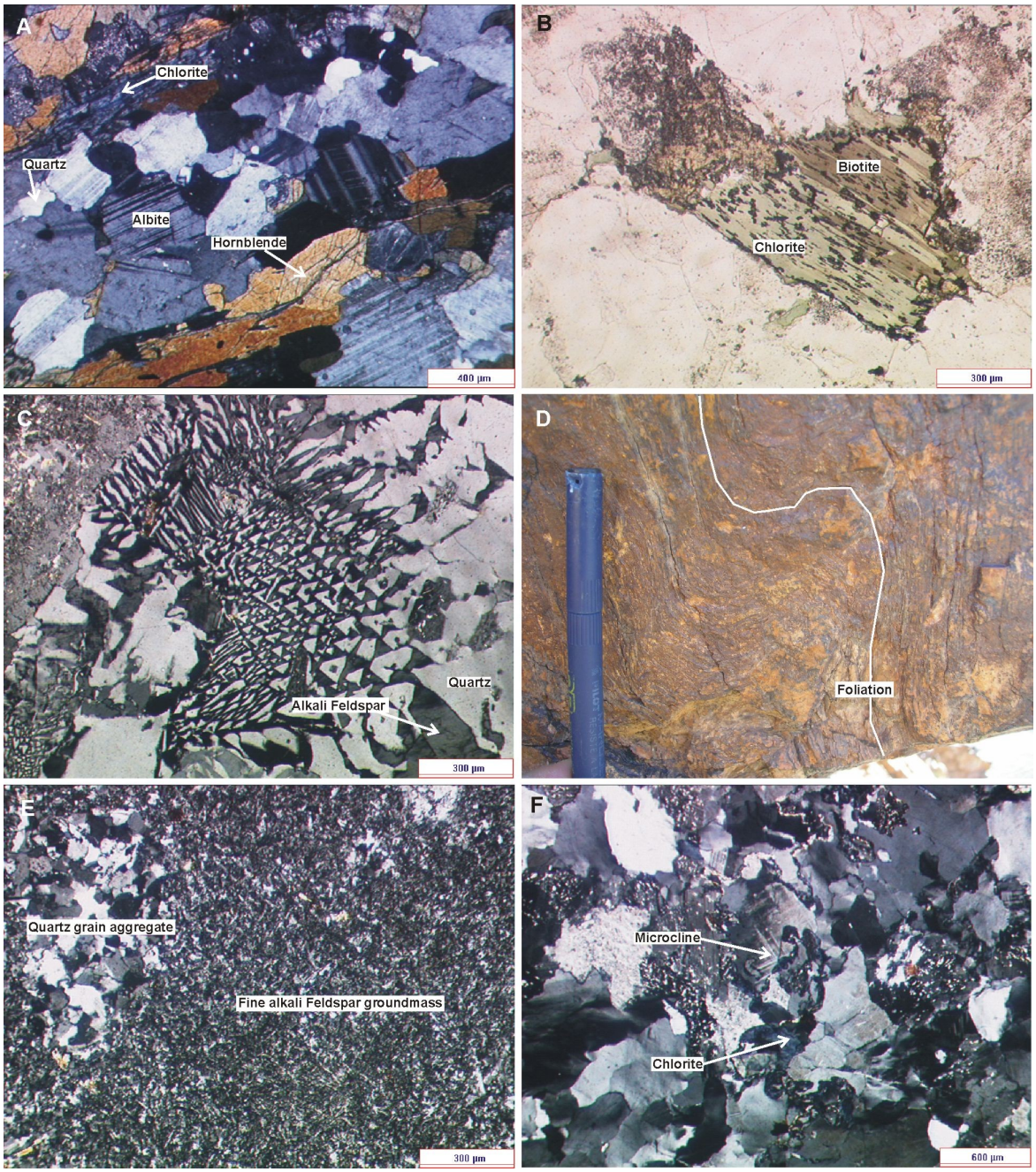

Fig. 2.34. Petrography and structure of the granites. A) Interlocking microcline and albite crystals (loc. 338). B) Inter-layered chlorite and biotite (338). C) Graphic texture in foliated pegmatite (Loc. 337). D) Folded fabric in granite (Loc. 334). E) Very fine alkali feldspar groundmass (Loc. 335). F) Microcline with chlorite (Loc. 332).

grain aggregates of recrystallised quartz (c. 20 %; Fig. 2.34E). Small amounts of chlorite (5-10 %) are present surrounding some of the feldspar crystals.

The leucogranite consists of large (0.5-1 mm) interlocking quartz (30-40 %), microcline (20-30 %) and albite crystals (15-25 %), often partially altered to chlorite (5-10 %; Fig. 2.34F).

Unfortunately, there are no geochronological age constraints on either generation of granite or the thrust faults. The older granite intruded the gneiss before the schist protolith was deposited on the Nemegt Basement Gneiss-North East-Nemegt Schist sequence unconformity (Fig. 2.32), suggesting it is much older than then leucogranite which cuts the unconformity. The granites contain chlorite and epidote, which are common products from the breakdown of feldspars during greenschist facies metamorphism (Bucher & Frey 1994). This suggests that the granites have been affected by the same regional metamorphic event as the rocks they have intruded.

2.9 The Altan Uul Ophiolite

Altan Uul and Nemegt Uul contain several fault bound mafic-ultramafic sequences consisting of peridotite, serpentinite, cumulate gabbro, sheeted dykes, pillow lavas and deep marine sediments, including jasperoids. A structural and lithological transect was recorded through the largest of these sequences in western Altan Uul (section 2.4). Similar mafic-ultramafic sequences crop out in central Altan Uul and western Nemegt Uul (Fig. 2.35B).

Gabbro is the most common rock-type in each of the mafic-ultramafic sequences. To determine the genetic origin of the mafic-ultramafic sequences, and to enable comparison between areas, samples of gabbro were taken along transects in western Altan Uul, and central Altan Uul for petrographic analysis. Samples of gabbro from Altan Uul were prepared for analysis using standard x-ray fluorescence spectroscopy (XRF) techniques at the University of Leicester (Tarney & Marsh 1991). All the zones that samples were taken from were fractured and multiply veined. Only the least deformed, veined and fractured samples were chosen for XRF analysis.

2.9.1 Gabbro petrography

There are variations in the percentage of each mineral, grain morphology and grain size across the samples (Fig. 2.9E-J). However, they all, with one exception, have similar petrography and on the basis of texture, similar crystallisation histories.

Small (0.1 mm) subhedral olivine crystals (c. 5 %), 0.25-8 mm subhedral plagioclase feldspar (typically 30-40 %), and 1-6 mm subhedral, interstitial, augite

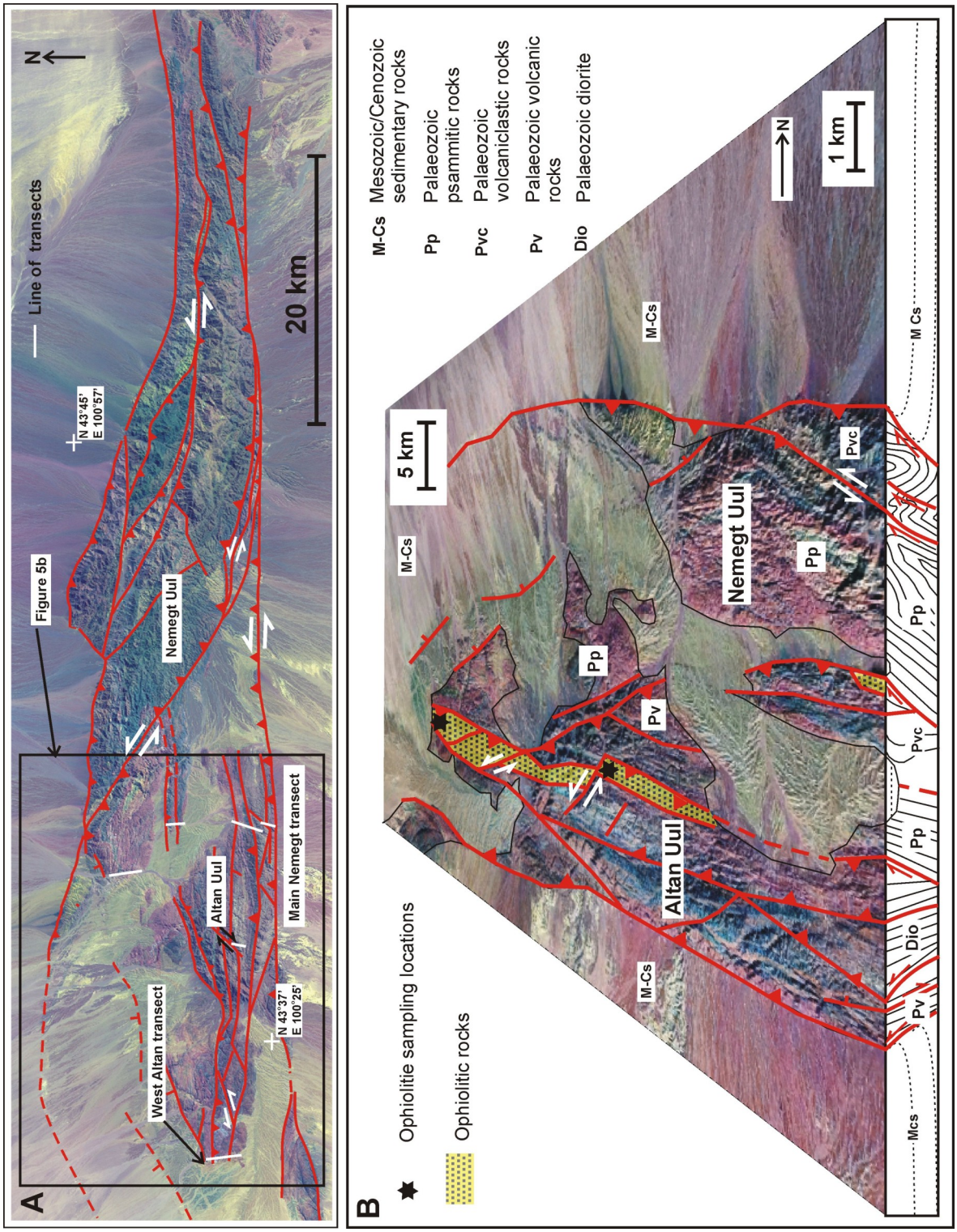

Fig.2.35. A) Photo-geological interpretation of Landsat TM image of Nemegt Uul and Altan Uul showing the location of the West Altan transect. B) Oblique westward view of western Nemegt Uul and Altan Uul, showing cross-strike basement structure of western Nemegt Uul and eastern Altan Uul, and the along-strike continuity of the Altan Uul Ophiolite sequence. Approximate locations of gabbro samples nalysed for major and trace element chemistry are marked. GPS coordinates are given in Table 1.

	A05/1/10	A05/1/12	A05/2/24	A05/2/25	A05/2/26a	A05/2/26b	A05/2/26c	A05/4/40	A05/4/43
Type	Gabbro	Gabbro	Gabbro	Fine gabbro	Gabbro	Gabbro	Gabbro	Gabbro	Gabbro
Lat	43°38'56"	42°38'59.1"	43°39'36.29"	43°39'29"	43°39'42.6	43°39'42.6	43°39'42.6	43°39'24.6"	43°39'31"
Long	100°19'18"	100°19'3.4"	100°19'21"	100°19'16.5"	100°19'11.1"	100°19'11.1"	100°19'11.1"	100°31'4.9"	100°30'58.6"
wt%									
SiO_2	52.58	47.750	49.620	50.59	49.990	51.04	51.28	46.56	50.18
TiO_2	0.28	0.2	0.26	0.29	0.17	0.14	0.14	0.2	0.36
Al_2O_3	16.62	19.38	14.96	16.44	19.68	20.57	19.19	17.05	15.4
Fe_2O_3	5.2	2.95	5.91	5.94	4.64	3.97	4.37	6.02	5.12
MnO	0.101	0.059	0.111	0.111	0.094	0.088	0.09	0.096	0.103
MgO	7.44	8.39	10.15	10.21	8.03	7.14	8.01	10.31	9.43
CaO	11.4	12.64	13.48	12.9	12.1	11.84	10.47	11.89	15.98
Na_2O	4.41	2.82	2.98	2.55	3.03	3.25	3.85	2.4	2.42
K_2O	0.315	0.722	0.105	0.249	0.558	0.75	0.577	0.02	0.026
P_2O_5	0.009	0.008	0.003	0.003	0.004	0.002	0.007	0.008	0.007
Total	98.36	94.92	97.58	99.28	98.30	98.79	97.98	94.55	99.03
ppm									
As	5.2	1.1	5.5	2.5	0.7	1.6	0.0	37.6	1.2
Ba	19.4	54.0	18.5	53.8	49.7	68.1	45.2	10.8	24.5
Co	19.8	11.3	26.5	25.5	18.8	15.8	19.3	30.4	22.7
Cr	105.8	2617.6	912.4	941.2	710.1	528.6	538.5	650.9	1402.3
Cu	38.5	31.0	20.7	49.8	80.1	73.9	81.6	141.2	56.2
Ga	11.8	11.1	11.7	13.0	12.9	12.1	11.3	12.4	11.9
Mo	1.1	1.5	1.7	1.4	0.8	0.7	1.0	0.6	1.7
Nb	-0.1	0.2	-0.9	-0.7	0.2	0.1	0.4	-0.2	1.4
Ni	38.6	57.7	140.4	149.6	198.0	165.7	181.2	237.2	111.6
Pb	1.5	1.1	-0.3	0.9	3.2	0.3	3.2	2.3	2.0
Rb	10.1	19.9	3.1	7.1	12.8	17.9	14.5	0.8	2.4
Sc	41.7	44.7	47.8	51.0	31.5	26.3	27.4	34.4	63.0
Sn	-0.4	0.4	-1.6	-0.9	1.4	-2.1	1.1	-1.3	-1.1
Sr	109.9	192.4	171.5	132.3	278.8	262.5	240.1	180.7	273.1
Th	1.7	1.9	3.4	4.1	2.8	3.3	4.1	4.3	0.3
U	0.0	-0.2	1.5	0.9	0.0	-0.2	-0.2	0.8	1.6
V	146.3	119.5	163.8	166.8	92.1	73.3	71.3	105.9	220.0
W	0.8	-2.2	-1.2	2.3	-0.1	1.3	0.3	0.9	0.6
Y	9.6	8.1	6.0	8.0	4.8	3.7	6.3	3.1	10.3
Zn	22.6	12.5	27.0	28.7	22.7	17.9	22.9	31.4	23.9
Zr	11.7	10.9	4.8	5.1	6.1	0.2	6.4	2.4	5.3

Table 1. XRF analyses of gabbro samples from Altan Uul.

(typically 5-30 %) are the primary minerals in the gabbro. Plagioclase feldspar crystals are heavily altered, making it difficult to estimate their anorthite content, although some retain lamellar twinning. They are commonly replaced with clusters of 0.02 mm stubby epidote grains (10-20 %). 0.5 mm anhedral calcite (5-15 %) cuts the epidote and plagioclase crystals. Fractures in the feldspars, and elsewhere in the samples, contain chlorite (c. 5 %). Chlorite also occurs as streaky patches within feldspar crystals. Augite crystals typically have a rim of actinolite (5-10 %). In some samples, there is a groundmass composed of very fine serpentine (up to 30 %) and brucite (up to 5 %). Where serpentine is present, 0.02-2 mm strands of fibrous chrysotile (20 %) and 1-2 mm streaky talc crystals (c. 5 %) can sometimes be seen overgrowing the groundmass. Knots of 0.5 mm subhedral hornblende (up to 30 %) are sometimes present, cutting the remains of augite, actinolite, calcite, chlorite, talc, chrysotile and the serpentine groundmass. All the samples have thin (0.5-1 mm) veins of epidote and sometimes quartz cutting all other minerals.

One gabbro sample (A05/4/43) has a slightly different mineralogy to the other samples. In this rock, 1 mm euhedral enstatite (50 %) crystals with augite exsolution lamella and 0.25 mm subhedral plagioclase feldspar crystals (10 %) are the primary minerals. The plagioclase is almost completely altered to small stubby epidote crystals (25 %) and chlorite (5 %). The enstatite has actinolite rims (5 %), and is locally surrounded by a groundmass of fine serpentine (5 %). The high percentage (50 %) of enstatite in this sample suggests it is a pyroxenitic gabbro.

The textural and cross-cutting relationships of key mineral phases in the samples, helps to identify the order of crystallisation, the likely tectonic setting (Pearce & Wanming 1988), and the types of alteration the rocks have undergone. There are small variations in the mineralogy of each sample, but they have all undergone the same metamorphic processes. Olivine, followed by plagioclase feldspar then augite, were the first phases to crystallise as the gabbro cooled from a magma. This crystallisation sequence is typical of a cumulate gabbro formed in a mid-ocean ridge setting (Pearce & Wanming 1988).

After crystallisation of the gabbro, observed mineral assemblages and textures suggest several prograde metamorphic reactions took place. First, olivine was serpentinized in the presence of H_2O, a reaction that has been demonstrated to occur at a temperature of just under 400 ^oC and a pressure c.2 kbar by Deer et al. (1966). As

temperatures increased, different serpentine polymorphs stabilised, resulting in an assemblage of lizardite and chrysotile (Deer et al. 1966). At about the same time, plagioclase feldspar, probably originally anorthite or labradorite, was albitised, and augite broke down. Simultaneous breakdown of augite and albitisation of feldspar resulted in a chemistry leading to secondary crystallisation of epidote and calcite within some feldspar crystals, actinolite rims around some augite crystals and chlorite forming around feldspar and augite.

At temperatures of c. 450 ^{o}C, some of the serpentine, and all the remaining olivine in the rocks, started to alter to talc and H_2O (Deer et al. 1962). The presence of hornblende with chlorite suggests the transition from greenschist to amphibolite grade metamorphism was reached (400-500 ^{o}C at 2 kbar; Moody et al. 1983).

The prograde metamorphic reactions in the gabbros are consistent with greenschist to epidote-amphibolite grade peak metamorphic conditions. It is possible the metamorphic reactions discussed occurred during regional metamorphism. However, greenschist to epidote-amphibolite grade meta-gabbro also forms in most mid-ocean ridge environments, where temperature conditions under the mid-ocean ridge crest are high and the fractured crust allows deep influx of seawater (Manning et al. 1996, Nicolas & Mainprice 2005). Extensive epidotisation and quartz veining is a characteristic feature of ocean-floor metamorphism related to convective circulation of large amounts of heated sea water, leading to chemical exchanges between the rock and seawater (Bucher & Frey 1994). However, crosscutting relationships described within the samples suggest that quartz and epidote veins formed after initial pro-grade metamorphism, either in an ocean-floor setting or after a later regional metamorphic event that affected Palaeozoic rocks throughout the Nemegt and Altan Uul area.

2.9.2 XRF analyses

Data Quality

The gabbros sampled for XRF analysis have been metamorphosed to greenschist-to epidote-amphibolite grade and then cut by quartz and epidote veins. “Any rock which has been subjected to hydrothermal alteration or metamorphism is likely to suffer element mobility” (Rollinson 1993).

The behaviour of major elements during alteration varies depending on the original mineralogy. However, most of the major elements are very susceptible to mobility during weathering (e.g. Fe_2O_3) or metamorphism (e.g. Al_2O_3; Pearce 1976). Consequently, ocean-floor metamorphism may have several effects on gabbros through the circulation of hot aqueous fluid through the fractured oceanic crust (Manning et al. 1996). CaO will be leached, SiO_2 becomes mobile in the greenschist facies, and Na_2O is often introduced directly from seawater. Trace elements are also mobile during hydrothermal alteration or metamorphism. In general, incompatible low field strength (LFS) elements (Cs, Sr, Rb, Ba) are most affected, and compatible high field strength elements (Sc, Y, Th, Zr, Hf, Ti, Nb, Ta and the REE) are least effected (Pearce 1983, Rollinson 1993).

In addition to metamorphism, hydrothermal alteration and possible chemical weathering in submarine and subaerial environments affects the compositions of the major and trace elements Nb, Pb, Sn, U, W. These elements were also measured at or below the detection limits for XRF, making their measured abundances unreliable. Other trace elements (As, Th, Zr) are present at concentrations marginally above the detection

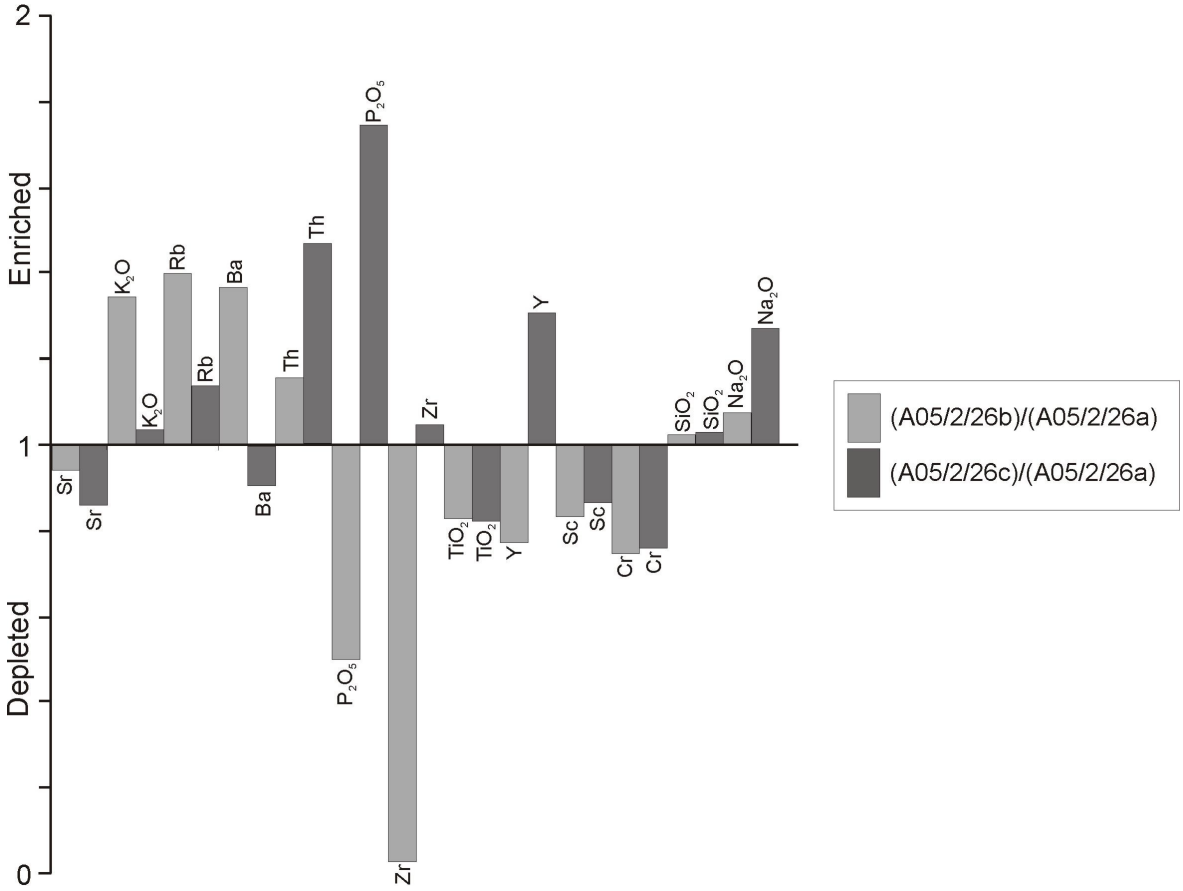

Fig. 2.36. – Enrichment/Depletion factors calculated for variably altered segments of sample A05/2/26 (after Rollinson, 1993). The more altered samples are enriched in K, Rb, Th, Si and Na, and depleted in Sr, Zr, Ti, Sc and Cr.

limits so should be treated with caution.

The method of Rollinson (1993, p159) was used to estimate the effect of alteration (enrichment factors) caused by the veining events affecting the gabbros. Sample A05/2/26, was a large block of gabbro containing an area that was fractured and intruded by epidote and quartz veins, and an area that was not visibly affected by veins. The samples was split into three separate samples; A05/2/26a was taken from the area of the specimen with the least visible alteration, away from any fractures or veins. A05/2/26b was taken from an area of the specimen in close proximity to the fractures and veins that ran throughout. A05/2/26c was taken from a fractured and veined segment of the sample. Splitting the rock into progressively more fractured and veined areas allowed a comparison of the effects of alteration on the analyses. Enrichment factors (Fig. 2.36) were calculated for major and trace elements used in interpreting the environment of formation of the gabbros. Element concentrations in the more visibly altered samples (A05/2/26b and A05/2/26c) were divided by the concentrations measured in the least visibly altered sample (A05/2/26a).

Elements with very small concentrations (e.g. P, Th, Zr, K) show very large enrichment factors with only very small increases in actual concentration. Rb, Ba and Sr are all LFS elements which would have been mobile during hydrothermal alteration of the gabbros, so they should show some enrichment or depletion. Ti, Cr and Sc are all depleted in the more altered samples. Ti is particularly susceptible to mobility during submarine weathering (Pearce 1976). Given an appreciation of these potential problems with the analyses, the geochemical data are conservatively interpreted.

2.9.3 Interpretation of XRF analyses

The mobility of silica and alkali elements during hydrous metamorphism means they are unsuitable for use in tectonic discrimination diagrams. Pearce & Cann (1977) use Zr and Ti, which are less mobile elements to generate a tectonic discrimination diagram suitable for basalts (Fig. 2.37A). Similarly, Winchester & Floyd (1977) use Nb/Y and Zr/ TiO_2 to produce a tectonic discrimination diagram suitable for basalts (Fig. 2.37B). Gabbro is chemically identical to basalt on a gross scale so these diagrams have been used to discriminate the Altan Uul meta-gabbros. However, the meta-gabbros have cumulate layering, so the whole-rock compositions of the gabbros are unlikely to represent the

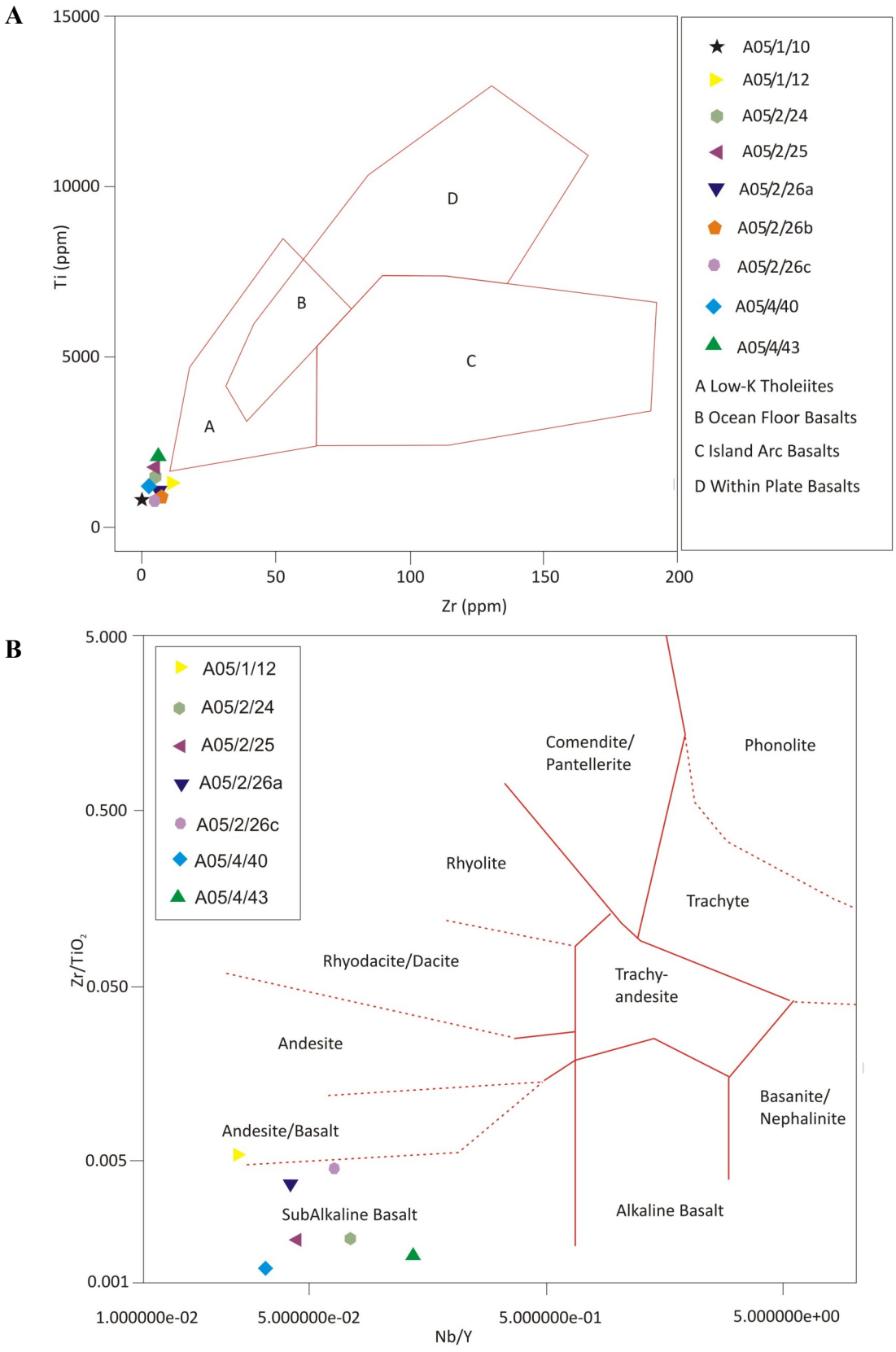

Fig. 2.37. – A) Zr against Ti tectonic discrimination plot (after Pearce & Cann 1973). The meta-gabbros do not plot within any of the fields, indicating that their composition has been altered by metamorphism. However, they plot closest to the low-K tholeiitic field, consistent with either an ocean-floor or oceanic-arc setting. B) Nb/Y against Zr/TiO_2 tectonic discrimination diagram (after Winchester & Floyd 1977). The meta-gabbros typically plot in the sub-alkaline basalt field, consistent with either an ocean-floor or oceanic-arc setting.

composition of the magma from which they crystallised. Consequently, caution should be used when interpreting the data plotted on the tectonic discrimination diagrams (Fig. 2.37),. The meta-gabbros do not fit within the tectonic discrimination fields defined by Pearce & Cann (1977; Fig. 2.37A). This could be because they are cumulates, or because metamorphism has altered their whole-rock chemistry. The enrichment/depletion factors shown in Figure 2.36 suggest that alteration of the meta-gabbros caused depletion of Zr and Ti. The meta-gabbros may also be depleted in Zr and Ti because these elements may have been taken into minerals in cumulate layers (e.g. spinel) that are absent from some of the samples. If this depletion is considered, the original meta-gabbro chemistry may have plotted in the low-K tholeiite field, consistent with an ocean-floor or oceanic island arc origin. The meta-gabbros typically plot in the sub-alkaline basalt field of the Winchester & Floyd (1977) discrimination plot (Fig. 2.37B). This is also consistent with an ocean-floor or oceanic arc setting.

Selected major and trace element analyses were normalised to MORB (Pearce 1983), and plotted on element abundance diagrams (Fig. 2.38). Gabbros from a back-arc setting (Lyngen, Norway), a forearc setting (Lyngen, Norway), and an island arc setting (Tianshui, China) are plotted for comparison (Fig. 2.38 A-C; Kvassnes et al. 2004, Pei et al. 2007). Cumulate olivine gabbros from the Oman ophiolite (Benoit et al. 1996) have a similar crystallisation sequence to the cumulate gabbros from Altan Uul, and are also plotted for comparison (Fig. 2.38 D).

The Altan Uul cumulate gabbros are enriched in the mobile elements K and Rb compared to both back-arc and fore-arc gabbros from Lyngen, Norway (Fig. 2.38 A-B). The main mineral in the Altan Uul gabbro samples containing K (and by substitution Rb) is hornblende which crystallised at the onset of epidote-amphibolite-grade metamorphism. The enrichment of these elements may therefore have occurred through interactions with hot aqueous fluids as epidote-amphibolite-grade metamorphism began. The Altan Uul gabbros are depleted in the relatively immobile elements P and Zr compared to the Lyngen back-arc gabbros (Fig. 2.38 A), and the immobile elements P, Y and Zr compared to the Lyngen fore-arc gabbros (Fig. 2.38 B).

Some samples of then Altan Uul gabbro are enriched and some are depleted in K and Rb compared to island arc gabbros from Tianshui, China (Fig. 2.32 C). The Altan Uul gabbros are depleted in the less mobile elements P, Zr, Ti and Y compared to the island arc gabbros.

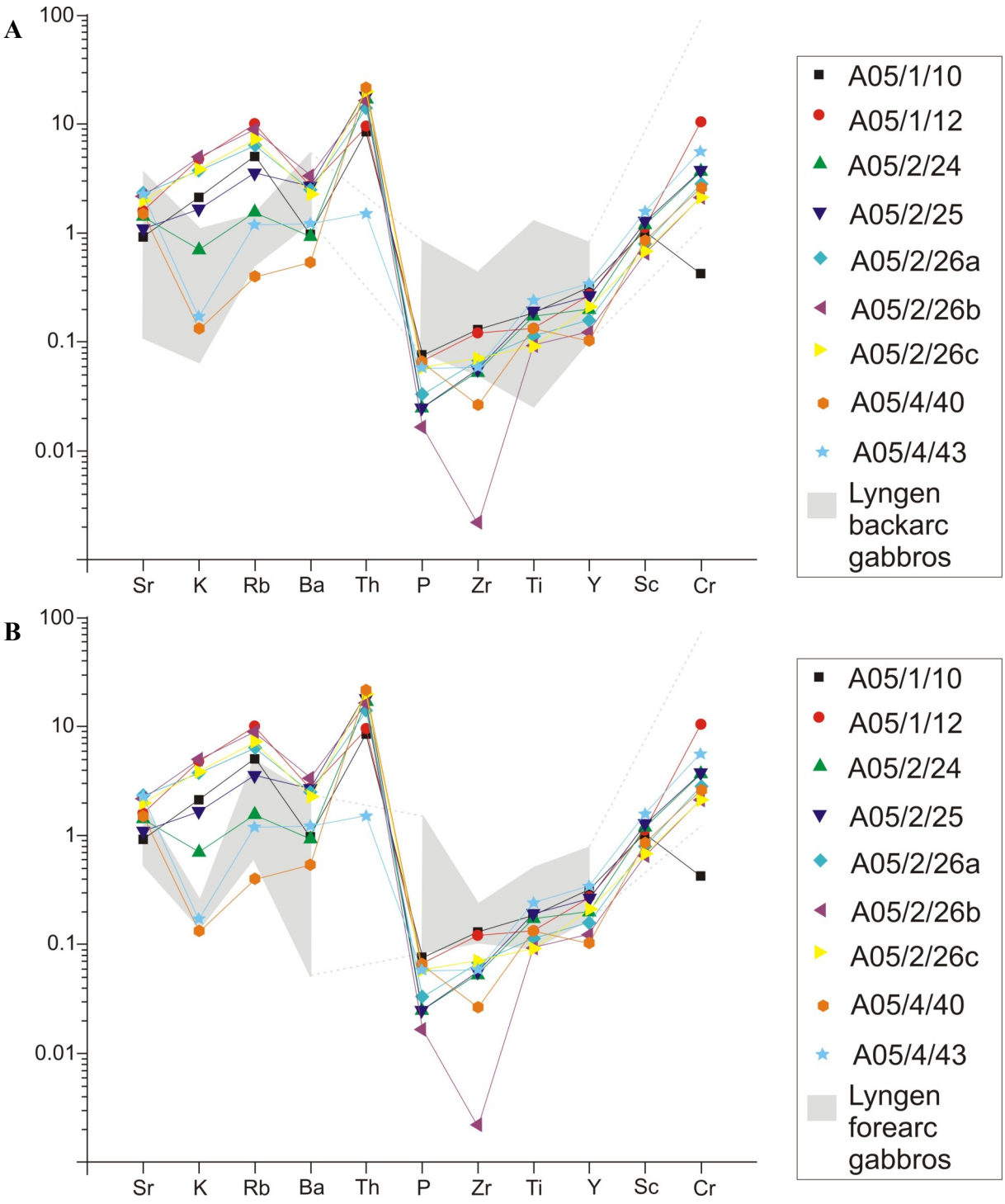

Fig. 2.38. Trace element abundance diagrams comparing the Altan Uul gabbros with gabbros from different tectonic environments. All data normalised to MORB (Pearce 1983). A) The Altan Uul gabbros are plotted with gabbros from Lyngen, Norway, interpreted to have formed in a backarc setting (Kvassnes et al. 2004). The Altan Uul gabbros are enriched in some mobile elements (K, Rb) and depleted in some immobile elements (P, Zr) compared to the gabbros from a back-arc setting. B) The Altan Uul gabbros are plotted with gabbros from Lyngen, Norway, interpreted to have formed in a forearc setting (Kvassnes et al. 2004). The Altan Uul gabbros are enriched in some mobile elements (Sr, K, Rb) and depleted in some immobile elements (P, Zr) compared to the gabbros from a fore-arc setting. (continued...)

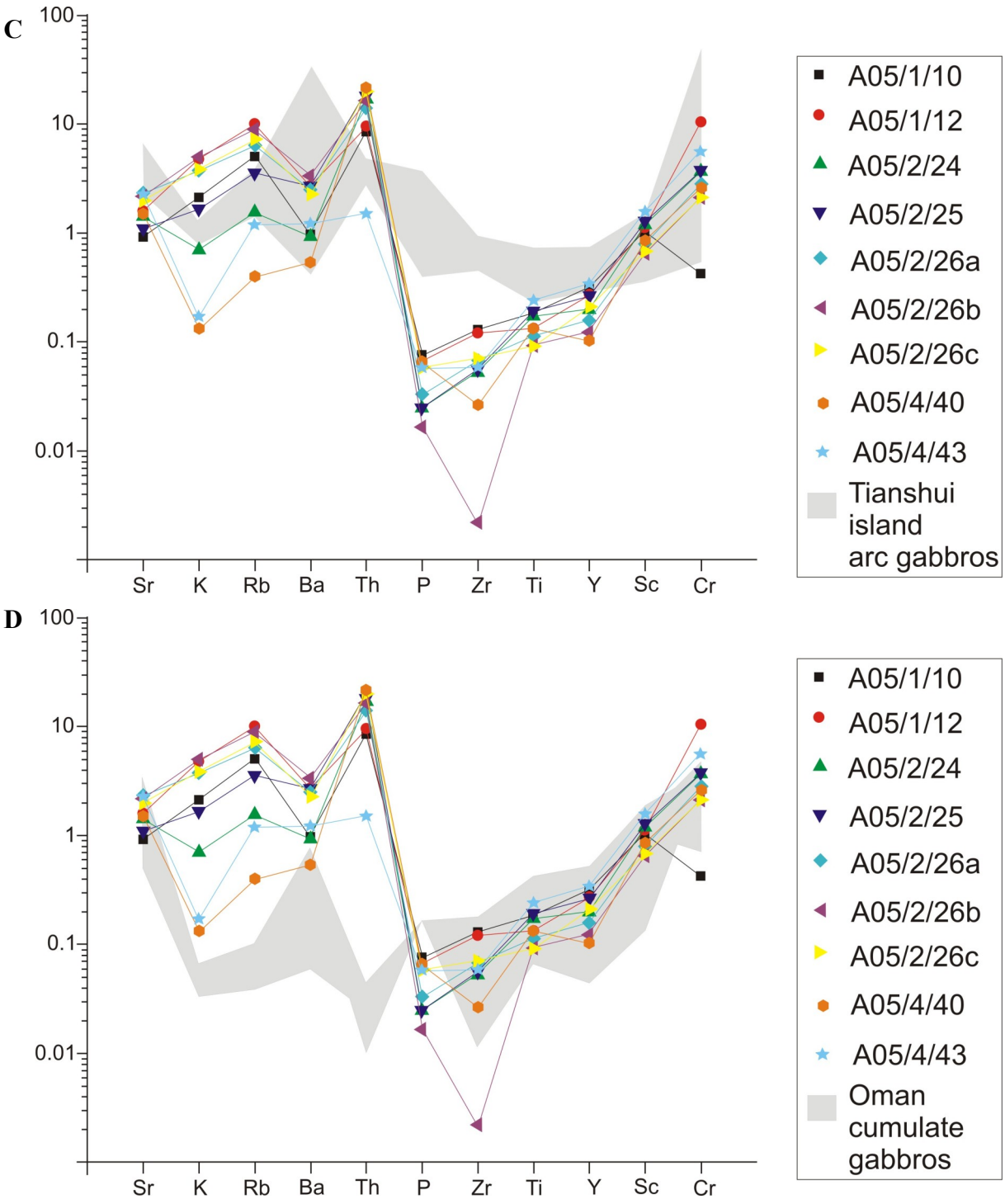

(...continued from the previous page) C) The Altan Uul gabbros are plotted with gabbros from Tianshui, China, interpreted to have formed in a island arc environment (Pei et al. 2007). The Altan Uul gabbros and the island arc gabbros are similarly enriched in mobile elements (Sr, K, Rb, Ba) to MORB. However, the Altan Uul gabbros are depleted in some immobile elements (Zr, Ti) compared to the island arc gabbros. D) The Altan Uul gabbros are plotted with gabbros from the Oman ophiolite (Benoit et al. 1996). The Altan Uul ophiolite is enriched in mobile elements (K, Rb, Ba) compared to the Oman cumulate gabbros. However, the trend for the immobile elements (Zr, Ti, Y, Sc, Cr) are similar for the Altan Uul gabbros and the Oman cumulate gabbros. The mobile elements have probably been enriched by metamorphic and weathering processes. The similarities between the immobile elements suggest that the Altan Uul gabbros have the closest affinity with the Oman cumulate gabbros.

The Altan Uul cumulate gabbros are enriched in the mobile elements K, Rb, Ba and Th compared to MORB and to the Oman cumulates. The main mineral in the samples containing K (and by substitution Rb and Ba) is hornblende which crystallised at the onset of epidote-amphibolite-grade metamorphism. The enrichment of these elements must therefore have occurred through interactions with hot aqueous fluids as epidote-amphibolite-grade metamorphism began. Thorium is generally found in silicate-rich melts, so enrichment in Th in the gabbros may be a result of later quartz veining. The HFS elements (Zr, Ti, Y, Sc) in the Altan Uul gabbros have similar normalised abundances to the Oman cumulates. Cr abundances are quite varied in the Altan Uul gabbros, which is interpreted as the result of the accumulation of spinel in the groundmass.

The Altan Uul gabbros have likely been enriched in mobile elements by metamorphic processes. Therefore, it is more important to consider the immobile elements to distinguish the likely tectonic environment in which they formed. The Altan Uul gabbros are depleted in some immobile elements compared to gabbros from back-arc, fore-arc and island arc settings, but have a similar trend to cumulate gabbros from the Oman ophiolite. This suggests that the trace element data for the Altan Uul gabbros are most consistent with an oceanic crustal origin.

2.10 Palaeozoic basement architecture of Nemegt Uul and Altan Uul

Field observations and petrographic analysis of samples taken along four south to north transects through Nemegt and Altan Uul have been used to define distinct fault-bound lithotectonic sequences (sections 2.4-2.7). In the following sections, the rocks documented along the transects are compared with each other to define across-strike (south to north) and along-strike (west to east) variations in lithology, structure and metamorphic grade. Photo-geological interpretation of Landsat TM imagery has been used to trace distinct lithologies and structures along-strike through areas that were not visited in the field, allowing interpretations of the along-strike continuity and connectivity of lithotectonic sequences and major structures within the ranges to be made (Figs. 2.39 and 2.40A-D).

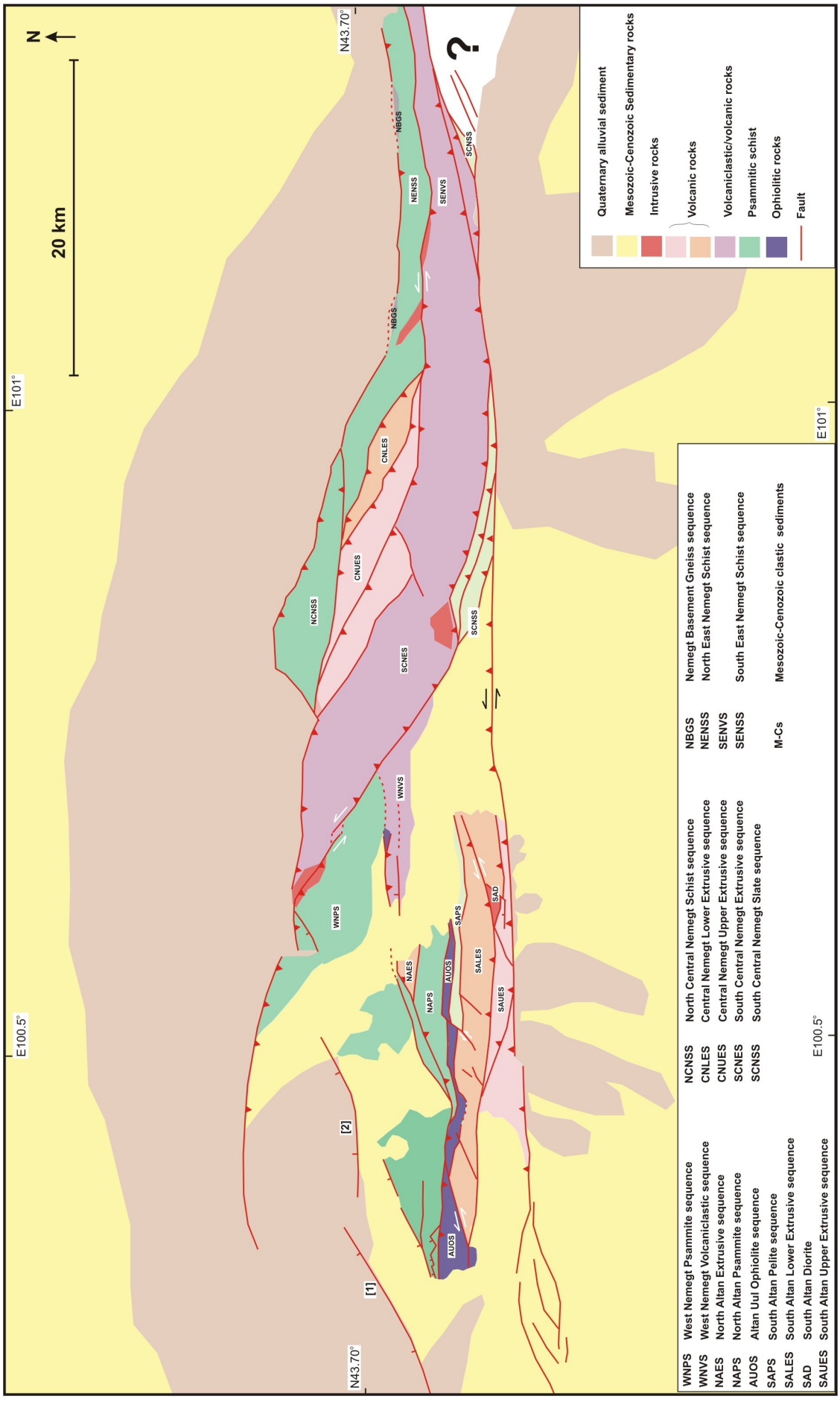

Fig. 2.39. Litho-tectonic map of Altan Uul and Nemegt Uul. Numbers in square brackets [#] mark locations referred to in the main text.

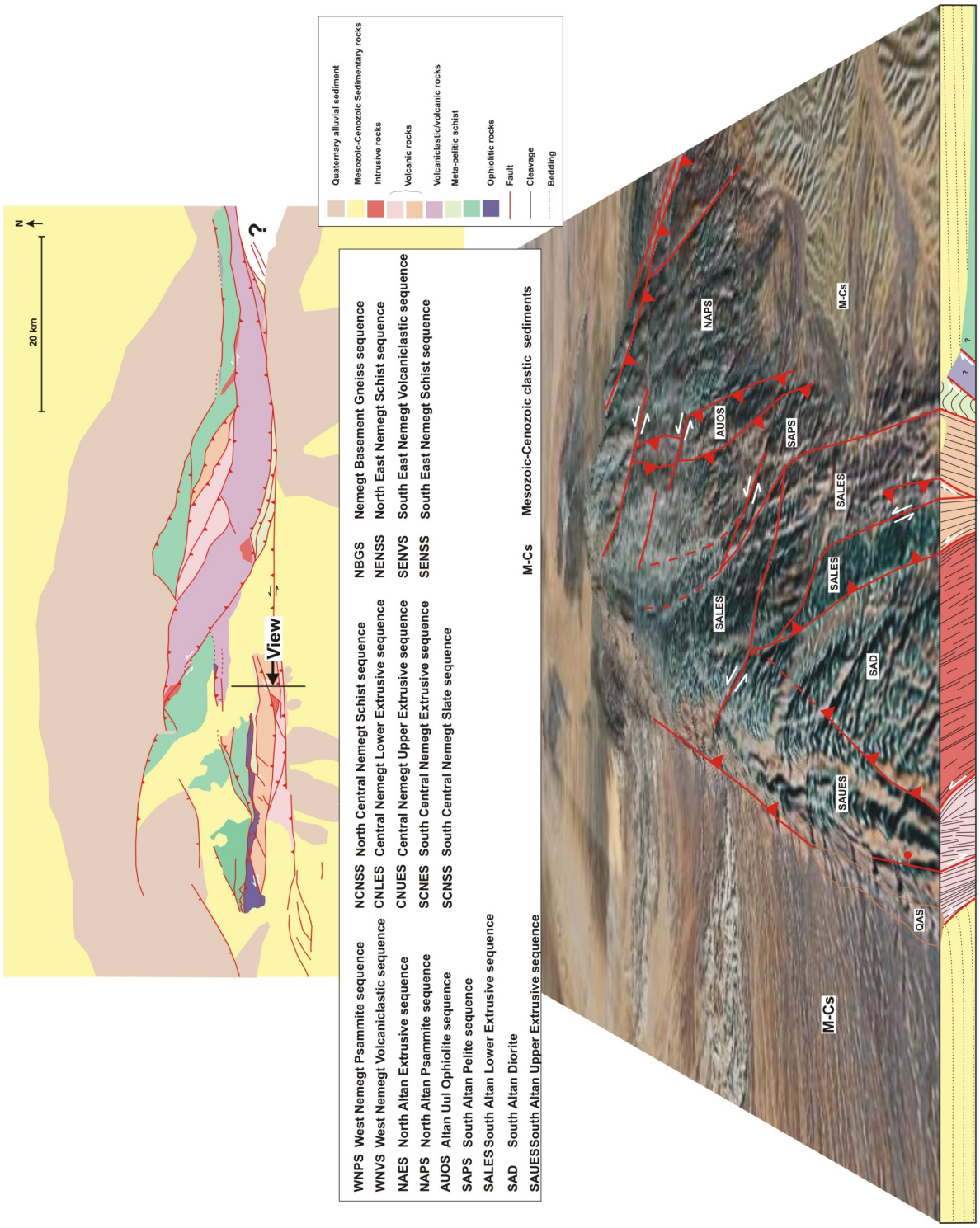

Fig. 2.40. Ai) Oblique cross-section, viewed west, showing lithological and structural distribution through southeast Altan Uul. Meta-basalts and volcaniclastic sedimentary and arkosic sandstones dominate the south of the area. They are thrust southwards over Mesozoic-Cenozoic sediments at the southern front of Altan Uul. To the north, the South Altan Diorite is thrust southwards over the volcaniclastic and arkosic sandstones. To the north, meta-andesites are thrust south over the South Altan Diorite. A steep north-dipping left-lateral oblique thrust places psammitic schists over the meta-andesites in the centre of the range. A south-dipping fault, possibly a thrust, separates psammitic schists in the South Altan Lower Extrusive sequence from meta-pelites to the north. The meta-pelites have a pervasive cleavage that has been folded into upright, open east-west trending folds. The meta-pelites are unconformably overlain in the transect area, but are seen to be thrust over the Altan Ophiolite sequence in the west.

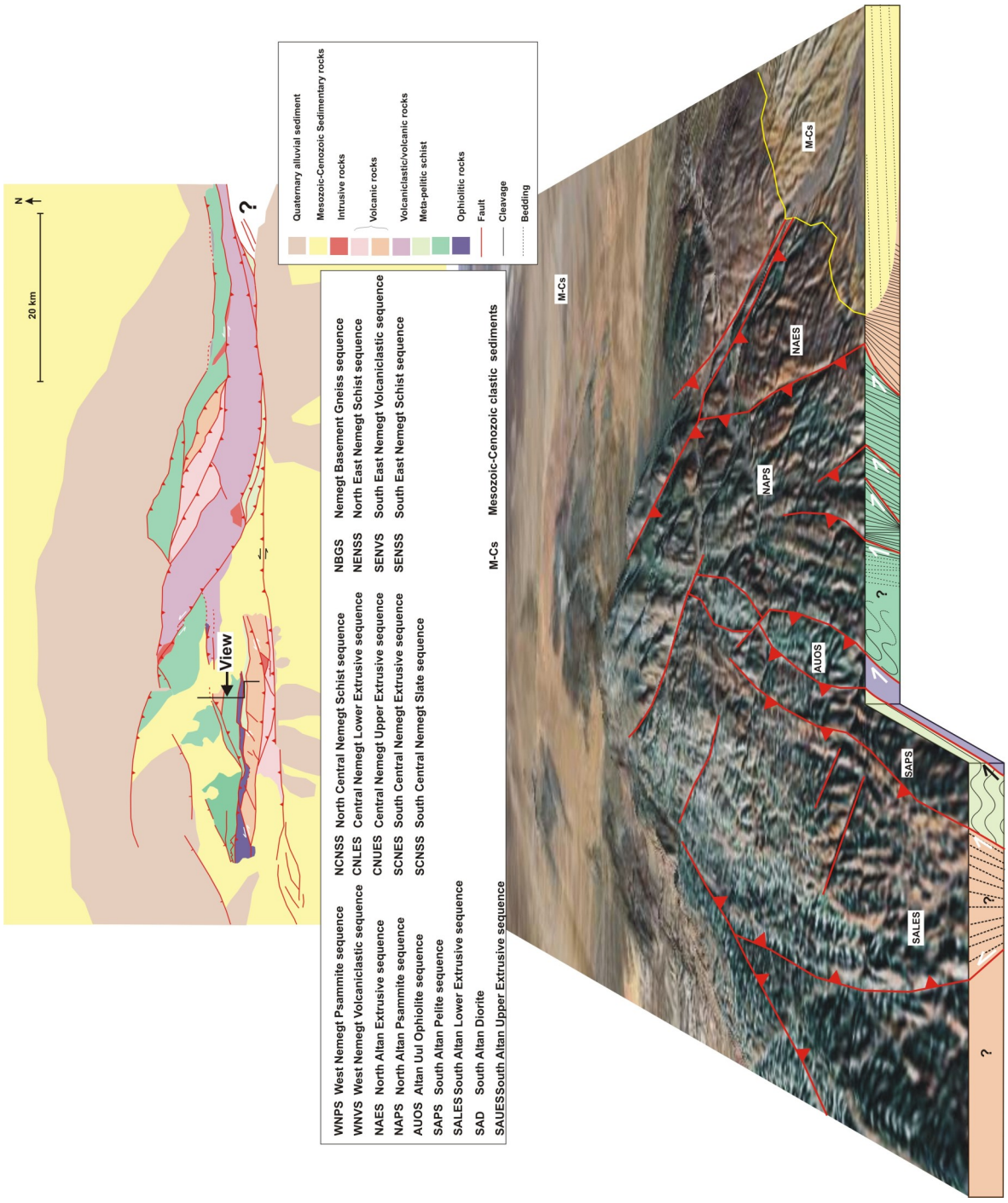

Fig. 2.40. Aii) Oblique cross-section, viewed west, showing lithological and structural distribution through northeast Altan Uul. The meta-pelites in the South Altan Pelite sequence are thrust north over the Altan Ophiolite sequence in central Altan Uul. Gabbros and serpentinite in the gabbros is thrust north over meta-psammites and meta-pelites in the North Altan Psammite sequence. The meta-psammites and meta-pelites have a pervasive steep north-dipping cleavage which becomes south-dipping further north. Close to the northern front of Altan Uul in this area, meta-psammite is thrust north over a belt of meta-andesite. Photo-geological interpretation of Landsat Tm imagery suggests the belt of meta-andesite widens to the west, where it is thrust north over more meta-psammites. Mesozoic-Cenozoic sediments unconformably overlay the Palaeozoic rocks at the northern front of Altan Uul.

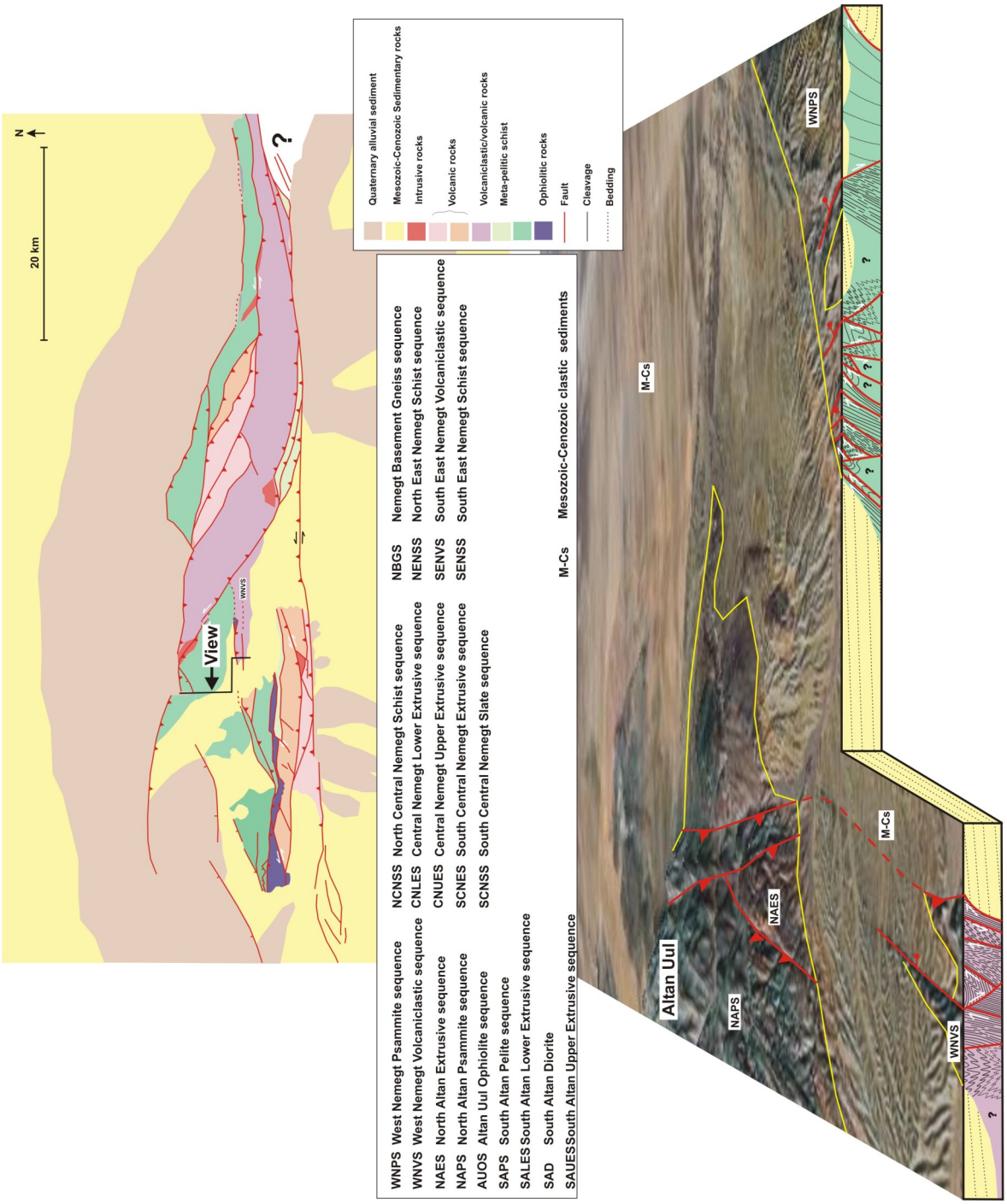

Fig. 2.40. Aiii) Oblique cross-section, viewed west, showing lithological and structural distribution through west Nemegt Uul. Mesozoic-Cenozoic sediments unconformably overlay volcaniclastic meta-conglomerate, and volcaniclastic and chloritic schist in the West Nemegt Volcaniclastic sequence. The schists have a pervasive cleavage that has been folded into tight upright folds in the south, and tight north-vergent folds to the north. Chloritic schist and meta-conglomerate are thrust north over Mesozoic-Cenozoic sediments that fill a basin between the West Nemegt Volcaniclastic sequence and the West Nemegt Psammite sequence to the north. The West Nemegt Psammite sequence consists of meta-psammitic and meta-pelitic schists, with a pervasive cleavage folded into tight north-vergent folds on a 10 cm to 10 m scale. North-directed thrust shear zones cut the schists and are cut by steep northeast-southwest trending brittle normal faults. At the northern front of Nemegt Uul, a zone of north-directed brittle thrust faults cuts Neogene gravels and places the West Nemegt Psammite sequence north over Mesozoic-Cenozoic sediments.

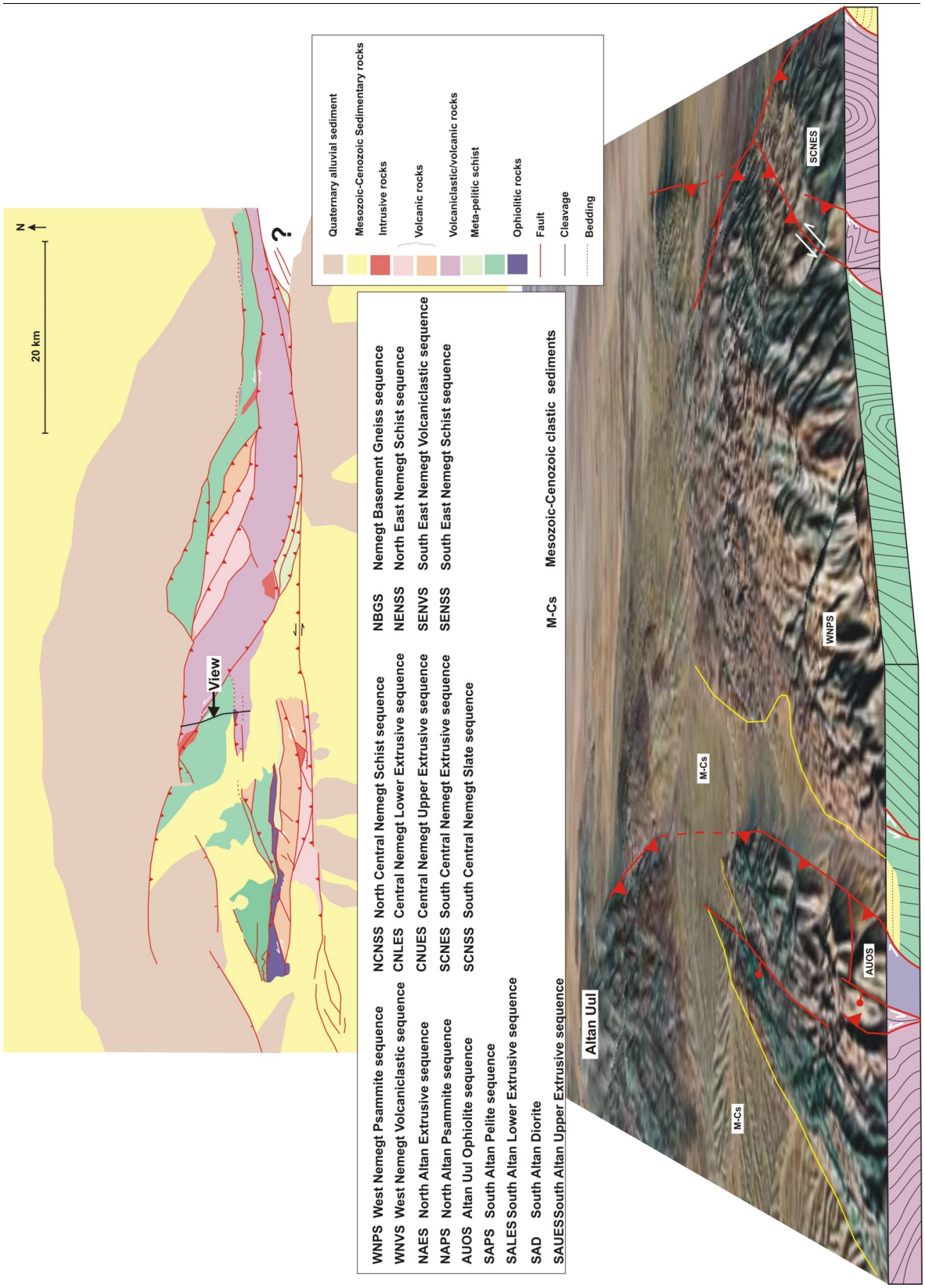

Fig. 2.40. B) Oblique cross-section, viewed west, showing lithological and structural distribution through northwest Nemegt Uul along Owen et al. (1999b) transect line. Meta-psammitic and meta-pelitic schists witha steep north-dipping cleavage are downthrown to the south against meta-gabbros, serpentinite and peridotite in a small fault-bound sliver of the Altan Uul ophiolite. The ophiolite sequence is thrust north over Mesozoic-Cenozoic sediments in a narrow westward-widening basin between the West Nemegt Volcaniclastic sequence and the West Nemegt Psammite sequence. The meta-psammites and meta-pelites to the north have a steep south-dipping cleavage which is folded into 20 m scale moderate upright to north-vergent folds in places.

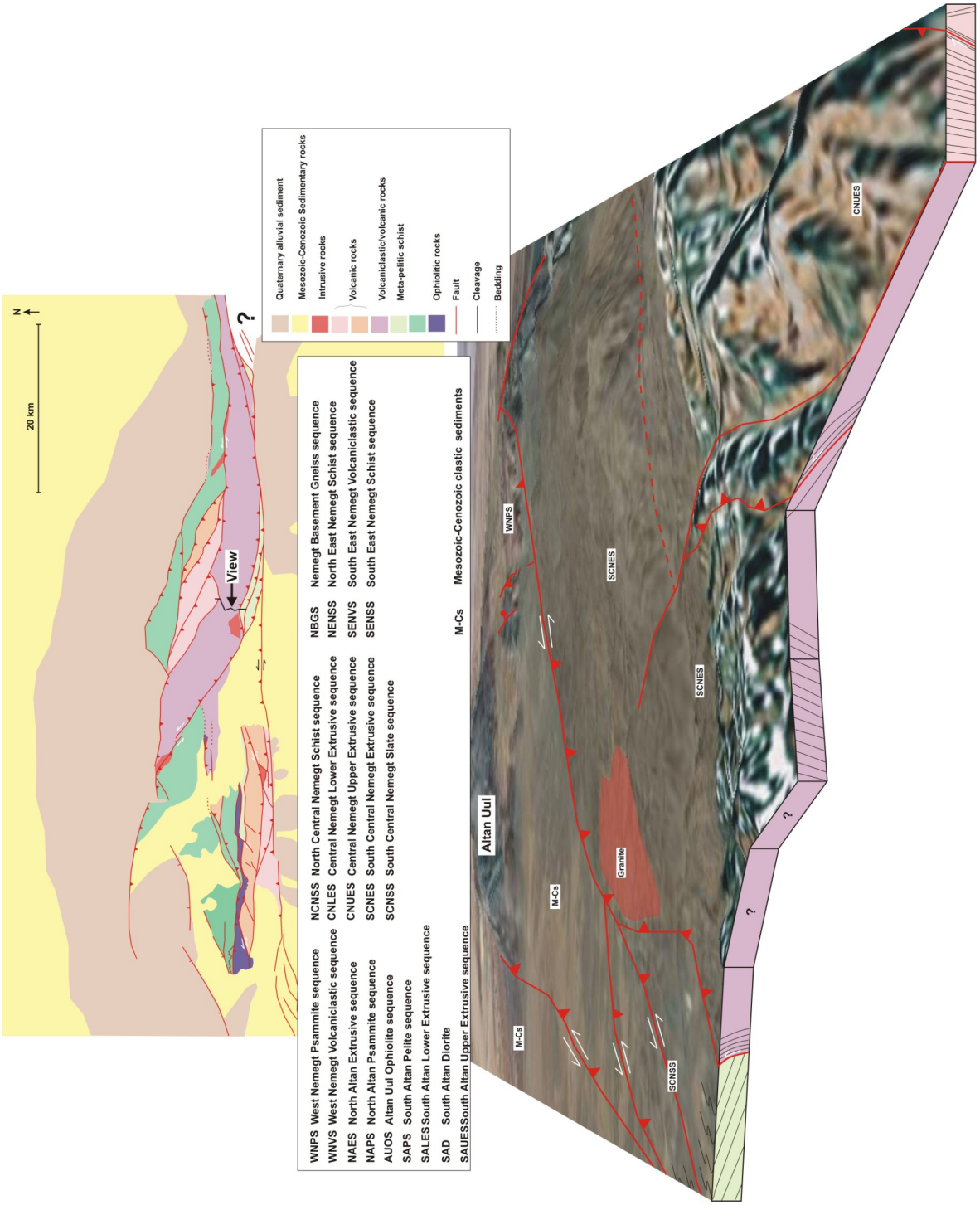

Fig. 2.40. Ci) Oblique cross-section, viewed west, showing lithological and structural distribution through south central Nemegt Uul. At the southern front of Nemegt Uul, slates in the south Central Nemegt Slate sequence are cut by left-lateral oblique thrust faults. To the north, the South Central Nemegt Extrusive sequence is thrust south over the slates. The volcaniclastic and meta-volcanic rocks in the South Central Nemegt Extrusive sequence form blocky exposures through southern Nemegt Uul. A linear southwest-northeast oriented valley likely marks the trace of a major fault separating the South Central Nemegt Extrusive sequence from the meta-andesites and volcaniclastic schists in the Central Nemegt Upper Extrusive sequence to the north.

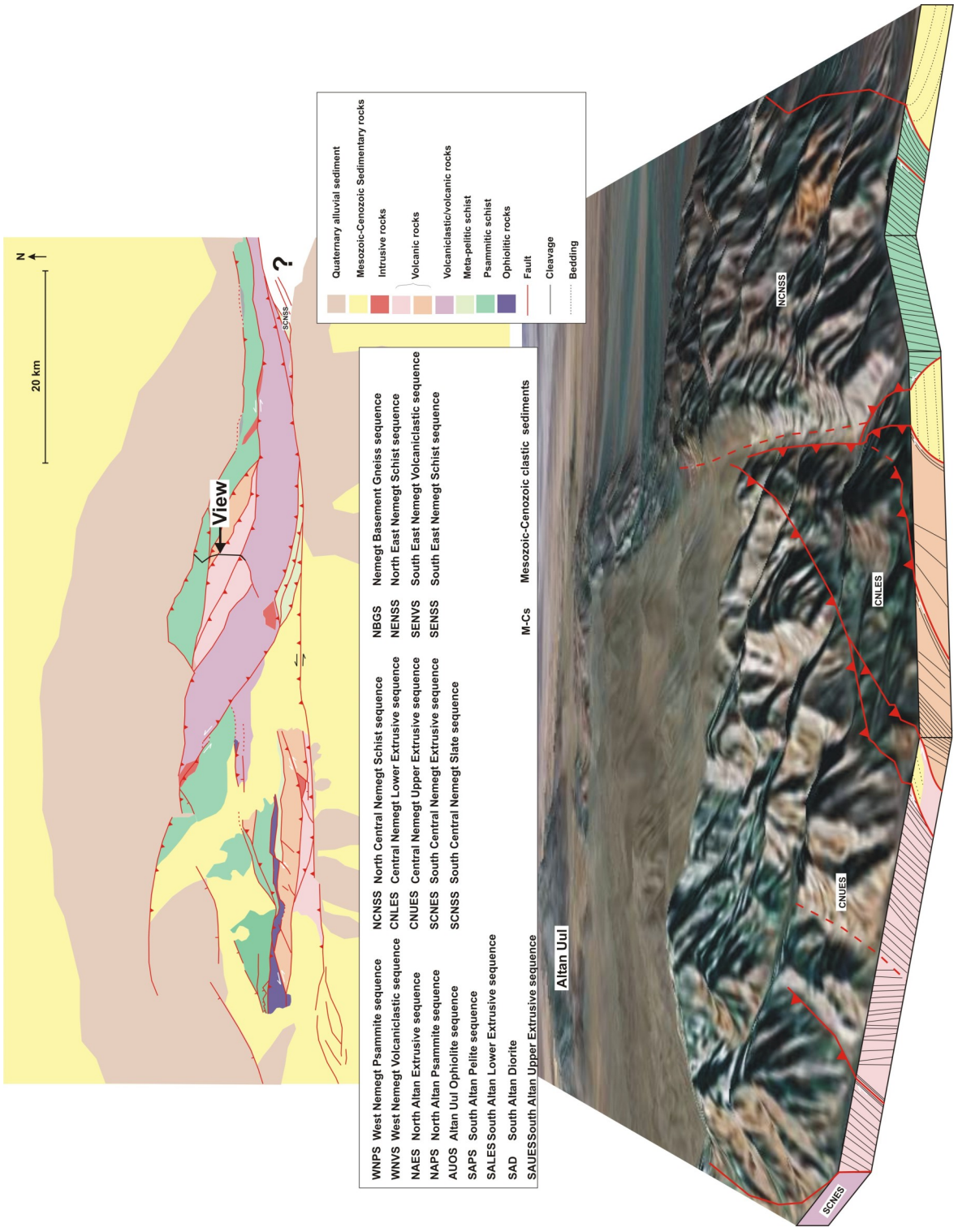

Fig. 2.40. Cii) Oblique cross-section, viewed west, showing lithological and structural distribution through north central Nemegt Uul. The Central Nemegt Upper Extrusive sequence consists of volcaniclastic schists which have a pervasive steep cleavage that typically dips south. Volcaniclastic schists in the sequence are thrust northeast over Mesozoic-Cenozoic sediments in the range. These cover sediments lie unconformably on the schists futher north. The Central Nemegt Upper Extrusive sequence is thrust north over meta-andesite, tuff and volcaniclastic schist in the Central Nemegt Lower Extrusive sequence. At the northern boundary of the sequence, rhyolite is thrust north over Mesozoic-Cenozoic sediments. A belt of phyllite and psammitic schist making up the North Central Nemegt Schist sequence is thrust south is thrust south over the Mesozoic-Cenozoic sediments to the north. The schists have a pervasive vertical to south-dipping cleavage. At the northern front of Nemegt Uul, the schists are thrust north over Mesozoic-Cenozoic basin fill.

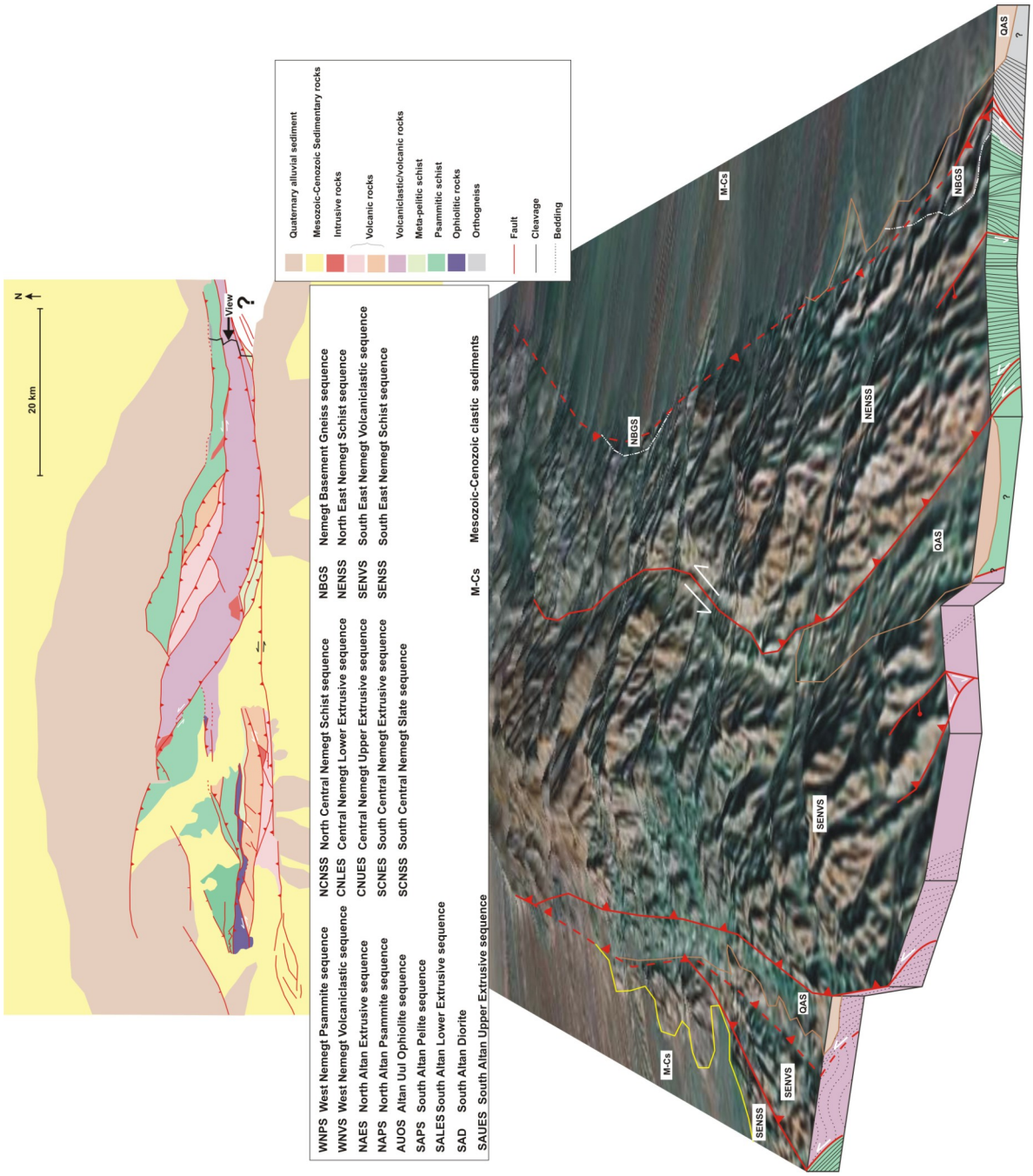

Fig. 2.40. D) Oblique cross-section, viewed west, showing lithological and structural distribution through east Nemegt Uul. In the south, meta-psammitic and meta-pelitic schists in the South East Nemegt Schist sequence are locally unconformably overlain by Cenozoic sediments. Farther west, the schists are thrust south over Mesozoic-Cenozoic sediments. In the transect area, fossiliferous and volcaniclastic meta-sandstones and minor meta-andesites are thrust south over the meta-psammitic and meta-pelitic schists along the south front. The fossiliferous meta-sandstones are folded into upright, open east-west trending folds. Two wide linear valleys cut southwest-northeast and east-west through the range and mark the trace of major range transecting faults. The northernmost of these faults has a proven left-lateral south-directed thrust component and separates the South East Nemegt Volcaniclastic sequence from the North East Nemegt Schist sequence. Meta-psammitic schist, chloritic schist and biotite schist in the north of Nemegt Uul have a pervasive cleavage dipping steeply north in the south of the North East Nemegt Schist sequence, and steeply south in the north. The schists rest unconformably upon foliated magmatic orthogneiss near the northern front of Nemegt Uul. At the northern front, Mesozoic-Cenozoic sediments rest unconformably upon the orthogneiss.

2.10.1 Lithological distribution

Altan Uul and western Nemegt Uul

In western Altan Uul, the Altan Uul Ophiolite sequence (section 2.4.1; Fig. 2.8) is a tectonically dismembered assemblage of pillow basalts, through cumulate gabbros, sheeted dykes, serpentinite, and arkosic psammites to jasperoids in the north. Petrographic analysis of the Altan Uul gabbros (section 2.9.1) and comparison of XRF analyses of the cumulate gabbros with cumulate gabbros from the Oman ophiolite (section 2.9.3) suggests that they are compatible with an oceanic crustal origin. The juxtaposition of the gabbros with related oceanic crustal rocks (serpentinite, pillow basalts and jasperoids) observed in the field makes a strong case for the exposure of a partial ophiolite sequence in western Altan Uul, which has been named the Altan Uul ophiolite (Rippington et al. 2008).

The Altan Uul ophiolite can be traced east on Landsat TM imagery to Central Altan Uul, where a fault-bound sequence of cumulate gabbros and serpentinite is exposed (section 2.4.1; section 2.9). Gabbros sampled from the exposure in central Altan Uul (samples A05/4/40 and A05/4/43; Table 1) have a similar petrography (section 2.9.1) and have similar major and trace element abundances (Table 1; Fig. 2.37; Fig. 2.38). In western Nemegt Uul, a c. 500 m^2 fault-bound sequence of peridotite, serpentinite, gabbro, meta-volcanic rocks and meta-sedimentary rocks is exposed (Fig. 2.35B; Rippington et al. 2008). This sequence was not sampled but the sequence is composed of rocks compatible with an oceanic crustal origin, and is interpreted to be part of the Altan Uul ophiolite. This exposure marks the easternmost documented exposure of the Altan Uul ophiolite.

The rocks to the south of the Altan Uul ophiolite are quite different to the rocks to the north. Along the eastern Altan Uul/western Nemegt Uul transect, the South Altan Upper Extrusive sequence, the South Altan Diorite, and the South Altan Lower Extrusive sequence, are exposed (Fig. 2.5 A-A_1; Fig. 2.11). These sequences consist of meta-basalts in the south, through arkosic sandstone, volcaniclastic breccia, diorite, and meta-andesite to arkosic psammite in the north (sections 2.5.1-2.5.3). To the north of the South Altan Lower Extrusive sequence, a sequence of phyllites is exposed (section 2.5.4; Fig. 2.11). To the west, in central Altan Uul, a sequence of meta-pelites is thrust north over the Altan

Uul ophiolite. Photo-geological interpretation of Landsat TM imagery suggests the phyllites south of the Altan Uul ophiolite in central Altan Uul are directly along-strike from the phyllites in eastern Altan Uul, and can be considered part of the South Altan Phyllite sequence (section 2.5.4; Fig. 2.11).

North of the Altan Uul ophiolite, along the eastern Altan Uul/western Nemegt Uul transect, the North Altan Psammite and Extrusive sequences, and West Nemegt Volcaniclastic and Psammite sequences are exposed (Fig. 2.5 C-H; Fig. 2.11). These sequences consist of interbedded arkosic meta-psammites and meta-pelites in the south, through limestone, volcaniclastic schist, meta-andesite, volcaniclastic meta-conglomerate with andesitic clasts (section 2.5.7), chloritic schist, meta-conglomerate, arkosic meta-pelitic schists, phyllites, and arkosic meta-psammites in the north (sections 2.5.5-2.5.8; Fig. 2.5 C-H; Fig. 2.11).

In summary, in eastern Altan Uul and western Nemegt Uul meta-andesites, with some meta-basalts, volcaniclastic meta-sedimentary rocks with andesitic and basaltic clasts, and rare meta-pelitic rocks are exposed directly south of the ophiolite (Fig. 2.5 A-B; Fig. 2.11). In contrast, the rocks to the north of the Altan Uul ophiolite (Fig. 2.5 C-H; Fig. 2.11) have dominantly arkosic meta-psammitic and meta-pelitic compositions with rare occurrences of meta-andesitic and volcaniclastic rocks. This defines a south to north meta-volcanic/volcaniclastic to ophiolitic to arkosic meta-psammitic/meta-pelitic sequence of rocks in eastern Altan Uul and western Nemegt Uul.

Central and Eastern Nemegt Uul

In central Nemegt Uul, the southernmost Palaeozoic rocks exposed are slates belonging to the South Central Nemegt Slate sequence (section 2.6.1). The slates define a narrow belt of meta-sedimentary rocks that can be traced eastward on Landsat TM imagery, to slates and phyllites first identified along the southern front of Nemegt Uul by Cunningham et al. (1996; Fig. 2.21). At the eastern extent of Nemegt Uul, chloritic schists of the South East Nemegt Schist sequence crop out (section 2.7.1; Fig. 2.7 A-A_1; Fig. 2.27). The slates in the South Central Nemegt Slate sequence (section 2.6.1; Fig. 2.21), the slates and phyllites documented by Cunningham et al. (1996; Fig. 2.21), and the chloritic schist in the South East Nemegt Schist sequence (section 2.7.1; Fig. 2.7 A-A_1; Fig. 2.27) are similar in appearance and can all be traced directly along-strike to the east

or west of each other on Landsat TM imagery (Fig. 2.39). The slates in the west (section 2.6.1) have a similar mineralogy to the chloritic schists in the east (section 2.7.1) although there is a higher percentage of feldspar in the chloritic schists in the east. Although these meta-sedimentary rocks do not appear to crop out continuously along the southern front of Nemegt Uul, the similarities in their appearance and mineralogy suggest the slates in the South Central Nemegt Slate sequence (section 2.6.1; Fig. 2.21), the slates and phyllites documented by Cunningham et al. (1996; Fig. 2.21), and the chloritic schists in the South East Nemegt Schist sequence (section 2.7.1; Fig. 2.7 A-A_1; Fig. 2.27) form a distinct east-west trending belt of meta-sediments in southern Nemegt Uul.

To the north of the slates in central Nemegt Uul, the South Central Nemegt Extrusive sequence, and Central Nemegt Upper and Lower sequences (sections 2.6.2-2.6.4) dominate exposure (Fig. 2.6 A-C; Fig. 2.21). These sequences consist of meta-andesitic volcanic breccias and conglomerates in the south, through tuffs, meta-andesites, volcaniclastic meta-breccias, volcaniclastic schists, meta-andesite, to interbedded meta-rhyolites and volcaniclastic meta-sandstones in the north (sections 2.6.2-2.6.4).

The Southeast Nemegt Volcaniclastic sequence crops out to the north of the chloritic schists along the southern front in eastern Nemegt Uul (section 2.7.2; Fig. 2.7A_1-D; Fig. 2.27). The sequence consists of interbedded arkosic volcaniclastic and meta-sandstones filled with brachiopod fragments in the south, through arkosic meta-psammite, and meta-andesite to volcaniclastic meta-conglomerate in the north (section 2.7.2).

The Southeast Nemegt Volcaniclastic sequence (section 2.7.2; Fig. 2.7A_1-D; Fig. 2.27) in eastern Nemegt Uul and the South Central Nemegt Extrusive sequence (section 2.6.2; Fig. 2.6 A-B; Fig. 2.21) in central Nemegt Uul are both dominated by similar meta-andesitic volcaniclastic meta-sedimentary rocks and meta-andesitic rocks. The mineralogy of volcaniclastic meta-conglomerates and breccias in both sequences are very alike, although there are less andesite clasts in the volcaniclastic meta-conglomerates in the east (5-10 %; section 2.7.2; Fig. 2.27) than the volcaniclastic meta-conglomerates and breccias in central Nemegt Uul (40-60 %; section 2.6.2; Fig. 2.21). The meta-andesites in central and eastern Nemegt Uul have the same mineralogy, although the meta-andesites in central Nemegt Uul have a higher feldspar phenocryst to groundmass ratio (25-40 % phenocrysts to 45-60 % groundmass) than the meta-andesites in eastern Nemegt Uul (5-10 % phenocrysts to 60-70 % groundmass). The Southeast Nemegt Volcaniclastic sequence and the South Central Nemegt Extrusive sequence are directly along-strike from

each other (Fig. 2.39). Similarities between their constituent lithologies suggest that they can be grouped together to define a single east-west belt of volcanic and volcaniclastic rocks through central and eastern Nemegt Uul. However, there are no comparable sequences to the Central Nemegt Upper and Lower sequences (sections 2.6.3-2.6.4) exposed in eastern Nemegt Uul, suggesting that the thickness of the combined meta-volcanic and volcaniclastic meta-sedimentary sequences is at its greatest in central Nemegt Uul (Fig. 2.39).

North of the meta-volcanic and meta-volcaniclastic rocks in central Nemegt Uul, the North Central Schist sequence crops out (section 2.6.5). The sequence consists of phyllites and meta-pelites in the south and grades north into arkosic meta-psammitic schists that are exposed along the northern front of Nemegt Uul (section 2.6.5; Fig. 2.6 C-D; Fig. 2.21). In eastern Nemegt Uul, the Northeast Nemegt Schist sequence crops out to the north of the meta-volcanic and volcaniclastic meta-sedimentary rocks (section 2.7.3; Fig. 2.21). The sequence consists of arkosic psammitic schists in the south, through quartz -biotite-chlorite schists to biotite schists in the north. Photo-geological interpretation of Landsat TM imagery combined with reconnaissance field work suggests that meta-psammitic schists are exposed along the northern front of Nemegt Uul forming a slightly arcuate east-west trending belt from the central transect to the eastern transect (Fig. 2.39). However, there are slight along-strike variations in the mineralogy of the meta-sedimentary rocks in northern Nemegt Uul. The meta-psammites at the northern front in central Nemegt Uul (section 2.6.5) are arkosic, with c.20-30 % alkali feldspar. The biotite schists at the northern front in eastern Nemegt are more mature, and contain no discernable feldspar grains (section 2.7.3). The schists in the Northeast Nemegt Schist sequence vary from arkosic in the south of the sequence to more mature in the north (section 2.7.3).

North of the biotite schist in the Northeast Nemegt Schist sequence in eastern Nemegt Uul, there is an orthogneiss (section 2.7.4; Fig. 2.7; Fig. 2.27). The biotite schist sits above an angular unconformity dipping 50-70^{o} to the south along the top of gneiss (section 2.7.3; Fig. 2.32), which suggests the protolith of the schist was deposited on an erosion surface above the orthogneiss. A sliver of orthogneiss is also exposed along the northern front of Nemegt Uul further to the west (Fig. 2.27) where meta-sediments are again seen unconformably above it. These are the only two documented occurrences of orthogneiss in Nemegt and Altan Uul.

In central and eastern Nemegt Uul, there is a clear south to north variation in the lithologies from meta-pelitic schist to meta-andesite, volcaniclastic meta-sandstone containing andesitic clasts, with meta-rhyolites exposed in central Nemegt Uul, to arkosic schists. In eastern Nemegt Uul, there are also schists with mature protoliths that were deposited on orthogneiss in the north of the area.

The south to north sequence in central and eastern Nemegt Uul is similar to the south to north sequence documented in western Nemegt and Altan Uul, although there are some important variations. In western Nemegt and Altan Uul, the meta-volcanic and meta -volcaniclastic sequences are dominantly exposed to the south of the Altan Uul ophiolite and the meta-sedimentary sequences are dominantly exposed to the north (Fig. 2.39). In central and eastern Nemegt Uul, no exposures of the Altan Uul ophiolite have been identified, although meta-volcanic and volcaniclastic meta-sedimentary sequences are still dominantly exposed to the south of the main meta-sedimentary sequences (Fig. 2.39). There are three possible reasons for this absence: 1) ophiolitic rocks do exist in the area and were not found due to their inaccessibility; 2) ophiolitic rocks were obducted but have been moved or eroded due to subsequent deformation and exhumation in the area; or 3) ophiolitic rocks were not obducted in the central and eastern areas.

From field observations, it is unclear if the meta-volcanic rocks and volcaniclastic meta-sedimentary rocks in southern Altan Uul are part of the same sequence as those documented in central and eastern Nemegt Uul. The meta-volcanic sequences in southern Altan Uul include meta-basalts (section 2.5.1) which are not seen in central and eastern Nemegt Uul. Conversely, the meta-volcanic sequences in central Nemegt Uul contain tuffs and meta-rhyolite (section 2.6.2) which are not seen anywhere else in either range. It is not clear if the slates and schists exposed along the southern front of Nemegt Uul have a counterpart in western Nemegt and Altan Uul (Fig. 2.39).

2.10.2 Polyphase deformation in Nemegt and Altan Uul

Before the spatial distribution of strain formed by Palaeozoic deformation events affecting the rocks of Nemegt and Altan Uul can be assessed, it is essential to consider the polyphase deformation sequence and to determine the relative temporal evolution of all the structures in the area. There are no geochronological data for the numerous faults in Nemegt Uul and Altan Uul. However, cross-cutting relationships between structures

make it possible to determine that the Palaeozoic rocks have been affected by four distinct deformation events.

The oldest evidence of strain in the area, is open east-west trending F1 folds of bedding seen in eastern Nemegt Uul (Fig. 2.29F). An axial planar S1 cleavage is seen in the core of these folds (Fig. 2.29F). Although F1 folds are only preserved in eastern Nemegt Uul, where they are not overprinted by subsequent deformation, S1 is widespread throughout Nemegt and Altan Uul. There are small variations in the orientation of the cleavage throughout the area, but S1 dominantly strikes east-west and has a moderate to steep south or north dip (Fig. 2.41A-B).

The effects of subsequent deformation events are not obvious in southeastern Nemegt Uul, allowing the cautious assumption that in this area, cleavage and fold hinges have not been significantly rotated about a vertical axis, with a possible exception adjacent to a major northeast-southwest valley where northeast plunging F1 folds may have been rotated in an anticlockwise direction (Fig. 2.7 stereonet 2; Fig. 2.27 B), suggesting the presence of a left-lateral fault. However, S1 cleavage is dominantly east-west trending throughout Nemegt and Altan Uul (Fig. 2.41A-B), which suggests that vertical axis rotations were rare. Therefore, the present-day orientations of the structures, can be cautiously interpreted to indicate the approximate orientations of the principal stress axes under which the structures actually formed. The first deformation event (D1) is therefore inferred to have been contractional, with an approximately north-south principal horizontal maximum stress, normal to the dominant east-west trend of F1 fold axes and S1 cleavage (Fig. 2.41A, C).

In the psammitic and volcaniclastic schists in western and northern Nemegt Uul (sections 2.5.7-2.5.8, 2.6.5; Fig. 2.5 E-H) and the jasperoids in northwest Altan Uul (section 2.4.1; Fig. 2.41), S1 cleavage has been folded by a second deformation event (D2), to form tight north-vergent F2 folds with an axial planar S2 cleavage (Fig. 2.20E-J; Fig. 2.41C-D). North-directed ductile shear zones cut through western Nemegt Uul (section 2.5.8; Fig. 2.20G), excising the long-limbs of F2 folds in the area. This suggests the north-vergent F2 folds tightened and locked-up under top to the north shear, causing north-directed shear zones to form and accommodate the strain. The orientation of D2 structures in Nemegt and Altan Uul (Fig. 2.41) suggests that it was also a northward-directed shearing event. The parallelism of D1 and D2 structures (Fig. 2.41) is either a consequence of crustal reactivation and/or due to parallel stress fields in the D1 and D2

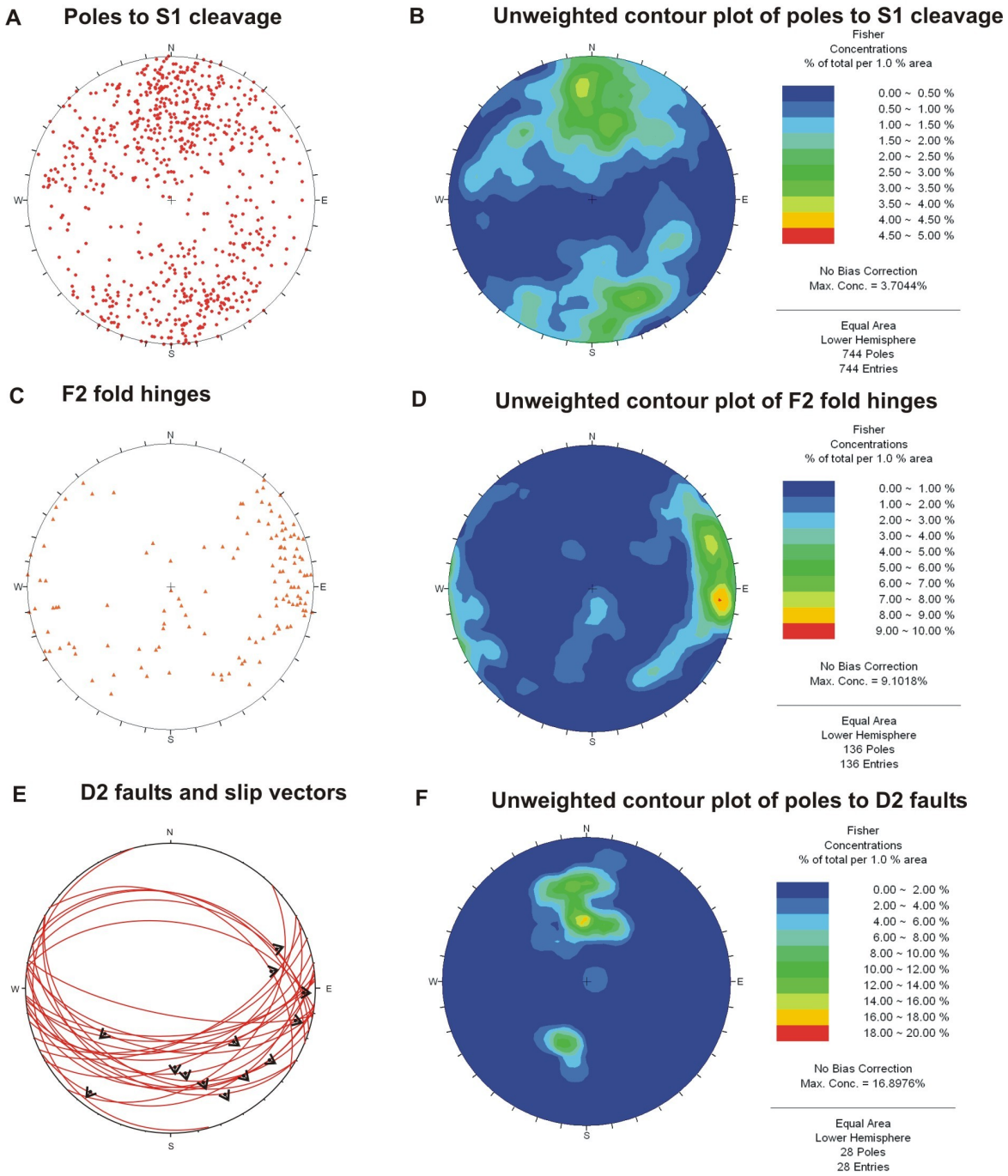

Fig. 2.41. A) All poles to S1 cleavage recorded in Nemegt and Altan Uul. The data is divided into two distinct groups; dominantly south-dipping cleavage and dominantly north-dipping cleavage B) Unweighted contour plot of all poles to S1 cleavage recorded in Nemegt and Altan Uul. The highest concentration of cleavage measurements indicate steep to moderate south-dipping cleavage. There is also a high concentration of steep north to northwest dipping cleavage. C) All F2 fold axes recorded in Nemegt and Altan Uul. The F2 fold hinges indicate southeast to northeast plunging fold hinges and some northeast to southwest plunging fold hinges. D) Unweighted contour plot of all F2 fold axes recorded in Nemegt and Altan Uul. The highest concentration of fold axis data is east plunging. E) Fault planes of all D2 faults with slip vectors where measured. The faults form two distinct groups; moderately south-dipping and moderately north-dipping. There are slip vectors indicating that left- and right-lateral oblique slip occurred. However, most of the slip vectors are close to dip-slip. F) Unweighted contour plot of all poles to fault planes of D2 faults. The highest concentration of data on the plot indicates that there are more south-dipping D2 thrust faults than north-dipping thrust faults.

deformation events, perhaps because the D2 event was progressive from the D1 event.

In western Nemegt Uul, S1 cleavage, F2 folds and D2 ductile shear zones are cut by ductile extensional shear zones and brittle normal faults (sections 2.5.7-2.5.8; Fig. 2.5 [21,25-26]; Fig. 2.20H) and the northern front of Altan Uul is marked by a northeast-southwest trending steep normal fault (Cunningham et al. submitted; section 2.4.1). The extensional shear zones and normal faults in Nemegt and Altan Uul are broadly parallel to Cretaceous basin forming faults north and south of the ranges (Cunningham et al. submitted; Fig. 2.39 [1,2]), and are interpreted as expressions of broadly north-south extensional deformation (D3) during Jurassic-Cretaceous basin formation across southern Mongolia (Meng et al. 2003). Deformation arising from this event is discussed further in chapter 3.

Nemegt Uul is bound by basinward-directed thrust faults on both sides (Fig. 2.6 [15]; Fig. 2.22A; Fig. 2.26D-E; Fig. 2.39). Altan Uul is bound to the south by a north-dipping thrust fault (Fig. 2.39). These faults thrust Palaeozoic rocks over Cretaceous-Cenozoic basin sediments. Within Nemegt Uul, several thrust faults carry metamorphosed Palaeozoic rocks over poorly consolidated Cretaceous-Cenozoic sediments (Fig. 2.5 [17]; Fig. 2.6 [4,9,13]; Fig. 2.19G). The structures are associated with a fourth distinct phase of deformation (D4) in the area which was a Cenozoic transpressional mountain building event. The deformation arising from this event is discussed in detail in chapter 3.

In summary, the structures from four deformation events have been documented in Nemegt and Altan Uul. The D3 extensional event formed normal faults that cut Cretaceous sediments in the basins north and south of Nemegt and Altan Uul, so most likely occurred in the Cretaceous, during widespread extensional basin formation in the region (Meng et al. 2003). The D4 transpressional structures formed the uplift at Nemegt and Altan Uul. D4 structures are seen to cut Cretaceous-Cenozoic sediments so mountain building must have occurred in the Cenozoic. D1 and D2 are the only pre-Cretaceous deformation events and are responsible for the Palaeozoic deformation in Nemegt and Altan Uul. The distribution of D1 and D2 strain and a discussion of their timings follows in section 2.10.3.

2.10.3 Strain variation

Palaeozoic strain and metamorphism in the rocks in Nemegt and Altan Uul are

closely linked. S1 cleavage is defined by the alignment of sheet silicate minerals and bands of recrystallised quartz. The dominant cleavage defining minerals are chlorite, muscovite, and sometimes biotite, especially in meta-sedimentary rocks (sections 2.5.7-2.5.8, 2.6.5, 2.7.3; Fig. 2.17A; Fig. 2.19B). Chlorite and muscovite are part of the mineral assemblage that indicates that many of the rocks, especially those with a meta-sedimentary composition, in Nemegt and Altan Uul have been metamorphosed in the greenschist facies (Bucher & Frey 1994). The alignment of metamorphic minerals to form the cleavage suggests that peak metamorphism occurred shortly before or contemporaneously with the D1 contractional deformation event.

It is important to note that only small areas of Altan Uul at its western and eastern extent were studied during this project, so a lack of evidence for structures may reflect the paucity of documentation in the area. Similarly, the main source of information about structures in Nemegt Uul is three transects through the range, so it is difficult to confidently state that structural trends documented here are representative of the entire area.

Finally, many of the faults in Nemegt and Altan Uul cannot confidently be assigned an age due to the lack of geochronology on the faults and the lack of cross-cutting relationships documented in the field. Where a fault can be dated relative to other structures by cross-cutting field relationships, faults in close proximity with the same orientation, width, fault rocks, slip direction and slip sense can be cautiously inferred to be of the same generation. The following sections discuss the distribution of structures formed by the D1 and D2 contractional deformation events. A discussion of the structures formed by the D3 extensional deformation event and D4 transpressional deformation event is included in chapter 3.

Altan Uul and western Nemegt Uul

The dominant expression of D1 contractional deformation in Altan Uul and western Nemegt Uul is a widespread S1 cleavage. However, S1 cleavage is not developed in all areas. It is ubiquitous in meta-sedimentary sequences north of the Altan Uul ophiolite (Fig. 2.5C-H; Fig. 2.39; sections 2.5.5-2.5.8), in which mica minerals, like chlorite and muscovite, are most common. Meta-volcanic sequences and coarse volcaniclastic meta-sedimentary sequences are cleaved, but cleavage is close-spaced and

is commonly localised near shear zones (Fig. 2.5A-B; Fig. 2.13D; Fig. 2.15G-H; sections 2.5.1-2.5.4).

F1 folds of bedding have not been documented in Altan Uul. F1 fold hinges can be seen in western Nemegt Uul, but the bedding has been tightly refolded by D2 (section 2.5.8; Fig. 2.20F). F2 folds of S1 cleavage are ubiquitous throughout the West Nemegt Volcaniclastic sequence and West Nemegt Psammite sequence north of the Altan Uul ophiolite (sections 2.5.7-2.5.8; Fig. 2.5E-H; Fig. 2.39), and the jasperoids at the northern extent of the Southwest Altan Ophiolite sequence (section 2.4.1; Fig. 2.4). F2 fold axes dominantly trend east-west and plunge gently to the east or west. However, the data suggests that there are more eastward plunging fold axes (Fig. 2.41C-D). In the South Altan Phyllite sequence (section 2.5.4), S1 cleavage is folded into upright and open east-west trending F2 folds (Fig. 2.5 [8-9]; Fig. 2.16B, C). This is unique in the Nemegt and Altan Uul region.

In western Altan Uul, a north-directed thrust fault striking 300^{o} and dipping 32^{o} to the southwest at the northern extent of the serpentinites in the Altan Uul ophiolite is truncated by a normal fault striking 105^{o} and dipping 75^{o} to the north (section 2.4.1; Fig. 2.10D). If the normal fault is an expression of D3 extensional deformation, the earlier north-directed thrust can be assumed to relate to D1 or D2. Photo-geological interpretation of GoogleEarth imagery of western Altan Uul suggests a fault that thrusts the jasperoids northwards over psammites is truncated by the normal fault (D3) at the northern front of Altan Uul and so is classified as a D2 structure (Cunningham et al. submitted; section 2.4.1; Fig. 2.4 [11,12]; Fig. 2.10F).

The only place in western Nemegt Uul where D2 thrust shear zones are cut by normal faults, assumed to have formed during the D3 extensional deformation event, is in the West Nemegt Psammite sequence (section 2.5.8; Fig. 2.5 G-H). The D2 thrust shear zones in this area excise the long-limbs of F2 folds of cleavage, and are all broadly east-west trending with shallow to moderate southerly dips (section 2.5.8; Fig. 2.20G).

In summary, there is a south to north variation in the intensity of D1 and D2 strain in Altan Uul and western Nemegt Uul. Some of this can be attributed to the ease with which the meta-sedimentary rocks north of the Altan Uul ophiolite are cleaved (sections 2.5.5-2.5.8; Fig. 2.39) compared to the meta-volcanic and volcaniclastic meta-sedimentary rocks south of the Altan Uul ophiolite (sections 2.5.1-2.5.4; Fig. 2.39). In western Altan Uul, basalts in the south of the Southwest Altan Ophiolite sequence

(section 2.4.1) contain sub-spherical unstrained amygdales of quartz and chlorite-filled vesicles (Fig. 2.9D). However, north of the mafic-ultramafic rocks in the sequence, jasperoids are folded into tight north-vergent F2 folds of cleavage (section 2.4.1; Fig. 2.4 transect).

The South Altan Phyllite sequence (section 2.5.4) to the south of the Altan Uul ophiolite in eastern Altan Uul is folded into open upright F2 folds (Fig. 2.16B, C) in contrast to the tight north-vergent F2 folds in the West Nemegt Psammite sequence (section 2.5.8; Fig. 2.20E) to the north of the Altan Uul ophiolite in western Nemegt Uul (Fig. 2.39), even though they consist of similar phyllite and meta-pelite rocks. This suggests that the Altan Uul ophiolite marks a boundary between less strained rocks to the south and more intensely strained rocks to the north. This may suggest that obduction of the Altan Uul ophiolite was contemporaneous with south to north contractional deformation during D1 and D2. Furthermore, more intense strain to the north of the ophiolite is consistent with northward obduction of the ophiolite over the rocks in northern Altan Uul and western Nemegt Uul (section 2.5.5-2.5.8; Fig. 2.39).

Central and Eastern Nemegt Uul

Upright open F1 folds of bedding are seen in the Southeast Nemegt Volcaniclastic sequence in eastern Nemegt Uul (section 2.7.2; Fig. 2.7 stereonets 1-2; Fig. 2.29F). D2 structures have not been identified in the area.

The dominant manifestation of D1 in central Nemegt Uul is S1 cleavage (Fig. 2.6). Throughout central Nemegt Uul, S1 cleavage trends east-west and mostly dips south (Fig. 2.6 B-D), although areas to the south have north-dipping cleavage (Fig. 2.6 A-B). Throughout central and eastern Nemegt Uul, meta-sedimentary rocks (sections 2.6.5, 2.7.3) are generally more intensely cleaved than blocky meta-volcanic and volcaniclastic meta-sedimentary rocks (sections 2.6.2, 2.6.4, 2.7.2) with the exception of the volcaniclastic schists in the Central Nemegt Upper Extrusive sequence, which have a matrix rich in sheet-silicate minerals like chlorite (section 2.6.3; Fig. 2.6). There are few faults in central or eastern Nemegt Uul that can confidently be assigned to D1 or D2. A belt of flysch between the Central Nemegt Lower extrusive sequence and the North Central Nemegt Schist sequence (section 2.6.4; Fig. 2.39), is ductile deformed in a north-directed shear zone, and has been overprinted by east-west trending left-lateral north-

directed brittle thrusts, suggesting that the shear zone is an older structure, possibly related to D1 or D2 deformation.

2.10.4 Metamorphic grade variation

It is not possible to calculate the exact P-T conditions of metamorphism in the rocks of Nemegt and Altan Uul with the data available. However, the mineral assemblages of the rocks along the four transects through the ranges (section 2.4-2.7) make it possible to assign the metamorphic facies to the peak metamorphic conditions that the rocks underwent. The mineral assemblages used to estimate the metamorphic facies in which peak metamorphism occurred are dependant on the bulk composition of the protoliths of the metamorphic rocks (Spear, 1993). Consequently, the meta-volcanic rocks in Nemegt and Altan Uul have a different metamorphic mineral assemblage to the meta-sedimentary rocks at the same pressures and temperatures.

To estimate P-T conditions from the metamorphic facies in which peak metamorphism occurred requires an assumption about the tectonic environment in which metamorphism occurred to be made. Miyashiro (1961) first recognised three facies series he called 'barric types', which are dependent on the ratio of pressure to temperature increase with increasing depth in the Earth (Fig. 2.42). The three 'barric types' define three geothermal gradients along which rocks might travel during burial, which determines the metamorphic mineral assemblages that form within them. The first facies series is the high P/T or glaucophane-blueschist series, typical of metamorphism in subduction zone settings. This series progresses through the zeolite – pumpellyite – blueschist – eclogite facies with increasing pressure and temperature (Fig. 2.42; Spear, 1993). The second facies series is the intermediate P/T or kyanite-sillimanite series, typical of metamorphism in continental orogenic belts. This series progresses through the greenschist – epidote amphibolite – amphibolite – granulite facies with increasing pressure and temperature (Fig. 2.42; Spear, 1993). The third facies series is the low P/T or andalusite-sillimanite series, typical of metamorphism in island arcs, ocean ridges and contact aureoles. This series progresses through the greenschist – amphibolite – granulite facies with increasing pressure and temperature (Fig. 2.42; Spear, 1993). To relate the metamorphic mineral assemblages in Nemegt and Altan Uul to a correct range of P-T conditions, it is essential to consider which facies series they belong to and therefore

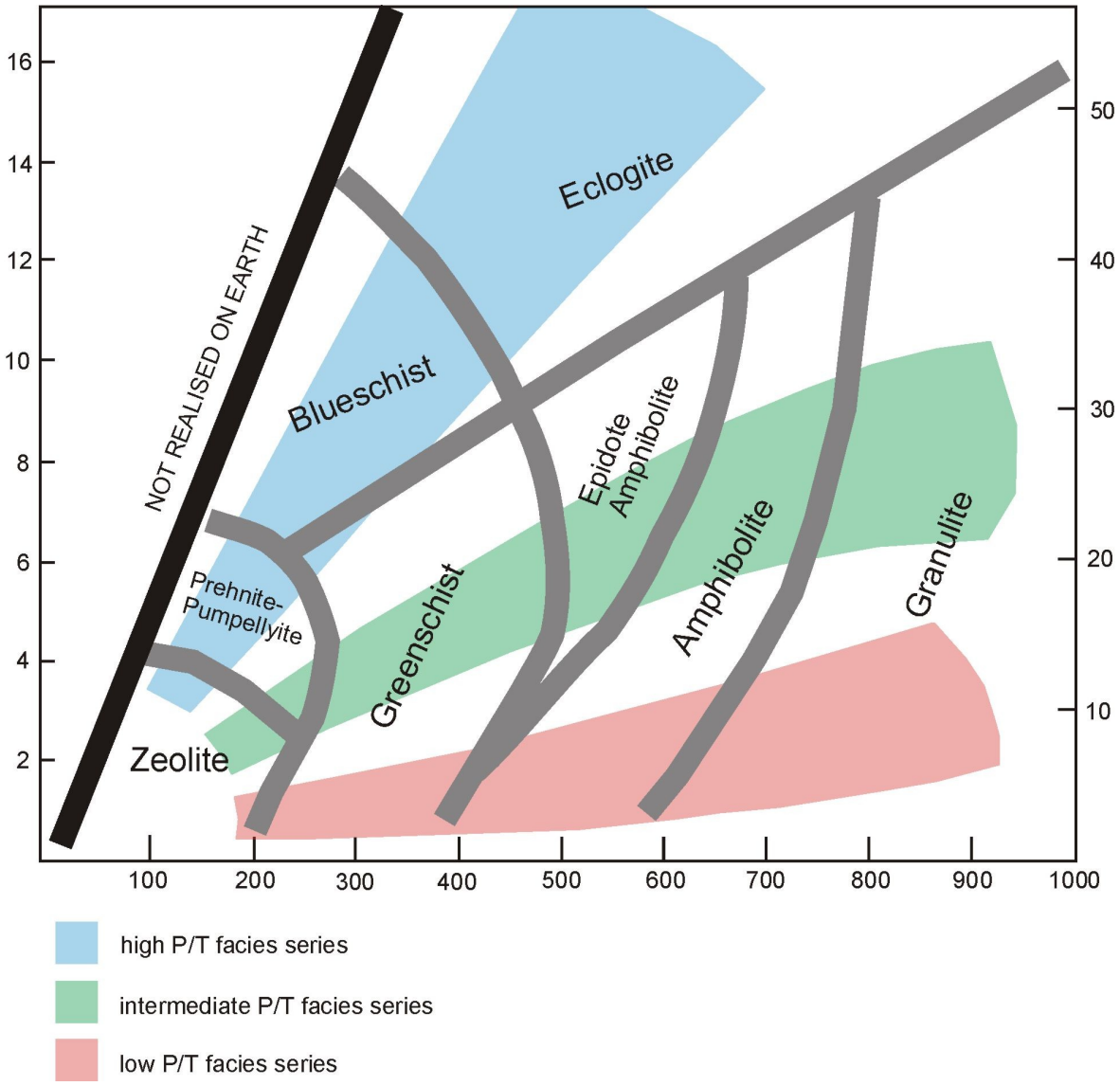

Fig. 2.42. P-T conditions of metamorphic facies from Spear (1993). High P/T, intermediate P/T, and low P/T facies series are marked for comparison.

which geothermal gradient should be used to estimate the P-T conditions, and depth at which peak metamorphism occurred.

Throughout most of Nemegt and Altan Uul meta-psammitic and meta-pelitic rocks have a metamorphic mineral assemblage of chlorite ± epidote ± biotite ± muscovite (e.g. the West Nemegt Volcaniclastic sequence, section 2.5.7) and most mafic rocks have a metamorphic mineral assemblage of chlorite ± epidote ± actinolite ± hornblende (e.g. the North Altan extrusive sequence, section 2.5.6) suggesting that these rocks are of greenschist facies (Bucher & Frey 1994). In the meta-sedimentary rocks, the presence of biotite suggests higher P-T conditions within the greenschist facies were achieved than where chlorite exists on its own (Bucher & Frey 1994).

In the West Nemegt Psammite sequence (Fig. 2.5 [26]; section 2.5.8), a fault bound block of meta-pelitic schist has the metamorphic mineral assemblage of biotite – garnet – epidote suggesting that the rocks are of epidote-amphibolite facies (Bucher & Frey 1994). The biotite crystals in the meta-pelitic schists in western Nemegt Uul are aligned to form the S1 cleavage. This suggests that these rocks were metamorphosed during the same regional D1 contractional deformation event as the other chlorite-rich meta-pelitic rocks throughout Nemegt and Altan Uul, but that they were at higher pressures and temperatures, and so were deeper.

The juxtaposition of greenschist and epidote-amphibolite grade rocks that were metamorphosed at the same time, but at different depths, suggests typical Barrovian metamorphism, or an intermediate P/T facies series, should be used to estimate the P-T conditions of peak metamorphism in the rocks of Nemegt and Altan Uul (Fig. 2.42).

The Miyashiro (1961) facies model identifies a set of P-T zones with transitional boundaries (Fig. 2.42). However, using the facies model in figure 2.42, and a geotherm of 25 ^{o}C/km, which runs through the centre of the intermediate P/T facies series, a range of possible P-T conditions for the metamorphic rocks of Nemegt and Altan Uul can be estimated (Spear, 1993). The P-T conditions for greenschist facies metamorphism along a 25 ^{o}C/km geotherm are c.280 ^{o}C at c. 3.2 kbar/c.12 km to c. 475^{o} at 5.75 kbar/c. 18 km (Spear, 1993). Greenschist facies range from chlorite zone rocks formed at lower pressures and temperatures to biotite zone rocks formed higher pressures and temperatures in the biotite zone (Bucher & Frey 1994). Some of the meta-pelitic rocks in the West Nemegt Volcaniclastic sequence contain biotite as the dominant cleavage defining mineral (section 2.5.7), indicating biotite zone metamorphism, nearer the top of the range of temperatures and pressures possible in the greenschist facies than the majority of meta-pelitic and meta-psammitic rocks in Nemegt and Altan Uul, which contain chlorite as the dominant cleavage defining mineral. The P-T conditions for epidote-amphibolite facies metamorphism along a 25^{o} C/km geotherm are c. 500 ^{o}C at c. 5.75 kbar/c. 18 km to c. 590 ^{o}C at c. 6.75 kbar/c.20 km (Spear, 1993).

Gabbros in the Altan Uul ophiolite were also metamorphosed at greenschist and epidote-amphibolite grade (section 2.9.1). However, this is thought to have occurred during ocean-floor metamorphism, before the D1 contractional deformation event and before regional metamorphism (section. 2.9.1; Rippington et al. 2008). Although Manning et al. (1996) demonstrate that greenschist to epidote-amphibolite facies

metamorphism occurs in oceanic crust, it is at the upper pressure limits of the low P/T facies series geotherm in the facies model presented in figure 2.42 (Miyashiro, 1961, Spear, 1993). Using the upper limits of the low P/T facies series, P-T conditions for peak ocean-floor metamorphism of the Altan Uul ophiolite were c. 450 ^{o}C at c. 2 kbar (Fig. 2.42). This is in agreement with the P-T conditions of experimentally determined reactions for prograde reactions by Deer (1966) and Moody et al. (1983) in the cumulate gabbros (section 2.9.1).

In the Northeast Nemegt schist sequence (section 2.7.3) where quartz-chlorite-biotite schists and biotite-schists are exposed in close association with granite intrusions, biotite and garnet overprint chlorite, which defines the cleavage, and large flakes of free muscovite can be seen all over the schist in hand specimen, suggesting the rocks were locally metamorphosed by the granites. This suggests the low P/T facies series should be used to estimate the P-T conditions during contact metamorphism, but the intermediate P/T facies series should be used to estimate the P-T conditions during the preceding regional metamorphic event. The overprinted chlorite defining the cleavage in these rocks suggests the schists were metamorphosed to greenschist facies. However, some biotite laths are also rotated into parallelism with the cleavage, suggesting they formed before or during the D1 cleavage-forming contractional deformation event. This indicates that these schists were metamorphosed to the biotite zone of the greenschist facies (Bucher & Frey, 1994; section 2.7.3), in P-T conditions nearer the top of the estimated range.

The only unmetamorphosed rocks in the area are volcaniclastic breccias and arkosic sandstones found at the northern extent of the South Altan Upper Extrusive sequence in southern Altan Uul (section 2.5.1; Fig. 2.39). These rocks have been downthrown on a north-dipping normal fault and show no evidence that they have been regionally metamorphosed.

2.11 Discussion

There is a south to north change of lithologies in Nemegt and Altan Uul, from meta-volcanic and volcaniclastic meta-sedimentary rocks through ophiolitic rocks in Altan Uul to arkosic meta-sedimentary rocks in the north, and mature meta-sedimentary rocks and orthogneiss in northeast Nemegt Uul.

Meta-volcanic and volcaniclastic meta-sedimentary rocks crop out in east-west

trending belts in southern Altan Uul and throughout central and eastern Nemegt Uul (Fig. 2.39). Based on estimated modal percentages of quartz, and alkali and plagioclase feldspars in samples in these areas, andesite is the dominant volcanic extrusive rock and is the dominant clast-type in volcaniclastic rocks (section 2.10.1). In Altan Uul, more meta-basaltic mineral assemblages were identified (section 2.10.1), and pillow basalts occur in southern Altan Uul (section 2.5.1; Fig. 2.13B). There is also a fault-bound diorite pluton exposed in southern Altan Uul (section 2.5.3; Fig. 2.39). In central Nemegt Uul, the meta-volcanic and volcaniclastic sequences also contain meta-rhyolite (section 2.6.4).

The assemblages of dominantly meta-andesitic volcanic and volcaniclastic rocks with meta-basaltic and rhyolitic components, and a large dioritic intrusion suggest the meta-volcanic and volcaniclastic sequences in southern Altan Uul and Nemegt Uul may represent the products of arc volcanism. This interpretation agrees with work by Helo et al. (2006) which suggests Silurian volcano-sedimentary sequences in Nemegt Uul and Altan Uul have a geochemistry compatible with an intra-oceanic island arc interpretation. Furthermore, Helo et al. (2006) showed that the geochemistry of meta-andesites and meta -basalts in Nemegt and Altan Uul are geochemically indistinguishable from volcanic sequences exposed in the Gurvan Sayhan range to the east (Fig. 2.1). This suggests the east-west trending belts of meta-volcanic and volcaniclastic meta-sedimentary rocks in southern Altan Uul and Nemegt Uul can be considered the products of a single arc.

North of the meta-volcanic and volcaniclastic meta-sedimentary rocks in Altan Uul, fault bound sequences consisting of pillow lavas, gabbros with cumulate layers, sheeted dykes, serpentinite, peridotite, and jasperoids are exposed. The primary mineral phases of the gabbros, and the order of crystallisation (olivine, plagioclase, augite) is the same as olivine gabbro cumulates found in the Oman ophiolite (Benoit et al. 1996). Cross -cutting relationships of primary and secondary mineral phases indicate that all of the samples were metamorphosed under greenschist conditions, and that some began the transition to epidote-amphibolite-grade metamorphism, consistent with an oceanic crust environment (Manning et al. 1996). Epidote and quartz veining post-dates metamorphism. Analyses of the Altan Uul cumulate gabbros shows enrichment in LFS elements, confirming that the rocks were altered by metamorphism and veining. However, the HFS elements follow the same trend seen in the cumulate gabbros from the Oman ophiolite, which are interpreted to have formed from fractional crystallisation of liquids with MORB characteristics (Benoit et al. 1996). The field, petrographical and petrological

evidence suggest there is an east-west trending, south-dipping ophiolitic suite of rocks in Altan Uul and western Nemegt Uul (Fig. 2.39).

The Altan Uul ophiolite is thrust north over arkosic meta-psammitic and meta-pelitic schists. To the east in central Nemegt Uul, meta-volcanic and volcaniclastic meta-sedimentary rocks are also thrust north over meta-psammitic and meta-pelitic schists (Fig. 2.39). The arkosic nature of the meta-sedimentary rocks north of Altan Uul ophiolite implies that they are proximal to their source. However, the arkosic meta-sedimentary rocks are overthrust by the ophiolite, suggesting they were deposited on the opposite side of the closing ocean basin from the arc rocks documented in southern Nemegt and Altan Uul. The arkosic meta-sediments may be derived from arc-type rocks to the north, which are now covered by the extensive Cretaceous-Cenozoic sedimentary sequences in the basin to the north, or from continental crust. Alternatively, the arkosic meta-sedimentary rocks may be derived from the arc-rocks to the south, and have been deposited to the north in the final stages of ocean basin closure, just before the ophiolite was obducted onto them.

In northeast Nemegt Uul, meta-volcanic and volcaniclastic meta-sedimentary rocks are thrust north over arkosic psammites, quartz-biotite-chlorite schists and quartz-biotite schists. The Northeast Nemegt Schist sequence varies from arkosic meta-sedimentary rocks in the south to mature meta-sedimentary rocks in the north. At the northern extent of the sequence, biotite schists lie with angular unconformity upon a discontinuous belt of orthogneiss. The unconformity suggests that the orthogneiss is significantly older than the meta-sedimentary rocks. The original tectonic setting of the gneiss is not certain. The schists contain no feldspar, suggesting the sediments that formed their protolith were probably formed in a marine setting. The unconformable relationship between the gneiss and the schists suggest it may represent a block of basement that marine sediments were later deposited on to.

The arkosic nature of the meta-sedimentary rocks in northern Nemegt and Altan Uul implies that they are proximal to their source. The arkosic meta-sediments may be derived from arc-type rocks to the north, which are now covered by the extensive Cretaceous-Cenozoic sedimentary sequences in the basin to the north, or from continental crust. Alternatively, the arkosic meta-sedimentary rocks may be derived from the arc-rocks to the south. However, they are overthrust by the ophiolite, suggesting they were deposited on the opposite side of the closing ocean basin from the arc rocks documented

in southern Nemegt and Altan Uul. It is possible that they were derived from dioritic and possibly gabbroic arc rocks to the south of the ophiolite, and deposited to the north in the final stages of ocean basin closure, just before the ophiolite was obducted onto them.

Four distinct phases of deformation have been identified by cross-cutting field relationships (section 2.10.2). D1 was a north-south contractional deformation event that folded bedding and formed an east-west trending S1 cleavage throughout Nemegt and Altan Uul. The S1 cleavage is defined by chlorite, muscovite and biotite, suggesting that peak metamorphism of the cleaved rocks in the area was shortly before or contemporaneous with D1. D2 was a south to north contractional deformation event that folded S1 cleavage into tight north-vergent F2 folds and cut S1 cleavage and F2 folds with north-directed shear zones. F2 folds are only found in meta-sedimentary rocks north of the Altan Uul ophiolite. There is no convincing evidence for D2 structures in southeast Nemegt Uul, so D2 seems not to have modified D1 structures in the area. D2 fold axes, and shear zones are approximately parallel to F1 fold axes and S1 cleavage, which might suggest that D2 formed under the same principal stress directions as, and may have followed on from, D1.

D3 was an extensional deformation event that formed Cretaceous basins to the north and south of Nemegt and Altan Uul. D4 was a transpressional mountain building event that uplifted the Palaeozoic rocks in Nemegt and Altan Uul to form the mountains that exist today (section 2.10.2). Further evidence for the timings and styles of deformation during the D3 and D4 deformation events is discussed in chapter 3.

D1 and D2 did not affect the Cretaceous-Cenozoic sediments to the north and south of Nemegt and Altan Uul. Sandstone petrographic data of Lamb and Badarch (1997, 2001) suggests that there was a shift from marine to terrestrial sedimentation in the late Carboniferous, suggesting that the crust was uplifted at this time (Rippington et al. 2008). D1 and D2 are the only contractional deformation events recorded in the rocks in Nemegt and Altan Uul, suggesting that D1 and/or D2 contraction may have caused late Carboniferous uplift in the area.

The majority of the Palaeozoic rocks in Nemegt and Altan Uul have been metamorphosed to greenschist facies, although there are some important exceptions. Volcaniclastic breccia and arkoses in southern Altan Uul (section 2.5.1) are unmetamorphosed and are the lowest grade Palaeozoic rocks in the area. Meta-pelitic schists in western Nemegt Uul contain biotite and garnet related to regional

metamorphism, and are the highest grade rocks seen in Nemegt and Altan Uul, and also the highest grade rocks yet documented in the Gobi Altai region, (Cunningham. Pers. Com.). They may mark a regional metamorphic culmination. The meta-psammites and meta-pelites north of the Altan Uul ophiolite are deformed into tight north-vergent F2 folds and cut by north-directed thrust shear zones. In contrast, F2 folds in phyllites to the south of the Altan Uul ophiolite are upright and open.

In summary, the Palaeozoic rocks with the highest metamorphic grade and the most intense strain are in north Altan Uul and western Nemegt Uul (section 2.5.5-2.5.8), to the north of the Altan Uul ophiolite. Palaeozoic rocks with the lowest metamorphic grade and the least strain are in southern Altan Uul, to the south of the Altan Uul ophiolite (section 2.5.1). Therefore, the tectonic event that drove northwards obduction of the Altan Uul ophiolite may have been the cause of the D1 and D2 contractional deformation in the late Carboniferous, and the rocks north of the ophiolite were more deeply buried and more intensely strained because they were overthrust by the ophiolite during obduction.

The evidence presented here is used to propose models for the original tectonic setting and obduction of the Altan Uul ophiolite, and to produce a synthesis of the Palaeozoic evolution of Nemegt and Altan Uul in chapter 4.

2.12 Conclusions

Documentation of the variation in lithologies, metamorphism, and strain across four transects in Nemegt Uul and Altan Uul, combined with analysis of Landsat TM satellite imagery and petrographical and petrological analyses of mafic-ultramafic sequences in the ranges allow several conclusions to be drawn.

1. There is a south to north variation in Palaeozoic lithologies in Nemegt and Altan Uul. In the south, east-west trending belts of meta-andesitic, meta-basaltic, meta-rhyolitic and dioritic rocks and volcaniclastic meta-sedimentary rocks with andesitic clasts are interpreted as the products of a volcanic arc. Geochronological and geochemical analysis of isolated volcano-sedimentary rocks in Nemegt and Altan Uul may suggest a single intra-oceanic arc/fore-arc system may have existed in the region during the mid-late Palaeozoic (Helo et al. 2006).

2. A discontinuous east-west trending south-dipping fault-bound belt of variably exposed mafic and ultramafic rocks is thrust northwards over dominantly arkosic meta-psammitic and meta-pelitic rocks in Altan Uul and western Nemegt Uul. The belt includes pillow basalts, gabbros with cumulate layers, sheeted dykes, serpentinite, peridotite and jasperoids. Trace elements of the gabbros have been compared to samples from fore-arc, back-arc, island-arc and ophiolitic environments. The immobile trace elements of the Altan Uul gabbros are most similar to those of cumulate gabbros from the Oman ophiolite. Therefore, the mafic and ultramafic rocks in Altan Uul are cautiously interpreted to represent a partial ophiolite sequence.

3. In northeast Nemegt Uul, a belt of schists displays a northwards transition from dominantly arkosic psammitic schists to more mature biotite schists. The biotite schists lie with angular unconformity upon orthogneiss in a discontinuous east-west trending belt exposed along the northern front of Nemegt Uul. The angular unconformity suggests that the protoliths of the schists, possibly marine sediments, were deposited on the gneiss, before burial and metamorphism.

4. Four deformation events affect the Palaeozoic rocks in Nemegt and Altan Uul. Only D1 and D2, both south-north contractional deformation events are considered to have occurred in the Palaeozoic. Parallelism between D2 and D1 structures, and a lack of evidence for subsequent modification of D1 structures in eastern Nemegt Uul suggests both deformation events occurred under the same regional stress orientations, and that D2 may have directly followed D1. Sandstone petrographic data of Lamb and Bardarch (1997, 2001) suggest the area was uplifted in the late Carboniferous. It is suggested that the D1 and D2 events may have produced this uplift.

5. The most strained and highest grade metamorphic rocks are north of the Altan Uul ophiolite and the least strained and the lowest grade metamorphic rocks are to the south. Thus, the event that drove obduction of the ophiolite may have caused the D1 and D2 deformation events.

Chapter 3

The post-accretionary evolution of Nemegt and Altan Uul

3.1 Introduction

Central Asia contains many diffuse regions of active transpressional deformation making it an ideal region in which to study the processes of continental intraplate deformation and active mountain building (Fig. 3.1; Tapponnier & Molnar 1979, Baljinnyam et al. 1993, Cunningham 2005, Cunningham 2007). However, the Palaeozoic and Mesozoic deformation may have affected the way in which Cenozoic stresses have been accommodated by the crust. In southern Mongolia, there is a complex history of Palaeozoic terrane accretion and continental amalgamation that has formed an approximately east-west trending structural grain throughout the region (Fig. 3.1 inset; Cunningham 1998, 2007, Badarch et al. 2002). Subsequent to terrane accretion and continental amalgamation, much of the region underwent Jurassic-Cretaceous extension, producing basins filled with palynomorph and dinosaur fossil-rich Cretaceous sediments (Jerzykiewicz et al. 1991, Traynor & Sladen 1995, Benton et al. 2000, Meng 2003, Meng et al. 2003), and Late Cenozoic transpressional deformation, uplifting the mountains seen today, caused by a northeasterly SH_{max} thought to be a result of the ongoing north-directed India-Eurasia collision approximately 2500 km to the south (Molnar & Tapponier 1975, Zoback, 1992, Baljinnyam et al. 1993).

The Gobi Altai in southern Mongolia is a region of left-lateral transpressional deformation with a basin and range physiography (Fig. 3.1; Cunningham 2005, 2007). It is dominated by two large intracontinental left-lateral strike-slip fault systems, the Bogd fault and the Gobi-Tien Shan fault system, which localise deformation and uplift at restraining bends and stepovers, forming distinct intraplate orogenic belts along their length (Fig. 3.1; Cunningham et al. 1996, Cunningham 2005, 2007). The left-lateral Bogd fault can be traced over 350 km from Artsa Bogd in the east, to its termination in the southeast Altai in the west (Fig. 3.1). On December 4, 1957, left-lateral slip along the Bogd fault produced a M = 8.3 earthquake and ruptured the surface over a distance of 260 km (Florensov & Solonenko 1967, Kurushin et al. 1997). The left-lateral Gobi-Tien Shan

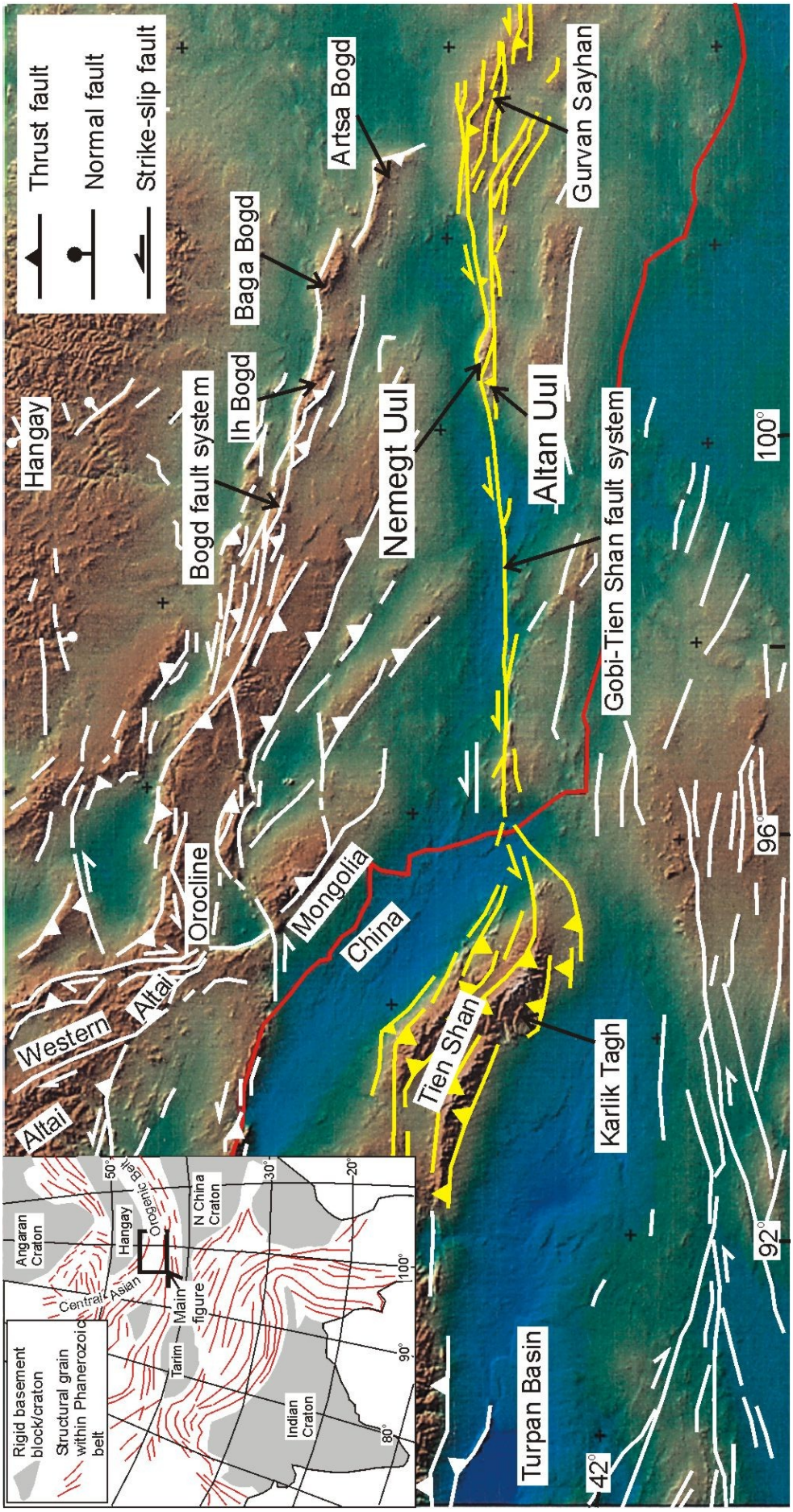

Fig. 3.1. Map of southern Mongolia showing modern fault trends (after Cunningham et al. 2003b). Nemegt and Altan Uul are situated along the left-lateral Gobi-Tien Shan fault system. Inset shows Palaeozoic structural grain (after Cunningham, 2005).

fault system is situated to the south of the Bogd fault in the Gobi Altai region. The eastern termination of the system is a horsetail splay that uplifts the Gurvan Sayhan range, and the western termination is a horsetail splay that uplifts Karlik Tagh in easternmost Tien Shan (Fig. 3.1; Cunningham et al. 2003b). The mountain belts in the Gobi Altai have an architecture of interlinked left-lateral strike-slip faults, pure-slip thrust faults and left-lateral oblique-slip thrust faults (Cunningham 2005). Geomorphological evidence, including low mountain front sinuosities, steeply incised valleys and large Quaternary alluvial fan arrays throughout the Gobi Altai region suggest the mountains are in the early stages of active orogeny (Cunningham et al. 1996, Owen et al. 1997, 1999b), although cosmogenic dating of summit plateaux along the Bogd fault suggest the summit peneplanes of some of the mountains may have been exposed since the Jurassic (Jolivet et al. 2007).

This chapter presents, a 3D model of the architecture of Nemegt and Altan Uul (Fig. 3.2), two Late Cenozoic uplifted mountain ranges situated along the left-lateral Gobi -Tien Shan fault system in southern Mongolia. Previous reconnaissance and geomorphological studies of Nemegt Uul have suggested that it has an asymmetric positive flower structure geometry (Cunningham et al. 1996, Owen et al. 1999b).

Nemegt Uul consists of fault-bound sequences of Palaeozoic greenschist grade meta-andesites, tuffs, meta-volcaniclastic schists, arkosic and mature meta-psammitic and meta-pelitic schists, epidote-amphibolite garnet schists and a small, fault-bound partial ophiolite sequence consisting of greenschist grade meta-gabbros, peridotite and serpentinite, extrusive volcanic rocks and marine sediments. Altan Uul consists of fault-bound sequences of Palaeozoic greenschist grade meta-psammites, meta-pelites, volcaniclastic schists, andesitic lavas, arkosic and volcaniclastic sandstones, mudstones and cherts, epidote-amphibolite grade meta-andesite, and a partial ophiolite sequence consisting of greenschist-grade meta-gabbros, serpentinites, and altered basaltic lavas (Rippington et al. 2008). In chapter 2, the Palaeozoic rocks of Nemegt and Altan Uul were used to define east-west trending litho-tectonic sequences interpreted to present a south to north sequence of arc volcanic and volcaniclastic rocks, an ophiolite, and marine sedimentary rocks which were accreted in the Late Carboniferous, forming an arc-continent suture zone (Rippington et al. 2008; chapter 2; Fig. 3.2).

Four structural and lithological transects through Nemegt Uul and Altan Uul were carried out in 2004 and 2005. Data from these were used to document the

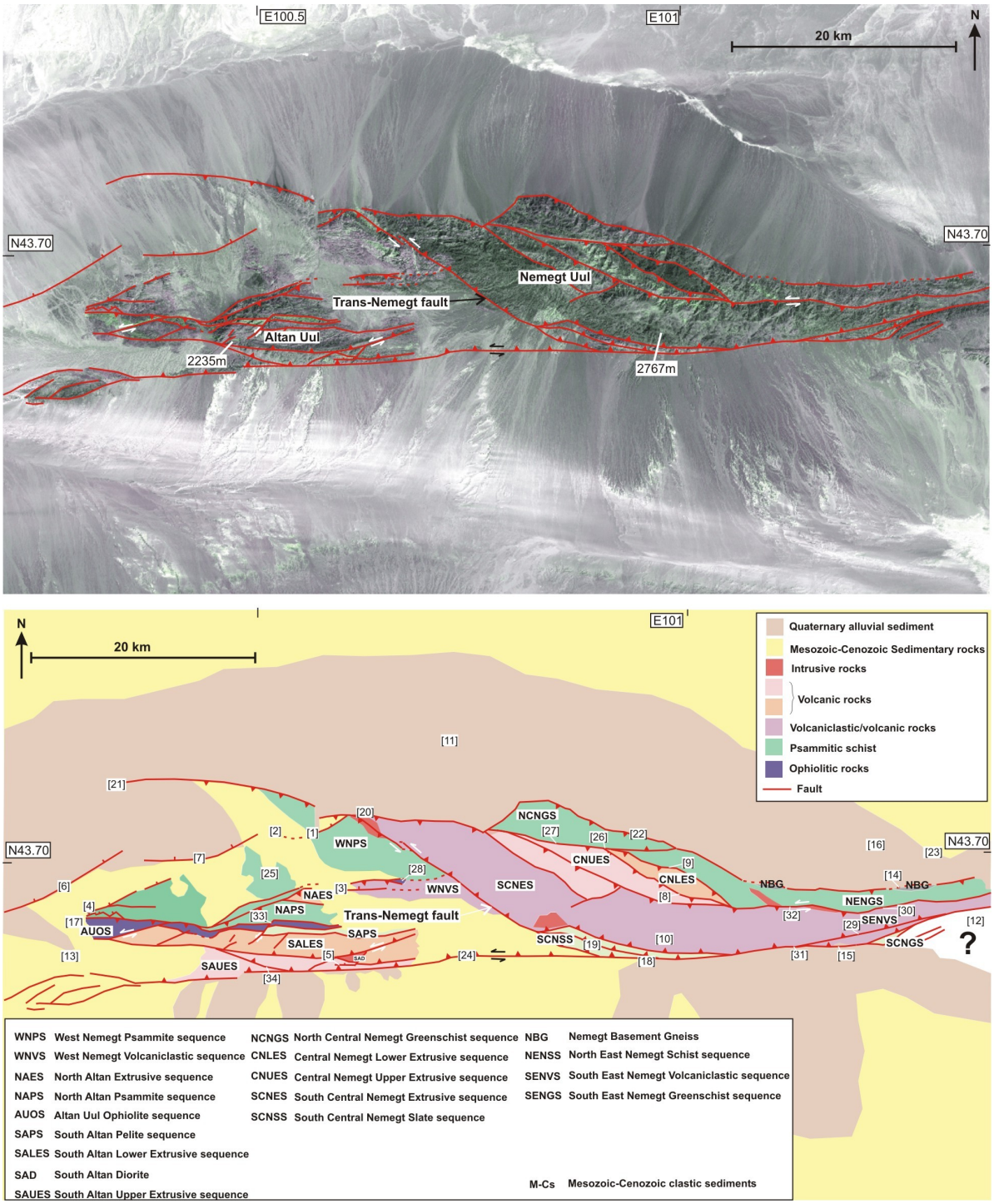

Fig. 3.2. Landsat TM image with major faults marked and litho-tectonic map of Nemegt and Altan Uul. Numbers in brackets refer to numbers in the text.

polydeformational history of basement lithologies (chapter 2). In this chapter, data presented in chapter 2 are reconsidered in the context of the post-accretionary evolution of Nemegt and Altan Uul. In addition, new data are presented that document the geometry and slip vectors of major Cenozoic fault zones. Landsat TM imagery was used to determine the along-strike continuity of major structures within the ranges and to gain geological information about areas not visited. Field observations and Landsat image analysis by the author are combined with results of a geomorphological study of Nemegt Uul by Owen et al. (1999b) to suggest a model for the 3D architecture, and Cenozoic structural and geomorphological evolution of the Nemegt and Altan Uul ranges.

3.2 Cretaceous and Cenozoic geological structure of Nemegt and Altan Uul

In chapter 2, four lithological and structural transects across Nemegt and Altan Uul were described (Fig. 2.4-2.7). There is a lack of geochronological data on the structures documented in Nemegt and Altan Uul. Where possible, cross-cutting lithological and structural relationships have been used to constrain the timing of distinct deformation events and the formation of associated structures. In chapter 2, the structures in Nemegt and Altan Uul were linked to distinct deformation events: late Carboniferous contractional strain (D1 and D2), Cretaceous extensional strain (D3), and Cenozoic transpressional strain (D4). In the following sections, the Cretaceous structures (D3) and Cenozoic structures (D4) of Nemegt and Altan Uul are described in more detail, and interpreted in the context of the Cretaceous and Cenozoic evolution of Nemegt and Altan Uul.

3.3 Cretaceous extensional structures

All the normal faults documented in Nemegt and Altan Uul cut Palaeozoic cleavage and in many places are seen to cut Palaeozoic folds and ductile shear zones, suggesting they formed after late Carboniferous contractional deformation events (D1 and D2). East west and northwest-southeast trending normal faults are broadly parallel to dominantly northwest-southeast trending normal faults that cut the Cretaceous sediments in the basins to the north and south of Nemegt and Altan Uul (Cunningham et al. submitted). The normal faults in the basins cut Cretaceous sedimentary rocks indicating that they post-

date deposition. There is no evidence of a second rifting event after the widespread Jurassic-Cretaceous extensional event in southern Mongolia (Johnson et al. 2001, Meng, 2003). Therefore, it is thought that sedimentation was syn-tectonic deposited and the normal faults that cut Cretaceous basin sedimentary rocks relate to the later phases of Cretaceous basin evolution (Cunningham et al. submitted). Based on this sub-parallelism and the cross-cutting relationships identified, it is suggested here that all of the approximately east-west trending normal faults documented in Nemegt and Altan Uul are Mesozoic.

3.3.1 Nemegt Uul

At several locations In western Nemegt Uul, extensional faults or shear zones cut Palaeozoic folds, cleavage, folds of cleavage and ductile shear zones. Just south of the northern front of northwest Nemegt Uul in a north-south trending canyon (Fig. 2.5 G-H; Fig. 3.2 [1]) a brittle extensional fault that strikes 055^{o} and dips 52^{o} to the northwest, marks the boundary between Palaeozoic cleaved and folded greenschist grade psammite and an unmetamorphosed Cretaceous sedimentary succession (Cunningham et al. submitted). On Landsat TM imagery, the fault can be traced semi-continuously through the Cretaceous rocks west of Nemegt Uul (Fig. 3.2 [2]; Cunningham et al. submitted).

In the north-south trending canyon south of this fault (Fig. 2.5 G-H; Fig. 3.2 [1]), four brittle normal faults strike 265-280^{o} and dip 35-74^{o} south, and cut Palaeozoic folds of cleavage and ductile thrust shear zones (Fig. 3.3A). Slickenline orientations on two of these faults suggest they slipped in a left-lateral normal oblique-slip sense, whilst slickenline data on another suggests dip-slip movement occurred (Fig.

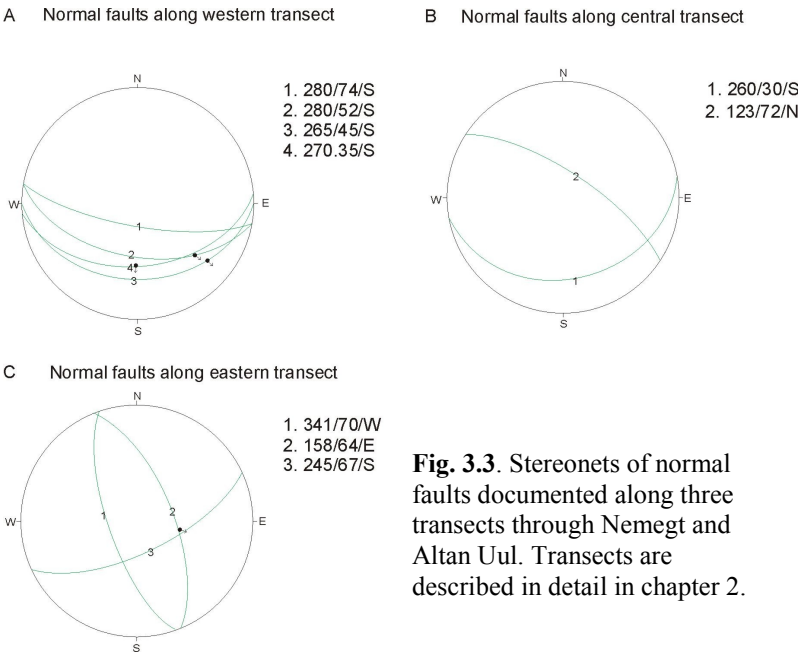

Fig. 3.3. Stereonets of normal faults documented along three transects through Nemegt and Altan Uul. Transects are described in detail in chapter 2.

3.3A). Distinct fault-dragged bedding planes offset by one of the normal faults suggest there has been less than 10 m of normal displacement across the fault (Fig. 2.20H; Fig. 3.3A fault 4). Slickenlines plunge 15° towards 130° on the fault plane which strikes 270° and dips 35° south. A maximum dip parallel offset of 10 m can be used to calculate a maximum net slip of c.14 m, which fault-dragged bedding indicates occurred in a left-lateral normal direction, suggesting the fault is a relatively insignificant structure. Displacement markers were not found on other normal faults in Nemegt Uul so it is not possible to deduce whether all the normal faults in Nemegt Uul have similarly small displacements.

In the West Nemegt Volcaniclastic sequence, a c. 1 m wide zone of brown and fractured zone of mylonite striking 132° and dipping 63° to the northeast marks a shear zone forming a gully that cuts across a north-south valley (section 2.5.7; Fig. 3.2 [3]). The mylonite zone is weathered and fractured and kinematic indicators are not obvious, but to the west a fault with the same orientation cuts the unconformity between the Palaeozoic rocks and Cretaceous sediments perched between Nemegt and Altan Uul, down-throwing the Cretaceous sediments to the north (Fig. 3.4). It is possible the mylonite zone is

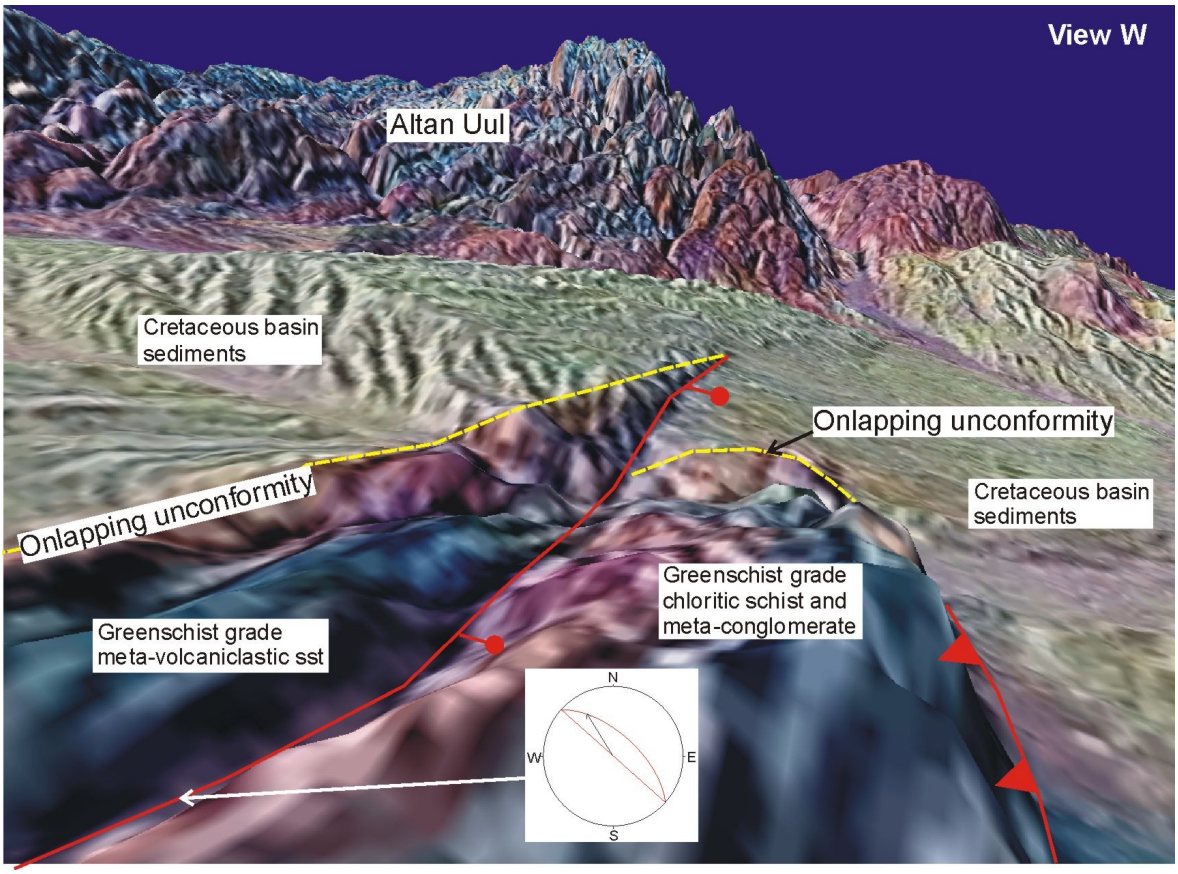

Fig. 3.4. Landsat TM image draped over SRTM-90 image, showing a normal fault cutting the Palaeozoic rocks in Nemegt Uul and the Cretaceous basin perched between Nemegt and Altan Uul.

fractured and weathered because it has been partially reactivated by the brittle normal fault that cuts the Palaeozoic-Cretaceous unconformity to the west (Fig. 3.4).

In central Nemegt Uul, there are very few normal faults. Along the transect detailed in section 2.6, only two normal faults were confidently identified: One cuts meta-volcanic rocks in the middle of the range and strikes 260^{o} and dips 30^{o} to the southeast (Fig. 2.6 B-C). A second strikes 123^{o} and dips 72^{o} to the north, and downthrows Cretaceous conglomerate to the north of a belt of flysch (Fig. 2.6 C; Fig. 3.3B). The amount of offset along these faults is unknown.

Three brittle normal faults were identified along the eastern transect detailed in section 2.7 (Fig. 2.7). In the north, a c.50 cm wide zone of cataclasite marks a normal fault that strikes 245^{o} and dips 67^{o} to the southeast, and cuts the cleaved North East Nemegt Schist sequence (Fig. 3.3C). The other two normal faults cut the South East Nemegt Volcaniclastic sequence and have a very different orientation to the other normal faults identified in Nemegt Uul. The first strikes 341^{o} and dips 70^{o} southwest (Fig. 2.29H; Fig. 3.3C). The second strikes 158^{o} and dips 64^{o} northeast (Fig. 3.3C). Fault slip sense was determined by fault dragged foliation in the fault zone. The fault orientations suggest they may have formed under different stress conditions to the broadly east-west trending Mesozoic faults in Nemegt and Altan Uul. The lack of cross-cutting field relationships at the locations of these faults makes it difficult to identify when they formed and how they fit into the deformation sequence.

3.3.2 Altan Uul

The northwestern front of Altan Uul (Fig. 3.2 [4]) is marked by a shallow extensional detachment fault, that dips 20-40^{o} to the northwest, and juxtaposes greenschist grade phyllites, meta-psammites and jasperoids against unmetamorphosed but intensely sheared and flattened breccias and conglomerates in the hanging-wall (Cunningham et al. submitted). Landsat TM imagery draped over a Shuttle Radar Topography Mission-90 (SRTM-90) DEM of the area, shows triangular facets, or ‘flatirons’, representing the remains of the normal fault footwall, between valleys that exit the range to the north of Altan Uul (Fig. 3.5).

Few normal faults were documented within Altan Uul. In westernmost Altan Uul, along the West Altan transect (section 2.4), a scree-filled gully truncates a thrust fault that

Fig. 3.5. Landsat TM image draped over SRTM-90 image, showing normal fault along the northern front of western Altan Uul. Cretaceous sediments drape over the mountain front. Uplifted Cretaceous sediments can also be seen perched on top of the Palaeozoic rocks in western Altan Uul.

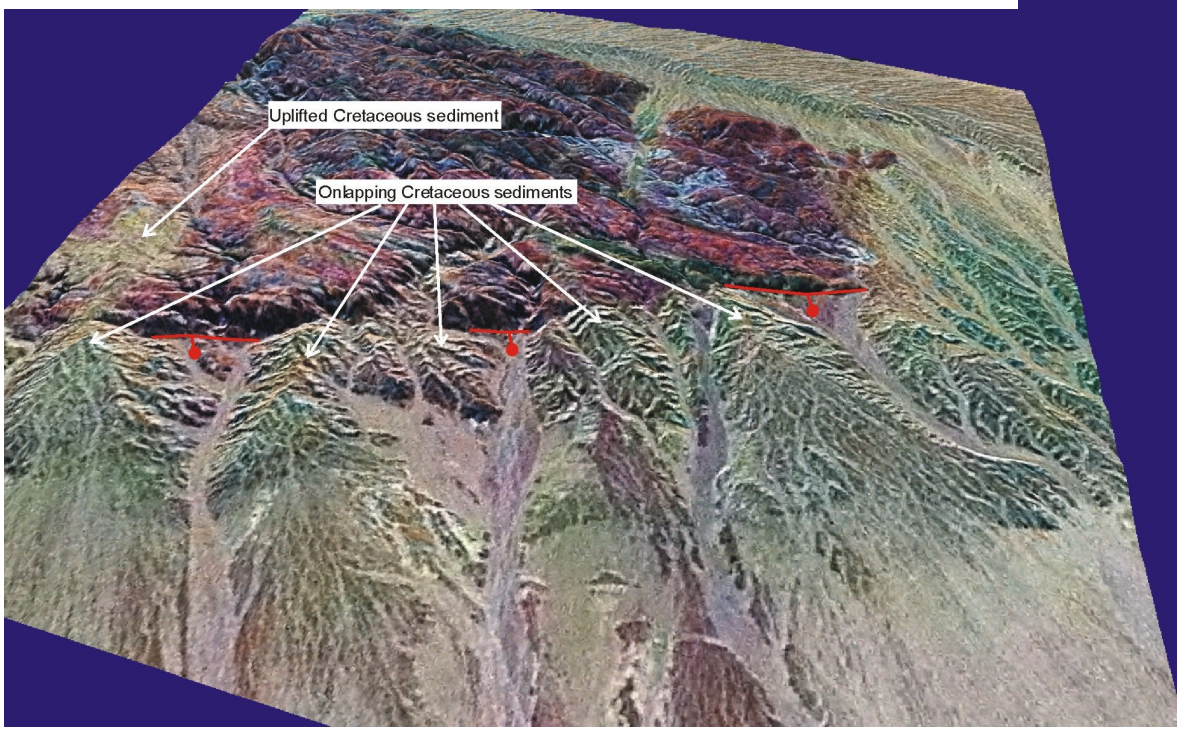

places gabbros over serpentinites in the Altan Uul ophiolite (Fig. 2.10D; Rippington et al. 2008). North of the gully greenschist-grade psammites are exposed. A 1 m wide zone directly north of the gully contains folded psammites. The narrow extent, size, and style of the folds suggest they formed by fault-drag in the hanging-wall of a normal fault (Fig. 2.10E). The gully between the serpentinites and psammites is cautiously inferred to represent the weathered out remains of a north-dipping normal fault zone (Fig. 2.10D).

In southern Altan Uul, along the West Nemegt Uul/East Altan Uul transect, an inferred steeply north-dipping normal fault, marks a metamorphic break between greenschist grade meta-andesite to the south and unmetamorphosed volcaniclastic sediments to the north (section 2.5; Fig. 2.5 [2]; Fig. 3.2 [5]). The fault zone was not directly measured, because it was weathered out into a c. 5 m-wide east-west trending valley, but is clearly visible in inaccessible cliffs east of the transect section (Fig. 2.13E). Slickenlines on isolated outcrops in the valley suggest the fault moved in a dip-slip direction (Fig. 2.13G). Normal slip sense is inferred by the obvious metamorphic break across the fault zone (section 2.5.1).

The most obvious products of extensional deformation in the region are the large basins to the north and south of Nemegt and Altan Uul (Fig. 3.2; Cunningham et al.

submitted). Normal faults within the basin to the west of Nemegt Uul and north of Altan Uul typically have a northeast-southwest trend and dip steeply to the northwest (Fig. 3.2 [6,7]; Cunningham et al. submitted). Cretaceous sediments are also seen between Nemegt Uul and Altan Uul and in several overthrust palaeovalleys in central Nemegt Uul, where they have been uplifted by Cenozoic deformation (Fig. 3.2 [2, 8-9]).

There are insufficient data to better constrain the timing of extensional faulting in Nemegt and Altan Uul. Most of the extensional shear zones and normal faults documented in the Nemegt and Altan Uul ranges (Fig. 3.3) dip steeply and are sub-parallel to the east-west to northeast-southwest trend of the normal faults in the Cretaceous sediment filled basins that surround Nemegt and Altan Uul. In at least one area in western Nemegt Uul, an east-west trending fault cuts the unconformity between the Palaeozoic basement and the Cretaceous cover (Fig. 3.4), which suggests that some faulting post-dates deposition of Cretaceous sediments in the basins surrounding Nemegt and Altan Uul. Similarly, normal faults described by Cunningham et al. (submitted) cut Cretaceous sediments dated by their Aptian fossil pollen to the north of Altan Uul and are interpreted to be associated with Cretaceous syndepositional rifting (Cunningham et al. submitted). This might suggest that normal faults in the range formed under similar stress conditions as the normal faults related to Cretaceous basin evolution to the north and south of Nemegt and Altan Uul.

3.4 Geomorphology

3.4.1 Nemegt Uul

Nemegt Uul is a sigmoidal-shaped elongate mountain range with a length-width ratio of approximately 1:8 (Owen et al. 1999b). It rises to 2769 m above sea-level from Cretaceous basins c.1800 m above sea-level in the south and c.1200 m above sea-level in the north. The difference in elevations of the basins that flank Nemegt and Altan Uul can be explained in one of three ways. 1) The south side of the range may have been higher before Cenozoic uplift began and so reflects the evolution of an earlier topographic variation across the area. 2) The Nemegt basin to the south of the range has received more sediment than the basin to the north. 3) The Nemegt basin to the south has been uplifted in the Cenozoic relative to the basin north of Nemegt Uul. An uplifted east-west trending

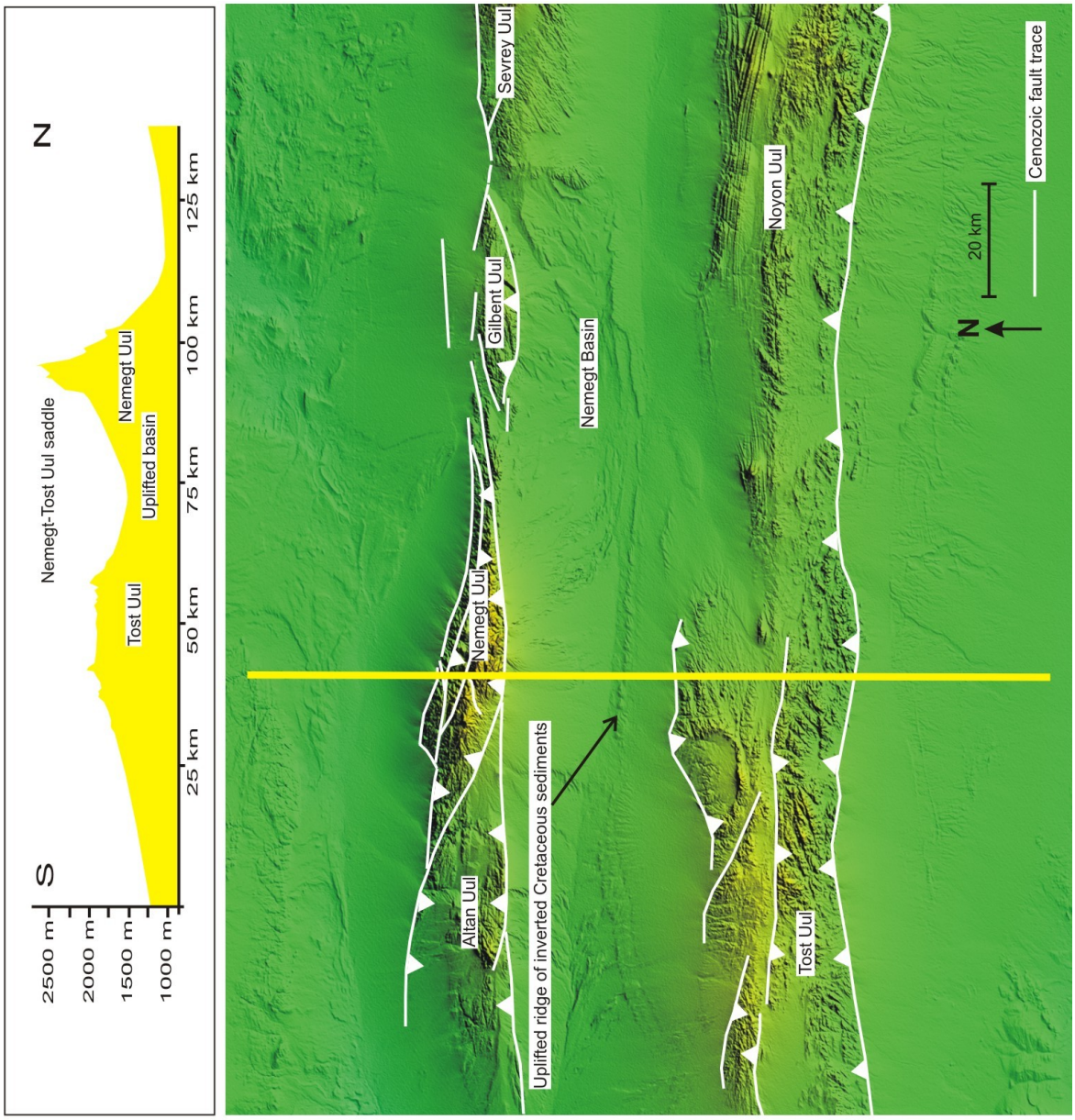

Fig. 3.6. Topographic traverse from the south of Tost Uul, over the Nemegt Basin and Nemegt Uul to the basin to the north (12.5 times vertical exaggeration). The Nemegt Basin is uplifted relative to the basins to the south and north. An uplifted ridge composed of Cretaceous sediments in the middle of the Nemegt Basin suggests there has been basin inversion, probably due to Cenozoic transpressional reactivation of Cretaceous basin faults.

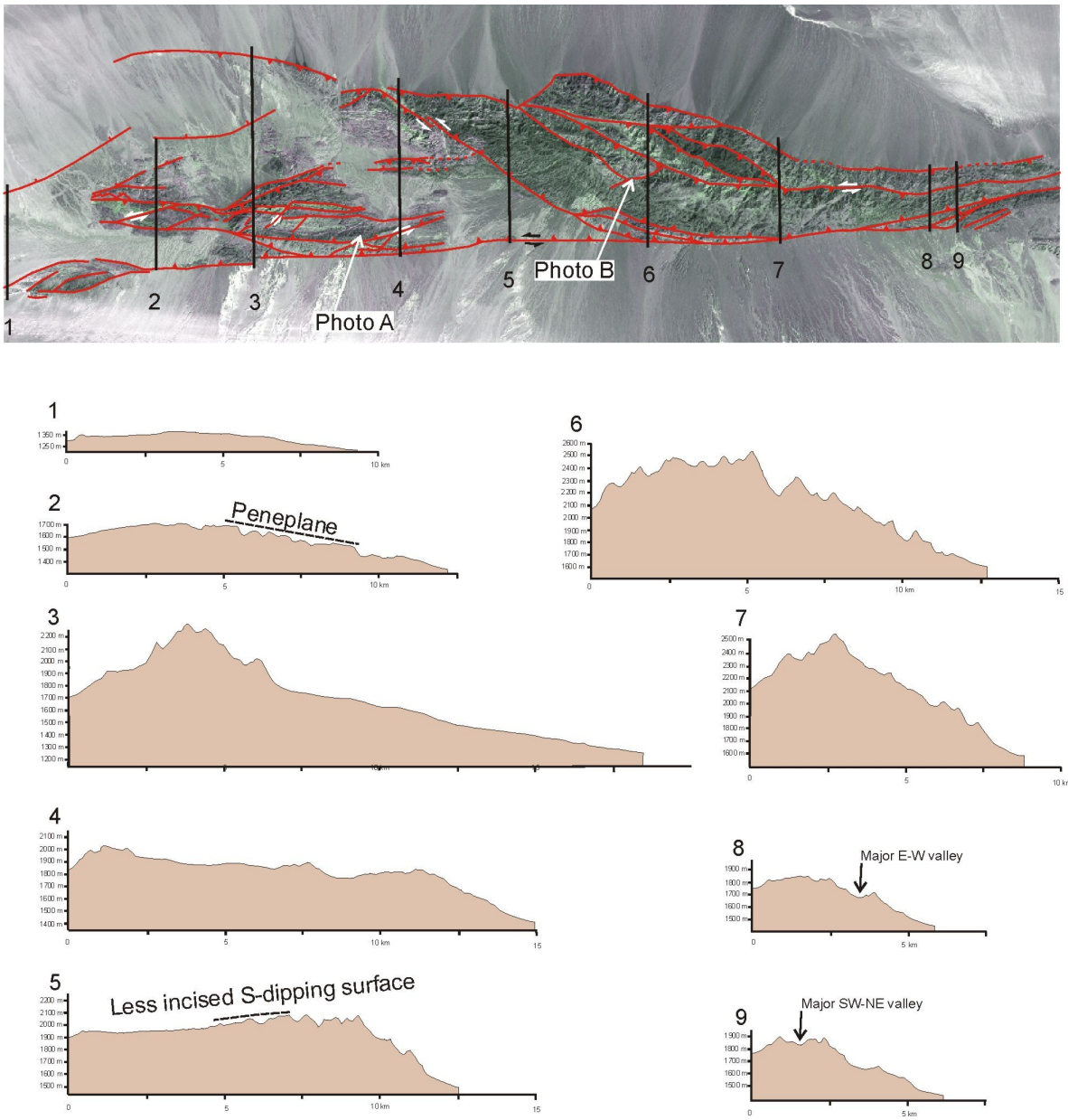

Fig. 3.7. Topographic traverses over Altan and Nemegt Uul (3.5 times vertical exaggeration), location map and photos of topography. The traverses are vertically exaggerated. All the traverses highlight the difference in elevation between the higher south front and lower north front of the Altan and Nemegt ranges Traverse 2 clearly shows the peneplane on top of western Altan Uul. Traverse 6 passes close to the summit of Nemegt Uul. Traverses 8 and 9 show major valleys cutting through the eastern end of Nemegt Uul.

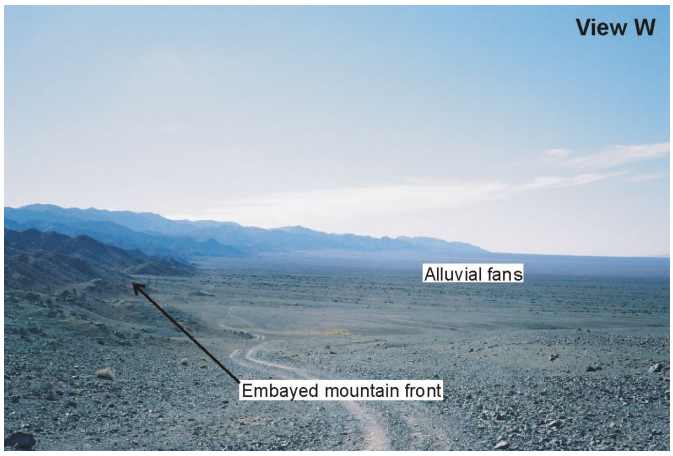

Fig. 3.8. Field photo of the northern front of Nemegt Uul viewed westward (Loc. 159). The front is embayed and an extensive alluvial fan array often conceals the structure along the front.

ridge of Cretaceous sediments in the centre of the Nemegt basin may represent a blind thrust (Fig. 3.6). This may be due to Cenozoic reactivation of Cretaceous faults in the basin and suggests that the Nemegt basin has been uplifted relative to other basins to the north and south (Fig. 3.6). This suggests that Cenozoic deformation is manifest in a wider zone of uplift through this area generating a topographic saddle across the Tost Uul and Nemegt Uul ranges and the basin separating them (Fig. 3.6).

Nemegt Uul is topographically asymmetric (Fig. 3.7), with the highest elevations in the southwest, coincident with the inside bend of the Trans-Nemegt fault (Fig. 3.2 [10]). The asymmetry of the range is highlighted by the comparatively larger catchment area to the north, feeding an extensive alluvial fan array at the north mountain front (Fig. 3.2 [11]; Owen et al. 1999b). At the eastern and western extents of Nemegt Uul (Fig. 3.2 [12-13]), northward flowing streams cross the range with much of their catchment on the southern side of the mountain, indicating that the topography of the range is tilted to the north (Owen et al. 1999b).

The north and south mountain fronts have a low sinuosity, especially in the west where the Trans-Nemegt fault transects the range. At the eastern extent of Nemegt Uul, both the north and south fronts are more embayed (Fig. 3.2 [14-15]; Fig. 3.8). Alluvial fans to the north and south of Nemegt Uul are commonly entrenched at their heads to the depth of a few metres (Owen et al. 1999b). However, Owen et al. (1999b) report alluvial fans to the northeast of Nemegt Uul (Fig. 3.2 [16]) where entrenchment is concentrated in the mid-fan stretches, possibly representing areas of localised uplift associated with north-directed foreland propagating blind thrusts.

Lower elevations at the edges of the Palaeozoic outcrop in Nemegt Uul, especially north of the drainage divide, have an active, incised morphology (Fig. 3.7; Fig. 3.9). However, the topographically higher mountain interior has a more mature, less incised topography (Fig. 3.7; Fig. 3.9). SRTM-90 DEM imagery shows a southward tilted

surface, possibly a peneplane, at the western end of Nemegt Uul (Fig. 3.9). This may represent an older erosional surface that has been uplifted during the Cenozoic.

3.4.2 Altan Uul

Altan Uul has a northward tilted peneplaned summit (Fig. 3.9; Fig. 3.10). On Landsat TM imagery, Cretaceous sediments can be seen onlapping the Palaeozoic rocks on this older erosion surface at the western end of the range (Fig. 3.2 [17]; Fig. 3.5). In the east, the peneplane is tilted north and is onlapped by Cretaceous sediments between Altan and Nemegt Uul (Fig. 3.9). To the northeast of the same Cretaceous sediments, a southward dipping peneplane in Nemegt Uul is onlapped by Cretaceous sediments (Fig. 3.9). This may suggest that the peneplane in eastern Altan Uul and western Nemegt Uul represent opposite sides of c. 2 km wide Mesozoic valley that was filled with Cretaceous sediments and then exhumed in the Cenozoic.

The highest topography in Altan Uul is in the south which coincides with the main drainage divide, with long streams draining to the north. In western Altan Uul, the drainage divide between north and south is situated south of the basement exposures (Fig. 3.10). Elevations drop steeply to the west of the high point in Altan Uul (2235 m) and then steadily decrease along the northward tilted peneplane to the western extent of the range (Fig. 3.7 traverse 1 and 2).

It is not possible to accurately calculate how much Cenozoic uplift there has been in Nemegt and Altan Uul. However, by projecting the peneplane surface in Altan Uul to the south, above the area where it has been eroded, and by projecting the south range-bounding thrust fault upto the projected elevation of the peneplane, it is possible to quantitatively evaluate the minimum amount of uplift and shortening on the southern front of Altan Uul. This method assumes the dip of the southern range bounding thrust fault remains the same to depth and does not account for the amount of shortening and uplift accommodated on smaller faults within the range. Nevertheless, it gives an approximate minimum of 236 m of shortening and 359 m of uplift in western Altan Uul, and a minimum of 158 m of shortening and 533 m of uplift in eastern Altan Uul (Fig. 3.11), suggesting there the western end of Altan Uul has not been uplifted as much as the eastern end. The south-dipping peneplanes on Nemegt Uul are not as obvious on topographic traverses, making it more difficult to apply this method to Nemegt Uul. The

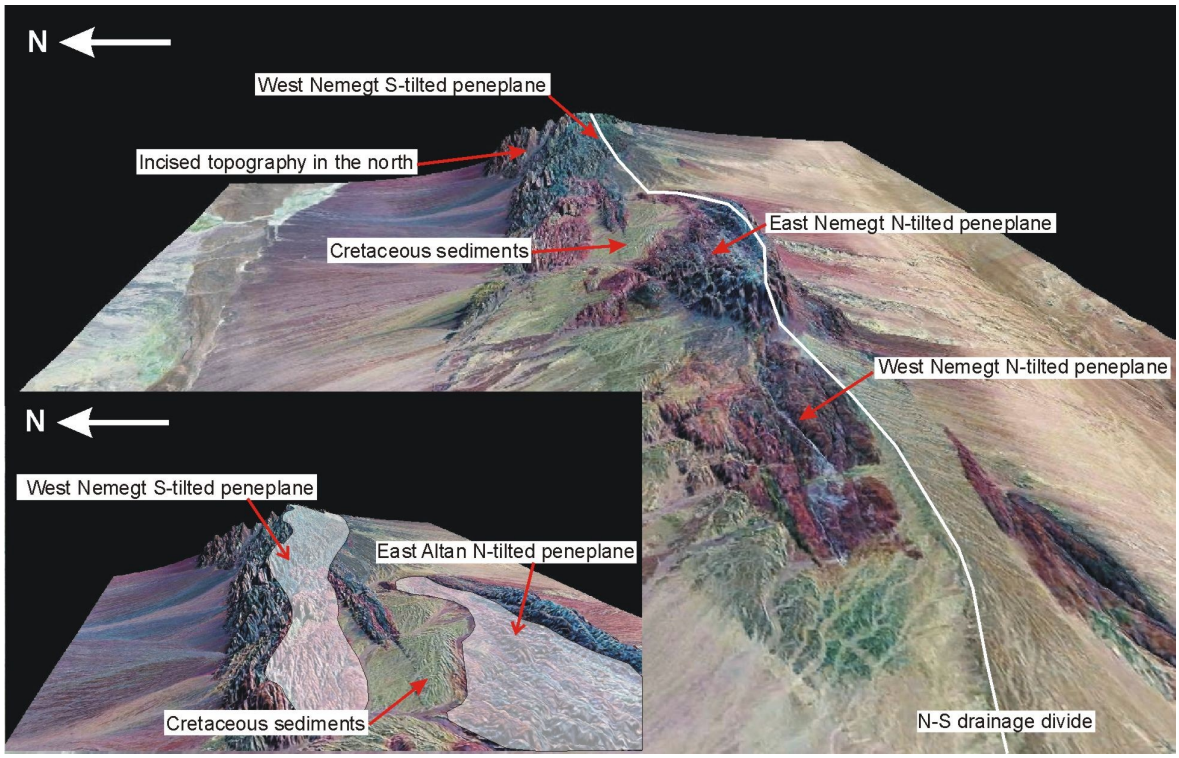

Fig. 3.9. A south-dipping peneplane in western Nemegt Uul and a north-dipping peneplane in Altan Uul are both onlapped by Cretaceous sediments between the range. It is suggested that these peneplanes may represent a Cretaceous erosion surface, possibly opposite sides of a valley that was filled with Cretaceous sediments.

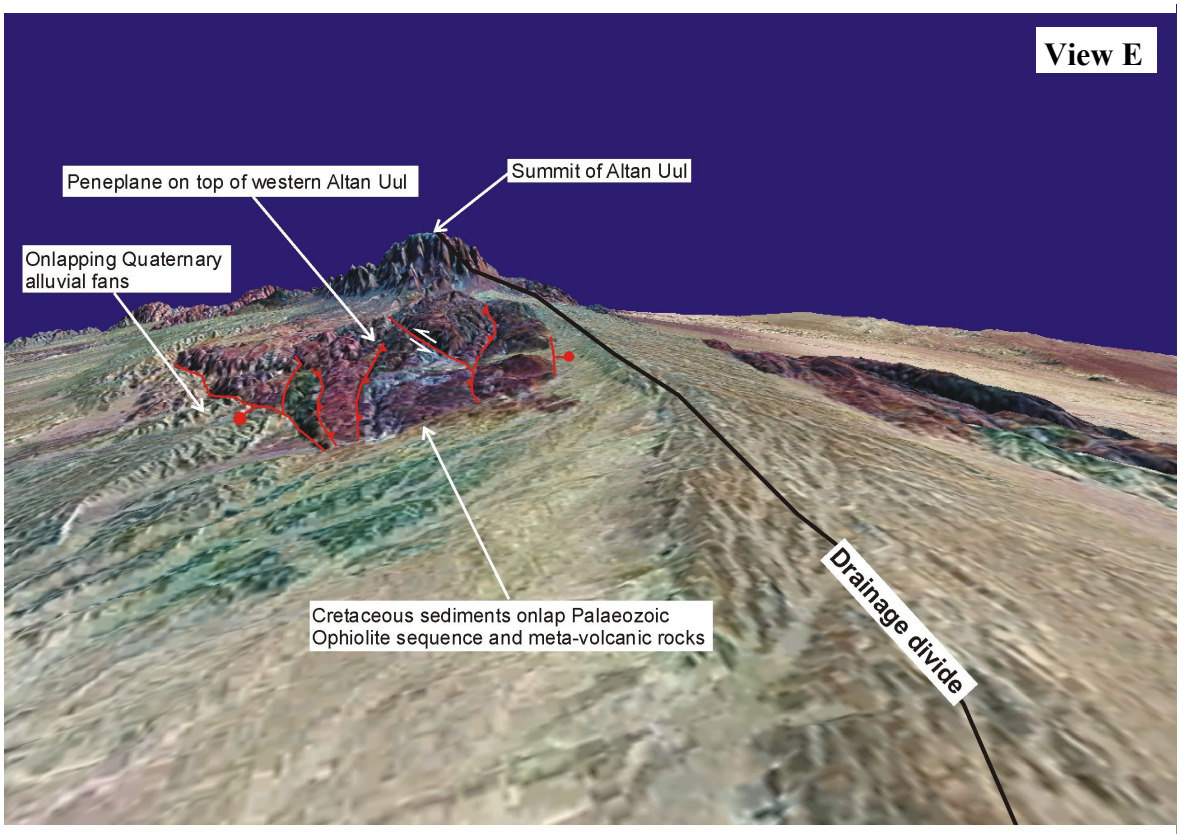

Fig. 3.10. Landsat TM image draped over SRTM-90 image, showing the drainage divide in western Altan Uul. Channels in the Cretaceous sediments that onlap the Palaeozoic rocks at the western extent of Altan Uul can be seen draining from south to north across the width of the range. The peneplane on top of western Altan Uul can be seen.

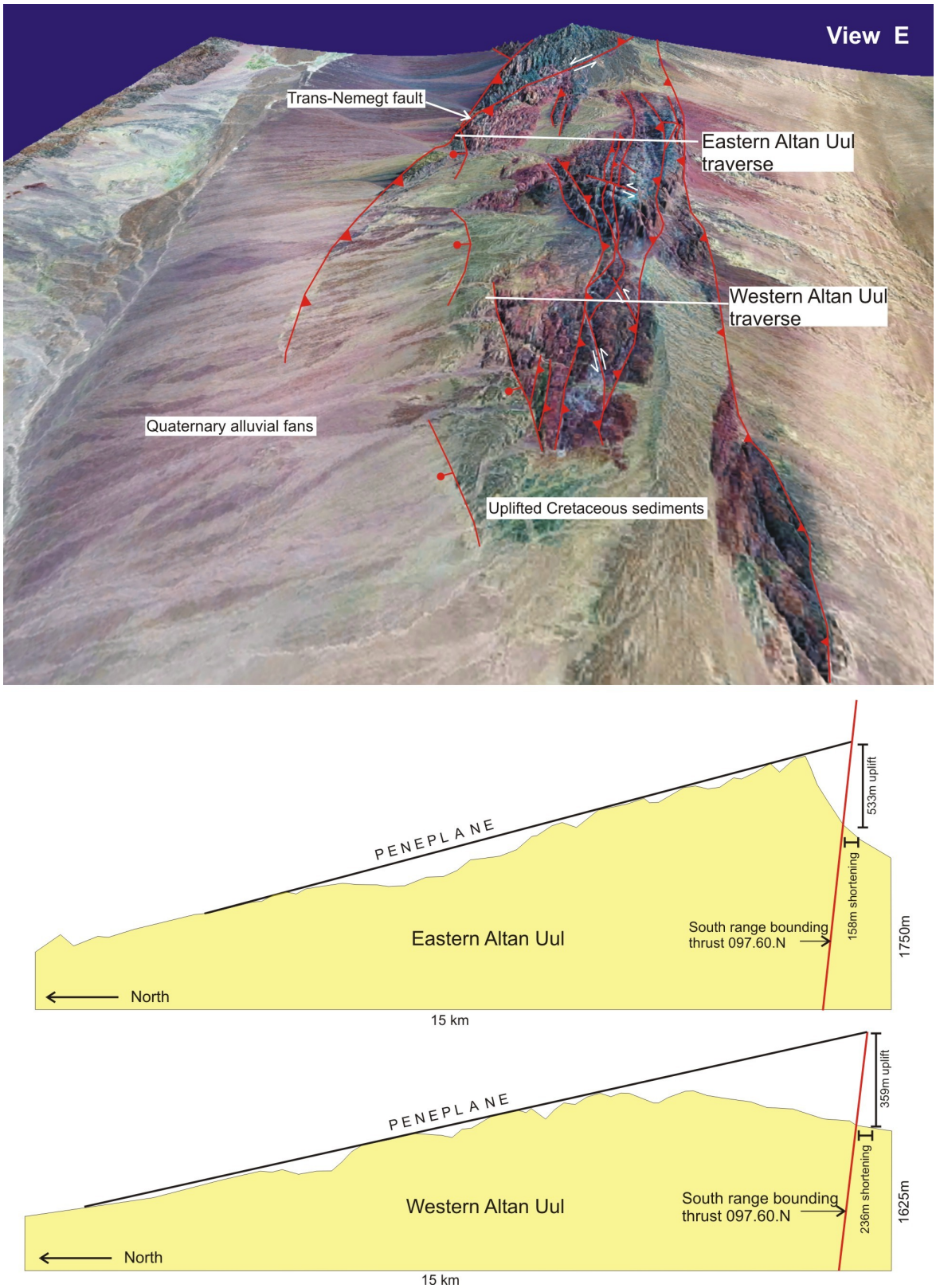

Fig. 3.11. Landsat TM image draped over SRTM-90 image. The Cretaceous sediments that onlap the Palaeozoic rocks at the western extent of Altan Uul are uplifted along the westward continuation of the north-directed Trans-Nemegt fault north of Altan Uul, and the south-directed thrust along the south side of Altan Uul. The north-dipping peneplane and the south-range bounding thrust fault are projected into space. Their point of intersection can be used to estimate the amount of shortening and uplift that has occurred on the south-side of the range.

exposure of mature topography and erosion surfaces at the top of the Palaeozoic basement suggests parts of the Nemegt Uul range have been exposed for longer than more incised topography at the northern front (Fig. 3.7; Fig. 3.9). If the erosion surfaces are Cretaceous, as is suggested in western Nemegt and eastern Altan Uul, it would indicate that the majority of uplift and exhumation required to expose the dominantly greenschist-grade metamorphic rocks of Nemegt and Altan Uul most likely occurred before or during Cretaceous extensional deformation. Consequently, the amount of Cenozoic uplift and exhumation is likely to be relatively small. Assuming the Cretaceous peneplane in Nemegt Uul was at the same elevation as the basin to the north of Nemegt Uul during the Cretaceous, it is possible to take the highest point (c. 2100 m) of the peneplane in western Nemegt Uul and subtract the elevation of the mountain front (c. 1600 m) to estimate there has been c. 500 m of uplift in western Nemegt Uul since the Cretaceous (Fig. 3.7 traverse 5).

3.5 Cenozoic transpressional structures

In the following section, the Cenozoic faults in Nemegt and Altan Uul are discussed. The structure of the mountain fronts is discussed first, before the Cenozoic structure within the ranges is considered.

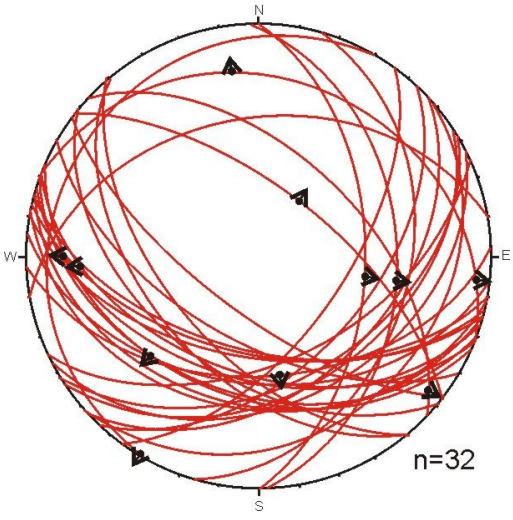

Fig. 3.12. A stereonet of all the strike, dip and slickenline data documented for faults identified as Cenozoic by cross-cutting field relationships in Nemegt and Altan Uul. Long faults (e.g. the Trans-Nemegt fault) have multiple measurements presented in this figure.

All the strike, dip and slickenline data from faults that are known to be Cenozoic based on cross-cutting field relationships are presented in Fig. 3.12.

3.5.1 Nemegt Uul mountain front structure

In Nemegt Uul, the range fronts are defined by low sinuosity basinward-directed brittle thrust faults. At the south front of Nemegt Uul, Palaeozoic greenschist grade meta-psammitic schist and meta-volcaniclastic schist are thrust south over locally steeply north-dipping overturned Cretaceous and Neogene clastic basin

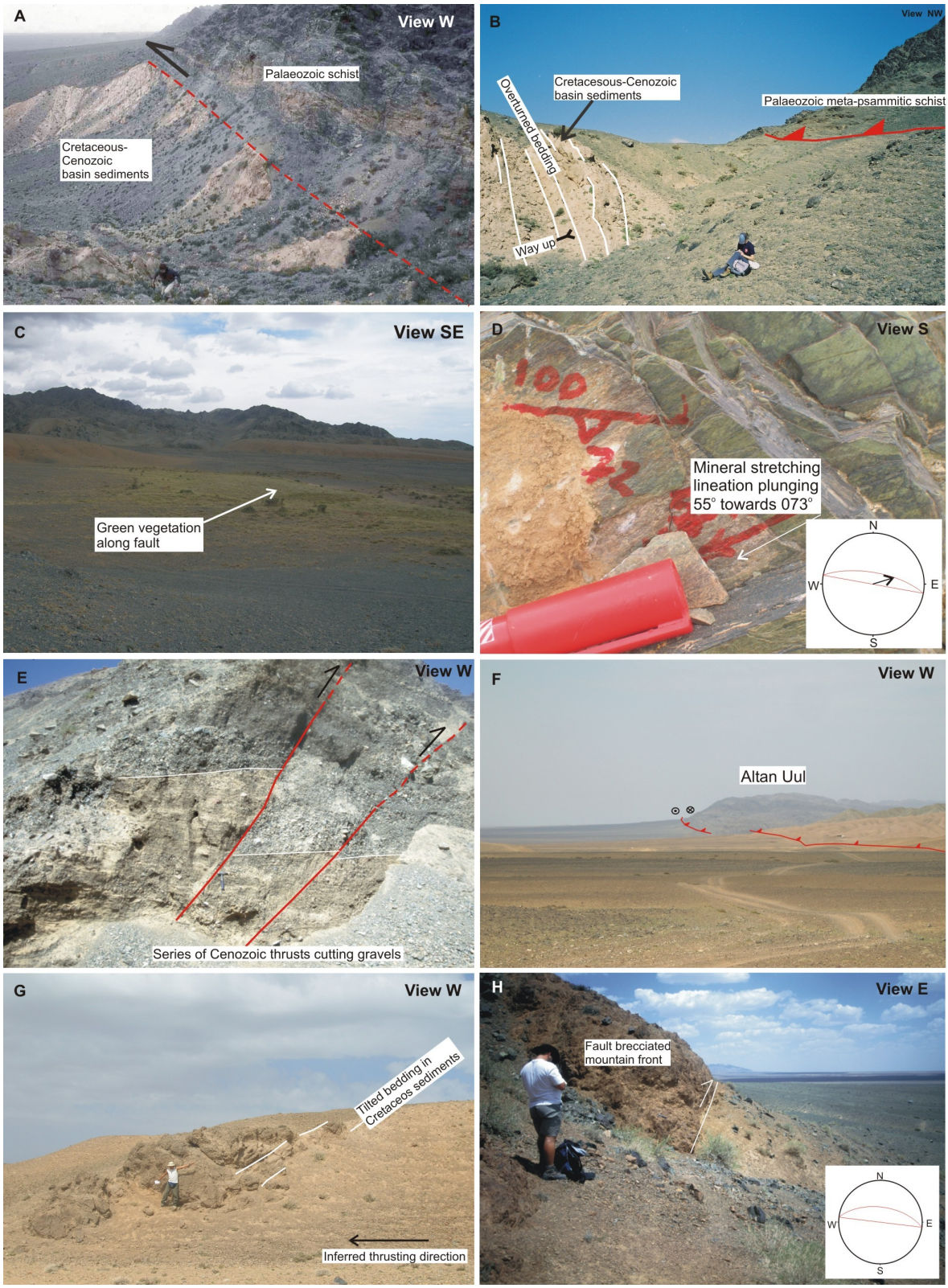

Fig. 3.13. Field photos of the Cenozoic mountain front structure in Nemegt and Altan Uul. A) Palaeozoic greenschist grade meta- volcaniclastic and meta-pelitic rocks are thrust south over Cretaceous and Neogene sediments along the south front of Nemegt Uul (200m east of Loc. 1). B) Cretaceous-Cenozoic sediments are overturned by the south range bounding thrust in Nemegt Uul (Loc. 1) C) Vegetation marks a spring line along faults in a strike-slip duplex south of the southeastern bend in the Trans-Nemegt fault in southwest Nemegt Uul (Loc. 301). D) Oblique-slip mineral stretching lineations on isolated slate exposure along the strike-slip fault in C (Loc. 304). E) North-directed thrusting in Quaternary alluvial gravels at the mountain front in northwest Nemegt Uul (Loc. 3). F) The fault connecting Nemegt and (continued...)

(continued from previous page) Altan Uul cuts through Cretaceous and Quaternary sediments. The fault is marked by wells dug along spring-lines at the surface, and a slight increase in elevation over the fault to the north (Loc. 307). G) Cretaceous sediments south of the fault between Nemegt and Altan Uul, are tilted to the southwest suggesting left-lateral oblique-slip thrusting may be the dominant sense of movement along the fault (seen in F; Loc. 308). H) Brown fault breccia associated with the range bounding thrust fault along the southern front of Altan Uul (Loc. 6).

sediments (Fig. 3.2 [18]; Fig. 3.13A; B; Cunningham et al. 1996; Owen et al. 1999b). The thrust fault dips c.45^{o} to the north but no slickenlines were identified.

In southwest Nemegt Uul, the southern frontal thrust curves towards the north, becoming the Trans-Nemegt fault (Fig. 3.2), and a strike-slip duplex consisting of at least three faults is traceable on the Landsat image (Fig. 3.2 [19]). With the exception of the Trans-Nemegt fault, these faults do not produce any significant topographic expression. However, the faults produce spring lines marking their trace (Fig. 3.13C). Isolated slate outcrops along the trace of one of the faults striking 100^{o} and dipping 72^{o} north contain mineral stretching lineations plunging c.55^{o} towards 073^{o} the east, indicating that movement along the fault was left-lateral oblique-slip (Fig. 3.13D). Where the faults defining the strike-slip duplex cut through the South Central Nemegt Slate sequence (Fig. 3.2 [19]; section 2.6.1), steep northeast plunging, northwest-vergent folds of cleavage are seen in close association with the faults, also suggesting the faults have moved left-laterally (Fig. 2.22C-F).

At the north front of Nemegt Uul in the northwest, Quaternary alluvial gravels are cut by a zone of north-directed brittle thrusts that strike 300^{o} and dip 60^{o} to the southwest (Fig. 3.2 [20]; Fig. 3.13E). This thrust zone can be traced west on Landsat TM imagery to where it meets the Trans-Nemegt fault, which then extends c.10 km west of the Palaeozoic outcrop in Nemegt Uul, between 5 and 10 km north of Altan Uul (Fig. 3.2 [21]; Fig. 3.11). To the east a thrust zone strikes c. 281^{o} and dips 34^{o} and marks the front of Nemegt Uul, where Palaeozoic schists are thrust north over Cretaceous basin sediments (Figs. 2.26D-E; Fig. 3.2 [22]).

The frontal thrusts of Nemegt Uul are most obvious in the west. In the east, the mountain fronts have been embayed by erosion and the range-bounding faults are obscured by Quaternary alluvial sediments (Fig. 3.2 [14-15]; Fig. 3.8) suggesting they have not been active as recently as those in the west. In the Cretaceous basin north of Nemegt Uul, uplifted Cretaceous sediments form an anticline in a northwest-southeast trending line of low hills clearly visible on Landsat TM and SRTM-90 imagery (Fig. 3.2 [23]; Fig. 3.14). The steepest Cretaceous sediments dip c.45-55^{o} southwest, suggesting

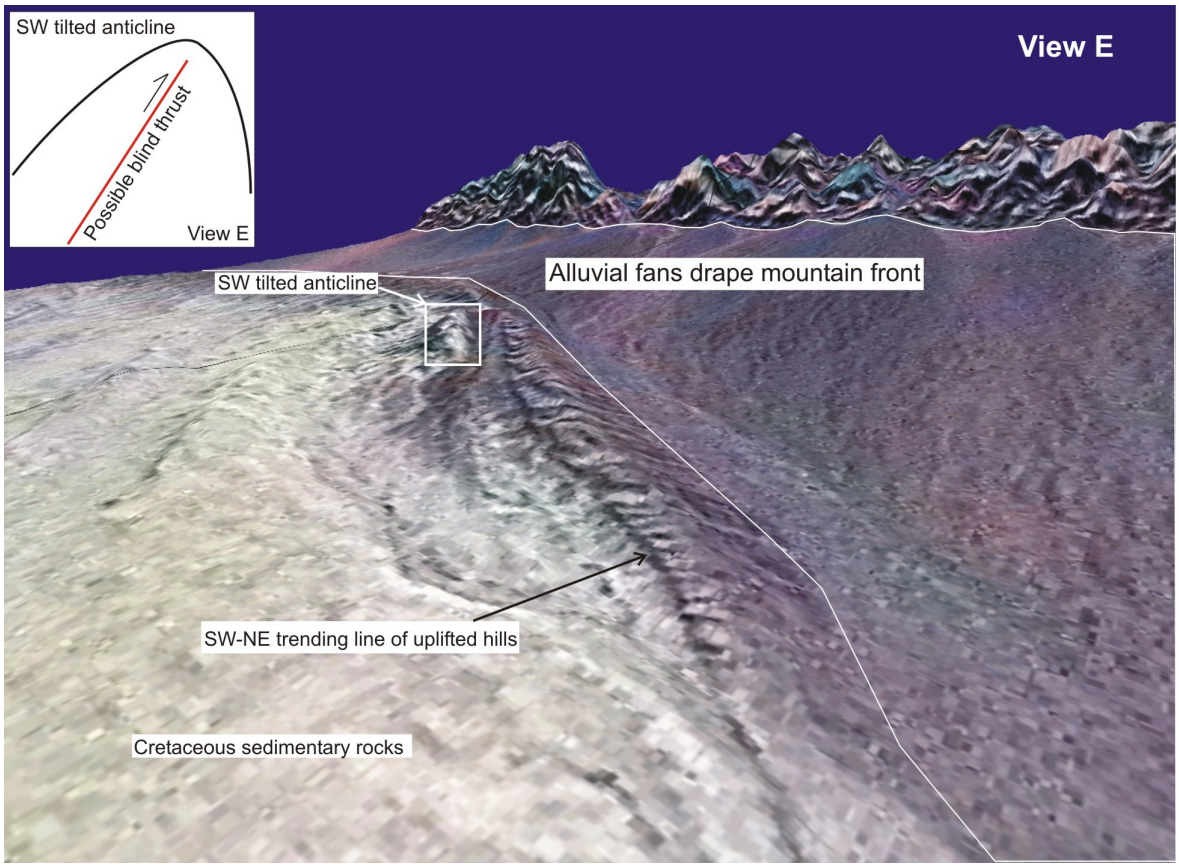

Fig. 3.14. Landsat TM image draped over SRTM-90 image, showing a low line of hills in eastern Nemegt Uul. Cretaceous sediments folded into a southwest-tilted anticline may mark a south-directed blind thrust, possibly reactivating a north-dipping Cretaceous normal fault. Location shown on Fig. 3.2 [23].

the anticline is verging towards Nemegt Uul. The anticline may have formed above a steeply northeast-dipping normal fault in the basin that has been reactivated in a southwest-directed thrust sense. This is the only outlying ridge in the Nemegt Uul foreland.

3.5.2 Altan Uul mountain front structure

In southern Nemegt Uul, an east-west trending fault branches off from the Trans-Nemegt fault and cuts Cretaceous and Quaternary sediments to connect with the southern front of Altan Uul and is marked by an obvious lineament on Landsat TM imagery (Fig. 3.2 [24]). The fault plane was not seen in the field but the trace of the fault is marked by a spring line, a series of wells, and a slight increase in topography to the north across the fault (Fig. 3.13F). Cretaceous sediments south of the predicted location of the fault have been tilted to the southwest suggesting there may have been left-lateral southwest-

directed oblique-slip thrusting on the fault (Fig. 3.13G). At the south front of Altan Uul, a c. 10 m wide zone of fault breccia is seen in places, containing fracture planes that strike approximately 097° and dip approximately 60° north (Fig. 3.13H). However, the frontal thrust fault is typically not visible because uncut Quaternary alluvial fans onlap the mountain front, but the front of the range has a low-sinuosity (Fig. 3.2), suggesting the southern range bounding thrust is the most active fault in the Altan Uul area. To the west of Altan Uul, the southern range bounding thrust can be traced past a sigmoidal dome consisting of uplifted Palaeozoic rocks (Fig. 3.15). Just west of this uplifted dome, Cretaceous-Cenozoic sediments look like they have been deformed into a southward tilted antiform defining an east-west trending ridge (Fig. 3.15). This may be the surface manifestation of a blind thrust, possibly the westward continuation of the Altan Uul southern range bounding thrust. The fault has not yet broken the surface, suggesting it may be young and undeveloped.

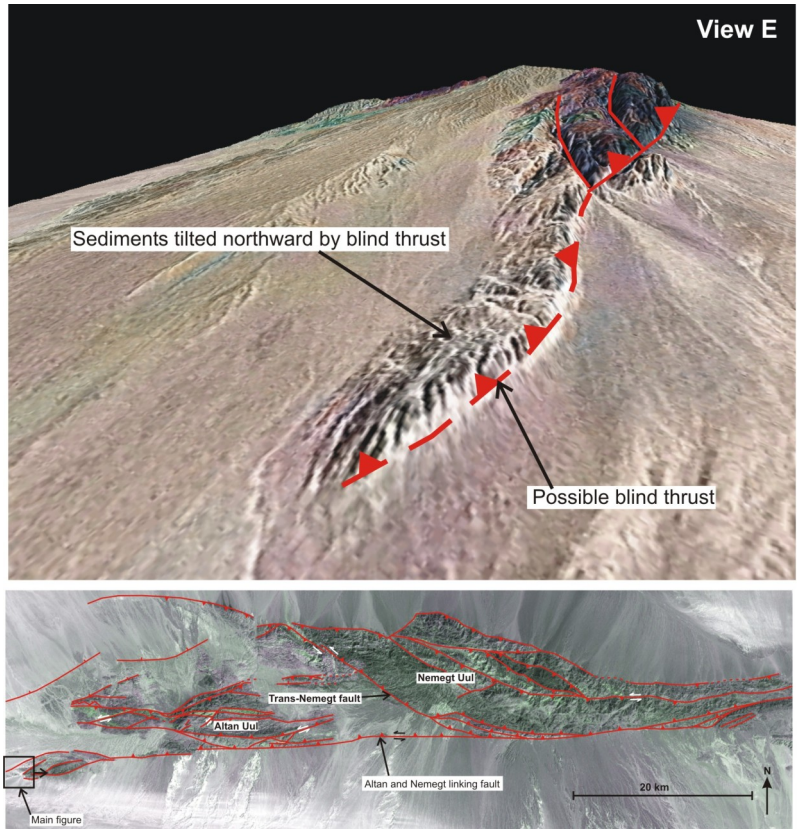

Fig. 3.15. Landsat TM image draped over SRTM-90 image, showing a Cretaceous-Cenozoic sediments at the western extent of Altan Uul, deformed into a southward-tilted antiform, suggesting there may be a blind thrust beneath the surface at this location.

The northern front of Altan Uul is bound by a Cretaceous northeast-southwest basin bounding normal fault in the west (Fig. 3.2 [4]), and is onlapped by Cretaceous sediments in the east (Fig. 3.2 [25]). The westward continuation of the Trans-Nemegt fault zone and the southern Altan range bounding thrust have uplifted the Cretaceous sediments directly west of Nemegt and Altan Uul and directly north of Altan Uul (Fig. 3.11).

3.5.3 Cenozoic structures within Nemegt Uul

Chapter 2 documents many faults within Nemegt and Altan Uul. Only a few of these thrust Palaeozoic rocks over Cretaceous-Cenozoic sediments and can be unequivocally designated as Cenozoic in age.

Section 2.6.4 describes a 100 m-wide zone of deformed black flysch marking a major north-directed ductile thrust shear zone along the central transect. The flysch marks the boundary (Fig. 3.16A, B) between the Central Nemegt Lower Extrusive sequence and the North Central Nemegt Greenschist sequence (section 2.6.4; Fig. 3.2 [26]). Approximately 100 m north along the central transect (Fig. 2.6) unmetamorphosed polymict conglomerate thought to be Cretaceous in age, is downthrown and juxtaposed with the flysch on a normal fault trending 123^{o} and dipping 72^{o} northeast presumed to be Cretaceous. (Fig. 3.16A). However, to the west of the central transect (Fig. 2.21 [8]), the flysch pinches out and meta-volcanic rocks in the Central Nemegt Lower Extrusive sequence are thrust north over phyllites in the North Central Nemegt Schist sequence (Fig. 2.6; Fig. 3.16A).

Many large rounded boulders of meta-volcanic rocks from the overthrusting meta-volcanic sheet were incorporated into the flysch which occupies the footwall of the north-directed thrust shear zone, during deposition (Fig. 3.16C). A brittle fault between the meta -volcanic rocks and the flysch is marked by a c. 50 cm wide south-dipping gouge zone that strikes 280^{o} and dips 54^{o} to the southwest, and suggests that there were later brittle movements on the ductile shear zone (Fig. 3.13D). A ductile fabric in the flysch is cut by the normal fault that downthrows the Cretaceous conglomerate (Fig. 3.13A), so ductile thrusting is assumed to have occurred during late Carboniferous contractional deformation events (section 2.10.2). Younger north-directed brittle thrust faults also cut the ductile thrust zone (Fig. 3.16E). Slickenlines in calcite veins that cut the earlier ductile fabrics, plunge 28^{o} towards 215^{o}. Fault drag of cleavage along localised brittle shear planes that cut all earlier fabrics suggests that more recent left-lateral oblique-slip thrust sense brittle movement has overprinted Carboniferous north-directed ductile thrust movements along the flysch shear zone (Fig. 3.16F), most likely during thrusting of the meta-volcanic rocks over the Palaeozoic phyllites to the west (Fig. 3.16A). To the west of the flysch and conglomerate, there is a major east-west linear valley (Fig. 3.2 [27]; Fig. 3.16A). The linearity of the valley suggests that its morphology is controlled by a fault.

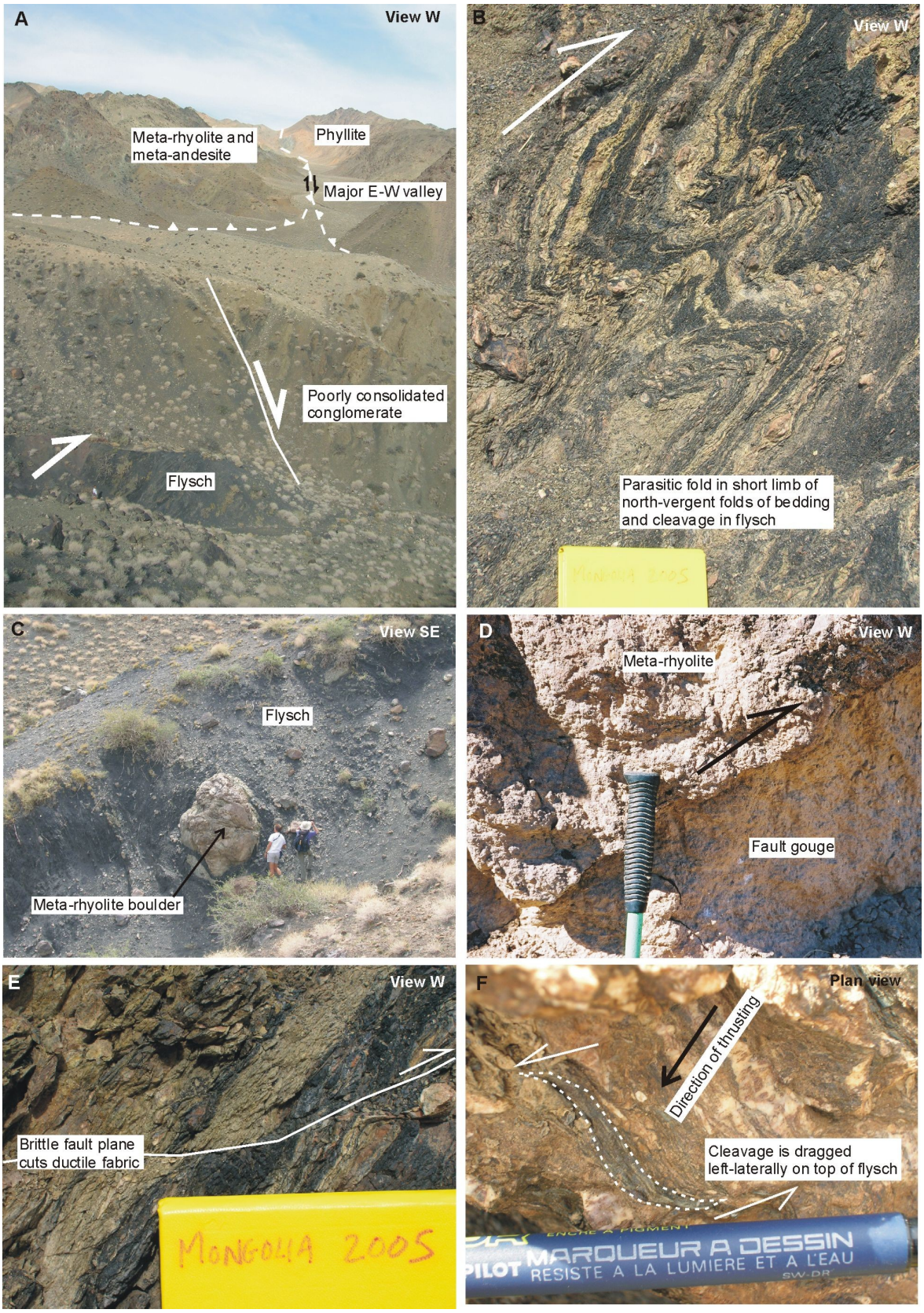

Fig. 3.16. Field photos of black flysch in northern Nemegt Uul (all photos taken around Loc. 187). A) A north-directed ductile thrust shear zone in the flysch formed by a north-directed overthrusting sheet of meta-rhyolite, is cut by a north-dipping normal fault down-throwing Cretaceous conglomerate to the north. West of the flysch, a major linear east-west trending valley may mark a Cenozoic fault where Palaeozoic meta-rhyolite is placed north over Paleozoic phyllites. (continued...)

(continued from previous page) B) Parasitic folds in the short limb of a north-vergent F2 fold in the flysch. Pale layers are interbedded volcanic material entrained in the flysch. C) The flysch contains meta-rhyolitic boulders from the Central Nemegt Lower Extrusive sequence. Some volcanic material is interlayered with the flysch (see B) so was entrained prior to thrusting, but some has been entrained into it during north-directed thrusting. D) Fault gouge in the fault zone between the meta-rhyolite and the flysch suggests there has been later brittle faulting E) North-directed brittle thrust faults cut ductile fabrics in the flysch zone. F) Fault dragged foliation associated with the brittle fabrics in the flysch indicate there may have been a left-lateral component to later brittle thrusting.

The valley is a major feature of the Cenozoic morphology of Nemegt Uul but there is insufficient data to date it precisely (Fig. 3.2 [27]). However, it is possible that left-lateral oblique-slip brittle kinematic indicators that overprint ductile fabrics in the flysch (Fig. 3.16F) may have been formed during brittle Cenozoic left-lateral thrusting of the meta-volcanic rocks in the south over the flysch and phyllites to the north (Fig. 2.6 [9]; Fig. 3.16D).

In western Nemegt Uul, the West Nemegt Volcaniclastic sequence (section 2.5.7) is thrust north over Cretaceous sediments on a c. 3 m wide fault zone consisting of gouge and incohesive fault breccia striking 230^{o} and dipping between 22-50^{o} to the southeast (Fig. 2.19G). No slickenlines were identified.

The Trans-Nemegt fault is the longest Cenozoic fault within Nemegt Uul (Fig. 3.2). It forms the northern boundary of a group of faults that define a strike-slip duplex in southwest Nemegt Uul (Fig. 3.2 [19]) but branches off through Nemegt Uul to the northwest and is the only fault to connect the southern and northern fronts of the range (Fig. 3.17). In the south, the fault strikes 080^{o} and dips 40^{o} to the north, with slickenlines that plunge 16^{o} towards 352^{o} (Fig. 3.17). To the northwest, the geometry of the Trans-Nemegt fault changes as it cuts through the range. The line of the fault forms a linear valley through Nemegt Uul (Fig. 3.17). The valley is filled with Quaternary alluvial sediment but at isolated outcrops at the edges of the valley, the fault is seen to steepen to 53^{o} NE (strike 133^{o}) with slickenlines plunging 20^{o} towards 118^{o} (Fig. 3.17). Further northwest along the valley the dip of the Trans-Nemegt fault changes through vertical to strike 307^{o}-279^{o} and dip 70^{o}-54^{o} to the southwest with slickenlines plunging from 60^{o}-47^{o} towards 270^{o}-228^{o} respectively (Fig. 3.17). The fault cuts a granite intrusion, thrusting it north over itself and displacing the northern footwall side c. 300 m left-laterally (Fig. 3.17). The fault is continuous through the granite intrusion and slickenlines and kinematic indicators suggest it thrust the granite in a left-lateral north-directed oblique thrust sense (Fig. 3.17). Just before the northern front, the fault strikes 287^{o} and dips 46^{o} to the southwest with slickenlines plunging 40^{o} towards 238^{o} (Fig. 3.17). At the northern front,

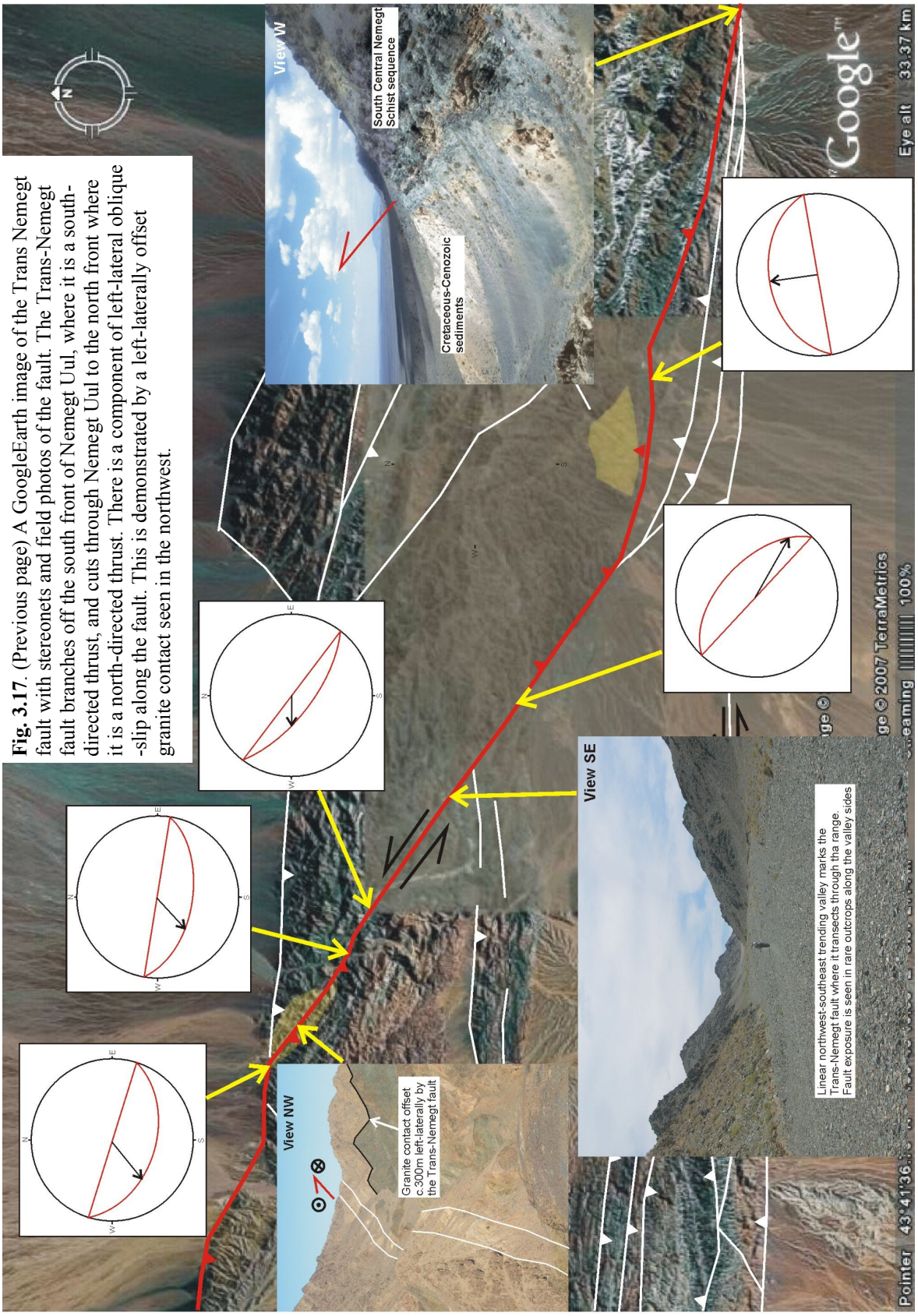

Fig. 3.17. (Previous page) A GoogleEarth image of the Trans Nemegt fault with stereonets and field photos of the fault. The Trans-Nemegt fault branches off the south front of Nemegt Uul, where it is a south-directed thrust, and cuts through Nemegt Uul to the north front where it is a north-directed thrust. There is a component of left-lateral oblique -slip along the fault. This is demonstrated by a left-laterally offset granite contact seen in the northwest.

the Trans-Nemegt fault bends to the west and is joined by the east-west trending range bounding thrust fault zone from the east (Fig. 3.17). Although the Trans-Nemegt fault changes its strike and dip over its length, slickenline data and kinematic indicators suggest that it maintains a left-lateral oblique-slip thrust sense (Fig. 3.17). By connecting the south and north fronts of Nemegt Uul, the Trans-Nemegt fault gives the range a double restraining bend geometry (Fig. 3.2). The Trans-Nemegt fault marks the low-sinuosity north and south fronts of Nemegt Uul before transecting the range. In the northwest, the Trans-Nemegt fault cuts Quaternary gravels, and overturns Neogene sediments on the south front (Fig. 3.13A,B,E), which combined with the low-mountain front sinuosity produced by the fault (Fig. 3.2), suggests that the Trans-Nemegt fault is the most recently active fault in Nemegt Uul.

A lack of convincing piercing points makes calculating the amount of slip along the Trans-Nemegt fault difficult. A section of Google Earth satellite imagery at a higher resolution than the Landsat TM imagery shows a small white band of rocks in the centre of the range being dragged in a left-lateral direction along the fault (Fig. 3.18). Field and petrographical analysis of this rock shows it to be a band of metamorphosed pelitic schist, rich in white mica. Approximately 3.3 km southwest, a band of the pelitic schist is cut by the fault and displaced 300 m left-laterally (Fig. 3.18). This displacement is the same as the displacement of a granite contact seen along the fault to the northwest (Fig. 3.17). Using the fault geometry and slickenline data documented along this segment of the Trans -Nemegt fault, the amount of fault dip-parallel movement (643-674 m) and the net slip (710-738 m) can be calculated. These data can be used to calculate the maximum vertical movement directly associated with slip along the Trans-Nemegt fault. Assuming that all of the vertical movement accommodated by the fault resulted in uplift of the surface, the data suggest there may have been c. 520-633 m of local vertical uplift around the northwest-southeast trending range-transecting segment of the Trans-Nemegt fault.

The Landsat imagery shows other sigmoidal faults that have the same northwest-southeast trending trace as the Trans-Nemegt fault, forming a small duplex in Central Nemegt Uul (Fig. 3.2 [8-9]). Two faults in the duplex bound the Central Nemegt Lower Extrusive Group (section 2.6.4). The southernmost of these northwest-southeast trending faults strikes 258^{o} and dips 47^{o} and slickenlines plunge 47^{o} towards 170^{o} and suggest dip-slip movement (Fig. 2.24G; Fig. 3.12). Field evidence on both faults suggests that they are moderate-steep south-southwest dipping north-directed brittle thrust faults that carry

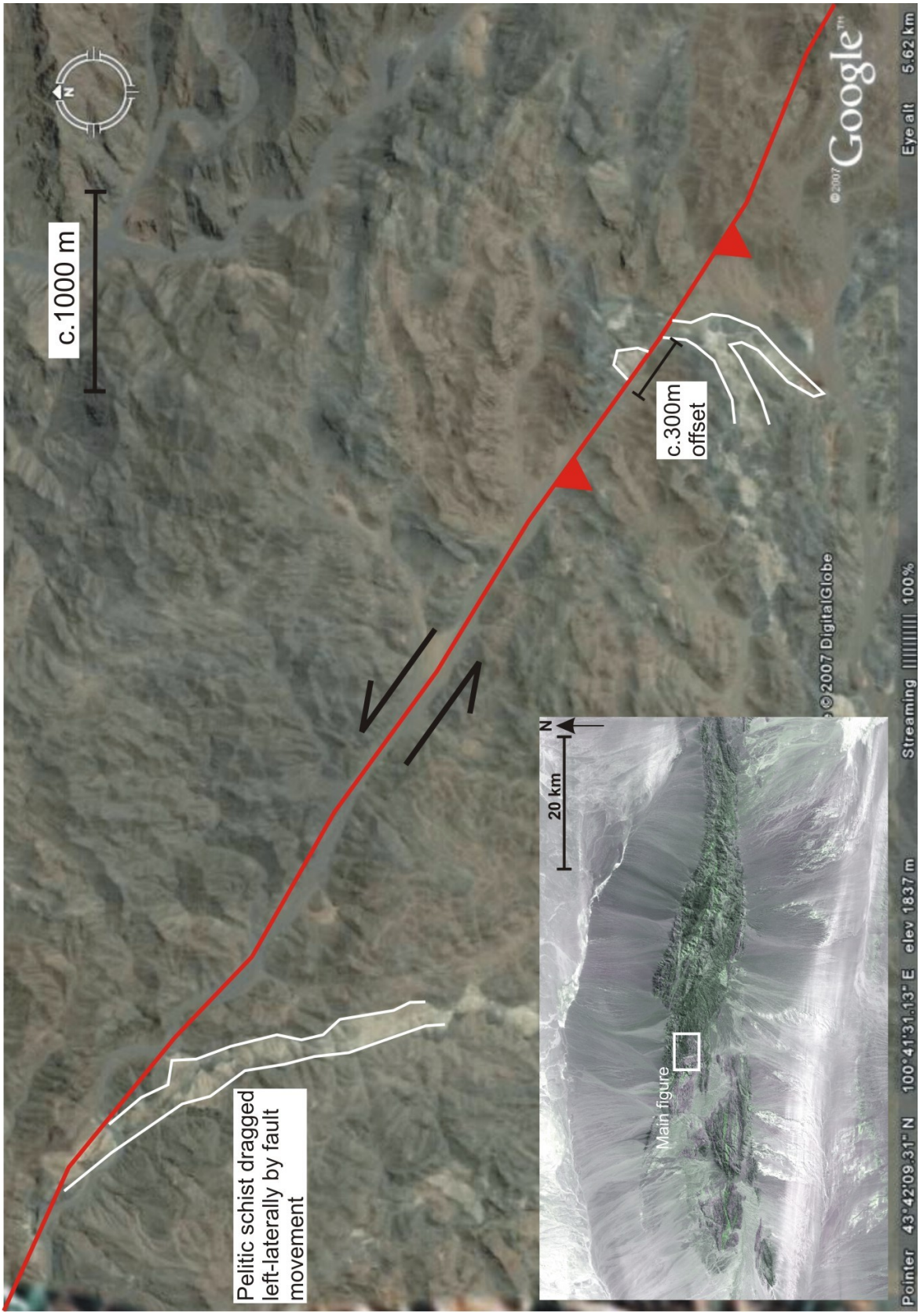

Fig. 3.18. A Google Earth image of the Trans-Nemegt fault showing bands of c.300 m left-laterally offset meta-pelitic schist. Centre of image is 43°42’31”N, 100°41’13”E.

Palaeozoic meta-volcanic rocks north over unconsolidated conglomerate in palaeovalleys within the range (Fig. 2.6 B-C). Although the age of the unconsolidated conglomerate is not known, it is not metamorphosed or strained and is similar to Cretaceous-Cenozoic conglomerates seen along the north front.

In eastern Nemegt Uul, two large straight valleys cut through the range (Fig. 3.2 [29-30]). In the south a c. 500 m wide linear northeast-southwest trending valley cuts through the South East Nemegt Volcaniclastic Group (section 2.7.2; Fig. 2.7 [3]), and eventually joins the southern frontal thrust to the west (Fig. 3.2 [31]). Although no fault plane is seen, the low sinuosity of the valley suggests there may be a fault present. In the north, a c.100 m wide east-west trending linear valley marks the northern boundary of the South East Nemegt Volcaniclastic Schist (section 2.7.2; Fig. 3.2 [30]). This valley can be traced to the west on Landsat TM imagery, where it strikes 285^{o} and dips 57^{o} to the southwest, cutting and offsetting a granite left-laterally by c.1.5 km (Fig. 3.2 [32]). Slickenlines were not found so the exact movement on the fault is not known. Further west in central Nemegt Uul, the fault forms the southern boundary of the duplex (Fig. 3.2 [8-9]) discussed in the previous paragraph.

3.5.4 Cenozoic structures within Altan Uul

Few Cenozoic structures have been documented within Altan Uul. However, many areas of Altan Uul are difficult to access and were not visited, so the paucity of evidence for Cenozoic deformation may simply reflect the poor data coverage for the area. Landsat TM imagery of Altan Uul shows several left-lateral offsets of Palaeozoic litho-tectonic sequences. In central Altan Uul, one of these faults is marked by a wide valley north of the Altan Uul ophiolite (Fig. 3.2 [33]). However, no fault planes were seen in the field and the age of the faults is not certain.

On Landsat TM imagery, a northwest-southeast trending fault can be seen branching off to the northwest from the southern front of Altan Uul (Fig. 3.2 [34]). The highest elevations in Altan Uul are next to this fault, suggesting that it may be a Cenozoic thrust fault, and that it may have moved more recently, or generated more uplift, than other faults in the Altan Uul area.

In this section, left-lateral displacements of 1.5 km and 300 m have been documented on two Cenozoic left-lateral faults in Nemegt Uul area (Fig. 3.2 [32]; Fig.

3.18). There are other left-lateral faults in Nemegt and Altan Uul, but their ages are unknown so they are not included in the calculation of the total left-lateral displacement. The evidence suggests there has been at least 1800 m of left-lateral deformation in the Nemegt and Altan Uul area.

3.6 Discussion

Normal faults and extensional shear zones in Nemegt and Altan Uul are dominantly east-west to northeast-southwest trending (Fig. 3.3). They cut Palaeozoic cleavage, folds and ductile shear zones and are sub-parallel to normal faults that cut Cretaceous rocks in the basins to the north and south of Nemegt and Altan Uul (Cunningham et al. submitted), and so may have formed under similar stress conditions, during Cretaceous basin evolution.

Nemegt Uul is bound to the north and south, and Altan Uul is bound to the south, by basinward-directed thrust faults that form low-sinuosity mountain fronts (Fig. 3.2; Fig. 3.13). Along the south front of Nemegt Uul, south-directed thrusting has overturned Cretaceous and Neogene basin sediments (Fig. 3.13A, B). On the north front of Nemegt Uul, an east-west range-bounding zone of thrusts cuts Quaternary gravels (Fig. 3.13E). This evidence suggests there has been Quaternary deformation in the range.

The Cenozoic faults within Nemegt Uul have a northwest-southeast to east-west trend, giving them a collective sigmoidal trace (Fig. 3.2). The Trans-Nemegt fault connects the north and south fronts of Nemegt Uul, giving the range a double restraining bend morphology. Left-lateral offsets on known Cenozoic faults total 1800 m. There are a number of areas which were not visited in Nemegt and Altan Uul, and a number of left-lateral faults which could not be assigned ages based on cross-cutting field relationships, suggesting that 1800 m is a minimum estimate of left-lateral displacement in Nemegt and Altan Uul. However, where slickenlines and kinematic indicators have been identified on Cenozoic faults, they typically suggest dip-slip or left-lateral oblique-slip movement (Fig. 3.12), suggesting there has not been a major component of Cenozoic pure strike-slip fault movement in Nemegt and Altan Uul.

Fault slip-vector data for the Trans-Nemegt fault suggests it has moved in a left-lateral oblique thrust sense (Fig. 3.17). Nemegt Uul has a low-mountain front sinuosity where it is bound by the Trans-Nemegt fault, and deformed Neogene gravels adjacent to,

and cut by the fault, indicates that there has been recent left-lateral oblique thrust movement on the Trans-Nemegt fault. The highest elevations in Nemegt Uul coincide with the inside bend of the Trans-Nemegt fault, suggesting that it has incurred the most thrust movement, or is the most recently active fault in Nemegt Uul. The geometry and cross-cutting relationships of the Cenozoic faults in Nemegt Uul at depth are unknown. However, conservative extrapolation of surface fault orientations to depth indicates that Nemegt Uul has an asymmetric positive flower structure geometry in cross-section. The geometry and slip-vectors of the Cenozoic faults in Nemegt Uul are consistent with a double restraining bend interpretation (Fig. 3.19).

Altan Uul is linked to Nemegt Uul by a Cenozoic left-lateral south-directed oblique-slip thrust fault, and also has an asymmetric positive flower structure in cross-section (Fig. 3.19). The highest elevations in Altan Uul are located to the south, close to the highly linear southern mountain front (Fig. 3.2), suggesting that the southern range bounding thrust fault may have caused a large proportion of the uplift seen in the range. Projecting the north-dipping peneplanes and north-dipping southern range-bounding thrust fault in western Altan Uul to the south, it is possible to calculate that the fault has accommodated approximately 158-236 m of shortening and approximately 359-533 m of uplift. The northwestern Palaeozoic basement-Cretaceous cover boundary of Altan Uul is marked by a normal fault, and the Palaeozoic rocks in the west are onlapped by Cretaceous sediments (Fig. 3.2; Fig. 3.5). However, the westward continuation of the Trans-Nemegt fault to the north of Altan Uul, and the south range bounding thrust fault have uplifted both Palaeozoic and Cretaceous rocks (Fig. 3.11), suggesting that Cenozoic uplift in Nemegt and Altan Uul has occurred within the same transpressional system.

There are different ways of classifying restraining bends based on bend morphology and the kinematics of the bend defining faults. Mann (2007) synthesises many of the studies of restraining bends to date and presents a global catalogue of restraining bends on active and ancient fault systems. Mann (2007) defines three restraining-bend types (Fig. 3.20): First, transpressional uplifts, for example the Southern Alps along the Alpine Fault system in New Zealand (Little et al. 2005, Mann 2007). Second, sharp restraining bends, for example the Almacik Mountains along the North Anatolian fault zone in Turkey (Saribudak et al. 1990, Mann 2007). Third, gentle restraining bends referred to as lazy-S or lazy-Z shaped, for example the Sutai range along the Tonhil fault in Altai of southern Mongolia (Cunningham et al. 2003a, Mann

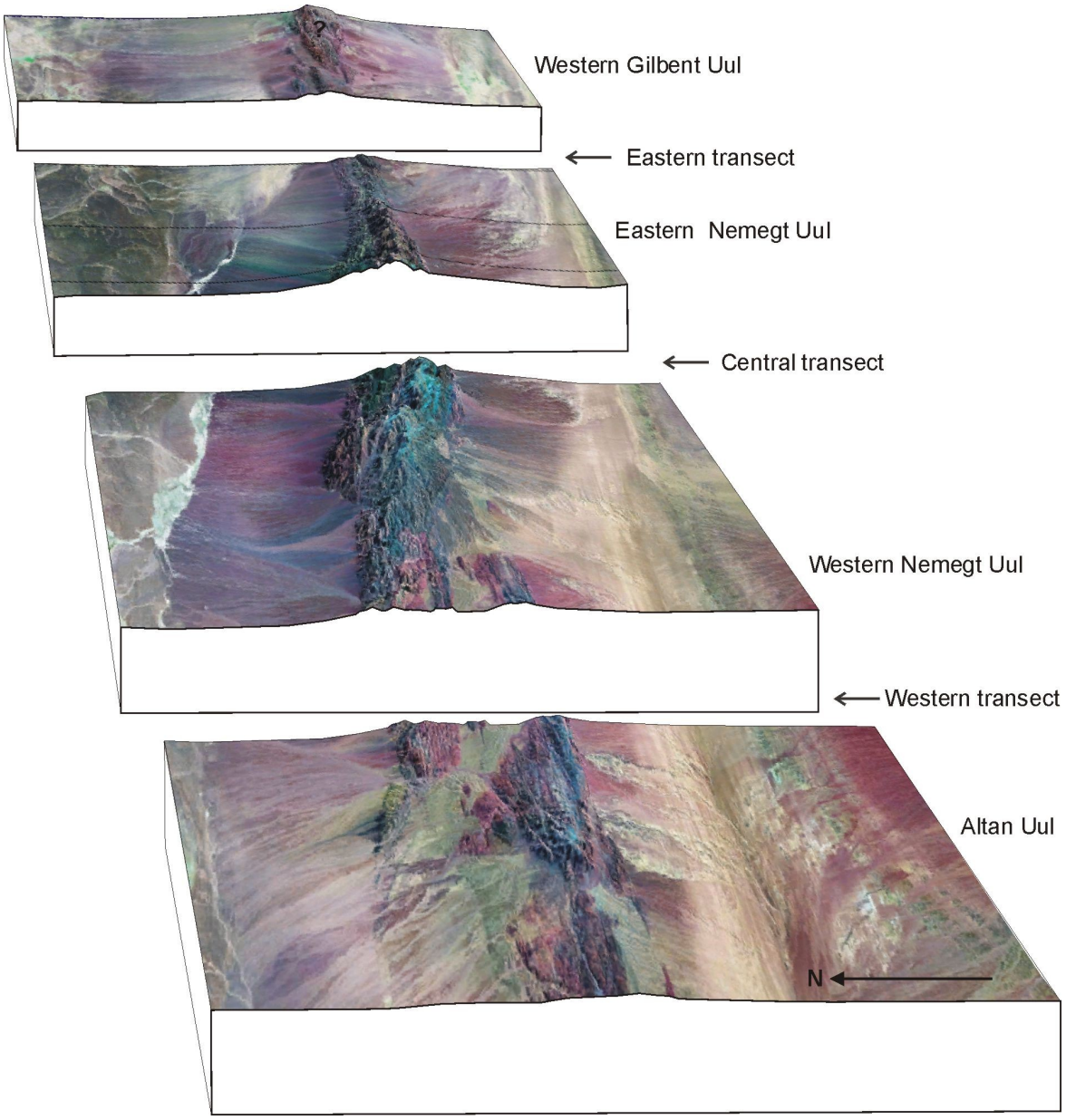

Fig. 3.19. A) Landsat TM imagery of Nemegt and Altan Uul viewed eastward B) The same Landsat TM imagery with structural interpretation (next page). C) 3D block model with litho-tectonic and structural interpretation and Landsat TM imagery removed (page after next).

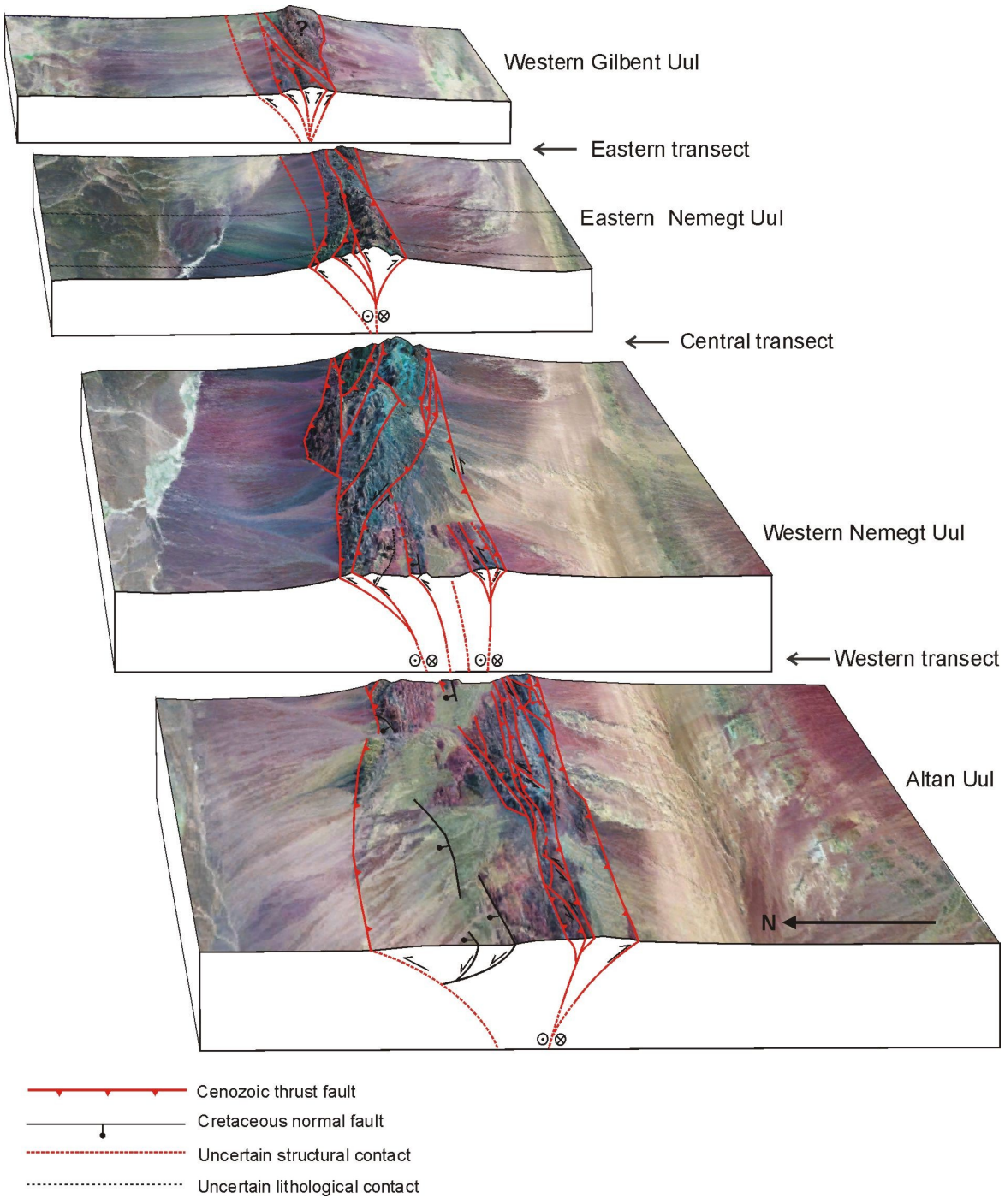
Western Gilbent Uul
Eastern transect
Eastern Nemegt Uul
Central transect
Western Nemegt Uul
Western transect
Altan Uul
N
Cenozoic thrust fault
Cretaceous normal fault
Uncertain structural contact
Uncertain lithological contact

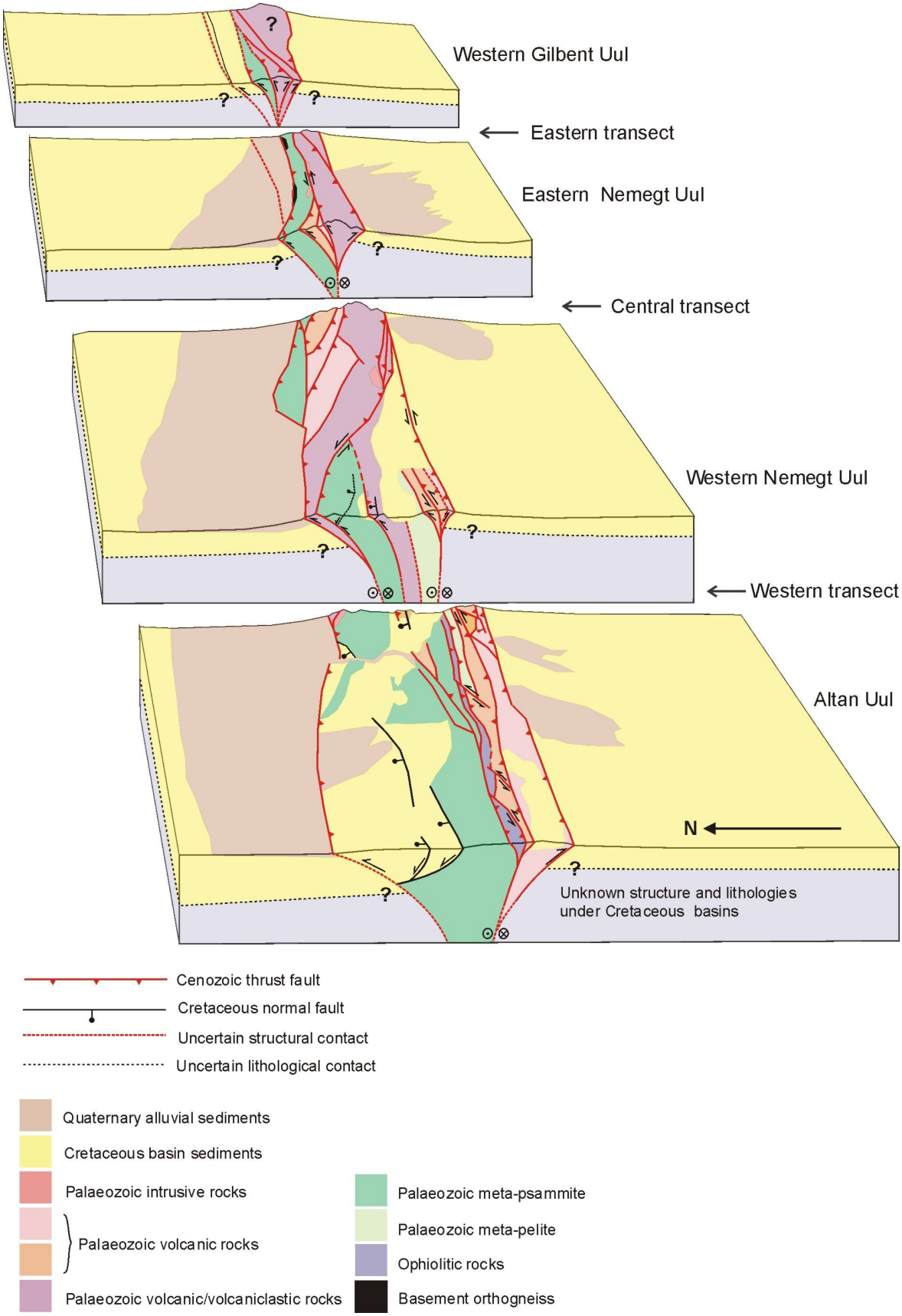
Western Gilbent Uul
Eastern transect
Eastern Nemegt Uul
Central transect
Western Nemegt Uul
Western transect
Altan Uul
N
Unknown structure and lithologies
under Cretaceous basins
Cenozoic thrust fault
Cretaceous normal fault
Uncertain structural contact
Uncertain lithological contact
Quaternary alluvial sediments
Cretaceous basin sediments
Palaeozoic intrusive rocks
Palaeozoic volcanic rocks
Palaeozoic volcanic/volcaniclastic rocks
Palaeozoic meta-psammite
Palaeozoic meta-pelite
Ophiolitic rocks
Basement orthogneiss

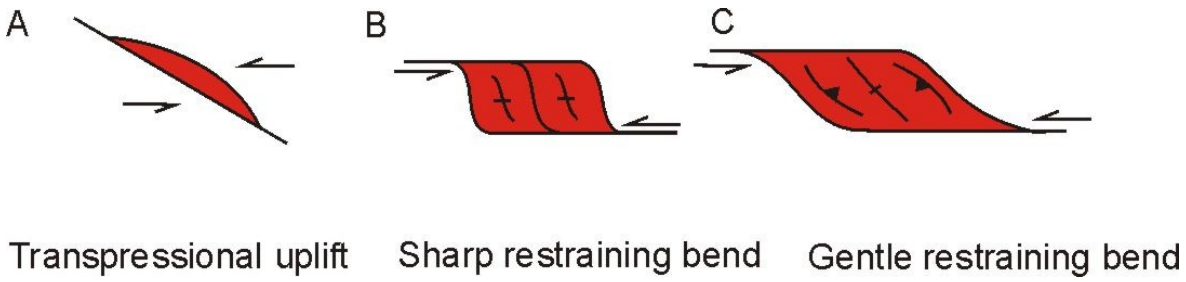

Fig. 3.20. Three types of restraining bend (after Mann, 2007). A) Transpressional uplift, B) Sharp restraining bends are typically rhomboidal in shape and aligned along major strike-slip faults. They range in scale up to several kilometres in length and up to hundreds of metres in width (Mann, 2007). C) Gentle restraining bends are more common than sharp restraining bends, and exhibit a lazy-S or lazy-Z shape depending on the sense of slip and overstep across the master faults. They range in size from small features a few kilometres across to the worlds largest bends up to 200 km wide and several kilometres in elevation (Mann, 2007).

2007). Cowgill et al. (2004b) discuss restraining bends in terms of the dominant type of slip along the faults defining a bend. Consequently, there are two end-member types of restraining bends. First, "thrust-dominated" bends, which are flanked by thrust faults, and second, "strike-slip dominated" bends, which are flanked by strike-slip faults (Cowgill et al. 2004b).

A lack of slickenline data on major Cenozoic faults makes it impossible at this time to be certain of the precise slip vectors along many of the Cenozoic faults that define the Nemegt Uul restraining bend. However, kinematic indicators on most of the Cenozoic faults documented in Nemegt and Altan Uul, especially the range-bounding faults and the Trans-Nemegt fault where it transects Nemegt Uul, suggest that most of the Cenozoic deformation in the area has a left-lateral oblique thrust, or pure thrust component (Fig. 3.12). This suggests that strain is not partitioned into a strike-slip and thrust components, unlike many "thrust-dominated" bends, e.g. the Santa Cruz Mountains, along the San Andreas fault, California (Anderson 1990, 1994) and "strike-slip dominated" restraining bends, e.g. the Akato Tagh bend, along the Altyn Tagh fault, Tibet (Cowgill et al. 2004a, Cowgill et al. 2004b). Combining the definitions of Mann (2007) and Cowgill (2004b), the author of this study cautiously defines Nemegt Uul as a gentle oblique-slip dominated restraining bend.

The asymmetry of the flower structure in Nemegt Uul and Altan Uul is mirrored by the topography, with higher elevations consistently found in the south, giving the ranges a northward tilt (Owen et al. 1999b). In Altan Uul, there is a north-dipping peneplane. The topographic asymmetry may reflect greater uplift along the southern range-bounding faults or may indicate that the Palaeozoic-Cretaceous unconformity had a

northward tilt that existed before Cenozoic uplift. Greenschist to epidote-amphibolite grade metamorphosed rocks in Nemegt and Altan Uul may have originally been buried at c. 12-20 km depth (section 2.10.4; Fig. 2.42), so there must have been c. 12-20 km of uplift and exhumation since the Carboniferous. A south-dipping erosion surface preserved in the Palaeozoic rocks in western Nemegt Uul and the north-dipping Altan Uul peneplane suggest that most of the c. 12-20 km uplift and exhumation required to expose these rocks, occurred before the Cretaceous. The lack of Cretaceous sediments preserved on top of the un-incised topography in western Nemegt Uul either suggests that Cretaceous sediments were never deposited there, indicating that topography may have persisted in this area from the late Carboniferous, or that erosion completely removed the Cretaceous sediments leaving the Cretaceous erosion surface.

The Trans-Nemegt fault is the longest fault in Nemegt and Altan Uul and the highest elevations in the region are located on its inside southeast bend, suggesting it may have accommodated the most slip in the area (Fig. 3.2 [10]; Owen et al. 1999b). The inside of the bend is where the maximum uplift has been documented in other restraining bends (Westaway 1995, Cunningham et al. 2003a, Cowgill et al. 2004b, Wakabayashi et al. 2004, Cunningham 2005, 2007). This suggests the bend of the through-going fault controls where maximum uplift occurs in a restraining bend. Fault geometry and slickenline data and documented lateral offset along the Trans-Nemegt fault were used to estimate a maximum vertical movement of 520-633 m associated with the Trans-Nemegt fault which defines the Nemegt Uul restraining bend. On the south front of Altan Uul, the estimated Cenozoic vertical movement is 359-533 m. Apatite fission track data from the Ih Bogd and Baga Bogd (Vassallo et al. 2007) to the north (Fig. 3.1) and the Tien Shan over 500 km to the west (Dumitru & Hendrix, 2001) have been used to constrain the cooling history and by association, the age of uplift, in these ranges. In the Tien Shan, apatite fission track data suggests there has been no more than 3 km of Cenozoic exhumation (Dimitru et al. 2001). In Ih Bogd and Baga Bogd, to the north of Nemegt and Altan Uul (Fig. 3.1), apatite fission track data suggests there has only been a few hundred metres of Cenozoic exhumation (Vassallo et al. 2007). The evidence from Ih Bogd and Baga Bogd is in agreement with the evidence in Nemegt and Altan Uul, which suggests there has been relatively little Cenozoic uplift in Nemegt and Altan Uul compared to the uplift and exhumation thought to have occurred during the late Carboniferous and Cretaceous.

In the east, the mountain fronts of Nemegt Uul are embayed and topography is lower (Fig. 3.2 [14-15]; Fig. 3.8), suggesting the mountain fronts have not been active as recently as in the west, where the mountain front sinuosity is low and the highest elevations are found (Fig. 3.2 [10,18,20]; Fig. 3.7). To the northeast of Nemegt Uul, the possibility of a foreland propagating blind thrust is indicated by the mid-fan entrenchment of alluvial fans (Fig. 3.2 [16]; Owen et al, 1999b). This could indicate that deformation is "stepping out" from the range, as is suggested for the restraining bend uplifted ranges along the Bogd fault to the north (Bayasgalan et al. 1999, Owen et al. 1999a). Low rates of rainfall in southern Mongolia result in low rates of erosion. Consequently, lower erosion rates result in less material being removed from the mountains, making it increasingly difficult mechanically for the faults that control uplift to work against gravity. Eventually the force required to act against gravity may become greater than the force required to form new basinward faults, and the system will widen (Bayasgalan et al. 1999, Owen et al. 1999a). This process of strain hardening is documented in several restraining bend systems in Central Asia. For example, the Ih Bogd, Artsa Bogd and Baga Bogd bends along the Bogd fault in southern Mongolia (Bayasgalan et al. 1999), and the Akato Tagh bend along the Altyn Tagh fault in Tibet (Cowgill et al. 2004a). However, there is only c.300 m of left-lateral offset documented along the Trans-Nemegt fault, suggesting 710-738 m of net left-lateral oblique thrust slip movement and a maximum of 520-633 m of vertical movement. Although the frictional properties of the Trans-Nemegt fault are unknown, 710-738 m of net slip seems to be a small amount of displacement for a fault of its length (c.70 km). The low-mountain front sinuosity, high elevations, and deformed Neogene sediments associated with the Trans-Nemegt fault also suggests that it is one of the more active faults in the area. If strain hardening was occurring, the Trans-Nemegt fault would be expected to have locked up. This makes it hard to justify a strain-hardening system.

There is another way to explain why the eastern end of Nemegt Uul appears less active than the west. The Trans-Nemegt fault in western Nemegt Uul defines the restraining bend in Nemegt Uul. The area immediately adjacent to the restraining bend is where the most thrust deformation and uplift is expected to occur (Westaway, 1995, McClay & Bonora, 2001). Eastern Nemegt Uul is farther away from the restraining bend, and so is less likely to display evidence for thrusting and uplift, and may have accommodated more strike-slip deformation. This hypothesis is supported by evidence for

1.5 km of left-lateral offset along an east-west trending fault in eastern Nemegt Uul (Fig. 3.2 [30]), in contrast with evidence of only 300 m of left-lateral offset along the Trans-Nemegt fault in the west.

3.7 Conclusions

Cautious interpretation of cross-cutting lithological and structural relationships, and consideration of geomorphological features allows several conclusions to be made about the evolution of Nemegt and Altan Uul.

1. Nemegt and Altan Uul both have an asymmetric positive flower structure and northward tilted topography in cross-section, although there is a south-dipping peneplane in western Nemegt Uul. The ranges are linked by a left-lateral south-directed oblique-slip thrust fault. Uplifted Cretaceous sediments along the westward continuation of the Trans-Nemegt fault to the north of Altan Uul suggest uplift in both ranges is controlled by the same transpressional system.

2. Low-mountain front sinuosity, overturned Neogene sediments along the south front, and cut Quaternary gravels at the north front of Nemegt Uul suggest that mountain building has occurred in the late Cenozoic, and may be ongoing.

3. The Trans-Nemegt fault connects the recently active north and south fronts of Nemegt Uul, giving the range a double restraining bend geometry. Maximum uplift is localised on the inside of the southeastern bend of the Trans-Nemegt fault. Slickenline data indicate the fault has moved in a left-lateral oblique-thrust sense. Displaced bedding on Google Earth imagery coupled with fault geometry and slickenline data were used to calculate that there has been a maximum of 710-738 m net slip along the Trans-Nemegt fault. There is little evidence for a major component of Cenozoic pure strike-slip faulting in the area, and kinematic indicators suggest an oblique thrust component to most of the Cenozoic faults in Nemegt and Altan Uul. Based on classification schemes used by Mann (2007) and Cowgill (2004b), the Nemegt Uul restraining bend is cautiously interpreted as a gentle oblique-slip dominated restraining bend.

4. The existence of relatively un-incised topography on metamorphosed Palaeozoic rocks in western Nemegt Uul, and a northward tilted peneplane in Altan Uul suggest most of the uplift required to expose the Palaeozoic rocks occurred before, or during the Cretaceous, most likely during late Carboniferous arc-continent collision. A lack of Cretaceous sediments preserved on the erosion surfaces in western Nemegt Uul may also suggest that some Palaeozoic rocks have been exposed since the late Carboniferous. Estimates of 520-633 m of maximum vertical uplift on the Trans-Nemegt fault, suggest there has not been a great deal of Cenozoic uplift.

5. Western Nemegt Uul has lower mountain front sinuosities and higher elevations than eastern Nemegt Uul. It is suggested that this disparity is a consequence of a variation in the style of deformation between western and eastern Nemegt Uul. In the west, there is a wider, thrust dominated deformation zone surrounding the restraining bend, defined by the Tran-Nemegt fault so elevations are higher. Contrastingly, the eastern extent of Nemegt Uul is farther away from the restraining bend, and has more documented evidence of left-lateral deformation, which may not be generating as much topography.

Chapter 4

The crustal evolution of Nemegt and Altan Uul: a synthesis

4.1 Introduction

Southern Mongolia has had a long complex history of polydeformation. In the middle to late Palaeozoic, a series of tectonic terranes were accreted in a northward direction to form the southward younging Central Asian Orogenic Belt (Fig. 2.1 inset), which passes through southern Mongolia and northern China (Zonenshain et al. 1990, Didenko 1992, Ruzhentsov & Pospelov 1992, Lamb & Badarch 1997, 2001, Badarch et al. 2002, Xiao et al. 2003, Xiao et al. 2004a). In the late Mesozoic widespread rifting occurred across southern Mongolia and northern China, forming extensive basins filled with Cretaceous sediments, rich in dinosaur fossils (Jerzykiewicz & Russell 1991, Benton et al. 2000, Johnson et al. 2001, Meng 2003, Meng et al. 2003). In the Cenozoic, continental extrusion tectonics, thought to have been caused by the northward indentation of India into Eurasia, resulted in the formation of a series of large right-stepping east-west trending left-lateral intracontinental transpressional fault systems from Tibet to Mongolia (Fig. 4.1 inset). In southern Mongolia, a corridor of intracontinental left-lateral transpression has localised uplift at push-up ridges, stepovers and restraining bends along left-lateral strike-slip faults (Fig. 4.1; Baljinnyam et al. 1993, Cunningham et al. 1996).

Nemegt and Altan Uul are Cenozoic uplifted mountains along the trace of the Gobi-Tien Shan fault system (Fig. 4.1). They consist of dominantly greenschist grade metamorphosed Palaeozoic volcanic, volcaniclastic, sedimentary and ophiolitic rocks. Consequently, they represent an opportunity to study the cross-cutting lithological and structural relationships caused by multiple deformation events that have affected the region from the Palaeozoic to the present.

In chapter 2, the cross-cutting relationships of the lithologies and structures in Nemegt and Altan Uul were established, and the Palaeozoic environment of lithological formation and deformation was discussed. In chapter 3, the Mesozoic and Cenozoic structures in the area were discussed and a 3D model of the present day architecture of Nemegt and Altan Uul was presented.

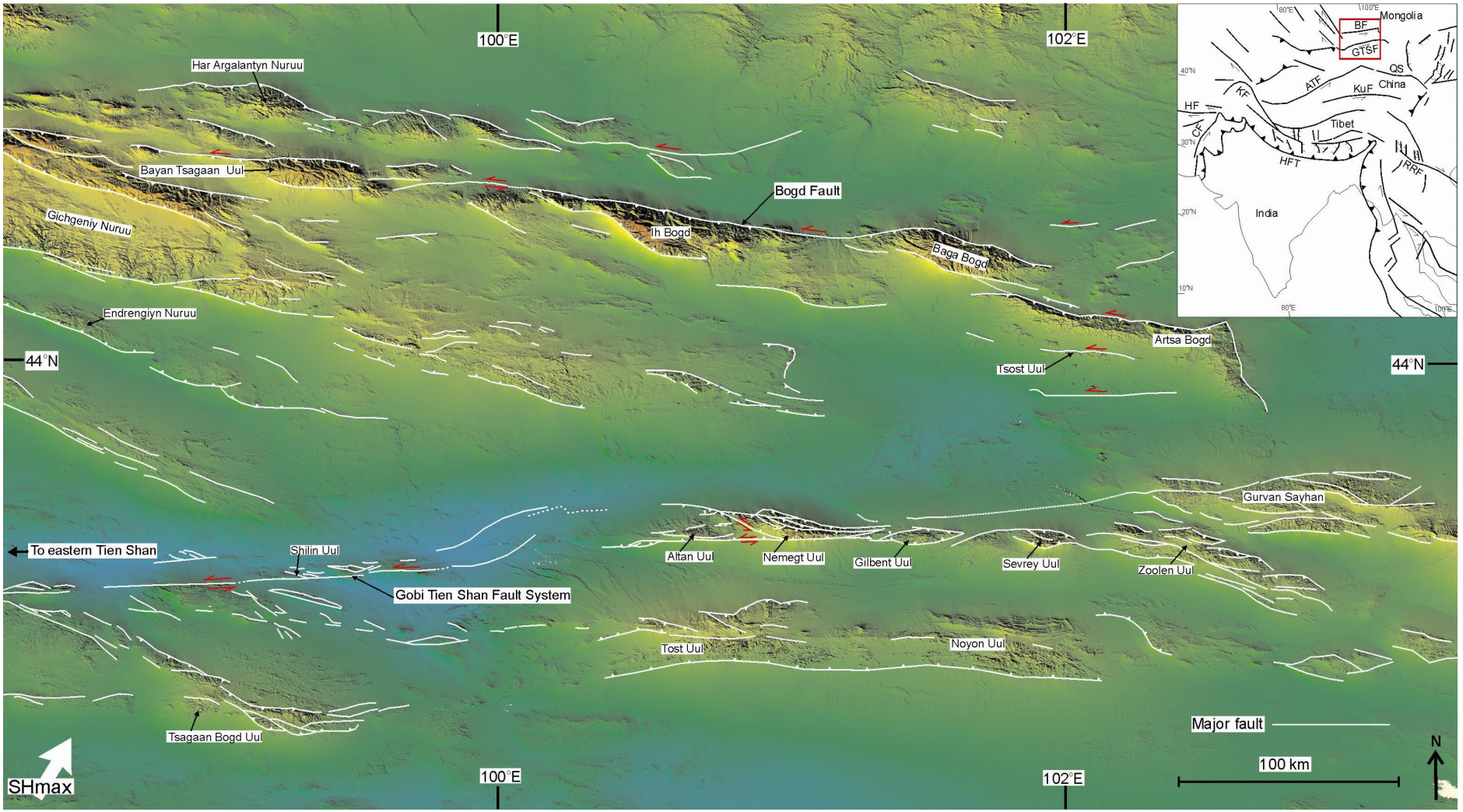

Fig. 4.1. SRTM-90 DEM of Gobi Altai. Inset shows major Cenozoic faults north of the India-Eurasia collision zone. ATF = Altyn Tagh fault, BF = Bogd fault, CF = Chaman fault, GTSF = Gobi Tien Shan fault system, HF = Herat fault, HFT = Himalayan frontal thrust, KF = Karakorum fault, KuF = Kunlun fault, QS = Qilan Shan fault, RRF = Red River fault (redrawn from Tapponier et al. 1982).

In this chapter, a brief review of the current models for the accretion of the Central Asian Orogenic Belt, and the Palaeozoic ophiolite belts in Mongolia is presented. The geology of the tectonic terranes surrounding Nemegt and Altan Uul is discussed and existing models for the Palaeozoic evolution of southern Mongolia are tested against evidence presented in the previous chapters from Nemegt and Altan Uul. The Cenozoic evolution of Nemegt and Altan Uul are considered in the context of the Gobi-Tien Shan fault system. The implications of these models to our understanding of intraplate mountain building processes in the region are discussed.

4.2 Palaeozoic terrane amalgamation models

The remoteness and vast area of southern Mongolia means there are still large regions where crustal rock types, major structures, and geochemical and geochronological characteristics of basement and cover sequences are poorly documented. Consequently, "early" tectonic models for the crustal evolution of the Central Asian Orogenic Belt in Mongolia (Ruzhentsov & Pospelov 1992, Sengor et al. 1993, Yakubchuk et al. 2001) can be regarded as working hypotheses to be tested and refined as new field data become available. Recently, several new syntheses of the evolution of the Central Asian Orogenic Belt have been published that challenge earlier models and incorporate new published field data (Zoneshain et al. 1990, Ruzhentsov & Pospelov 1992, Dorjnamjaa et al. 1993, Sengor et al. 1993, Buslov et al. 2001, Yakubchuk et al. 2001, Badarch et al. 2002). A brief summary of these models is given here to provide a context for this study.

The development of the Central Asian Orogenic Belt began with the rift separation of the Angaran and North China cratons. Palaeomagnetic reconstructions (Pisaravesky et al. 2003) and the intrusion of basic dyke swarms with isotopic ages in the range 974-900 Ma into the margins of the Angaran craton (Dobretsev et al. 2003), suggest the onset of rifting occurred in the Neoproterozoic. At the same time several small gneissic micro-continents also rifted away from the cratons (Zoneshain et al. 1990, Ruzhentsov & Pospelov 1992, Sengor et al. 1993, Khain et al. 2003). Between 900 Ma and 544 Ma, island-arcs, seamounts and oceanic crust were formed between and around these microcontinents (Khain et al. 2003, Windley et al. 2007). The presence of a belt of Neoproterozoic ophiolites around the Angaran craton suggests that these microcratons were re-attached by subduction-accretion. These Neoproterozoic ophiolites were thrust

onto the margins of their respective micro-cratons in several different directions, suggesting that there was no single direction of subduction at this time (Sengor et al. 1993, Windley et al. 2007).

The evolutionary models diverge at this point. The Kipchak-arc model of Sengor et al. (1993) proposes that a single large arc formed between the Angaran and North China cratons, and grew at a constant rate throughout the Palaeozoic to produce the continental crust that makes up the Central Asian Orogenic Belt. Yakubchuk et al. (2001) propose a three-arc variation of the same model. The Kipchak-arc models propose that the amalgamated Palaeozoic crust was later reshuffled into its present configuration by strike-slip faulting during oroclinal bending of the arc or arcs, and by subsequent Mesozoic-Cenozoic intraplate strike-slip deformation. However, the Kipchak-arc models lack sufficient kinematic data from proposed major strike-slip faults to support the conclusions made regarding terrane reshuffling in the Palaeozoic. Palaeogeographic plate configurations based on recent palaeomagnetic data (Smethurst et al. 1998, Hartz & Torsvik 2002, Meert & Lieberman 2004, Murphy et al. 2004, Cocks & Torsvik 2005, Popov et al. 2005) also suggest that the Angaran and North China cratons were not in the palaeogeographical positions required by the Sengor et al. (1993) Kipchak-arc model in the Lower Palaeozoic (Windley et al. 2007).

Zonenshain (1990) suggested an alternative model which compares the amalgamation of the Central Asian Orogenic Belt to the geology and tectonics of the modern western Pacific; a theme developed in a number of subsequent studies (Ruzhentsov & Pospelov 1992, Dorjnamjaa et al. 1993, Buslov et al. 2001, Badarch et al. 2002, Laurent-Charvet et al. 2002, Xiao et al. 2003). These models all propose that rifting apart of the Angaran and North China cratons was soon followed by the development of the Palaeo-Asian ocean, which contained microcontinents and several intra-oceanic subduction zones with juvenile arc systems. Accretion of these microcontinent and arc elements began in the northern Central Asian Orogenic Belt in the early Palaeozoic, then progressed southwards with dominantly north-dipping subduction producing progressively younger arc rocks and ophiolite belts in southern Mongolia and bordering regions of China (Badarch et al. 2002). Terminal closure of the Palaeo-Asian ocean was completed in the Permo-Triassic with final suturing of the North China craton against the extensive collage of terranes separating it from the Angaran craton to the north (Xiao et al. 2003). Many studies use the archipelago-type (Indonesian) model summarised by

Windley at al. (2007), in interpreting the rocks of southern Mongolia as a series of discrete arcs that were separated by ocean basins (Hendrix et al. 1996, Lamb & Badarch 1997, 2001, Laurent-Charvet et al. 2002, Xiao et al. 2003, Helo et al. 2006). However, the exact nature and extent of these arcs and ocean basins is poorly understood.

4.3 Ophiolite belts of Mongolia

Ophiolitic rocks in southern Mongolia occur as discrete slivers of peridotite, serpentinite, gabbro, sheeted dyke complexes, pillow basalts and ocean-floor sediments, and follow a broadly east-west basement fabric (Fig. 4.2). Following Palaeozoic thrust emplacement, the ophiolitic assemblages have been variably subjected to younger deformation events recorded in the Gobi Altai region, including Late Jurassic-Cretaceous extensional deformation (Johnson et al. 2001, Meng 2003, Meng et al. 2003), and Late Cenozoic sinistral transpressional deformation (Cunningham et al. 1996). A paucity of radiometric age data for ophiolitic rocks in southern Mongolia and widespread Cretaceous sedimentary cover make it difficult to correlate Palaeozoic suture zones along-strike in the region.

Five main ophiolite belts can be identified in Mongolia. In the north, the Hug accretionary wedge terrane, Zavhan craton, Lake and Bayangol island arc terranes, Dariv terrane, and Ilchir and Bayankhongor ophiolite terranes (Fig. 4.2) contain slivers of Neoproterozoic-Cambrian ophiolites (Badarch et al. 2002, Buchan et al. 2002, Windley et al. 2007). The Bayankhongor ophiolite has a Sm-Nd gabbro age of 569 ± 21 Ma (Kepezhinskas et al. 1991), and a SHRIMP U/Pb zircon crystallisation age of 665 ± 15 Ma for an anorthosite (Kovach et al. 2005). Regardless of controversy surrounding the age of oceanic crust formation, granite plutons and dykes intruding the ophiolite and its boundary have a mean $^{207}Pb/^{206}Pb$ zircon evaporation age of 539 ± 5 Ma, giving a minimum age for accretion and obduction of the ophiolite (Buchan et al. 2002). The Khantaishir ophiolite in the Lake terrane has a $^{207}Pb/^{206}Pb$ zircon age of 568 ± 4 Ma, and the Bayannor ophiolite in the Dariv terrane has a mean $^{207}Pb/^{206}Pb$ zircon age of 571 ± 4 Ma. All these ophiolites were obducted in different directions around microcratons and arcs in the Neoproterozoic-Early Cambrian .

To the south, there is a belt of Ordovician-Silurian ophiolites. The Bidz terrane (31 on Fig. 4.2) contains ophiolitic rocks thought to represent displaced fragments of

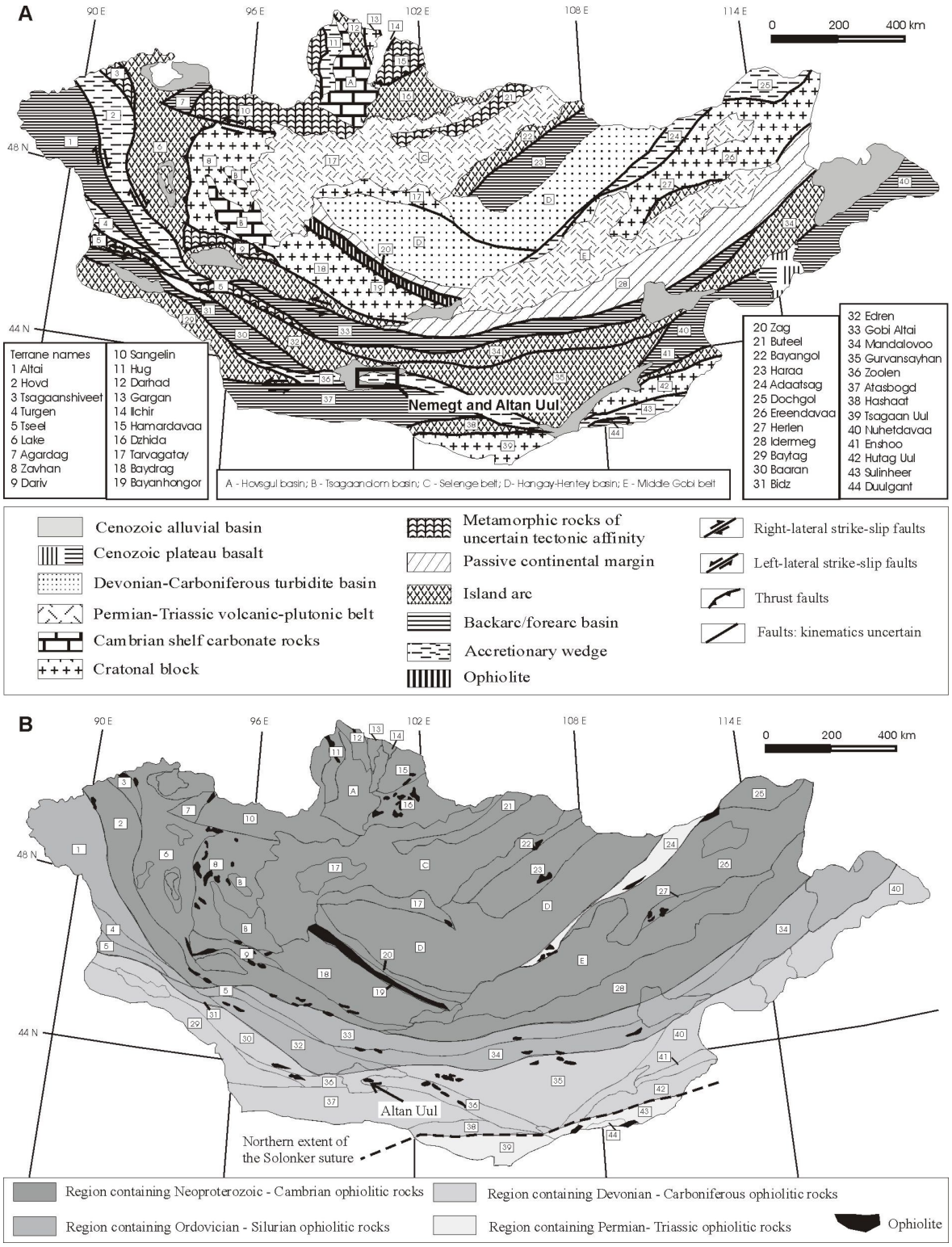

Fig. 4.2. A) Palaeozoic terrane map of Mongolia (after Badarch et al. 2002), B) Ophiolite occurrences overlaid with Palaeozoic terrane map (after Badarch et al. 2002, Buchan et al. 2002).

oceanic crust that were adjacent to a possible Ordovician island arc to the west in the Chinese Altai (He & Han 1991, Windley et al. 1994, Badarch et al. 2002).

To the southeast, the Zoolen and Gurvansayhan terranes (36 and 35 on Fig. 4.2) contain slivers of possible ophiolite. Although radiometric age determinations are not available for these rocks, they are along strike from the Hegenshan ophiolite in Inner Mongolia, China. Low potassium concentrations, preventing its use in radiometric dating, and difficulties with dating finely zoned amphiboles in basaltic dikes, cutting serpentinised harzburgite in the Hegenshan ophiolite, have caused some controversy about its age (Robinson et al. 1999). However, red cherts interlayered with pillow lavas contain radiolarian fossils including *Entactina* sp., *Tetrentactinia* sp., and *Cenellipsis* sp., suggesting a Middle-Late Devonian age of oceanic crust formation (Robinson et al. 1999, Zhou et al. 2003). Depleted tholeiitic basaltic dykes in the ultramafic sequence of the Hegenshan ophiolite have a flat chondrite-normalized REE pattern. Strong depletion in incompatible elements and the presence of large chromite deposits suggest that the Hegenshan ophiolite formed in an island-arc/back-arc environment (Robinson et al. 1999, Zhou et al. 2003).

Just north of the Chinese-Mongolia border, ophiolites in the Sulinheer, Tsagaan Uul and Hashaat terranes (39 and 38 on Fig. 4.2) mark the Solonker suture, which formed during the terminal closure of the Palaeo-Asian Ocean. Post-collisional S-type granites intruded into and across the suture zone have a Triassic whole rock Rb-Sr age of 228 ± 21 Ma (Chen et al. 2000).

In northeast Mongolia, the Adaatsag ophiolite represents a small part of the Mongol-Okhotsk suture (24 on Fig. 4.2). A single-zircon mean $^{207}Pb/^{206}Pb$ evaporation age of 325.4 ± 1.1 Ma for a leucogabbro pegmatite dyke records the time of formation of the oceanic crust in the Mongol-Okhotsk ocean (Tomurtogoo et al. 2005). Mid-Jurassic U -Pb secondary ionization mass spectrometry and evaporation zircon ages of 173.6 ± 0.8 Ma and 172.7 ± 1.2 Ma for a mylonitised granite provides a maximum age for the Muron shear zone, associated with the left-lateral Mongol-Okhotsk suture. Closure of the Mongol-Okhotsk ocean is thought to be diachronous from the Early Permian in the west to the Late Permian-Early Triassic in the east (Tomurtogoo et al. 2005). The Mongol-Okhotsk suture represents the termination of continental amalgamation in the Central Orogenic Belt.

4.4 Palaeozoic terranes of southern Mongolia

Badarch et al. (2002) described and identified 44 terranes in Mongolia. The quality of the data and implications for the interpretations presented in the Badarch et al. (2002) study are discussed in section 2.2. Despite the unknown quality of some of the palaeontological data and poor age constraints on many of the Palaeozoic rocks, the Badarch et al. (2002) terrane synthesis provides a useful model to test using new field and geochemical data.

Nemegt and Altan Uul have previously been placed in the Zoolen terrane (Badarch et al. 2002; 36 on Fig. 4.2). The characteristics of this terrane were discussed in section 2.2. In order to place the Zoolen terrane in a regional tectonic context, the geology of the surrounding terranes in southern Mongolia as outlined by Badarch et al. (2002) is discussed below.

The Zoolen terrane (36 on Fig. 4.2) is surrounded by several other Palaeozoic terranes described and identified by Badarch et al. (2002). To the northwest, is the Edren terrane (Fig. 4.2), which is divided into two main sequences. The northern sequence is dominated by Devonian and Carboniferous meta-sedimentary argillaceous rocks, fossiliferous limestone, and minor chert intruded by Permian alkaline granite plutons, all of which have undergone intense brittle deformation, shearing and upright folding. The southern sequence is dominated by Devonian to Lower Carboniferous greenschist grade metamorphosed meta-basaltic/andesitic volcanic and volcaniclastic rocks, constrained by uncited palaeontological data, with some minor meta-limestone and clastic meta-sedimentary rocks overlain by Permian felsic meta-volcanic rocks intruded by Carboniferous-Permian diorite, granodiorite, and leucogranite plutons (Badarch et al. 2002). Major and trace element geochemical analysis of Devonian basalts in the southern sequence, suggests an arc origin (Lamb & Badarch 2001).

To the northeast of the Edren terrane, and north of the Zoolen terrane, is the Mandalovoo terrane (34 on Fig. 4.2). It is a long narrow east-west trending belt extending over 1000 km east into northeast China (34 on Fig. 4.2). It has a deformed stratigraphic succession divided into an Ordovician to Mid-Devonian dominantly marine sedimentary sequence with sandstone, mudstone and fossiliferous limestone (contains *T. gigantea* sp.), chert, and felsic tuff, and an Upper Devonian dominantly volcanic sequence with pillow basalt, andesite, volcaniclastic sandstone and chert. Devonian diorite and granodiorite

plutons are widespread. There are also Lower Carboniferous marine sediments throughout the area constrained by uncited palaeontological evidence (Badarch et al. 2002). Major and trace element geochemical analysis of Devonian pillow basalts suggests an arc origin (Lamb & Badarch 2001). The volcanic rocks in the area are widely interpreted to represent a Devonian volcanic arc (Badarch et al. 2002). A palaeomagnetic survey suggests that the Devonian arc formed near the equator and has moved approximately 40^{o} north while rotating 70^{o} clockwise to reach its present location and attitude (Didenko 1992). The area is covered by Upper Carboniferous to Permian post-accretionary sequences of volcanic and sedimentary rocks, granite plutons and Jurassic to Cretaceous clastic rocks constrained by uncited palaeontological evidence (Badarch et al. 2002), suggesting that the Mandalovoo terrane (34 on Fig. 4.2) was accreted to the terranes to the north by the Mid-Carboniferous.

The Gurvansayhan terrane (35 on Fig. 4.2) is situated northeast of the Zoolen terrane and directly south of the Mandalovoo terrane in southern Mongolia. It is composed of several slivers of dismembered ophiolite and melange. It is divided into an Ordovician to Silurian dominantly greenschist grade meta-sedimentary sequence with meta-psammite, meta-pelite, chert and volcaniclastic rocks, an Upper Silurian to Lower Devonian dominantly ocean-floor volcanic and sedimentary sequence with radiolarian chert, tholeiitic pillow basalt, and andesitic tuff, and a Mid-Devonian to Lower Carboniferous dominantly marine sequence of fossiliferous chert, olistostromes with coral and limestone clasts, and volcaniclastic rocks. There are several melanges zones, consisting of blocks of pillow lava, fossiliferous limestone, sandstone, gabbro, diabase dykes and amphibolite (Badarch et al. 2002). Major and trace element geochemical analyses of Devonian pillow basalt suggest they were erupted in an island arc environment (Ruzhentsov & Pospelov 1992, Lamb & Badarch 2001, Helo et al. 2006). Helo et al. (2006) suggest that volcanic rocks in this island arc have indistinguishable geochemical characteristics from volcanic rocks to the southwest in Nemegt Uul in the Zoolen terrane. The terrane is deformed into imbricated thrust sheets, melanges and high strain zones. A post-accretionary syenite pluton with a K-Ar biotite age of 307 ± 4 Ma (Lamb & Cox 1998) and post-accretionary monzanite dyke with an Ar-Ar age of 313 ± 2.9 Ma (Lamb & Cox 1998, Perello et al. 2001) suggest that the arc elements of the Gurvansayhan terrane were accreted to the terranes to the north by the Mid-Upper Carboniferous. The terrane is overlain by Carboniferous, Permian and Jurassic-

Cretaceous volcanic and sedimentary rocks. Triassic sedimentary rocks are noticeably absent in the Gurvansayhan terrane, which might suggest the area was uplifted above sea-level at this time.

The Atasbogd terrane (24 on Fig. 4.2) lies directly south of the Zoolen terrane and extends beyond 800 km west into the Tien Shan region of northern China (Badarch et al. 2002). It is divided into an Ordovician to Silurian sequence of dominantly greenschist grade metamorphosed meta-sedimentary rocks including meta-psammite, meta-pelite, phyllite and marble, pillow basalt, and a Devonian succession of volcanic and sedimentary rocks including conglomerate, sandstone, siltstone, andesite, dacite, rhyolite, tuff, breccia, radiolarian chert and fossiliferous limestone (Ruzhentsev, 1985; Badarch et al. 2002). In the southwest of the terrane, the Ordovician to Silurian meta-sedimentary succession is intruded by granite plutons and disconformably overlain by Devonian sedimentary rocks (Badarch et al. 2002). The dominantly volcaniclastic meta-sedimentary content of the Atasbogd pre-accretionary sequences is consistent with a forearc/backarc origin (Badarch et al. 2002). Devonian to Carboniferous and Permian granodiorite and granite plutons intrude the Ordovician to Devonian rocks. Lower Carboniferous shallow marine rocks, upper Carboniferous to lower Permian volcanic and volcaniclastic rocks, upper Permian to lower Triassic non-marine clastic rocks with terrestrial fossils and lower -middle Jurassic alluvial and lake sedimentary rocks, form an extensive post-accretionary assemblage in the area (Badarch et al. 2002). This suggests that accretion of the Atasbogd terrane to the Zoolen terrane in the north had occurred by the middle Carboniferous. A disconformity in the Upper Silurian-lower Devonian and an unconformity in the middle Cretaceous in the area (Meng et al. 2003), suggest that the Atasbogd terrane was uplifted more than once in the Palaeozoic-Mesozoic.

4.5 A synthesis of the Palaeozoic evolution of Nemegt and Altan Uul

In chapter 2, the distribution of lithologies in Nemegt and Altan Uul was discussed and preliminary interpretations about the tectonic environment of their formation were made. The distribution of lithologies in Nemegt and Altan Uul suggests there is a general south to north transition from greenschist grade mafic meta-volcanic rocks, with arc-like characteristics (section 2.10.1; Fig. 2.39) and volcaniclastic meta-sedimentary rocks, through a sequence of ophiolitic rocks in Altan Uul, to immature meta

-sedimentary rocks and mature meta-sedimentary rocks in the north. In northeast Nemegt Uul, mature meta-sedimentary rocks sit unconformably above orthogneiss along the northern front of the range (section 2.7.3-2.7.4; Fig. 3.32). Although the Palaeozoic rocks have been deformed by subsequent deformation events in the Mesozoic and Cenozoic (chapter 2), there is little evidence to suggest that subsequent deformation events have caused major rotation or modification of Palaeozoic structural trends (section 2.10.2; chapter 3). Therefore the south to north transition from arc-like meta-volcanic rocks through volcaniclastic, and ophiolitic to arkosic and mature meta-sedimentary rocks is probably a Palaeozoic trend, and has not been significantly reorganised by Mesozoic and Cenozoic deformation events. Consequently, a model for the tectonic environment of the area in the late Palaeozoic can be formulated and tested against existing models of the tectonic environment of southern Mongolia (Lamb & Badarch, 1997, 2001; Badarch et al. 2002).

4.5.1 Late Palaeozoic arc systems of southern Mongolia

Sandstone petrographic data presented by Lamb & Badarch (1997, 2001) and a synthesis of field data by Badarch et al. (2002) suggest that rocks in the Edren and Mandalovoo terranes to the northwest and north of Nemegt and Altan Uul (Fig. 4.2) contain greenschist grade Devonian arc meta-volcanic and volcaniclastic rocks. Devonian provenance data from marine meta-sedimentary rocks to the north of the Devonian arc rocks in the Mandalovoo terrane point to an arc-source, but also contain a continental signature (Fig. 4.2; Lamb & Badarch, 1997, 2001; Badarch et al. 2002). Lamb & Badarch (2001) suggest an east-west trending Devonian intra-oceanic arc constructed across the Edren and Gurvansayhan terranes north of Nemegt and Altan Uul, and may have occupied a location south of a small ocean basin separating the arc from the continent in the north (Fig. 4.3A; Lamb & Badarch 2001).

Helo et al. (2006) present geochemical and geochronological data suggesting Silurian-Devonian volcano-sedimentary sequences in Nemegt and Altan Uul are geochemically indistinguishable from volcano-sedimentary sequences in the Gurvansayhan range to the east (section 2.2). The east-west belt of greenschist grade arc meta-volcanic and volcaniclastic rocks in southern Altan and Nemegt Uul may therefore represent a fragment of a much larger Palaeozoic arc system stretching across much of

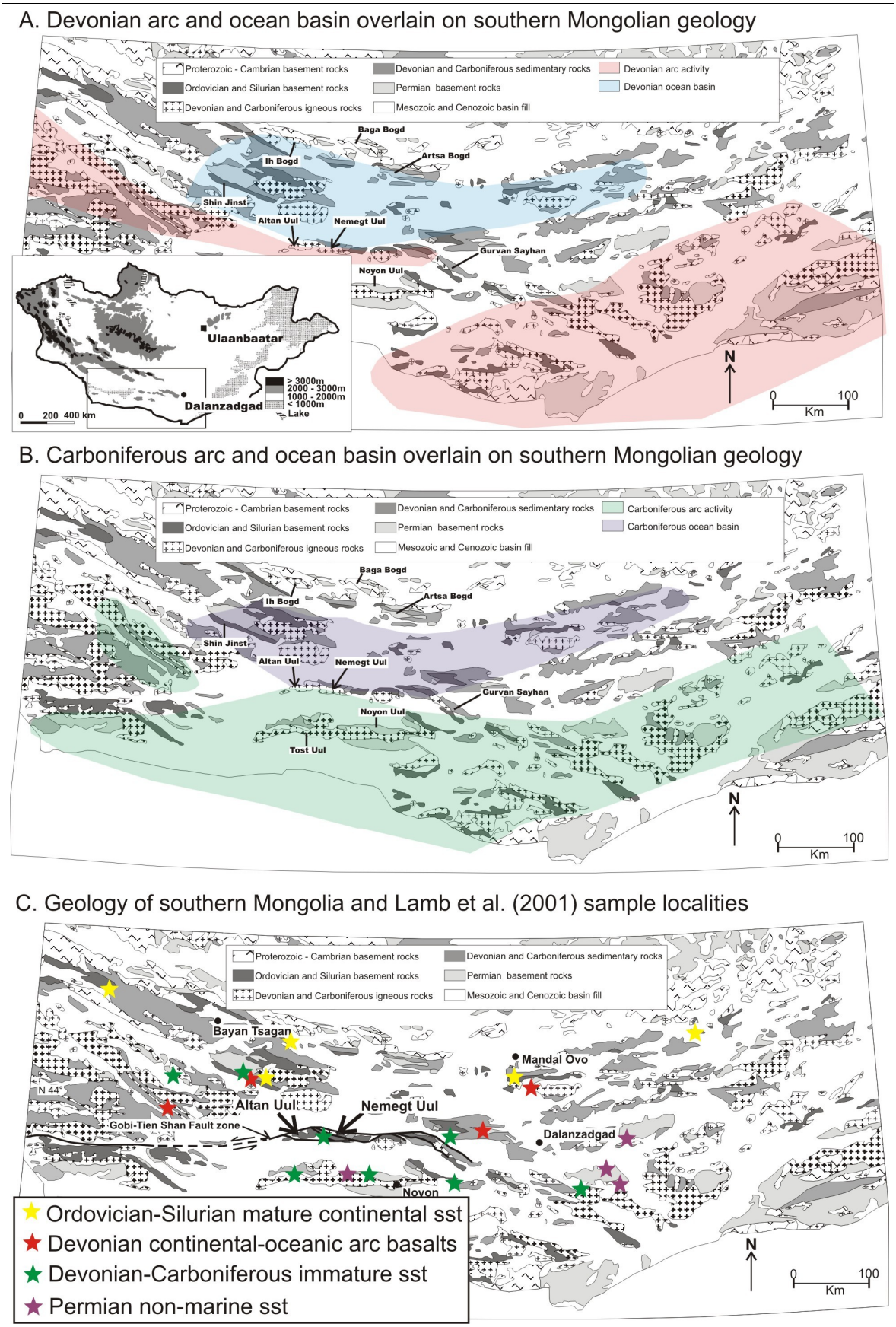

Fig. 4.3. Maps of geology of southern Mongolia redrawn from Lamb et al. (2001) to incorporate new data from this study A) Geology of southern Mongolia with position of Devonian arc and ocean basin, B) Geology of southern Mongolia with position of Carboniferous arc and ocean basin, C) Geology of southern Mongolia with sandstone sandstones from Lamb & Badarch (2001) study, showing a marine to terrestrial transition in the depositional environment from the Devonian and Carboniferous to the Permian.

southern Mongolia.

Sandstone petrographic data presented by Lamb & Badarch (2001) and synthesised field data presented by Badarch et al. (2002) suggest that greenschist grade Carboniferous meta-volcanic and volcaniclastic arc rocks in the Zoolen and Gurvansayhan terranes in southern Mongolia may represent a second Carboniferous oceanic arc, partially built on the foundations of the earlier Devonian arc. Their data show Carboniferous marine meta-sedimentary sequences in a basin to the north of Nemegt and Altan Uul (Fig. 4.3B). One interpretation of this data is that a back-arc basin existed north of an east-west trending Carboniferous arc in southern Mongolia (Lamb & Badarch, 2001). However, the data could also suggest that the small marine basin that existed between the arc and the continent in the Devonian, may have persisted as a trapped oceanic basin into the Carboniferous, or that an intra-arc basin existed (Fig. 4.3B).

To the north of the east-west trending belt of arc-type rocks in Nemegt and Altan Uul, there are sequences of east-west trending greenschist grade volcaniclastic, arkosic and mature meta-sediments (section 2.10.1; Fig. 2.39). The dominantly volcaniclastic and arkosic nature of the meta-sedimentary rocks directly north of the meta-volcanic rocks in the area may suggest they were deposited in a fore-arc/back-arc environment, possibly at the margins of the Devonian-Carboniferous marine basin that Lamb et al. (2001) and Badarch et al. (2002) suggest existed across southern Mongolia at the time. In northeast Nemegt Uul, biotite schists containing little or no immature clasts or grains are suggested to represent a more mature protolith, that may have been deposited in deeper water, distal from any arc or continental source (section 2.7.3; section 2.10.1). The schists sit unconformably above an east-west trending belt of orthogneiss, suggesting the orthogneiss is a fragment of older basement: the orthogneiss may represent a fragment of continental basement or the eroded root of an older arc that the sediments were deposited upon.

4.5.2 Late Palaeozoic terrane accretion in southern Mongolia

In order to document the spatial and temporal evolution of a terrane mosaic it is arguably most important to identify the suture zones between amalgamated terranes. Such sutures usually mark the location of former seaways and oceans floored by oceanic crust. Consequently, the presence of obducted ophiolitic rocks is the most important feature in

locating and identifying possible suture zones.

In Altan Uul, a south-dipping east-west trending fault-bound mafic-ultramafic belt consisting of pillow basalts, gabbros with cumulate layers, sheeted dykes, serpentinites and jasperoids has been interpreted as a partial ophiolite sequence (Rippington et al. 2008; chapter 2; Fig. 2.39). The Altan Uul ophiolite separates meta-volcanic arc-type rocks in southern Altan Uul from meta-sedimentary rocks to the north. Epidote-amphibolite psammitic schists to the north of the ophiolite represent a regional metamorphic culmination (Cunningham. pers comm., 2007). Contractional deformation in the rocks to the north of the ophiolite is contemporaneous with peak metamorphism. The contractional deformation in these rocks, and in the ophiolite itself, is dominantly north-directed suggesting that it was obducted northward over the meta-sedimentary rocks exposed in northwest Nemegt Uul (Rippington et al. 2008; chapter 2). There is a lack of direct evidence to indicate the polarity of subduction that occurred in the area. However, northward subduction of the Altan Uul ophiolite suggests that subduction was most likely southward directed beneath the arc-like meta-volcanic and volcaniclastic rocks in southern Nemegt and Altan Uul. Sandstone petrographic data presented by Lamb & Badarch (2001) indicates a marine to terrestrial transition of the depositional setting in southern Mongolia from the Carboniferous to the Permian, suggesting the area was uplifted in the late Carboniferous during ophiolite obduction and arc-continent accretion (section 2.11).

Southward subduction in southern Mongolia contrasts with some previous studies that interpret the majority of Palaeozoic subduction in southern Mongolia to be north directed (Badarch et al. 2002). There is a south to north transition across east-west trending litho-tectonic sequences and similar evidence of north-directed thrusting interpreted to suggest a south-dipping Carboniferous suture zone approximately 500 km to the west in the Tien Shan (Allen et al. 1993, Guo et al. 1993, Gao et al. 1998, Laurent-Charvet et al. 2002, Shu et al. 2002, Xiao et al. 2004b, Charvet et al. 2007). However, there is insufficient evidence to correlate between the proposed south-dipping suture in Altan Uul and the south-dipping Yili-North Tien Shan suture at this time.

Northward obduction of the Altan Uul ophiolite over southward subducting oceanic crust leaves four possibilities for the origin of the ophiolite resulting in a similar litho-tectonic configuration of the rocks in Nemegt and Altan Uul. First, the Altan Uul ophiolite is the obducted remnant of normal oceanic crust emplaced during terminal

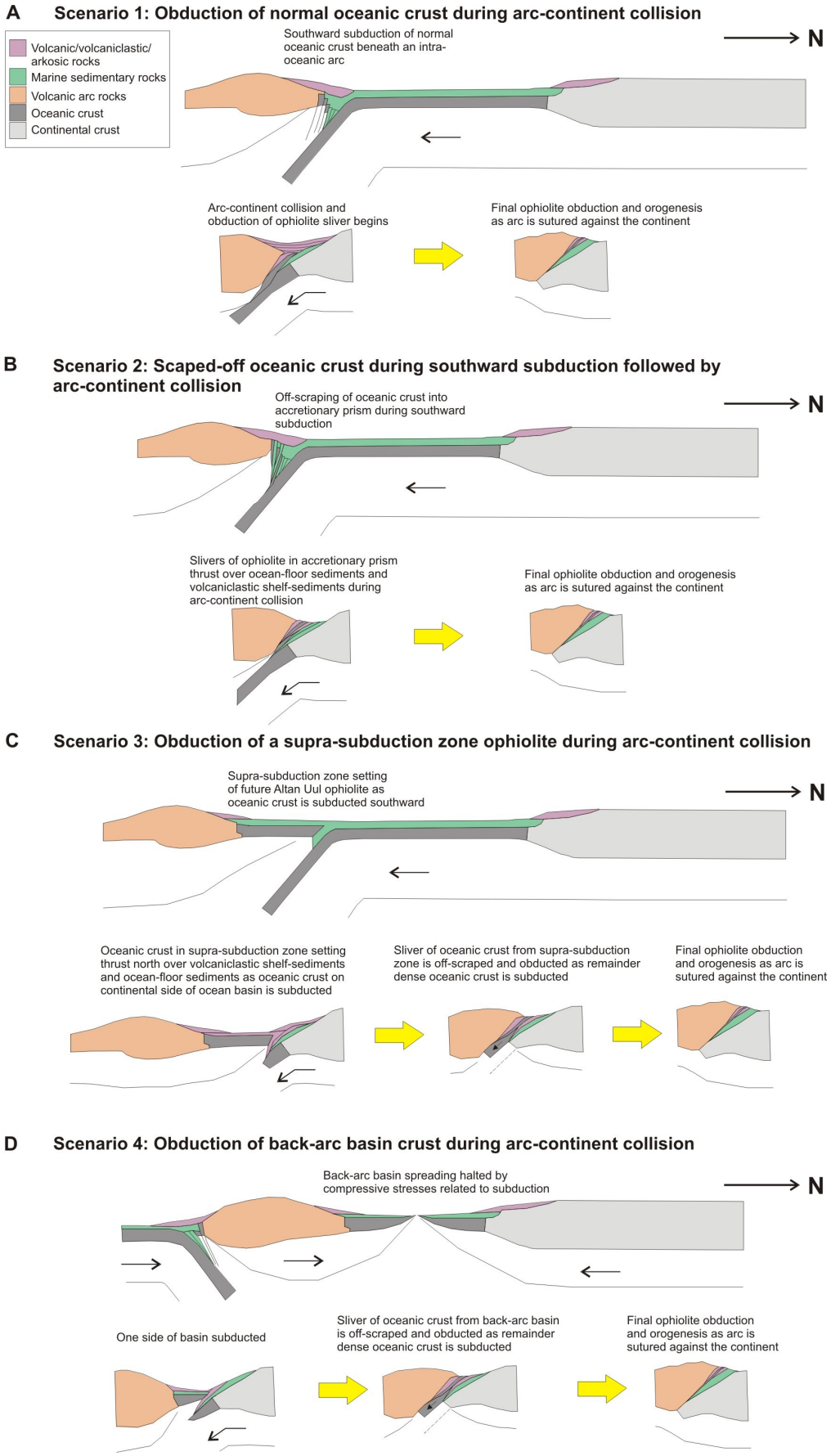

Fig. 4.4. Schematic models of obduction of the Altan Uul ophiolite. A) Obduction of normal oceanic crust, B) Obduction of an off-scraped fragment of oceanic crust, C) Obduction of supra-subduction zone oceanic crust, D) Obduction of back-arc basin oceanic crust.

ocean basin closure and arc or continental collision (Fig. 4.4A). Second, the Altan Uul ophiolite is an scraped-off fragment of accreted oceanic crust in a subduction accretion complex (Fig. 4.4B). Third, it was a supra-subduction zone ophiolite that formed in the extending hanging wall above a southward dipping intra-oceanic subduction zone (Fig. 4.4C). Fourth, the ophiolitic rocks represent back-arc basin oceanic crust obducted during back-arc basin inversion and closure (Fig. 4.4D).

Identifying back-arc basin ophiolites vs. supra-subduction zone ophiolites using major and trace element geochemistry is difficult. Back-arc oceanic crust often has a geochemical signature that is transitional to arc rocks, manifest as a higher ratio of low field strength (LFS) to high field strength (HFS) elements. This ratio may be caused by enhanced stability of certain minerals (ilmenite, rutile) which retain HFS elements in the hydrous environment above a subduction zone, or could be a result of hydrous fluids transporting LFS elements into back-arc mantle source regions from the subducting slab or via incipient melting within the mantle wedge (Tarney et al. 1981). Unfortunately, the LFS elements in the Altan Uul gabbros appear to have been enriched by metamorphic processes (section 2.9). It is not known how much enrichment there has been, but unless this can be quantified, the original ratio of LFS to HFS elements will remain unknown. With the data available (Table 1, Fig. 2.38), it is not possible to say if the Altan Uul ophiolite is an obducted fragment of back-arc oceanic crust or a supra-subduction zone ophiolite that formed in an arc or fore-arc setting.

Structural and petrographic evidence from transects across Nemegt and Altan Uul (section 2.4-2.7) suggests Silurian-Carboniferous arc-type rocks are juxtaposed against meta-sedimentary rocks, possibly deposited in a marine basin, which may have separated the arc from a continent to the north (Lamb & Badarch 1997, 2001, Badarch et al. 2002). Considering this palaeo-geographical configuration and the geographical configuration today (Fig. 4.3C), the arc must have collided with the continent at some point, most probably in the late Carboniferous when sandstone petrographic provenance data is interpreted to suggest the region was uplifted (Lamb & Badarch 2001; Fig. 4.3C). Regardless of whether the Altan Uul ophiolite is an scraped-off fragment of normal oceanic crust obducted during southward subduction, or a fragment of normal oceanic crust obducted during arc-continent collision, a similar tectonic arrangement of arc-type volcanic rocks thrust north over ophiolitic rocks, in turn thrust north over meta-sedimentary rocks, would have resulted. Either way, assuming the Altan Uul ophiolite

represents an obducted fragment of normal oceanic crust would suggest that it marks a suture zone between two tectonic terranes.

Based on collective evidence presented here, the author cautiously favours a collisional suture zone interpretation (Fig. 4.4A) for the ophiolitic rocks in Altan and Nemegt Uul for the following reasons. First, the ophiolitic rocks are bordered on the south by volcanic lithologies with arc-like characteristics and on the north with deep marine sediments deposited on possible continental crust. This spatial arrangement of lithotectonic units is most consistent with collision of an arc terrane against a continental block to the north with intense contractional deformation of marine sedimentary rocks caught in between. Second, no melange assemblage has been identified anywhere in Nemegt Uul, suggesting that the ophiolitic rocks are not part of a major accretionary prism terrane. Finally, the Nemegt and Altan Uul basement rocks north of the ophiolite represent a metamorphic and structural culmination in southern Mongolia consistent with levels of strain and metamorphism typically found in the internal zones of orogens near the collisional suture.

The suture zone interpretation for the ophiolitic rocks in Nemegt and Altan Uul, combined with evidence that the volcanic sequences in Nemegt and Altan Uul are part of the same intra-oceanic arc system identified in the Gurvansayhan terrane to the east (Helo et al. 2006) suggests that the most recent terrane model for southern Mongolia (Badarch et al. 2002; Fig. 4.2A), which places Nemegt and Altan Uul in the Zoolen accretionary wedge terrane (Fig. 4.2) requires modification. Further fieldwork is required to redefine the boundaries of Palaeozoic terranes in the area, but Nemegt and Altan Uul might be considered as straddling the suture zone between an island arc terrane to the south, possibly a westward extension of the Gurvansayhan terrane (Fig. 4.2), and a marine basin or forearc/backarc terrane to the north. This may require the redefinition of parts of the Mandalovoo island arc terrane to the north (Fig. 4.2), so that documented Devonian and Carboniferous marine sedimentary rocks (Badarch et al. 2002) can be considered part of marine basin in a forearc/backarc terrane.

4.6 Post-accretionary tectonic evolution of southern Mongolia

Terrane accretion in the Central Asian Orogenic Belt ended with the terminal closure of the Palaeo-Asian Ocean in the Permian-Triassic, forming the north-dipping

Solonker suture in southern Mongolia and northern China (Xiao et al. 2003; Fig. 4.2). Unconformities in the Triassic, Jurassic and the early Cretaceous throughout much of southern Mongolia and northern China indicate parts of the region were uplifted through much of the Mesozoic (Hendrix et al. 1996, Zheng et al. 1996, Meng 2003). The causes of this uplift may include late Palaeozoic terrane accretion, closure of the Monghol-Okhotsk Ocean to the north, and closure of Tethyan Ocean basins to the south (Hendrix et al. 1996, Meng et al. 2003). However, no evidence for Mesozoic contractional or uplift events was documented in Nemegt and Altan Uul during this study.

In the Cretaceous, large east-west trending Cretaceous continental sediment filled basins opened to the north and south of Nemegt and Altan Uul and across much of the Mongolia-China border region (Jerzykiewicz & Russell 1991, Benton et al. 2000, Johnson et al. 2001, Meng 2003, Meng et al. 2003). A shallow northwest-dipping northeast-southwest trending extensional fault at the northern front of Altan Uul, and northeast-southwest and east-west trending normal faults in the basins north of the Nemegt and Altan Uul ranges are thought to be the result of a regional Cretaceous extensional deformation event (Cunningham et al. submitted; Fig. 2.39). In Nemegt and Altan Uul, occasional northeast-southwest and east-west trending normal faults cut Palaeozoic contractional structures. Cross-cutting relationships do not help to further constrain the age of the normal faults in the ranges. However, the normal faults in the ranges are sub-parallel to the normal faults in the basins to the north and south, suggesting they are also the result of Cretaceous extensional deformation.

Suggested causes of extensional deformation and basin formation in the region include gravitational collapse of tectonically thickened crust following Palaeozoic terrane accretion and subsequent contractional events relating to distant collisional events in China in the early Mesozoic (Graham et al. 2001), back-arc extension caused by subduction zone rollback in the Palaeo-Pacific plate which was being subducted over 1000 km to the south (Watson et al. 1987, Traynor & Sladen 1995), and magmatic underplating from an unknown source resulting in hotter thinned crust (Shao et al. 2000). However, no evidence for these models is presented here so contributing to the ongoing debate about the driving mechanism of Cretaceous extension in southern Mongolia is beyond the scope of this study.

4.7 Cenozoic intraplate mountain building

The recognition of several large east-west trending intracontinental strike-slip fault systems through Tibet (Kunlun fault, Altyn Tagh fault), northern China and southern Mongolia (Qilan Shan fault, Gobi-Tien Shan fault system, Bogd fault) has led to the development of the popular hypothesis of eastward extrusion of central Asia due to the continued northward indentation of India following the India-Eurasian collision (Fig. 4.1; Molnar & Tapponier 1975, Tapponnier & Molnar 1979, Tapponnier et al. 1982). In southern Mongolia, the Gobi-Altai left-lateral corridor of transpressive deformation defines a zone of active left-lateral strike-slip and thrust faulting stretching from Artsa Bogd to the western Altai and Gurvan Sayhan to the eastern Tien Shan (Fig. 4.1; Fig. 4.5; Cunningham et al. 1997).

The Gobi corridor of left-lateral transpression is structurally dominated by two major approximately east-west trending left-lateral fault systems flanked by smaller left-lateral strike-slip systems (Cunningham et al. 1996). In the north, the Bogd fault has localised uplift at several large restraining bends: Artsa Bogd, Baga Bogd, Ih Bogd and Bayan Tsagaan Uul to the west (Fig. 4.1). At 3957 m above sea-level, Ih Bogd marks the topographic culmination in the Gobi Altai. The Bogd fault terminates at Artsa Bogd in the east and persists for c. 350 km to the west where it terminates to the east of the west Altai orocline (Baljinnyam et al. 1993, Cunningham et al. 1997). In the south, the Gobi-Tien Shan fault system is a zone of left-lateral transpressional deformation extending c. 1000 km from its eastern termination in the Gurvan Sayhan range of southern Mongolia to its western termination in the Barkol Tagh and Bogda Shan ranges in the eastern Tien Shan of northern China, and localises uplift at a number of push-up ridges, restraining bends and stepovers along discrete fault strands (Fig. 4.5; Cunningham et al. 1997, Cunningham et al. 2003b).

4.7.1 The Bogd fault vs. the Gobi-Tien Shan fault system

Photo-geological interpretation of SRTM-90 DEM imagery of the Bogd fault (Fig. 4.1) and the Gobi-Tend Shan fault system in southern Mongolia (Fig. 4.5) provides an opportunity to suggest how the left-lateral fault systems in the Gobi-Altai link along-strike and the implications of these linkages are for the evolution of Nemegt and Altan

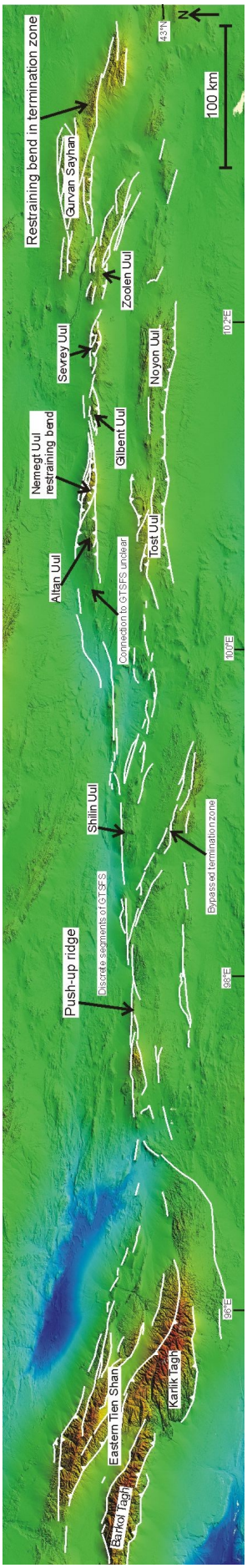

Fig. 4.5. Photo-geological interpretation of SRTM-90 DEM imagery of the entire Gobi-Tien Shan fault system based on maps in by Cunningham et al. (2003b). It is clear that the fault system consists of discrete east-west fault strands that are not as well connected as the fault strands in the Bogd fault (Fig. 4.1).

Uul and the system as a whole. There are obvious differences between the Bogd fault and the Gobi-Tien Shan fault system. The Bogd fault defines a 20-30 km zone of continuous left-lateral transpressional deformation trending west northwest-east southeast for c. 350 km from Artsa Bogd in the east to the Bayan Tsagaan Uul in the west (Fig. 4.1; Baljinnyam et al. 1993, Cunningham et al. 1997). The well known 1957 M = 8.3 earthquake along the fault formed surface ruptures over a length of 260 km (Kurushin et al. 1997). The Bogd fault bounds several large 60-100 km long ranges in the Gobi Altai, including Ih Bogd, the regional topographic high.

In contrast, the Gobi-Tien Shan fault system defines an east-west trending zone of transpressional deformation that is c. 100 km wide at its eastern termination in the Gurvan Sayhan range of southern Mongolia and stretches over 1000 km to its c. 100 km wide western termination in the eastern Tien Shan of northern China (Fig. 4.5). Areas of obvious Cenozoic faulting coincide with push-up ridges and restraining bends along the fault system (Fig. 4.5). In several places along the length of the Gobi-Tien Shan fault system it is difficult to identify linkages between discrete fault strands where topography is subdued (Fig. 4.5). Moving east from the western termination of the system in the Tien Shan, a number of northwest-southeast horsetail splays branch off from the main east-west trending fault system (Cunningham, 2003b; Fig. 4.5). To the east of Nemegt Uul, the Zoolen range defines a northwest-southeast trending horsetail splay, and at the eastern termination of the Gobi-Tien Shan fault system, the Gurvan Sayhan range marks another northwest-southeast trending horsetail splay. One explanation for this architecture is that these horsetail splays mark old termination zones that formed along smaller east-west trending fault strands (Cunningham et al. 1996). As east-west trending fault strands along the fault system have connected, it became more efficient to transfer strain along the system, bypassing the termination zones. These failed termination zones all branch off to the south of the obvious east-west linear segments of the Gobi-Tien Shan fault system. This suggests that while individual fault strands may have propagated to the east and/or west as they grew in length, the Gobi-Tien Shan fault system as a whole has propagated eastward through time. This photo-geological interpretation of SRTM-90 imagery is not robust evidence that the Gobi-Tien Shan system is not a single coherently linked fault system, but it certainly suggests the Gobi-Tien Shan fault system is a wider, diffuse system consisting of discrete fault strands than the more continuous Bogd fault to the north (Fig. 4.1; Fig. 4.5).

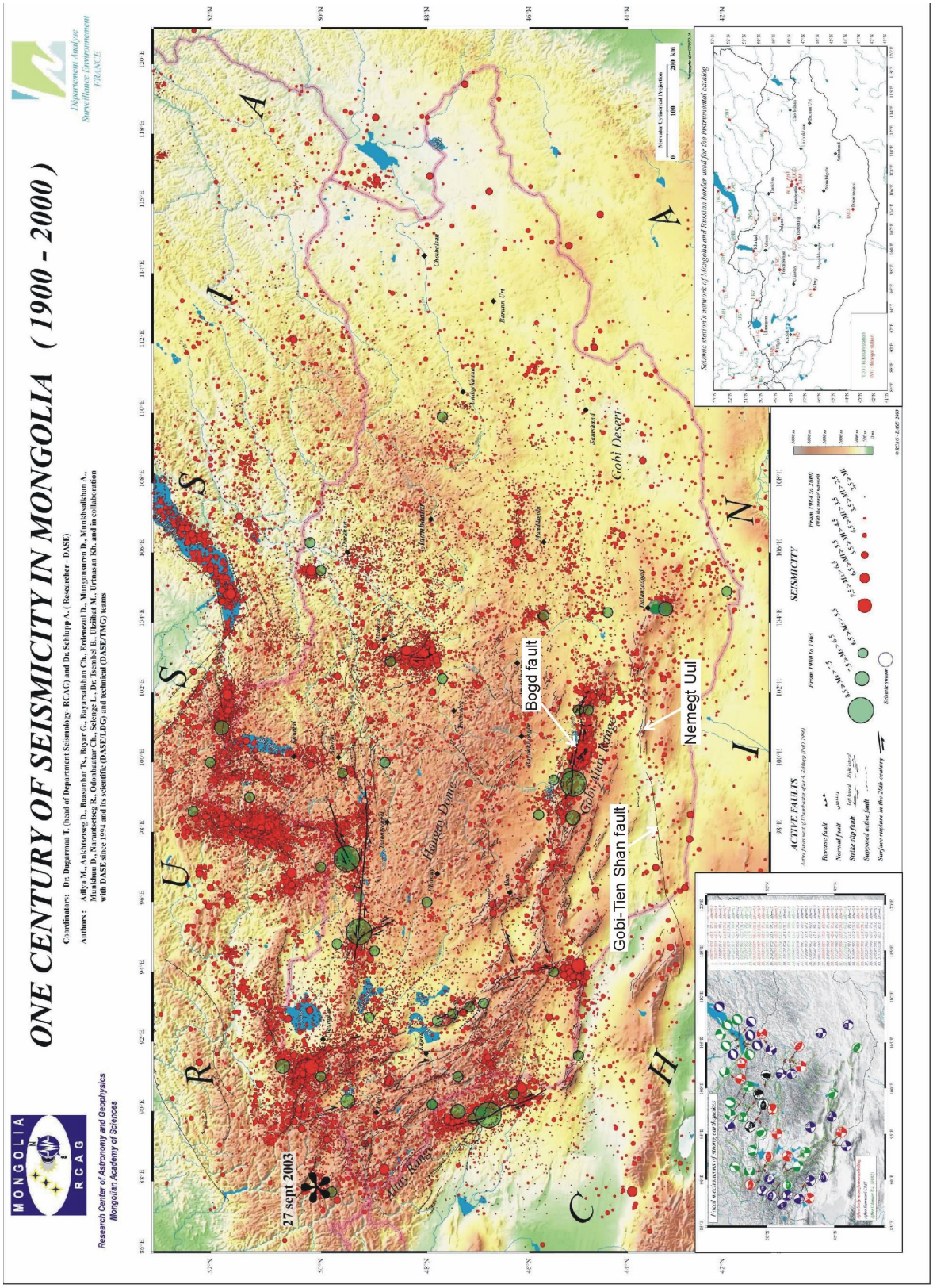

Fig. 4.6. Map of seismicity in Mongolia (Adiya et al. 2003). The Gobi-Tien Shan fault system was less seismically active than the Bogd fault between 1900-2000.

A map of seismicity in Mongolia between the years 1900-2000, shows a high frequency of earthquakes along the Bogd fault, and earthquakes of higher magnitude than along the Gobi-Tien Shan (Fig. 4.6). Focal mechanisms of strong earthquakes along the Bogd fault suggest it has moved in a left-lateral strike-slip sense (Fig. 4.6). The only focal mechanism presented along the Gobi-Tien Shan fault system indicates thrust sense movement in the Gurvan Sayhan termination zone. However, slickenlines on the Trans-Nemegt fault in Nemegt Uul, suggest that the fault has moved in a left-lateral oblique-slip sense (Fig. 3.17). Although 100 years of earthquake data is not a sufficient dataset on which to base firm conclusions about the active tectonics of southern Mongolia, the differences in frequency and magnitude of seismicity between the Bogd fault and the Gobi-Tien Shan fault system might be interpreted to suggest that the Bogd fault has had more frequent, and larger earthquakes because it is a longer, better connected fault system. In contrast, the Gobi-Tien Shan fault system may actually define an east-west trending belt of incompletely connected left-lateral strike-slip, thrust and oblique-slip fault strands, so is unable to accommodate larger earthquakes.

Assuming the Gobi-Tien Shan fault system is a zone of transpressional deformation comprising discrete fault segments as opposed to a coherent intracontinental strike-slip fault zone has clear implications for the amount of strain accommodated along individual fault strands. Although the whole system may have accommodated offset on the order of tens of kilometres, individual fault strands can only accommodate strain proportional to the length of their trace (Cowie & Scholz 1992). If the Gobi-Tien Shan fault system consists of discrete segments of connected strike-slip and thrust faulting, restricting the amount of movement on individual fault strands, how did the Nemegt restraining bend form, and how can the uplift at Nemegt and Altan Uul be explained?

4.7.2 Models for the evolution of the Nemegt Uul double restraining bend

In chapter 3, different definitions of restraining bends were discussed. By the definition of Mann (2007), Nemegt Uul represents an example of a lazy-Z shaped gentle restraining bend (Fig. 3.20), which are the most common type of restraining bend identified in the geological record at this time. There are numerous ways in which restraining bends can evolve, depending on local stress conditions and pre-existing structure, but there are essentially four main mechanisms that can form a bend along a

strike-slip fault.

1) Vertical axis rotations relative to a constant orientation of SH_{max}. Three-dimensional strain in strike-slip systems typically involves vertical axis rotations (Jackson et al. 1990). A straight strike-slip fault segment can be affected by vertical axis rotations during progressive fault evolution, resulting in changes in the strike of the fault and the kinematics of fault movement as it rotates relative to the external stress field (Cunningham et al. 2003a, Cunningham et al. 2007; Fig. 4.7A). Such a bend might be manifest as a single bend, commonly at the termination of a strike-slip fault, or as a double bend along the faults length.

2) Reactivation of pre-existing structure. Continental crust preserves fabrics and faults formed by early deformation events. Consequently, pre-existing structures may be partially or wholly reactivated. (Holdsworth et al. 2001). Reactivated pre-existing structures may link strike-slip fault segments, guide fault propogation, and effectively compartmentalise the stress field leading to locally anomalous fault orientations. All of these processes may form single or double restraining bends (Fig. 4.7B).

3) Coalescing termination zones. Two offset parallel faults may form and terminate into horsetail splays, locally uplifting the crust. The restraining bends formed in these termination zones may grow and coalesce through time to form a wide areas of transpressional deformation and uplift (Cunningham, 2007; Fig. 4.7C).

4) Restraining bend formed in overstepping zone. Two offset parallel master faults can form, propagate, and form an overstep. As the master faults overstep, the shear stress in the stepover zone increases and the fault tips bend towards each other and link up to form a double bend (Westaway 1995; Fig. 4.7D). The stress field between the master faults is determined by geometry of the stepover: the length of the master faults in the stepover zone and the distance between the master faults across the stepover determine the shape of the eventual bend (Westaway 1995). McClay and Bonora (2001) successfully simulate the evolution of different stepover zone geometries using sandbox models. The results of these experiments confirmed that the shape of restraining bend mountains corresponds to the geometry of the stepover zone. Wider stepover zones produce wider zones of deformation and lower elevations when the total displacement remains the same. Decreasing the amount of overlap between the parallel master faults at the stepover produces more sigmoidal gentle bends, whereas higher levels of overlap result in sharp restraining bends (McClay & Bonora, 2001).

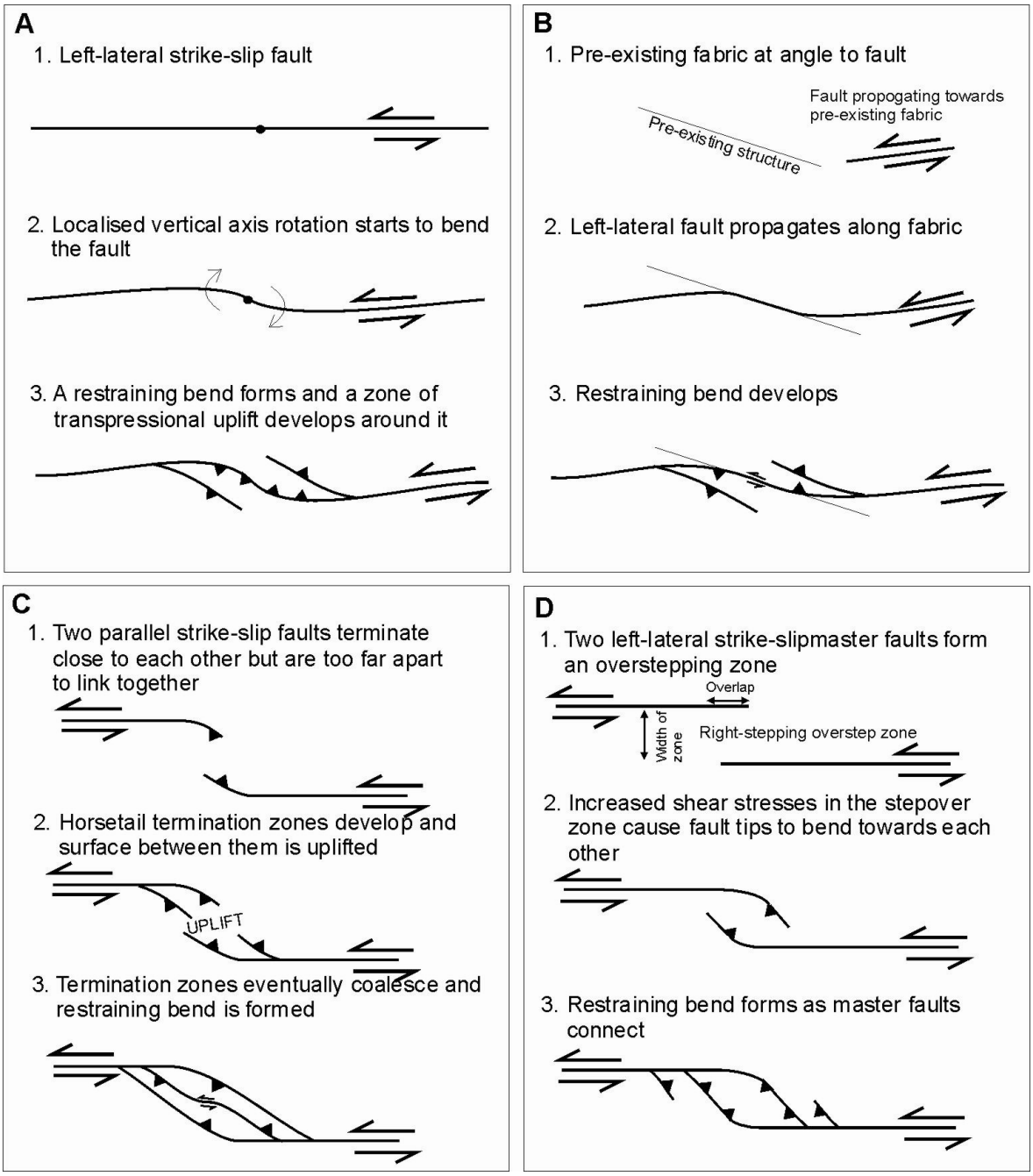

Fig. 4.7. Four ways of forming a restraining bend. A) Vertical axis rotations relative to a constant orientation of SHmax. B) Reactivation of pre-existing structure. C) Coalescing termination zones. D) Restraining bend formed in overstepping zone.

In Nemegt and Altan Uul, the Palaeozoic fabric formed by cleavage and ductile thrust shear zones is dominantly east-west trending and south dipping along the transects documented in chapter 2, with only small local variations to its geometry (section 2.10.2-2.10.3), suggesting it is unlikely that the Nemegt Uul restraining bend formed by bending a large pre-existing Cenozoic strike-slip fault by vertical axis block rotation. The Trans-Nemegt fault, which defines the Nemegt Uul restraining bend, cuts across local Palaeozoic fabric, suggesting the bend did not form by following a non-linear pre-existing structure. Nemegt Uul is a narrow elongate mountain range, making it unlikely that it has formed by the coalescence of strike-slip termination zones. Consequently, the most likely mechanism for the formation of the Nemegt Uul double restraining bend is that two offset parallel east-west trending master faults overlapped and locally bent towards each other, leading to the formation of the Trans-Nemegt fault, linking the two master faults. Nemegt Uul is a gentle restraining bend so we can assume the amount of overlap of the master faults was low. Assuming this overstepping mechanism formed the double restraining bend at Nemegt Uul, it is necessary to explain how two parallel east-west trending master faults formed in the area.

4.7.3 Structural inheritance

There is a degree of parallelism between some of the D4 faults, which trend east-west, D1 cleavage, and D2 shear zones in Nemegt and Altan Uul (Fig. 4.8). In chapter 2, the hypothesis that D2 followed on from D1 and occurred under similar south-north maximum horizontal stresses during Carboniferous arc-continent collision was presented. However, the maximum horizontal stress in southern Mongolia from the Cenozoic to the present, is orientated approximately northeast (045-060^{o}), and thought to be caused by continental extrusion in response to the continued northward indentation of India into Eurasia (Molnar & Tapponier 1975, Baljinnyam et al. 1993, Cunningham, 1998; Fig. 4.1). Therefore, the parallelism between some Cenozoic and Palaeozoic structures (Fig. 4.8), which have formed in different stress conditions, suggests structural inheritance may have played a role in the Cenozoic evolution of Nemegt and Altan Uul.

It has been suggested that the mechanical behaviour of the lithosphere is probably influenced by lateral rheological heterogeneities which significantly modify its total strength over a large enough area to modify the deformation at a continental scale

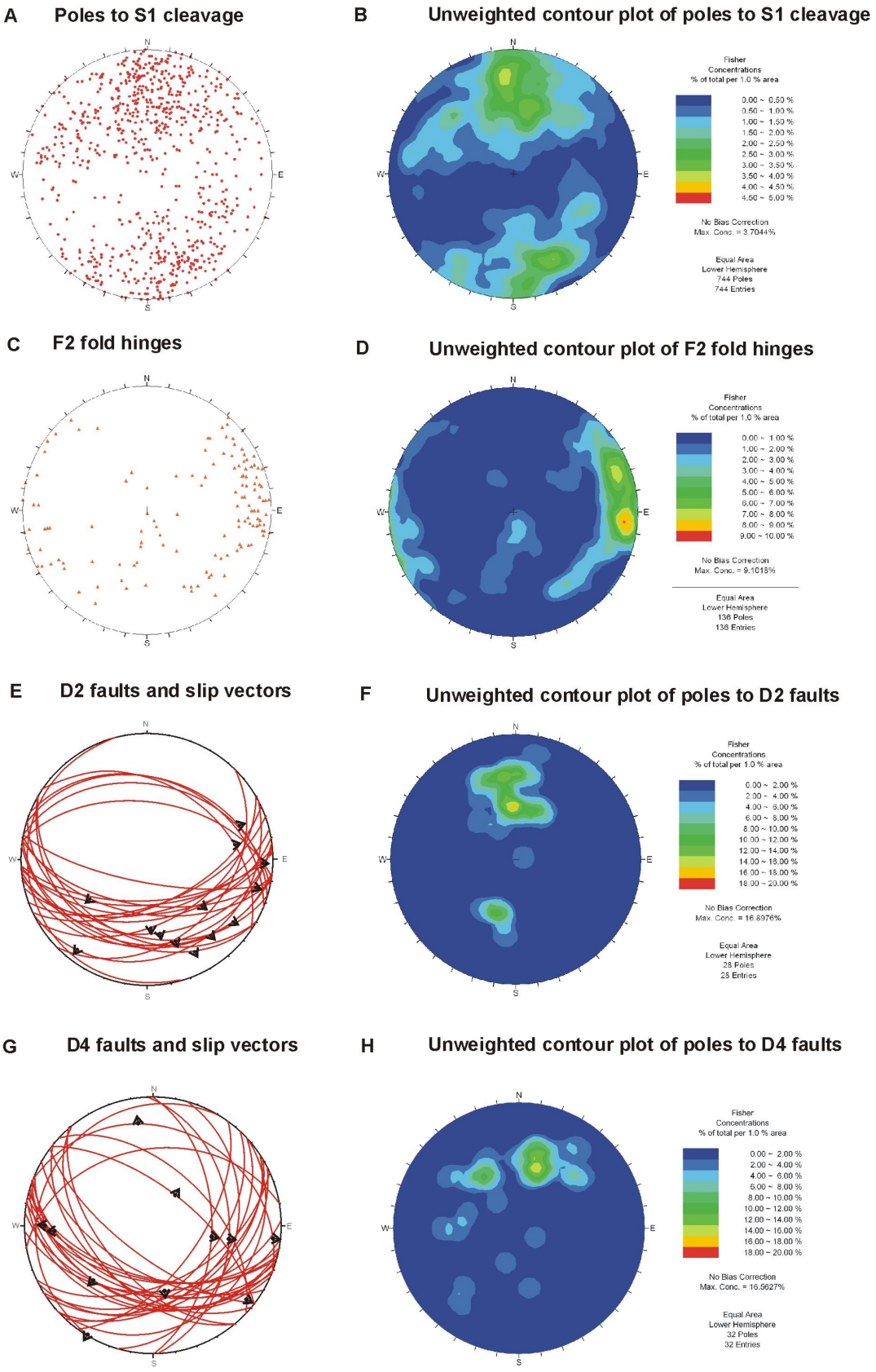

Fig. 4.8. Stereonets of S1, F2, D2 and D4 data. S1 is dominantly east-west trending. D2 faults are also dominantly east-west trending with most dipping to the south. There is also a high concentration of south-dipping east-west trending D4 faults. The parallelism between D2 cleavage and faults and D4 faults may indicate that D4 faults inherited the geometries of D2 structures.

(Tommasi 1995, Vauchez et al. 1998). Mechanical anisotropy is one way in which lateral heterogeneities can be generated in the continental lithosphere. Mica-rich rocks in the crust, and olivine in the lithospheric mantle, have planar anisotropies caused by their crystal structure which make them develop preferred orientations in the presence of a stress field, and making them sources of mechanical anisotropy in the lithosphere (Tommasi et al. 2000, Vauchez et al. 1998, Bai et al. 1991). Lithospheric mantle rocks develop crystallographic preferred orientations of olivine during deformation by dislocation creep (Vauchez et al. 1998). Direct observation of a consistent tectonic fabric in lithospheric mantle is possible where undisturbed lithospheric mantle structures are retained in the core of lherzolite massifs like the Ivrea zone in the Alps (Peselnik et al. 1977, Vauchez et al. 1998). Crystallographic preferred orientation in the lithospheric mantle is regarded as the main source of teleseismic wave splitting (Vauchez et al. 1998). Teleseismic shear wave splitting measurements often show that the fast split shear wave is polarised sub-parallel to orogenic structural trends (Silver 1996, Vauchez et al. 1998) and magnetotelluric soundings of the lithospheric mantle can also show an electrical anisotropy, suggested to be caused by the existence of conductive graphite films along grain boundaries, with highest conductivity parallel to foliation (Senechal et al. 1996, Vauchez et al. 1998). Consistency between data from teleseismic wave splitting and magnetotelluric measurements strongly support the hypothesis that the lithospheric mantle displays a tectonic fabric and that this fabric is laterally coherent over several tens to hundreds of kilometres (Vauchez et al. 1998). It follows that if the olivine-rich lithospheric mantle has a pervasive fabric and mica-rich crustal rocks are mechanically anisotropic, the whole lithosphere may deform anistropically in response to tectonic forces (Vauchez et al. 1998). It is also suggested that mechanical anisotropies formed during a major tectonic event, like terrane accretion, might result in bulk rheological heterogeneities in the crust that may be reactivated by subsequent deformation events, resulting in the inheritance of ancient tectonic trends (Vauchez et al. 1998).

Seismic anisotropy data for the lithospheric mantle along a north-south transect c. 500 km to the east of Nemegt and Altan Uul indicate that the fast polarization direction is oriented approximately east-west, broadly parallel to the surface trend of the Palaeozoic structural grain through central southern Mongolia (Gao et al. 1994, Cunningham, 1998). In the Nemegt and Altan Uul region, the transition from arc-type meta-volcanic rocks in the south through volcaniclastic meta-sedimentary and ophiolitic rocks to arkosic and

mature meta-sedimentary marine rocks in the north (Fig. 2.39) and the dominance of north-directed thrusting and north-vergent folding (Fig. 2.4-2.7) suggests that north-directed ophiolite obduction and arc-continent collision occurred in the Carboniferous (Rippington et al. 2008; Chapter 2). Arc-continent collision produced a dominantly east-west trending south-dipping cleavage, and south-dipping thrust faults across Nemegt and Altan Uul (Fig. 4.9A-C), and may have formed a crustal scale anisotropy in the region. Furthermore, serpentinized rocks have been demonstrated to be mechanically weak (Escartin et al. 1997), so the east-west trending ophiolite belt, consisting of serpentinites and olivine-rich rocks may mark a significant rheological weakness in the crust in this area. Assuming there has only been minor rotation of the northeasterly SHmax in the Cenozoic (Tapponnier et al. 1982, Zoback 1992, Cunningham et al. 1996), it is possible to consider the effect of the planar fabrics and bulk rheological heterogeneities formed during the Palaeozoic may have been affected by Cenozoic stresses.

Planar weaknesses like faults and cleavage, may be reactivated when placed under stress (Holdsworth et al. 1997). When faults slip, the stress acting upon them is split into two components: normal stress, acting orthogonal to the fault plane, and a shear stress acting along the fault plane. The normal stress acts against the fault plane increasing friction upon it and stopping it from moving. A fault can only slip when the shear stress is high and the normal stress is low. When the maximum stress direction is at 45^{o} to a fault, the shear stress is at its maximum. However, faults usually fail at a lower angle of c. 30-40^{o} to the maximum horizontal stress when the normal stress is also lower, so a vertical dipping fault plane at 30-40^{o} to the maximum horizontal stress direction may fail and the shear stress will cause it to slip in a pure strike-slip sense. However, if we consider a fault that is dipping 45^{o} and is at an angle of 30-40^{o} to the maximum horizontal stress direction, the fault may fail and the shear stress component will make it slip in an oblique sense.

In Nemegt and Altan Uul, the Palaeozoic structures (faults and cleavage) are at c.45^{o} to the present maximum horizontal stress direction, suggesting they are close to a favourable orientation for reactivation. However, the majority of the Palaeozoic structures documented in the area are dipping to the south. Consequently, they would be expected to reactivate in a left-lateral oblique-slip sense. This is demonstrated by slickenline data on the longest Cenozoic fault in the area, the Trans-Nemegt fault and east-west trending faults that branch off from the fault in the south (Fig. 3.17; Fig. 4.8). The geometrical argument for reactivation of east-west trending Palaeozoic fabrics in Nemegt and Altan

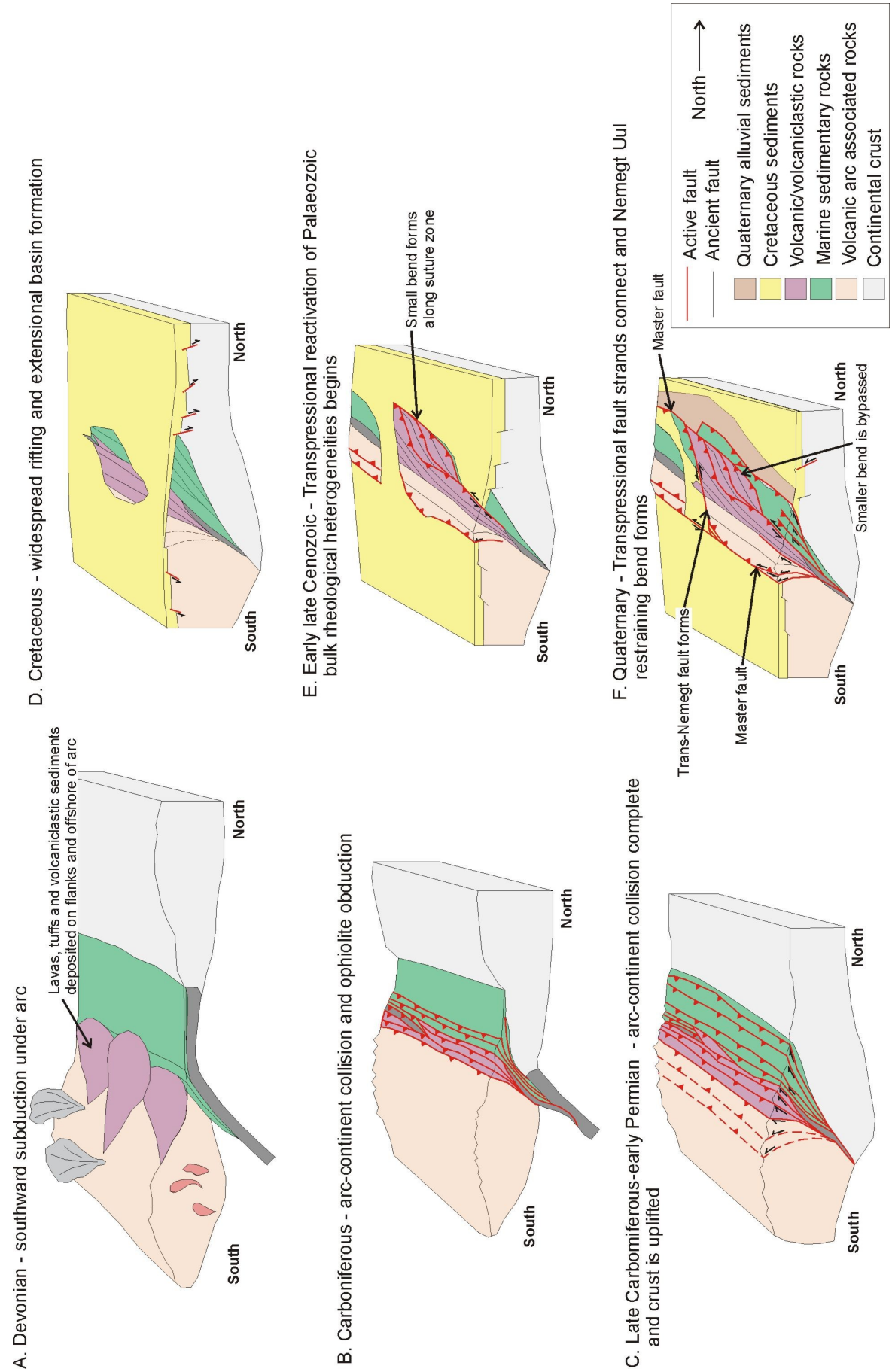

Fig. 4.9. Schematic block model showing evolution of the Nemegt Uul and Altan region from the Devonian to the Quaternary.

Uul is compelling. However, the evidence for reactivation of individual Palaeozoic faults is limited. The lack of field evidence for reactivation of individual faults, and the compelling geometrical argument for the reactivation of the east-west Palaeozoic structural trends is difficult to justify. It may suggest that it is a south-dipping east-west trending bulk rheological weakness caused by pervasive cleavage formation and obduction of mechanically weak serpentinised ophiolitic rocks during late Carboniferous arc-continent accretion that has been reactivated by the northeasterly Cenozoic SHmax.

4.7.4 A model for the Cenozoic evolution of Nemegt and Altan Uul

Most of the Cenozoic slickenline data from Nemegt and Altan Uul suggests there has been pure thrust or left-lateral oblique thrust movement on Cenozoic faults in the area (Fig. 4.8). Evidence for pure strike-slip deformation is confined to a short vertical segment of the Trans-Nemegt fault where it changes from a south-directed thrust fault on the south front of Nemegt Uul to a northeast-directed oblique-slip thrust fault on the north front and approximately 1.5 km of left-lateral displacement on an east-west trending fault in eastern Nemegt Uul (Fig. 3.2 [32]; Fig. 3.17). This suggests that, at the surface, strain is not partitioned into thrust and strike-slip components in Nemegt and Altan Uul.

The development of Cenozoic east-west trending south-dipping left-lateral oblique thrust faults in Nemegt and Altan Uul may suggest that dominantly east-west trending south-dipping Palaeozoic fabrics (cleavage and ductile shear zones) presented a bulk rheological weakness that was reactivated with the imposition of a northeasterly SH_{max} in the Cenozoic. It is proposed that a number of discrete east-west trending north-directed left-lateral transpressional faults formed in the Nemegt and Altan Uul area, and propagated to the east and west in the early late Cenozoic (Fig. 4.9E). In central Nemegt Uul, northwest-southeast trending faults between the South Central Nemegt Extrusive sequence, the Central Nemegt Upper Extrusive sequence and the Central Nemegt Lower extrusive sequence (section 2.6.2-2.6.4; Fig. 2.39) connect two east-west trending north-directed oblique thrust faults that form the southern boundary of the North Central Nemegt Schist sequence in central Nemegt Uul (section 2.6.5) and the North East Nemegt Schist sequence in eastern Nemegt Uul (section 2.7.3; Fig. 2.39; Fig. 4.9E). These northwest-southeast trending faults may have been part of an early bend formed in a right -stepping stepover in the area. Interestingly, the master faults for this smaller bend define

the boundary between Palaeozoic arc-type volcanic rocks and meta-sedimentary rocks (Fig. 2.39), suggesting they may have reactivated an east-west trending zone of weakness, represented by the suture zone formed during north-directed arc-continent collision.

Nemegt Uul and Altan Uul are bound to the south by south-directed Cenozoic thrust faults (Fig. 2.39). Palaeozoic cleavage dips to the north, broadly parallel to Cenozoic faults, on the southern side of Nemegt and Altan Uul, and dips to the south, parallel to Palaeozoic and Cenozoic faults on the northern side of the ranges. However, it is not clear if the cleavage has been rotated during Cenozoic south-directed faulting in the area, or if Cenozoic faults formed by reactivating north-dipping Palaeozoic planar weaknesses, which may have formed by south-directed back-thrusting related to northward obduction and arc-continent collision in the Palaeozoic. Regardless, it is suggested that the overstep formed by the southern range bounding thrust faults and the northern range bounding thrust faults led to the formation of the Trans-Nemegt fault (Fig. 3.2; Fig. 4.9F). When the Trans-Nemegt fault linked through the overstep, linking two large fault strands on the south and northern fronts, it formed the Nemegt Uul restraining bend and a wider thrust-dominated zone of deformation. This hypothesis is supported by low-mountain front sinuosity and higher elevations in the west, contrasting with the lower elevations and more sinuous mountain fronts to the east, out of the overstep zone, where there is evidence for more left-lateral dominated deformation. This scenario is demonstrated in figure 4.7D.

This model for the nucleation and evolution of the Nemegt Uul restraining bend is only one possible way in which the system could have formed. However, there are factors that make it the most compelling. First, the apparent parallelism between many Cenozoic and Palaeozoic structures combined with the suggestion that Nemegt Uul may mark a Palaeozoic collision zone containing anisotropic, weak serpentinised ophiolitic rocks, and south-dipping east-west trending pervasive Palaeozoic cleavage and ductile shear zones, so may represent a crustal-scale bulk rheologically weak zone in a favourable orientation for reactivation under Cenozoic boundary stresses. Second, the concept of short transpressive fault strands connecting to form a larger transpressive system helps explain the apparent small amount of strike-slip offset along the Trans-Nemegt fault, by suggesting strain could have been distributed across the system rather than localised on a single large strike-slip or transpressional fault.

Chapter 5

Conclusions and future work

5.1 Conclusions

Based on the evidence presented in the previous chapters, it is possible to make several conclusions about the polyphase evolution of Nemegt and Altan Uul and the implications of this study to existing models for the Palaeozoic, Mesozoic and Cenozoic evolution of southern Mongolia.

1. Nemegt and Altan Uul are an important geological locality in southern Mongolia, offering an opportunity to study rocks that have undergone a long polyphase tectonic evolution.

2. D1 and D2 contractional deformation events formed east-west trending upright folds of bedding, cleavage, north-vergent folds of cleavage and north-directed ductile thrust shear zones, and probably occurred in succession under similar south-north stress conditions in the late Carboniferous. D3 extensional deformation formed basins filled with dinosaur-rich Cretaceous sediments to the north and south of Nemegt and Altan Uul, and is thought to be a widespread rifting event. D4 transpressional deformation formed a series of east-west and northwest-southeast trending brittle faults in Nemegt and Altan Uul, thrusting Palaeozoic rocks exposed in the mountain ranges to the north and south over Cretaceous and Neogene sediments in the range-flanking basins and producing the modern architecture of the ranges.

3. Nemegt and Altan Uul consist of a south to north sequence of Palaeozoic greenschist grade meta-volcanic and volcaniclastic rocks, a partial ophiolite sequence, greenschist to epidote amphibolite grade arkosic and mature meta-sedimentary rocks, and orthogneiss. Garnet schists in western Nemegt Uul are the highest grade metamorphic rocks exposed in the Gobi Altai region.

4. The meta-volcanic and volcaniclastic rocks in the south fit established models which suggest that there was a Devonian-Carboniferous arc system in southern Mongolia (Lamb & Badarch, 2001). The arkosic and mature meta-sedimentary rocks in northern Nemegt and Altan Uul may be the remnants of a Devonian-Carboniferous ocean basin/back-arc basin, partially deposited on to a continental or micro-continental shelf.

5. A late Carboniferous collisional suture zone interpretation is cautiously favoured for the ophiolitic rocks in Nemegt and Altan Uul. The suture zone interpretation combined with evidence that suggests volcanic rocks in Nemegt and Altan Uul are part of the same intra-oceanic arc system identified in the Gurvansayhan terrane to the east (Fig. 4.2) indicates that the current terrane model (Badarch et al. 2002) requires modification. It is suggested that Nemegt and Altan Uul straddle an important east-west trending boundary between the Gurvansayhan island arc terrane to the south and east (Fig. 4.2), and parts of the Mandalovoo terrane (Fig. 4.2) containing Devonian-Carboniferous marine sediments to the north (Badarch et al. 2002). This requires redefinition of parts of the Mandalovoo terrane which is currently classified as an island-arc terrane (Badarch et al. 2002). The northern marine basin or forearc/backarc terrane may have been deposited on a micro-continental sliver or the eroded root of an ancient volcanic arc, represented by orthogneiss exposed in northeast Nemegt Uul.

6. Broadly east-west trending south-dipping structures in Nemegt and Altan Uul suggest late Carboniferous arc-continent accretion and ophiolite obduction were north-directed, and may have produced bulk rheological heterogeneities in the crust below Nemegt and Altan Uul.

7. Gaps between east-west trending fault strands along the Gobi-Tien Shan fault system, identified by photo-geological interpretation of SRTM-90 DEM imagery, and the relative low frequency and magnitude of earthquakes in the area compared to other intracontinental left-lateral strike-slip fault systems in Central Asia, suggests the Gobi-Tien Shan fault system may be evolving by the growth and linkage of discrete fault strands.

8. Nemegt and Altan Uul have a northward-tilted positive flower structure in cross-section and formed during Cenozoic uplift at a 'gentle restraining bend' formed at a right-stepping overstep between broadly east-northeast trending master faults (Fig. 4.9F) in the Gobi-Tien Shan fault system.

9. The northward obduction of the Altan Uul ophiolite, consisting of mechanically weak serpentinised rocks, and the formation of dominantly south-dipping east-west trending planar fabrics in the Palaeozoic rocks of Nemegt and Altan Uul during late Carboniferous arc-continent collision may have produced a bulk rheological heterogeneity in the crust. It is suggested this was a zone of rheological weakness which may have aided the reactivation of favourably orientated east-west trending planar fabrics in a left-lateral transpressional sense by the northeast SH_{max} resulting from the ongoing northward indentation of India into Eurasia c. 2500 km to the south. The eastward and westward propagation of Cenozoic fault strands reactivating Palaeozoic planar fabrics may have resulted in the formation of a right-stepping overstep zone along the Gobi-Tien Shan fault system, suggesting that the pre-existing crustal architecture of the region was a major controlling factor in the genesis and geometry of Cenozoic mountain building in the Nemegt and Altan Uul area.

5.2 Recommendations for future work

This is the first in-depth study of Nemegt and Altan Uul, and as such only deals with the evolution of a small part of southern Mongolia and the Central Asian Orogenic Belt. There are several avenues of investigation that should be targeted by future field work. Areas of Nemegt and Altan Uul were not visited during this study, and any future work should attempt to verify interpretations made, and to better constrain the models presented here. Future fieldwork should also be carried out in adjacent areas with the objective of constraining the along-strike continuity of the Palaeozoic rocks and structures exposed in Nemegt and Altan Uul and to ground-truth interpretations made about the Gobi-Tien Shan fault system based on SRTM-90 DEM and Landsat TM imagery. More evidence from areas along-strike is also needed to determine if the Altan Uul ophiolite really represents a major Palaeozoic suture zone and to identify possible linkages between Nemegt and Altan Uul and the Gobi-Tien Shan fault system. Further fieldwork to

constrain the palaeo-environment of Palaeozoic rocks to the north and south of Nemegt and Altan Uul may help to test models for the evolution of the area. The hydrocarbon potential and architecture of the basement beneath the Cretaceous basins to the north and south of Nemegt and Altan Uul is largely unknown. Seismic profiling across this area would benefit models for the basin evolution and may constrain links between the mountain and basin structure at depth. Cretaceous and Cenozoic sediments in the Nemegt and Altan Uul, especially in the area between the ranges and along the northern front of Altan Uul contain placer gold deposits that have been exploited by Mongolian nomads. The sediments containing the gold are the result of erosion from the ranges, suggesting there may be gold mineralisation in the Palaeozoic rocks in Nemegt and Altan Uul. The cumulate gabbros in Altan Uul may also contain significant chromite deposits. In western Altan Uul, numerous veins cut the ophiolitic and volcanic rocks in the range and may host economic minerals. The cross-cutting relationships of the vein systems and source of the vein material is poorly understood. It is suggested that Altan Uul, specifically vein-rich areas in the volcanic and ophiolitic sequences, should be targeted for future mineral exploration.

Further geochemical and geochronological work would vastly improve current models of the relationships between the rocks and structures exposed in Nemegt and Altan Uul. Pressure-temperature work and $^{40}Ar/^{39}Ar$ dating of micas may help to constrain the age of metamorphism and the P-T-t path of the rocks in some areas, with the necessary rock chemistry, as well as establishing the deformation histories of many of the ductile shear zones. Apatite fission track data from the Ih Bogd and Baga Bogd (Vassallo et al. 2007) to the north (Fig. 4.1) and the Tien Shan over 500 km to the west (Dumitru & Hendrix, 2001) have been used to constrain the cooling history and by association, the age of uplift, in these ranges. Apatite fission track dating in rocks from Nemegt and Altan Uul would establish the age of uplift, and place age constraints on the transpressional deformation identified. ^{206}Pb-^{238}U dating of zircons from the different volcanic sequences in Nemegt and Altan Uul would constrain their ages and combined with further major, trace and rare earth element analysis of the volcanic rocks, may constrain the evolution of the proposed Devonian-Carboniferous arc. The same geochemical and geochronological techniques should also be employed in the wider region where relevant, allowing the construction of a robust database of field, geochemical and geochronological data on which to interpret the evolution of southern Mongolia.

Appendix A.

GPS data for all localities referred to in Appendix B

All GPS data given in WGS 84 UTM projection (sector 47T).

Location	GPS ref	Easting	Northing
1	005	0658085	4831793
2	006	0654913	4831552
3	007	0632177	4844563
4	008	0634227	4839263
4	009	0634061	4839367
5	010	0633623	4839997
5	011	0633480	4840004
6	012	0632739	4830840
7	013	0632420	4830824
8	014	0632406	4830906
9	018	0651274	4832079
10	019	0651250	4832105
12	020	0651269	4832140
13	021	0651300	4832216
14	022	0651365	4832344
15	023	0629649	4838549
15	024	0629638	4838524
16	025	0629589	4838461
17	026	0329534	4838421
18	027	0629493	4838336
19	029	0626395	4841146
19	028	0651250	4841001
20	030	0626380	4841172
20	031	0626494	4841384
21	032	0626552	4841385
21	033	0626463	4841530
22	034	0626404	4841498
22	035	0626410	4841700
23	038	0626438	4841921
23	037	0626465	4841699
24	040	0626493	4842001
24	039	0626461	4841922
25	042	0626303	4842253
25	043	0626441	4842063
25	041	0626468	4842030
26	044	0626207	4842359
26	045	0626244	4842320
27	046	0625987	4842538
28	047	0629295	4842618
29	048	0626169	4842776
30	049	0626001	4842955
31	050	0626192	4843034
32	051	0626418	4845494
33	052	0626416	4845386
34	053	0626184	4845162
35	054	0626253	4844172

36	055	0626265	4844029
37	056	0626396	4843248
38	057	0626429	4843197
39	058	0626319	4843443
40	059	0626065	4844015
41	060	0625837	4844032
42	061	0625693	4843886
43	062	0626438	4844209
44	063	0626149	4845596
45	064	0629614	4838291
45	065	0629735	4838239
46	066	0629735	4838233
46	067	0629738	4836079
46	068	0629823	4833022
47	069	0624513	4838261
48	070	0629870	4838000
48	071	0629984	4837789
48	072	0629988	4837880
49	073	0629965	4837796
49	074	0629902	4837633
49	075	0699878	4837446
50	076	0626395	4840945
51	077	0626116	4836924
51	078	0626094	4836885
52	079	0626099	4836884
52	080	0626093	4836831
53	081	0626109	4836659
54	082	0626139	4836655
54	083	0626245	4836657
55	084	0626243	4836568
55	085	0626265	4836431
56	086	0626383	4836345
56	087	0626214	4836190
57	088	0626258	4836086
57	089	0626225	4835963
57	090	0626204	4835939
58	091	0626319	4835944
58	092	0626293	4835865
59	093	0626255	4835849
60	094	0626416	4835783
60	095	0626435	4835771
60	096	0626381	4835719
61	097	0626366	4835671
61	098	0626412	4835595
62	099	0626555	4835610
62	100	0626541	4835541
63	101	0626690	4835497
64	102	0626778	4835437
64	103	0626803	4835354
65	104	0632794	4838430
66	105	0634047	4838495
67	106	0633991	4838386
68	107	0633825	4838445
69	108	0633963	4838341
70	109	0633933	4838339
72	110	0633954	4838377
73	111	0633964	4738387
74	112	0633939	4838396

75	113	0633959	4838401
76	114	0633989	4838422
77	115	0634000	4838426
78	116	0634009	4838432
79	117	0634047	4838470
79	118	0634038	4838470
79	119	0634018	4838465
80	120	0633996	4838469
81	121	0633999	4838484
81	122	0633999	4838471
81	123	0633993	4838462
81	124	0633993	4838469
82	125	0633939	4838451
83	126	0634008	4838488
84	127	0634096	4838506
84	128	0634015	4838498
84	129	0633979	4838495
85	134	0633953	4838533
86	135	0633910	4838479
87	136	0633885	4838476
88	137	0633908	4838476
89	138	0633875	4838474
90	139	0633854	4838460
91	140	0633933	4838538
92	141	0634111	4838571
92	142	0634106	4838592
92	143	0634092	4838609
92	144	0633975	4838616
93	145	0633740	4838594
94	146	0633870	4838542
94	147	0633834	4838518
95	148	0633816	4838465
96	149	0633761	4838415
97	150	0633740	4838422
98	151	0633719	4838434
98	152	0633847	4838417
98	153	0633864	4838427
98	154	0633875	4838429
98	155	0633894	4838435
98	156	0633929	4838442
98	157	0633941	4838455
99	158	0633732	4838577
100	159	0633758	4838521
101	160	0633691	4838449
102	161	0633683	4838429
103	162	0634438	4838493
104	163	0634350	4838347
104	164	0634204	4838348
105	165	0634090	4838510
105	166	0634078	4838525
105	167	0634060	4838551
105	168	0633996	4838561
105	169	0633941	4838552
107	170	0633911	4838533
108	171	0633875	4838487
109	172	0633888	4838454
110	173	0633998	4838471
111	176	0644262	4843459

111	175	0644411	4843733
112	177	0644490	4843805
112	178	0644202	4843969
113	179	0643854	4844395
113	180	0643936	4844245
114	181	0643818	4844390
114	182	0643854	4844491
115	183	0643878	4844531
115	184	0643768	4844687
116	185	0639661	4843793
117	186	0639660	4843591
119	187	0653297	4841069
119	188	0653167	4840932
119	189	0653182	4840898
120	190	0633184	4840862
120	191	0653408	4840702
121	192	0653431	4840593
122	193	0653484	4840400
123	194	0653677	4840019
123	195	0653592	4840234
124	196	0653391	4839792
124	197	0653568	4839988
125	198	0653378	4841097
125	199	0653217	4841329
126	200	0653180	4841372
126	201	0652983	4841775
127	202	0653479	4839788
127	203	0653563	4839666
127	204	0653548	4839422
128	205	0653451	4839497
128	206	0653233	4839057
129	207	0653252	4838705
129	208	0653191	4838644
130	209	0652927	4842135
130	210	0653095	4841793
131	211	0652876	4842251
131	212	0652400	4842686
131	213	0652521	4842569
131	214	0652648	4842507
132	215	0652356	4842684
132	216	0652667	4843134
133	217	0652878	4843282
134	218	0653010	4838443
134	219	0652967	4837935
135	220	0652079	4837258
135	221	0652114	4837166
136	222	0652118	4837197
136	223	0652238	4837152
137	224	0652114	4836972
137	225	0651972	4837092
138	226	0651650	4836762
138	227	0651732	4836697
139	228	0651749	4836570
140	229	0651899	4836563
141	230	0651926	4836557
141	231	0651865	4836388
142	232	0651905	4836327
142	233	0651826	4836387

143	234	0651954	4836354
143	235	0651875	4836255
144	236	0652555	4836323
144	237	0652589	4836063
145	238	0652678	4836161
145	239	0652763	4836022
146	240	0652842	4836051
146	241	0652922	4835876
147	242	0678186	4829731
148	243	0678188	4829783
149	244	0678191	4829836
150	245	0678176	4830002
151	246	0678147	4830109
152	247	0678044	4830250
153	248	0677047	4833025
153	249	0677038	4833116
154	250	0677215	4833117
154	251	0677105	4833225
155	252	0677037	4833197
155	253	0676945	4833236
156	254	0676959	4833274
156	255	0676954	4833377
157	256	0676903	4833400
157	257	0676864	4833447
158	258	0676817	4833431
159	259	0680037	4838205
159	260	0680049	4838252
160	261	0679936	4838078
160	262	0679909	4838198
161	263	0679877	4837940
162	264	0679917	4837791
163	266	0676864	4833647
163	265	0676831	4833486
164	267	0676651	4833705
164	268	0676774	4833739
165	269	0676769	4833752
165	270	0676780	4833809
166	271	0676683	4833904
166	272	0676726	4833831
167	273	0676758	4834005
167	274	0676820	4833959
167	275	0676803	4833920
168	276	0677950	4834425
168	277	0677960	4834194
169	278	0678820	4834792
169	279	0678691	4834573
169	280	0678705	4834744
170	281	0678829	4834843
170	282	0678894	4834972
171	283	0680009	4837777
171	284	0680069	4837685
172	285	0680165	4837578
172	286	0680072	4837680
173	287	0680395	4837288
173	288	0680171	4837564
174	289	0680333	4837235
174	290	0680301	4837161
175	291	0680058	4836844

175	292		0680035	4836724
176	293		0680081	4836685
177	294		0680150	4836483
177	295		0680094	4836573
178	296		0679687	4835355
178	297		0679729	4835240
179	298		0679607	4835423
180	299		0679559	4835463
180	300		0679557	4835410
181	301		0679564	4835557
181	302		0679582	4835631
182	303		0679805	4835741
182	304		0679811	4835818
182	305		0679764	4835854
183	306		0680033	4836168
183	307		0680034	4836204
186		308	0652837	4841458
187		309	0652612	4841431
188		310	0626165	4842900
189		311	0626525	4843411
190		312	0605703	4835272
191		315	0626221	4842342
191		314	0626273	4842295
192		316	0626177	4842763
192		317	0626157	4842815
193		318	0606625	4832873
194		319	0606652	4833066
195		320	0606629	4833124
196		321	0606629	4833212
197		322	0606535	4833349
198		323	0606485	4833419
199		324	0606436	4833496
200		325	0606344	4833671
201		326	0606363	4833721
202		327	0606302	4833818
203		328	0606392	4833845
204		329	0606394	4833896
205		330	0606410	4833928
206		331	0606399	4834001
207		332	0606348	4834043
208		333	0606298	4834210
209		334	0606217	4834372
210		335	0606198	4834707
211		336	0606096	4834902
212		337	0606634	4834971
213		338	0606532	4835061
214		339	0606410	4835162
215		340	0606410	4835183
216		341	0606370	4835291
217		342	0605818	4835287
218		343	0605852	4835306
219		344	0605929	4835379
220		345	0605914	4835413
221		346	0605894	4835541
222		347	0605904	4835675
223		348	0605851	4835772
224		349	0605687	4835791
225		350	0605723	4835932

226	351	0622499	4834639
227	352	0622480	4834659
228	353	0622472	4834678
229	354	0622477	4834732
230	355	0622462	4834766
232	356	0622444	4834840
233	357	0622406	4834880
235	358	0622415	4834986
236	359	0622262	4835073
237	360	0622386	4835144
328	361	0622218	4835282
239	362	0629275	4830704
239	363	0629294	4830849
240	364	0629275	4830845
240	365	0629304	4830936
241	366	0629256	4830985
242	367	0629344	4831131
243	368	0629359	4831187
244	369	0629135	4831164
245	370	0629062	4831206
246	371	0629059	4831234
248	372	0629094	4831389
249	373	0629153	4831475
250	374	0629136	4831530
251	375	0629301	4831653
253	376	0629013	4831594
254	377	0629153	4831692
254	378	0629173	4831753
255	379	0629322	4831864
256	380	0629216	4832053
257	381	0629288	4832223
258	382	0629214	4832294
259	383	0629127	4832428
259	384	0629123	4832395
260	385	0629126	4832527
260	386	0629216	4832584
261	387	0629396	4832656
261	388	0629407	4832785
262	389	0629485	4833144
263	390	0629510	4833245
264	391	0629570	4833306
265	392	0629918	4833863
266	393	0632312	4842840
267	394	0632161	4842873
268	395	0631968	4842973
269	396	0631579	4843257
270	397	0631422	4843329
271	398	0631345	4843466
272	399	0631106	4843564
273	400	0630751	4843739
274	401	0630580	4843853
275	402	0630456	4843975
276	403	0629700	4844359
277	404	0629331	4844551
278	405	0629126	4844640
279	406	0632567	4842726
280	407	0632869	4842590
281	408	0633052	4842418

282	409	0633454	4842093
283	410	0633570	4841950
284	411	0633775	4841768
285	412	0634095	4841619
286	413	0634406	4841531
287	414	0634796	4841423
288	415	0637334	4839684
289	416	0636118	4840455
290	417	0635716	4840693
291	418	0635393	4840797
293	419	0647858	4835566
294	420	0648200	4835180
295	421	0648361	4835085
296	422	0649004	4834709
297	423	0649142	4834624
298	424	0649389	4834465
299	425	0649734	4884292
300	426	0650186	4834069
301	427	0649657	4833832
302	428	0647143	4834427
303	429	0646906	4834211
304	430	0646733	4834076
305	431	0646517	4834308
306	432	0645827	4834428
307	433	0645011	4831994
308	434	0642643	4831983
309	435	0642953	4832133
310	436	0653177	4838329
311	437	0647091	4834039
312	438	0647319	4834239
313	439	0647567	4834064
314	440	0647726	4833956
315	441	0647981	4834320
316	442	0671446	4836895
317	443	0671311	4836589
318	444	0670865	4836363
319	445	0667962	4836295
320	446	0667701	4836270
321	447	0668226	4838117
322	528	0679518	4838171
323	538	0679805	4838172
324	540	0679902	4838172
325	548	0679900	4838052
326	554	0679863	4838094
327	563	0679542	4838133
338	565	0679571	4838130
329	580	0679997	4838012
330	582	0680087	4837873
331	593	0680308	4837885
332	606	0679855	4837817
333	610	0680048	4837820
334	611	0679888	4837890
335	612	0679889	4837991
336	613	0679915	4838119
337	614	0680049	4838239
338	615	0679852	4838084
339	616	0679746	4838072

Appendix B
Structural data

Refer to Appendix A for GPS references for all localities

Bedding data

Locality	Strike	Dip	Dip direction
1	85	64	N
16	310	70	SW
20	90	32	N
27	280	12	SW
27	258	13	SE
28	61	20	NW
28	32	22	NW
30	340	7	SW
30	4	10	NW
33	187	24	E
36	337	16	W
39	40	16	NW
40	305	26	SW
42	275	50	S
97	278	35	SW
113	127	86	N
131	283	90	
132	290	57	SW
132	264	67	SE
132	264	72	SE
132	281	48	SW
132	223	60	SE
132	317	39	SW
132	262	48	SE
133	81	60	N
141	292	65	SW
141	340	44	SW
141	321	65	SW
142	314	57	SW
142	314	54	SW
142	318	58	SW
143	312	64	SW
143	308	63	SW
143	320	68	SW
143	317	62	SW
144	273	60	S
147	333	28	SW
154	143	15	NE
154	100	20	NE
154	177	16	E
156	136	30	NE
156	106	33	NE
156	106	23	NE
156	107	20	NE

156	105	36	NE
156	153	30	NE
156	170	32	NE
156	137	24	NE
156	181	33	E
156	183	38	SE
156	170	22	NE
156	190	55	SE
156	180	30	E
156	180	48	E
156	170	30	NE
156	161	26	NE
156	162	42	NE
156	184	21	SE
156	187	30	SE
156	183	34	SE
156	181	32	E
157	194	41	SE
157	191	41	SE
157	196	32	SE
157	204	25	SE
157	210	28	SE
157	230	50	SE
157	205	40	SE
157	230	42	SE
157	216	62	SE
157	209	60	SE
157	220	58	SE
158	223	43	SE
158	220	50	SE
158	201	52	SE
158	197	44	SE
158	203	40	SE
158	204	42	SE
158	201	42	SE
158	183	37	SE
158	191	38	SE
158	189	34	SE
163	232	56	SE
163	218	46	SE
163	233	58	SE
163	225	57	SE
163	229	62	SE
163	230	55	SE
163	243	58	SE
163	239	64	SE
163	245	60	SE
163	235	60	SE
163	233	56	SE
163	244	70	SE
163	233	64	SE
163	249	68	S
163	242	86	SE
163	248	68	SE
163	242	65	SE
163	250	70	SE

165	244	40	SE
165	240	45	SE
165	235	45	SE
166	62	63	NW
166	55	77	NW
166	53	74	NW
166	64	75	NW
166	51	52	NW
166	60	70	NW
166	55	72	NW
166	64	73	NW
166	62	65	NW
166	55	62	NW
167	50	85	NW
167	51	72	NW
167	41	76	NW
167	44	76	NW
167	39	43	NW
167	59	62	NW
167	44	66	NW
167	40	67	NW
167	40	70	NW
168	195	42	SE
168	185	60	SE
168	180	56	E
168	149	68	NE
168	155	75	NE
168	149	72	NE
168	154	72	NE
168	150	66	NE
168	165	47	NE
168	142	68	NE
168	169	63	NE
168	173	55	NE
168	175	60	NE
168	165	66	NE
168	150	45	NE
168	120	40	NE
168	188	36	NE
168	119	38	NE
168	100	48	NE
168	101	32	NE
168	112	37	NE
168	100	33	NE
169	115	27	NE
169	117	25	NE
169	136	36	NE
170	107	28	NE
175	65	48	NW
175	40	72	NW
175	65	48	NW
178	20	82	NW
178	23	76	NW
178	25	78	NW
178	29	82	NW
178	24	84	NW

178	34	80	NW
178	30	52	NW
178	51	52	NW
179	39	55	NW
179	42	62	NW
179	50	62	NW
179	48	55	NW
180	144	82	NE
180	150	72	NE
180	144	80	NE
180	149	73	NE
180	140	75	NE
180	142	81	NE
180	142	78	N
180	144	80	NE
180	135	82	NE
180	126	75	NE
180	149	75	NE
181	87	80	N
181	79	65	NW
181	83	78	NW
181	97	88	NE
181	113	59	NE
181	104	86	NE
183	18	59	NW
183	22	62	NW
192	360	27	W
220	295	70	SW
308	278	64	SW
308	260	43	SE
308	285	75	SW
308	288	26	SW
308	267	24	SE
308	263	50	SE
308	277	52	SW
308	319	50	SW
308	315	48	SW
308	307	45	SW
308	310	32	SW
308	312	51	SW
308	263	50	SE
308	277	52	SW

Cleavage/foliation data

Locality	Strike	Dip	Dip direction	Additional notes
4	205	38	SE	cleavage
4	204	42	SE	cleavage
4	270	45	S	cleavage
5	212	24	SE	cleavage
5	251	25	SE	cleavage
5	250	11	SE	cleavage
7	113	64	NE	cleavage
7	105	53	NE	cleavage
7	97	60	NE	cleavage

9	81	57	NW	cleavage
10	71	65	NW	cleavage
13	86	72	N	cleavage
14	69	52	NW	cleavage
14	81	74	N	cleavage
14	77	79	N	cleavage
14	78	84	N	cleavage
14	76	80	N	cleavage
14	85	79	N	cleavage
14	84	88	N	cleavage
14	80	90		cleavage
14	258	82	S	cleavage
14	266	74	S	cleavage
14	83	90		cleavage
14	278	70	S	cleavage
14	85	90		cleavage
14	268	74	S	cleavage
14	266	76	S	cleavage
14	262	74	S	cleavage
14	90	90		cleavage
14	259	82	S	cleavage
14	263	64	S	cleavage
14	259	71	S	cleavage
14	254	65	S	cleavage
14	259	72	S	cleavage
14	257	64	S	cleavage
14	93	90		cleavage
14	270	57	S	cleavage
14	82	55	N	cleavage
14	78	80	N	cleavage
14	80	85	N	cleavage
14	91	85	N	cleavage
14	260	70	S	cleavage
14	271	78	S	cleavage
14	266	75	S	cleavage
16	328	54	SW	cleavage
16	318	58	SW	cleavage
16	309	82	SW	cleavage
16	319	82	SW	cleavage
16	124	68	NE	cleavage
16	308	50	SW	cleavage
17	132	70	NE	cleavage
17	310	89	NE	cleavage
19	273	62	S	cleavage
19	258	78	S	cleavage
19	265	68	S	cleavage
19	284	45	SW	cleavage
19	263	70	S	cleavage
19	254	42	SE	cleavage
19	251	30	SE	cleavage
20	88	72	N	cleavage
20	90	32	N	cleavage
20	255	72	S	cleavage
20	263	80	S	cleavage
20	241	33	S	cleavage
20	79	45	N	cleavage

20	269	40	S	cleavage
21	142	22	E	cleavage
21	100	50	NE	cleavage
21	237	35	SE	cleavage
21	257	35	S	cleavage
21	252	37	S	cleavage
21	260	44	S	cleavage
21	266	57	S	cleavage
21	264	35	S	cleavage
22	260	39	S	cleavage
22	249	51	SE	cleavage
22	264	58	S	cleavage
22	210	15	SE	cleavage
23	87	42	NE	cleavage
23	292	68	SW	cleavage
23	57	90		cleavage
23	122	35	NE	cleavage
23	100	90		cleavage
23	310	18	SW	cleavage
23	344	12	W	cleavage
23	84	87	N	cleavage
24	205	5	E	cleavage
24	254	48	SE	cleavage
24	280	12	S	cleavage
25	313	25	NE	cleavage
28	243	16	S	cleavage
28	264	16	S	cleavage
31	40	12	NW	cleavage
31	60	27	NW	cleavage
38	152	32	SW	cleavage
38	45	42	NW	cleavage
38	136	26	SW	cleavage
38	310	34	SW	cleavage
38	347	34	SW	cleavage
38	100	29	NW	cleavage
38	67	35	NW	cleavage
45	321	53	SW	cleavage
45	306	58	W	cleavage
45	122	69	N	cleavage
45	174	48	E	cleavage
45	332	84	SW	cleavage
45	326	76	SW	cleavage
45	292	73	SW	cleavage
46	266	55	S	cleavage
46	281	52	S	cleavage
46	238	2	S	cleavage
46	229	40	SE	cleavage
46	323	26	SW	cleavage
46	308	65	SW	cleavage
46	131	71	NE	cleavage
46	151	63	NE	cleavage
46	84	84	N	cleavage
46	281	28	S	cleavage
48	238	32	SE	cleavage
48	208	24	SE	cleavage
48	278	45	S	cleavage

48	285	56	S	cleavage
48	204	64	SE	cleavage
48	156	38	NE	cleavage
48	267	68	S	cleavage
49	113	61	NE	cleavage
49	55	46	N	cleavage
49	280	80	SW	cleavage
49	134	83	N	cleavage
49	20	36	NW	cleavage
49	271	84	S	cleavage
49	262	68	S	cleavage
49	268	88	S	cleavage
49	274	82	S	cleavage
51	287	79	SW	cleavage
51	282	71	S	cleavage
51	282	64	S	cleavage
51	280	73	S	cleavage
52	278	64	S	cleavage
52	245	75	SE	cleavage
52	273	48	S	cleavage
53	290	48	SW	cleavage
53	303	50	SW	cleavage
53	292	68	SW	cleavage
53	290	60	S	cleavage
53	293	53	SW	cleavage
53	280	36	SW	cleavage
54	186	40	E	cleavage
54	299	50	SW	cleavage
54	290	60	SW	cleavage
54	306	54	SW	cleavage
55	236	25	SE	cleavage
55	285	50	SW	cleavage
55	286	35	SW	cleavage
55	285	58	SW	cleavage
55	268	68	S	cleavage
55	262	60	SE	cleavage
55	272	50	S	cleavage
56	305	40	SW	cleavage
56	261	30	SE	cleavage
56	245	40	SE	cleavage
56	270	45	S	cleavage
57	275	45	SW	cleavage
57	280	45	SW	cleavage
57	267	60	SE	cleavage
57	245	47	SW	cleavage
57	278	40	SW	cleavage
57	261	56	SE	cleavage
58	261	54	SE	cleavage
58	261	42	SE	cleavage
58	259	68	S	cleavage
58	265	60	SE	cleavage
58	277	58	SW	cleavage
59	260	54	SE	cleavage
60	273	73	SW	cleavage
60	269	59	S	cleavage
60	251	50	SE	cleavage

62	295	50	SW	cleavage
62	270	36	S	cleavage
63	292	60	SW	cleavage
64	278	72	SW	cleavage
69	290	32	SW	cleavage
70	292	58	SW	cleavage
72	310	60	SW	cleavage
73	251	60	SE	cleavage
79	255	22	SE	cleavage
80	273	75	SW	cleavage
85	194	48	SE	cleavage
88	308	64	SW	cleavage
87	272	74	SW	cleavage
90	200	62	SE	cleavage
90	198	67	SE	cleavage
90	192	40	SE	cleavage
90	186	78	SE	cleavage
90	188	63	SE	cleavage
90	210	70	SW	cleavage
94	198	50	SE	gps146
94	185	60	SE	gps147
94	202	34	SE	gps148
96	245	57	SE	cleavage
97	278	35	SW	//bedding
101	231	40	S	cleavage
101	243	50	S	cleavage
106	247	50	SW	cleavage
111	116	90		cleavage
111	136	84	NE	cleavage
111	280	67	SW	cleavage
111	306	84	SW	cleavage
111	128	90		cleavage
112	281	86	SW	cleavage
112	302	72	SW	cleavage
112	315	79	SW	cleavage
112	315	50	SW	cleavage
112	315	60	SW	cleavage
113	320	46	SW	cleavage
113	0	46	W	cleavage
113	302	72	SW	cleavage
113	127	86	NE	//bedding
113	319	64	SW	cleavage
114	305	78	SW	cleavage
114	305	70	SW	cleavage
114	146	75	NE	cleavage
114	120	90		cleavage
115	320	84	SW	cleavage
115	322	60	SW	cleavage
115	325	64	SW	cleavage
116	290	35	SW	cleavage
116	300	30	SW	cleavage
120	1	60	W	cleavage
120	45	50	NW	cleavage
121	207	50	SE	cleavage
122	269	77	S	cleavage
123	274	45	SW	cleavage

123	287	56	SW	cleavage
123	64	68	NW	cleavage
126	291	68	SW	cleavage
126	115	83	NE	cleavage
126	119	85	NE	cleavage
126	126	66	NE	cleavage
127	259	50	SE	cleavage
127	308	78	SW	cleavage
128	297	50	SW	cleavage
128	310	50	SW	cleavage
128	319	47	SW	cleavage
128	320	46	SW	cleavage
129	137	82	NE	cleavage
129	139	80	NE	cleavage
129	153	76	NE	cleavage
129	119	73	NE	cleavage
129	118	78	NE	cleavage
130	312	60	SW	cleavage
130	290	70	SW	cleavage
130	301	80	SW	cleavage
130	297	62	SW	cleavage
130	300	66	SW	cleavage
130	108	58	NE	cleavage
130	269	50	S	cleavage
130	289	70	SW	cleavage
130	308	68	SW	cleavage
131	113	83	NE	cleavage
131	286	90		cleavage
131	79	43	NW	cleavage
131	265	60	SW	cleavage
131	280	86	SW	cleavage
131	100	59	NE	cleavage
131	120	85	NE	cleavage
131	266	82	SW	cleavage
131	305	90		cleavage
131	275	78	SW	cleavage
131	283	90		//bedding
131	94	85	NE	cleavage
131	292	82	SW	cleavage
132	290	57	SW	//bedding
132	264	67	SE	//bedding
132	264	72	SE	//bedding
132	281	48	SW	//bedding
132	223	60	SE	//bedding
132	317	39	SW	//bedding
132	262	48	SE	//bedding
134	287	43	SW	cleavage
134	274	34	S	cleavage
134	260	23	SE	cleavage
134	359	10	W	cleavage
135	83	61	N	cleavage
135	83	75	N	cleavage
135	88	64	N	cleavage
135	75	63	NW	cleavage
136	65	80	NW	cleavage
136	33	72	NW	cleavage

136	345	65	SW	cleavage
136	318	86	SW	cleavage
136	350	60	SW	cleavage
137	63	40	NW	cleavage
137	65	30	NW	cleavage
137	70	30	NW	cleavage
137	87	40	N	cleavage
137	50	90		cleavage
138	48	38	NW	cleavage
138	51	60	NW	cleavage
138	51	58	NW	cleavage
138	75	68	N	cleavage
138	42	25	NW	cleavage
139	325	58	SW	cleavage
139	15	63	NW	cleavage
141	292	65	SW	//bedding
141	340	44	SW	//bedding
141	321	65	SW	//bedding
142	314	57	SW	//bedding
142	314	54	SW	//bedding
142	318	58	SW	//bedding
145	103	26	NE	slaty cleavage
146	322	36	SW	cleavage
153	120	70	NE	cleavage
153	115	55	NE	cleavage
153	120	63	NE	cleavage
153	112	68	NE	cleavage
153	97	73	N	cleavage
153	103	55	NE	cleavage
154	90	80	N	cleavage
155	335	86	SW	cleavage
155	280	83	SW	cleavage
155	310	80	SW	cleavage
155	123	72	NE	cleavage
156	57	57	NW	cleavage
156	70	57	NW	cleavage
157	85	76	NW	cleavage
157	84	75	NW	cleavage
159	142	37	NE	met fabric
159	177	22	E	met fabric
160	276	78	SW	cleavage
160	280	46	SW	cleavage
160	264	78	SE	cleavage
160	119	87	NE	met fabric
161	277	80	SW	cleavage
161	273	45	SW	//met fabric
161	130	78	NE	met fabric
162	85	63	NW	met fabric
162	255	74	SE	//met fabric
162	87	73	NW	//met fabric
162	267	75	SE	met fabric
162	245	88	SE	met fabric
163	86	72	N	cleavage

164	330	66	SW	cleavage
168	275	72	SW	cleavage
168	284	68	SW	cleavage
171	277	65	SW	cleavage
171	293	80	SW	cleavage
171	293	75	SW	cleavage
171	136	50	NE	cleavage
173	257	80	SE	cleavage
173	262	67	SE	cleavage
173	76	71	NW	cleavage
173	75	78	NW	cleavage
173	265	66	SE	cleavage
173	210	54	SE	cleavage
173	270	70	S	cleavage
173	257	66	SE	cleavage
173	250	62	SE	cleavage
173	279	81	SW	cleavage
173	233	82	SE	cleavage
174	116	84	NE	cleavage
311	210	84	SE	cleavage
311	213	90		cleavage
311	223	86	SE	cleavage
311	59	79	NW	cleavage
311	55	82	NW	cleavage
311	55	75	NW	cleavage
311	63	74	NW	cleavage
311	61	74	NW	cleavage
311	63	70	NW	cleavage
311	65	72	NW	cleavage
311	52	77	NW	cleavage
311	64	68	NW	cleavage
311	67	74	NW	cleavage
311	53	56	NW	cleavage
311	61	67	NW	cleavage
311	64	64	NW	cleavage
311	65	59	NW	cleavage
311	60	68	NW	cleavage
311	64	63	NW	cleavage
311	70	64	NW	cleavage
311	74	65	NW	cleavage
311	72	68	NW	cleavage
311	65	70	NW	cleavage
311	54	72	NW	cleavage
311	58	52	NW	cleavage
311	41	48	NW	cleavage
311	30	50	NW	cleavage
311	65	58	NW	cleavage
311	29	60	NW	cleavage
311	40	55	NW	cleavage
311	5	50	NW	cleavage
311	23	44	NW	cleavage
311	360	43	W	cleavage
311	33	50	NW	cleavage
311	32	49	NW	cleavage
311	13	52	NW	cleavage
311	27	42	NW	cleavage

311	29	52	NW	cleavage
311	33	51	NW	cleavage
311	22	58	NW	cleavage
311	23	50	NW	cleavage
311	31	63	NW	cleavage
311	20	53	NW	cleavage
311	13	52	NW	cleavage
311	8	72	NW	cleavage
311	25	63	NW	cleavage
311	43	46	NW	cleavage
311	35	44	NW	cleavage
311	23	63	NW	cleavage
311	25	59	NW	cleavage
311	21	55	NW	cleavage
311	19	65	NW	cleavage
311	11	54	NW	cleavage
311	31	56	NW	cleavage
311	14	38	NW	cleavage
311	23	38	NW	cleavage
311	325	66	SW	cleavage
311	337	43	SW	cleavage
311	320	45	SW	cleavage
311	328	55	SW	cleavage
311	319	66	SW	cleavage
311	327	78	SW	cleavage
311	322	76	SW	cleavage
311	340	72	SW	cleavage
311	345	55	SW	cleavage
311	351	46	SW	cleavage
311	352	81	SW	cleavage
311	344	82	SW	cleavage
311	340	65	SW	cleavage
311	335	64	SW	cleavage
311	325	76	SW	cleavage
313	70	71	NW	cleavage
313	60	75	NW	cleavage
313	56	67	NW	cleavage
313	79	58	NW	cleavage
313	78	57	NW	cleavage
313	77	53	NW	cleavage
313	60	69	NW	cleavage
313	57	72	NW	cleavage
313	67	60	NW	cleavage
313	71	67	NW	cleavage
313	71	63	NW	cleavage
313	58	57	NW	cleavage
313	70	49	NW	cleavage
313	55	56	NW	cleavage
313	60	56	NW	cleavage
313	41	51	NW	cleavage
313	56	60	NW	cleavage
313	36	42	NW	cleavage
313	18	55	NW	cleavage
313	39	64	NW	cleavage
313	46	66	NW	cleavage
313	29	58	NW	cleavage

313	51	72	NW	cleavage
313	51	71	NW	cleavage
313	43	73	NW	cleavage
313	74	73	NW	cleavage
313	83	53	NW	cleavage
313	63	69	NW	cleavage
313	65	65	NW	cleavage
313	59	60	NW	cleavage
313	69	60	NW	cleavage
313	48	74	NW	cleavage
313	47	75	NW	cleavage
313	20	90		cleavage
313	23	76	NW	cleavage
313	29	80	NW	cleavage
313	186	75	SE	cleavage
313	187	74	SE	cleavage
313	190	72	SE	cleavage
313	195	72	SE	cleavage
313	190	75	SE	cleavage
313	167	75	NE	cleavage
313	189	75	SE	cleavage
313	164	64	NE	cleavage
313	171	66	NE	cleavage
313	167	62	NE	cleavage
313	172	65	NE	cleavage
313	360	80	W	cleavage
313	189	70	SE	cleavage
313	187	60	NE	cleavage
314	257	54	SE	cleavage
314	250	43	SE	cleavage
314	263	51	SE	cleavage
314	259	65	SE	cleavage
314	241	67	SE	cleavage
314	250	56	SE	cleavage
314	239	66	SE	cleavage
314	243	70	SE	cleavage
314	244	75	SE	cleavage
314	235	80	SE	cleavage
314	246	77	SE	cleavage
314	241	81	SE	cleavage
314	243	79	SE	cleavage
314	245	76	SE	cleavage
314	243	70	SE	cleavage
314	239	78	SE	cleavage
314	265	77	SE	cleavage
314	222	74	SE	cleavage
314	223	80	SE	cleavage
314	221	89	SE	cleavage
314	220	67	SE	cleavage
314	225	60	SE	cleavage
314	209	66	SE	cleavage
314	207	68	SE	cleavage
314	227	67	SE	cleavage
314	193	40	SE	cleavage
314	192	44	SE	cleavage
314	188	45	SE	cleavage

314	191	66	SE	cleavage
314	210	38	SE	cleavage
314	177	72	NE	cleavage
314	175	50	SE	cleavage
314	193	58	SE	cleavage
314	191	78	SE	cleavage
314	199	87	SE	cleavage
314	194	75	SE	cleavage
314	194	70	SE	cleavage
187	320	46	SW	cleavage
192	240	38	S	cleavage
224	272	84	S	cleavage
227	270	48	S	cleavage
239	79	60	NW	cleavage
239	67	65	NW	cleavage
239	70	63	NW	cleavage
239	75	55	NW	cleavage
239	120	55	NE	cleavage
239	76	43	NW	cleavage
239	100	50	NE	cleavage
239	130	58	NE	cleavage
240	95	36	N	cleavage
240	98	42	NE	cleavage
240	105	27	NE	cleavage
240	111	33	NE	cleavage
241	78	40	NW	cleavage
241	77	33	NW	cleavage
241	83	32	NW	cleavage
241	77	28	NW	cleavage
241	92	46	N	cleavage
242	100	66	NE	cleavage
242	121	35	NE	cleavage
242	117	37	NE	cleavage
242	110	33	NE	cleavage
242	85	82	N	cleavage
242	265	80	S	cleavage
242	255	80	S	cleavage
243	90	85	N	cleavage
243	102	90		cleavage
243	279	59	S	cleavage
250	77	70	NW	cleavage
250	77	80	NW	cleavage
250	85	79	NW	cleavage
250	88	75	NW	cleavage
250	84	76	NW	cleavage
250	82	70	NW	cleavage
250	70	81	NW	cleavage
250	71	90		cleavage
257	11	42	SW	cleavage
257	22	20	NW	cleavage
257	14	36	NW	cleavage
257	20	22	NW	cleavage
257	3	32	NW	cleavage
257	357	38	SW	cleavage
258	47	63	NW	cleavage
258	45	61	NW	cleavage

258	56	67	NW	cleavage
258	46	69	NW	cleavage
258	45	73	NW	cleavage
259	229	90		cleavage
259	225	90		cleavage
261	264	65	S	cleavage
261	263	64	S	cleavage
261	272	65	S	cleavage
261	280	80	SW	cleavage
261	96	76	N	cleavage
261	279	60	SW	cleavage
261	95	74	N	cleavage
261	103	70	NE	cleavage
262	88	56	NW	cleavage
262	92	72	N	cleavage
262	97	85	N	cleavage
263	274	67	S	cleavage
263	285	60	S	cleavage
263	267	52	S	cleavage
264	70	60	NW	cleavage
264	70	56	NW	cleavage
264	69	39	NW	cleavage
264	68	63	NW	cleavage
264	72	32	NW	cleavage
264	83	49	NW	cleavage
264	85	60	NW	cleavage
264	91	39	NW	cleavage
264	78	25	NW	cleavage
264	87	53	NW	cleavage
264	108	57	NE	cleavage
264	89	37	NW	cleavage
264	82	52	NW	cleavage
264	82	57	NW	cleavage
264	95	50	NE	cleavage
264	102	49	NE	cleavage
264	93	47	NE	cleavage
264	280	35	SW	cleavage
264	279	52	S	cleavage
264	284	30	NW	cleavage
264	290	43	SW	cleavage
264	288	40	SW	cleavage
264	289	46	SW	cleavage
264	282	30	SW	cleavage
264	281	31	SW	cleavage
264	289	25	SW	cleavage
264	292	40	SW	cleavage
264	288	29	SW	cleavage
264	294	30	SW	cleavage
264	279	35	SW	cleavage
264	290	33	SW	cleavage
264	285	45	SW	cleavage
284	222	52	SE	cleavage
284	208	52	SE	cleavage
284	224	56	SE	cleavage
284	220	65	SE	cleavage
284	218	56	SE	cleavage

284	207	72	SE	cleavage
284	203	36	SE	cleavage
284	209	43	SE	cleavage
284	225	60	SE	cleavage
284	217	52	SE	cleavage
284	227	46	SE	cleavage
284	231	56	SE	cleavage
284	221	53	SE	cleavage
284	222	59	SE	cleavage
284	230	54	SE	cleavage
284	235	55	SE	cleavage
284	219	56	SE	cleavage
284	227	52	SE	cleavage
284	229	50	SE	cleavage
284	219	58	SE	cleavage
284	202	56	SE	cleavage
284	208	53	SE	cleavage
284	189	50	SE	cleavage
284	198	60	SE	cleavage
284	200	50	SE	cleavage
284	230	62	SE	cleavage
284	216	65	SE	cleavage
284	225	37	SE	cleavage
284	235	28	SE	cleavage
284	242	20	SE	cleavage
284	253	28	SE	cleavage
284	246	48	SE	cleavage
284	249	55	SE	cleavage
284	261	48	SE	cleavage
284	239	35	SE	cleavage
284	230	29	SE	cleavage
284	263	20	SE	cleavage
284	275	16	SW	cleavage
284	220	18	SE	cleavage
284	245	56	SE	cleavage
284	283	62	SE	cleavage
284	237	36	SE	cleavage
284	249	70	SE	cleavage
284	263	55	SE	cleavage
284	209	64	SE	cleavage
284	239	41	SE	cleavage
284	230	62	SE	cleavage
284	257	42	SE	cleavage
284	306	43	SW	cleavage
284	270	42	S	cleavage
284	280	46	SW	cleavage
284	290	52	SW	cleavage
284	286	46	SW	cleavage
284	285	45	SW	cleavage
284	294	49	SW	cleavage
284	291	44	SW	cleavage
284	325	36	SW	cleavage
284	284	43	SW	cleavage
284	232	54	SE	cleavage
284	284	33	SW	cleavage
284	267	23	SE	cleavage

284	300	12	SW	cleavage
284	270	16	S	cleavage
284	288	10	SW	cleavage
284	301	44	SW	cleavage
284	293	34	SW	cleavage
284	303	45	SW	cleavage
284	320	25	SW	cleavage
284	239	16	SE	cleavage
284	292	77	SW	cleavage
284	291	80	SW	cleavage
284	285	70	SW	cleavage
301	302	55	SW	cleavage
301	309	75	SW	cleavage
301	110	75	NE	cleavage
301	124	73	NE	cleavage
301	126	62	NE	cleavage
301	298	78	SW	cleavage
301	320	47	SW	cleavage
301	299	50	SW	cleavage
301	299	40	SW	cleavage
303	153	56	NE	cleavage
304	126	78	NE	cleavage
304	120	74	NE	cleavage
304	113	85	NE	cleavage
304	294	78	SW	cleavage
304	288	72	SW	cleavage
304	284	78	SW	cleavage
304	290	90		cleavage
304	98	85	NE	cleavage
304	100	76	NE	cleavage
304	274	78	SW	cleavage
306	103	76	NE	cleavage
306	110	90		cleavage
306	107	69	NE	cleavage
310	210	25	SE	cleavage
312	118	82	NE	cleavage
312	121	84	NE	cleavage
312	208	32	SE	cleavage
312	212	56	SE	cleavage
312	142	73	NE	cleavage
312	129	75	NE	cleavage
312	210	68	SE	cleavage
312	202	68	SE	cleavage
312	102	72	NE	cleavage
312	91	68	NE	cleavage
312	82	70	NW	cleavage
312	17	78	NW	cleavage
315	81	60	NW	cleavage
315	87	88	NW	cleavage
315	267	86	SE	cleavage
315	277	82	SE	cleavage
322	243	46	SE	cleavage
322	250	38	SE	cleavage
322	248	68	SE	cleavage
322	253	45	SE	cleavage
322	251	62	SE	cleavage

322	273	56	SE	cleavage
322	308	55	SW	cleavage
323	115	78	N	cleavage
323	119	65	NE	cleavage
323	95	74	NE	cleavage
323	118	70	NE	cleavage
324	286	50	SW	cleavage
324	256	40	SE	cleavage
324	267	60	SE	cleavage
324	261	50	SE	cleavage
324	260	48	SE	cleavage
324	245	50	SE	cleavage
324	273	57	SE	cleavage
325	264	88	SE	cleavage
325	300	85	SW	cleavage
325	286	86	SW	cleavage
329	260	84	SE	cleavage
329	266	67	SE	cleavage
329	269	90		cleavage
330	81	74	NW	cleavage

Fold axes data

Locality	Plunge	Trend	Notes
16	16	320	NE vergence F2
18	28	146	NE vergence F2
18	5	310	NE vergence F2
18	6	320	NE vergence F2
18	30	150	NE vergence F2
18	28	137	NE vergence F2
19	28	87	NE vergence F2
20	18	260	NE vergence F2
20	12	76	NE vergence F2
20	20	235	NE vergence F2
20	40	227	NE vergence F2
20	0	252	NE vergence F2
20	20	241	NE vergence F2
20	7	78	NE vergence F2
20	7	67	NE vergence F2
20	0	260	NE vergence F2
20	22	82	NE vergence F2
20	13	79	NE vergence F2
20	20	94	NE vergence F2
20	7	100	NE vergence F2
20	10	97	NE vergence F2
20	9	73	NE vergence F2
22	0	283	F2
22	20	111	F2
22	20	130	F2
23	14	273	F2
23	5	261	F2
23	5	261	F2
24	10	67	F2
24	12	98	F2
24	10	83	F2
25	20	57	F2

25	15	98	F2
25	1	41	F2
25	0	50	F2
25	2	243	F2
25	12	94	F2
25	5	85	F2
25	14	63	F2
25	14	47	F2
25	11	50	F2
26	5	100	F2
26	10	95	F2
26	10	273	F2
28	11	63	F2
28	19	64	F2
31	10	57	F2
46	33	154	NE vergence F2
46	27	151	NE vergence F2
46	32	136	NE vergence F2
49	20	260	F2
50	22	114	F2
50	15	109	F2
50	27	96	F2
50	30	123	F2
100	14	141	F2
100	28	135	F2
126	24	329	F2
130	35	123	F2
131	88	170	F2
161	26	100	N verging F2
171	6	300	F2
19	35	108	F2
19	22	96	F2
19	27	119	F2
21	22	75	F2
21	22	260	F2
21	0	275	F2
21	2	85	F2
21	0	240	F2
21	24	41	F2
21	28	78	F2
23	6	43	F2
23	16	209	F2
23	16	220	F2
24	4	63	F2
24	19	70	F2
24	11	60	F2
24	8	77	F2
24	23	64	F2
25	20	70	F2
25	2	70	F2
25	10	250	F2
25	7	85	F2
25	5	242	F2
25	24	82	F2
25	10	95	F2
25	12	90	F2

25	19	76	F2
25	13	53	F2
25	5	69	F2
25	15	67	F2
191	15	90	F2
191	17	90	F2
191	17	71	F2
191	18	97	F2
191	6	97	F2
191	50	65	F2
224	22	238	F2
224	13	241	F2
224	40	200	F2
239	22	110	F2
284	28	213	F2
284	19	87	F2
284	50	207	F2
284	55	191	F2
284	69	190	F2
284	53	193	F2
284	76	195	F2
284	66	190	F2
284	40	181	F2
285	13	108	F2
285	5	102	F2
285	0	100	F2
285	3	305	F2
285	8	288	F2
288	35	55	F2
288	33	44	F2
288	11	42	F2
288	24	53	F2
288	25	40	F2
312	57	144	F2
312	65	155	F2
312	72	152	F2
312	78	150	F2
312	82	144	F2
312	63	338	F2
312	75	360	F2
312	66	325	F2
318	5	92	F2
324	52	254	F2
330	36	195	F2
330	70	97	F2
330	45	60	F2
330	52	52	F2
330	60	40	F2

Fault data

Locality	Strike	Dip	Dip dir	Fault type	Lin. plunge	Lin. trend	Lin. type
3	300	60	SW	brittle thrust			
8	104	74	NE	brittle normal			
8	84	74	NW	brittle normal			
10	78	62	NW	high strain zone			
15	230	22	SW	brittle thrust			
19	240	35	SE	brittle thrust			
20	315	82	SW	brittle normal			
23	225	35	SE	brittle thrust	33	153	slickenline
46	132	63	NE	brittle normal	43	341	slickenline
51	284	56	SW	brittle thrust			
52	277	74	S	brittle thrust			
53	325	38	SW	brittle thrust			
53	321	86	SW	brittle thrust			
58	255	48	SE	?			
58	107	86	NE	brittle normal			
59	293	30	SW	brittle thrust			
61	267	50	S	thrust	33	145	slickenline
61	280	28	SW	brittle thrust			
64	263	80	SE	ductile thrust shear zone	75	126	stretching
64	243	80	SE	ductile thrust shear zone	43	160	stretching
64	276	39	SW	brittle thrust			
64	79	65	NW	brittle			
74	235	50	SE	brittle thrust			
77	348	30	SW	brittle thrust			
78	356	33	W	brittle thrust			
87	246	69	SE	brittle thrust			
88	120	45	NE	ductile			
111	65	54	NW	brittle back-thrust			
111	130	38	NE	brittle thrust?			
113	265	45	SE	brittle thrust			
113	284	38	SW	?			
114	308	34	SW	brittle thrust			
119	113	30	NE	brittle thrust			
120	235	35	SE	?			
120	251	56	SW	?			
120	110	51	NE	brittle thrust			
121	200	10	SE	brittle thrust			
121	50	45	NW	late brittle normal			
122	225	50	SE	?			
123	243	20	SE	brittle	4	217	slickenline
123	29	12	NW	brittle			
123	260	30	SE	brittle thrust			
123	279	65	SW	brittle normal			
123	227	42	SE	brittle thrust			
123	237	40	SE	?			
124	245	52	SE	brittle thrust			
126	83	47	NW	brittle thrust			
126	243	36	SE	brittle thrust			
127	239	44	SE	brittle thrust			
127	136	48	NE	small brittle normal			

127	314	45	SW	brittle thrust			
130	155	30	NE	brittle thrust			
130	168	20	NE	brittle thrust			
133	281	34	SW	Cz N frontal thrust			
138	72	60	SE	brittle thrust			
144	137	48	NE	ductile	38	109	stretching
149	62	76	NW	brittle oblique thrust	24	239	slickenline
153	120	63	NE	ductile thrust zone	310	40	stretching
154	100	55	NE	?			
154	117	30	NE	brittle thrust			
155	13	48	NW	?			
157	173	60	NE	brittle	24	32	slickenline
159	94	45	N	brittle normal			
159	266	27	SE	shallow brittle normal			
160	260	32	SE	brittle thrust			
160	240	42	S	?			
160	258	42	S	?			
161	280	32	SW	brittle thrust			
161	305	68	SW	brittle thrust			
161	305	45	SW	brittle thrust			
161	317	44	SW	brittle thrust			
162	295	55	SW	brittle thrust			
163	86	30	N	brittle thrust			
163	179	63	E	brittle thrust			
166	202	48	SW	brittle thrust			
166	187	87	E	brittle thrust			
167	158	64	NE	brittle normal	61		
171	134	40	NE	brittle normal	62		
172	282	78	SW	ductile shear zone	60	105	stretching
172	286	65	SW	ductile shear zone	33	6	stretching
173	75	46	NW	brittle thrust			
173	48	44	NW	brittle thrust	55	319	slickenline
173	245	67	SE	?			
173	71	50	NW	brittle normal			
173	94	30	N	brittle thrust			
174	86	32	N	brittle thrust			
174	50	63	NW	brittle normal			
174	297	41	SW	brittle thrust			
174	73	34	NW	brittle thrust			
175	110	30	NE	CZ brittle thrust	45	49	slickenline
175	265	40	SE	brittle normal	36	176	slickenline
175	295	20	SW	brittle			
175	70	68	NW	brittle	59	351	slickenline
177	82	35	N	brittle			
177	110	50	NE	brittle thrust			
177	55	65	NW	late brittle normal			
177	81	50	NW	brittle thrust	16	276	slickenline
177	40	60	NW	brittle thrust			
178	99	50	NE	brittle thrust	61	355	slickenline
179	47	52	NW	brittle thrust			
179	185	85	E	brittle			
179	5	16	W	brittle thrust			
179	135	45	NE	brittle thrust			
182	35	22	N	brittle thrust	14	303	slickenline

182	293	46	SW	brittle thrust			
182	320	23	SW	brittle thrust			
182	151	46	NE	brittle thrust	44	29	slickenline
182	246	40	SE	?			
182	243	52	SE	?			
182	252	55	SE	brittle no kin			
182	247	47	SE	brittle no kin			
182	223	36	SE	brittle normal	34	144	slickenline
182	90	38	N	brittle			
124	196	35	SE	brittle			
124	223	50	SE	brittle			
127	258	47	SE	brittle	48	170	slickenline
186	280	54	S	ductile thrust shear zone			
186	123	72	NE	brittle normal			
187	345	5	SW	ductile thrust shear zone			
19	254	58	SE	britle thrust	58	171	slickenline
188	88	80	NE	brittle normal	20	273	slickenline
19	266	54	S	ductile thrust shear zone	10	92	slickenline
19	265	60	S	ductile thrust shear zone	16	126	slickenline
19	280	74	S	brittle normal			
19	267	63	S	ductile thrust shear zone			
19	256	40	S	?			
20	287	38	S	ductile thrust shear zone			
20	280	52	SW	brittle normal	25	132	slickenline
20	262	32	S	ductile thrust shear zone			
20	264	40	S	ductile thrust shear zone	42	170	slickenline
20	256	55	S	ductile thrust shear zone	40	130	slickenline
21	278	32	S	ductile thrust shear zone	32	161	slickenline
21	240	48	S	ductile thrust shear zone	45	235	slickenline
21	260	36	S	ductile thrust shear zone	45	177	slickenline
21	300	38	SW	ductile thrust shear zone			
21	260	50	S	ductile thrust shear zone			
21	278	60	S	ductile thrust shear zone	13	105	slickenline
22	242	23	S	ductile thrust shear zone	22	140	slickenline
22	278	65	S	?			
23	225	35	SE	ductile thrust shear zone	10	153	slickenline
23	265	45	S	brittle normal	46	182	slickenline
24	270	35	S	brittle normal	15	130	slickenline
24	276	30	S	ductile thrust shear zone			
24	260	40	S	ductile thrust shear zone			
25	97	37	N	brittle thrust			

25	250	30	S	ductile thrust shear zone	14	218	slickenline
25	252	72	S	normal fault	10	250	slickenline
190	175	55	E	briitle thrust			
193	290	65	S	brittle normal			
193	268	48	S	brittle normal			
200	243	72	SE	brittle thrust	2	240	slickenline
201	310	57	SW	brittle thrust	45	290	slickenline
220	300	32	SW	ductile thrust shear zone			
220	285	75	S	brittle normal			
223	240	52	SE	brittle normal			
226	250	60	S	ductile thrust shear zone			
228	272	62	S	brittle normal	40	245	slickenline
230	283	90		brittle thrust	14	116	slickenline
232	280	72	SW	brittle thrust			
233	124	40	NE	ductile thrust shear zone			
237	270	62	S	brittle thrust			
239	107	35	N	ductile thrust shear zone			
239	112	36	NE	ductile thrust shear zone			
239	105	70	NE	brittle normal			
239	140	42	NE	brittle thrust	23	70	slickenline
240	85	36	NW	brittle thrust			
240	83	46	NW	?			
240	86	45	N	brittle thrust			
242	74	23	N	brittle thrust			
242	98	52	NE	ductile thrust shear zone			
243	73	50	NW	brittle thrust	45	10	slickenline
243	140	43	NE	brittle thrust	21	17	slickenline
243	110	75	NE	brittle normal			
244	97	60	NE	brittle normal	53	9	slickenline
251	280	66	SW	brittle normal	50	137	slickenline
253	67	66	NW	brittle thrust	50	328	slickenline
254	30	64	NW	brittle thrust	50	255	slickenline
258	22	44	NW	brittle thrust	41	340	slickenline
259	57	72	NW	brittle thrust			
259	62	75	NW	brittle normal			
260	105	62	NE	brittle thrust	37	80	slickenline
260	102	40	NW	ductile thrust shear zone			
261	245	60	SE	ductile thrust shear zone			
261	257	70	SE	brittle thrust			
263	269	70	S	brittle normal	62	168	slickenline
266	309	48	SW	brittle thrust			
268	287	46	SW	brittle thrust	40	227	slickenline
271	279	54	SW	brittle normal	26	228	slickenline
272	320	49	SW	brittle thrust			
274	283	55	SW	brittle thrust			
275	291	48	SW	brittle thrust	23	267	slickenline
275	276	44	SW	brittle thrust			
275	285	36	SW	brittle thrust			
276	290	40	SW	brittle thrust			

276	293	37	SW	brittle thrust			
281	320	57	SW	brittle thrust			
282	307	70	SW	brittle thrust	25	270	slickenline
286	281	75	SW	ductile thrust shear zone			
288	133	53	NE	brittle thrust	20	128	slickenline
289	178	40	E	brittle normal	20	100	slickenline
290	180	52	E	brittle normal	43	100	slickenline
297	80	40	NW	brittle thrust	16	352	slickenline
305	143	15	NE	brittle thrust			
305	111	24	NE	brittle thrust	10	96	slickenline
309	292	56	SW	brittle thrust			
325	302	36	SW	brittle thrust	36	186	slickenline
325	278	38	SW	?			
327	259	48	SE	?			

Appendix C:

Geochemical data

	A05/1/10 Gabbro	A05/1/12 Gabbro	A05/2/24 Gabbro	A05/2/25 Gabbro	A05/2/26a Gabbro
LAT N	43°38'56	43°38'59.1	43°39'36.29	43°39'39.29	43°39'42.6
LONG E	100°19'18	100°19'5.4	100°19'21	100°19'16.5	100°19'11.1
SiO_2	53.89	50.05	51.27	51.4	51.33
TiO_2	0.29	0.21	0.27	0.29	0.17
Al_2O_3	17.03	20.31	15.46	16.7	20.21
Fe_2O_3	5.33	3.09	6.11	6.03	4.76
MnO	0.103	0.062	0.115	0.113	0.097
MgO	7.62	8.79	10.49	10.37	8.25
CaO	11.68	13.25	13.93	13.11	12.42
Na_2O	4.52	2.96	3.08	2.59	3.11
K_2O	0.323	0.757	0.108	0.253	0.573
P_2O_5	0.009	0.008	0.003	0.003	0.004
Total	100.79	99.47	100.83	100.86	100.93
LOI	2.44	4.57	3.25	1.59	2.64
As	5.2	1.1	5.5	2.5	0.7
Ba	19.4	54.0	18.5	53.8	49.7
Co	19.8	11.3	26.5	25.5	18.8
Cr	105.8	2617.6	912.4	941.2	710.1
Cu	38.5	31.0	20.7	49.8	80.1
Ga	11.8	11.1	11.7	13.0	12.9
Mo	1.1	1.5	1.7	1.4	0.8
Nb	-0.1	0.2	-0.9	-0.7	0.2
Ni	38.6	57.7	140.4	149.6	198.0
Pb	1.5	1.1	-0.3	0.9	3.2
Rb	10.1	19.9	3.1	7.1	12.8
Sc	41.7	44.7	47.8	51.0	31.5
Sn	-0.4	0.4	-1.6	-0.9	1.4
Sr	109.9	192.4	171.5	132.3	278.8
Th	1.7	1.9	3.4	4.1	2.8
U	0.0	-0.2	1.5	0.9	0.0
V	146.3	119.5	163.8	166.8	92.1
W	0.8	-2.2	-1.2	2.3	-0.1
Y	9.6	8.1	6.0	8.0	4.8
Zn	22.6	12.5	27.0	28.7	22.7
Zr	11.7	10.9	4.8	5.1	6.1
%Fe_2O_3	5.11	2.81	5.76	5.77	4.51
%TiO_2	0.27	0.19	0.26	0.29	0.17
%CaO	11.35	12.96	13.57	12.65	11.71
La	-0.6	-1.8	-0.9	-2.2	-1.9
Nd	4.5	4.1	1.8	-0.5	0.7
Cs	1.9	3.0	0.8	3.0	1.2
K_2O	0.323	0.757	0.108	0.253	0.573
P_2O_5	0.009	0.008	0.003	0.003	0.004

	A05/2/26b Gabbro	A05/2/26c Gabbro	A05/4/40 Gabbro	A05/4/43 Gabbro	A05/9/61 Diorite	A05/9/63 Diorite
LAT N	43°39'42.6	43°39'42.6	43°39'24.6	43°39'31	43°37'39.2	43°37'42.7
LONG E	100°19'11.1	100°19'11.1	100°31'4.9	100°30'58.6	100°36'4.2	100°35'10.9
SiO_2	52.22	52.73	49.32	51.32	62.14	62.98
TiO_2	0.14	0.14	0.21	0.37	0.83	0.7
Al_2O_3	21.05	19.73	18.06	15.75	16.91	17.06
Fe_2O_3	4.06	4.49	6.38	5.24	6.71	6.31
MnO	0.09	0.093	0.102	0.105	0.076	0.092
MgO	7.31	8.24	10.92	9.64	2.55	2.95
CaO	12.11	10.77	12.59	16.34	5.89	5.19
Na_2O	3.33	3.96	2.54	2.47	3.95	3.88
K_2O	0.767	0.593	0.021	0.027	1.155	1.77
P_2O_5	0.002	0.007	0.008	0.007	0.178	0.122
Total	101.08	100.76	100.15	101.26	100.38	101.05
LOI	2.29	2.76	5.60	2.24	1.93	2.22
As	1.6	0.0	37.6	1.2	4.7	4.7
Ba	68.1	45.2	10.8	24.5	180.4	328.4
Co	15.8	19.3	30.4	22.7	21.3	20.0
Cr	528.6	538.5	650.9	1402.3	18.0	16.1
Cu	73.9	81.6	141.2	56.2	88.6	31.5
Ga	12.1	11.3	12.4	11.9	17.2	18.4
Mo	0.7	1.0	0.6	1.7	1.4	0.6
Nb	0.1	0.4	-0.2	1.4	3.1	2.5
Ni	165.7	181.2	237.2	111.6	6.7	5.7
Pb	0.3	3.2	2.3	2.0	3.8	0.2
Rb	17.9	14.5	0.8	2.4	23.9	28.4
Sc	26.3	27.4	34.4	63.0	14.5	23.7
Sn	-2.1	1.1	-1.3	-1.1	2.9	4.3
Sr	262.5	240.1	180.7	273.1	443.3	238.1
Th	3.3	4.1	4.3	0.3	5.3	2.6
U	-0.2	-0.2	0.8	1.6	-1.4	-1.4
V	73.3	71.3	105.9	220.0	136.3	157.6
W	1.3	0.3	0.9	0.6	0.1	2.1
Y	3.7	6.3	3.1	10.3	12.7	18.7
Zn	17.9	22.9	31.4	23.9	45.3	59.1
Zr	0.2	6.4	2.4	5.3	180.8	94.7
%Fe_2O_3	3.73	4.40	6.66	4.97	7.46	6.86
%TiO_2	0.13	0.14	0.21	0.39	0.95	0.77
%CaO	11.45	10.49	11.96	15.27	5.59	4.90
La	-0.9	-1.1	-0.5	-2.5	5.8	3.2
Nd	4.8	0.5	-2.1	-0.2	10.0	10.1
Cs	5.3	3.5	-1.6	1.8	2.6	-1.1
K_2O	0.767	0.593	0.021	0.027	1.155	1.77
P_2O_5	0.002	0.007	0.008	0.007	0.178	0.122

Bibliography

1990. Mongolian National Atlas, Ulaan Baatar, Moscow.

Adiya, M., Ankhtsetseg, D., Baasanbat, Ts., Bayar, G., Bayarsaikhan, Ch., Erdenezul, D., Mungunsuren, D., Munkhsaikhan, A., Munkhuu, D., Narantsetseg, R., Odonbaatar, Ch., Selenge, L., Tsenbel, B., Ulziibat, M., Urtnasan, K. 2003. One century of seismicity in Mongolia (1900-2000). *Research Centre of Astronomy and Geophysics, Mongolian Academy of Sciences and Département Analyse Surveillance Environnement France.*

Allen, M. B., Windley, B. F. & Chi, Z. 1993. Palaeozoic collisional tectonics and magmatism of the Chinese Tien Shan, central Asia *Tectonophysics,* **220**(4), 89-115.

Anderson, R. S. 1990. Evolution of the Northern Santa Cruz Mountains by Advection of Crust Past a San Andreas Fault Bend. *Science,* **249**, 397-401.

Anderson, R. S. 1994. Evolution of the Santa Cruz Mountains, California, through tectonic growth and geomorphic decay. *Journal of Geophysical Research,* **99** (B10), 20,161-20,179.

Aydin, A. & Nur, A. 1985. The types and role of stepovers in strike-slip tectonics. *The Society of Economic Palaeontologists and Mineralogists,* 35-44.

Badarch, G., Cunningham, D. & Windley, B. F. 2002. A new terrane subdivision for Mongolia: implications for the Phanerozoic crustal growth of Central Asia. *Journal of Asian Earth Sciences,* **21**, 87-110.

Bai, Q., Mackwell, S. J. & Kohlstedt, D. L. 1991. High-temperature creep of olivine single cyrstals 1. Mechanical results for buffered samples. *Journal of Geophysical Research,* **96**(B2), 2441–2463.

Baljinnyam, I., Bayasgalan, A., Borisov, B. A., Cisternas, A., Dem'yanovich, M. G., Ganbaatar, L., Kochetkov, V. M., Kurushin, R. A., Molnar, P., Philip, H. & Vashchilov, Y. Y. 1993. *Ruptures of Major Earthquakes and Active Deformation in Mongolia and its Surroundings*. Geological Society of America Memoir, Boulder, Colorado.

Bayasgalan, A., Jackson, J., Ritz, J.-F. & Carretier, S. 1999. 'Forebergs', flower structures,

and the development of large intra-continental strike-slip faults: the Gurvan Bogd fault system in Mongolia. *Journal of Structural Geology,* **21**, 1285-1302.

Benoit, M., Polve, M. & Ceuleneer, G. 1996. Trace element and isotopic characterization of mafic cumulates in a fossil mantle diapir (Oman ophiolite). *Chemical Geology,* **134**, 199-214.

Benton, M. J., Shishkin, M. A., Unwin, D. M. & Kurochkin, E. N. 2000. *The Age of Dinosaurs in Russia and Mongolia*. Cambridge University Press.

Best, M. G. & Christiansen, E. H. 2001. *Igneous Petrology*. Blackwell Science.

Blight, J., Cunningham, D. & Petterson, M. 2008. Crustal evolution of the Saykhandulaan Inlier, Mongolia: Implications for Palaeozoic arc magmatism, polyphase deformation and terrane accretion in the Southeast Gobi Mineral Belt. *Journal of Asian Earth Sciences,* **in press**.

Buchan, C., Pfander, J., Kroner, A., Brewer, T. S., Tomurtogoo, O., Tomurhuu, D., Cunningham, D. & Windley, B. F. 2002. Timing of accretion and collisional deformation in the Central Asian Orogenic Belt: implications of granite geochronology in the Bayankhongor Ophiolite Zone. *Chemical Geology,* **192**, 23-45.

Bucher, K. & Frey, M. 1994. *Petrogenesis of Metamorphic Rocks. 6th Edition*. Springer-Verlag.

Buslov, M. M., Saphonova, I. Y., Watanabe, T., Obut, O. T., Fujiwara, Y., Iwata, K., Semakov, N. N., Sugai, Y., Smirnova, L. V. & Kazansky, A. Y. 2001. Evolution of the Paleo-Asian Ocean (Altai-Sayan Region, Central Asia) and collision of possible Gondwana-derived terranes with the southern marginal part of the Siberian continent. *Geosciences Journal,* **5**(3), 203-224.

Calais, E., Vergnolle, M., San'kov, V., Lukhnev, A., Mirotschnitchenko, A., Amarjargal, S. & De´Verchere, J. 2003. GPS measurements of crustal deformation in the Baikal–Mongolia area (1994–2002): implications for current kinematics of Asia. *Journal of Geophysical Research,* **108**.

Charvet, J., Shu, L. & Laurent-Charvet, S. 2007. Paleozoic structural and geodynamic evolution of eastern Tianshan (NW China): welding of the Tarim and Junggar plates *Episodes,* **30**(3).

Chen, B., Jahn, B.-m., Wilde, S. & Xu, B. 2000. Two contrasting palaeozoic magmatic belts in northern Inner Mongolia, China: petrogenesis and tectonic implications.

Tectonophysics, **328**, 157-182.

Christie-Blick, N. & Biddle, K. T. 1985. Deformation and basin formation along strike-slip faults. In: *Strike-slip Deformation, Basin Formation and Sedimentation* (edited by Biddle, K. T. & Christie-Blick, N.) **37**. SEPM Special Publications, 1-34.

Cocks, L. R. M. & Torsvik, T. H. 2005. Baltica from the late Precambrian to mid-Palaeozoic times: the gain and loss of a terrane's identity. *Earth Science Reviews,* **72**, 39-66.

Coleman, R. G. 1994. Terranes (Units) in the Western half of the geodynamic map. *Stanford-China Geosciences Industrial Affiliates Program Annual Review,*, 1-8.

Collins, W. J. 2002. Hot orogens, tectonic switching, and creation of continental crust. *Geology,* **30**(6), 535-538.

Cowgill, E., Arrowsmith, J. R., Yin, A., Feng, W. X. & Zhengle, C. 2004a. The Akato Tagh bend along the Altyn Tagh fault, northwest Tibet 2: Active deformation and the importance of transpression and strain hardening within the Altyn Tagh system. *GSA Bulletin,* **116**(11/12), 1443-1464.

Cowgill, E., Yin, A., Arrowsmith, J. R., Feng, W. X. & Shuanhong, Z. 2004b. The Akato Tagh bend along the Altyn Tagh fault, northwest Tibet 1: Smoothing by vertical-axis rotation and the effect of topographic stresses on bend-flanking faults. *GSA Bulletin,* **116**(11/12), 1423-1442.

Cowie, P. A. & Scholz, C. H. 1992. Displacement-length scaling relationship for faults : data synthesis and discussion. *Journal of Structural Geology,* **14**(10), 1149-1156.

Cox, S. F. 1999. Deformational controls on the dynamics of fluid flow in mesothermal gold systems. In: *Fractures, fluid flow and mineralization* (edited by McCaffrey, K. J. W., Lonergan, L. & Wilkinson, J. J.) **155**. Geological Society, London, Special Publictions.

Crowell, J. C. 1974. Origin of late Cenozoic basins of southern California In: *Tectonics and Sedimentation* (edited by Dickinson, W. R.) **22**. SPEM Special Publications, 190-204.

Cunningham, D., Windley, B. F., Dorjnamjaa, D., Badamgarov, J. & Saandar, M. 1996. Late Cenozoic transpression in southwestern Mongolia and the Gobi Altai-Tien Shan connection. *Earth and Planetary Science Letters,* **140**, 67-81.

Cunningham, D., Windley, B. F., Owen, L. A., Barry, T., Dorjnamjaa, D. & Badamgarov,

J. 1997. Geometry and style of partitioned deformation within a late Cenozoic transpressional zone in the eastern Gobi Altai Mountains, Mongolia. *Tectonophysics,* **277**, 285-306.

Cunningham, D. 1998. Lithospheric controls on late Cenozoic construction of the Mongolian Altai. *Tectonics,* **17**(6), 891-902.

Cunningham, D., Davies, S. & Badarch, G. 2003a. Crustal architecture and active growth of the Sutai Range, western Mongolia: a major intracontinental, intraplate restraining bend. *Journal of Geodynamics,* **36**, 169-191.

Cunningham, D., Owen, L. A., Snee, L. W. & Jiliang, L. 2003b. Structural framework of a major intracontinental orogenic termination zone: the easternmost Tien Shan, China. *Journal of the Geological Society, London,* **160**, 575-590.

Cunningham, D. 2005. Active intracontinental transpressional mountain building in the Mongolian Altai: Defining a new class of orogen. *Earth and Planetary Science Letters,* **240**, 436-444.

Cunningham, D. 2007. Structural and topographic characteristics of restraining-bend mountain ranges of the Altai, Gobi Altai and easternmost Tien Shan. In: *Tectonics of Strike-Slip Restraining and Releasing Bends* (edited by Cunningham, D. & Mann, P.) **290**. Geological Society, London, Special Publications, 219-237.

Cunningham, D. & Mann, P. 2007. Tectonics of strike-slip restraining and releasing bends. In: *Tectonics of Strike-Slip Restraining and Releasing bends* (edited by Cunningham, D. & Mann, P.) **290**. Geological Society, London, Special Publications, 1-12.

Cunningham, D., Davies, S. & Mclean, D. submitted. Exhumation of a Cretaceous metamorphic core complex within a late Cenozoic restraining bend, Altan Uul, southern Mongolia. *Journal of Geology,*.

Deer, W. A., Howie, R. A. & Zussman, J. 1962. *Rock-forming minerals Vol. 3 Sheet Silicates*. Longmans.

Deer, W. A., Howie, R. A. & Zussman, J. 1966. *An introduction to the Rock Forming Minerals*. Longman.

Didenko, A. N. 1992. Magnetism of South Mongolian Middle Palaeozoic ophiolites. *Physics of the Earth and Planetary Interiors,* **74**, 223-277.

Dobretsev, N. L., Buslov, M. M. & Vernikovsky, V. A. 2003. Neoproterozoic to Early Ordovician evolution of the Paleo-Asian ocean: implications to the break-up of

Rodinia. *Gondwana Research.* **6**, 143-159.

Dorjnamjaa, D., Badarch, G. & Orolmaa, D. 1993. The geodynamic evolution of the mobile fold belts of the territory of Mongolia. In: *29th International Geological Congress,* (edited by Coleman, R. G.) **Reconstruction of the Paleo-Asian ocean**. VSP International Sci. Publ., Kyoto, Japan: Utrecht, Netherlands,, 63-76.

Dumitru, T. A. & Hendrix, M. S. 2001. Fission-track constraints on Jurassic folding and thrusting in southern Mongolia and their relationship to the Beishan thrust belt of northern China. In: *Paleozoic and Mesozoic tectonic evolution of central Asia: From continental assembly to intracontinental deformation* (edited by Hendrix, M. S. & Davis, G. A.) **194**. Geological Society of America Memoir, Boulder, Colorado, 2105-229.

Eenzhin, G. 1983. The Southern Mongolian Hercynian Eugeocynaclinal Zone (Dzolen Range-Mandal-Ovoo) during Early Devonian time. *Geotectonics,* **17**, 326-334.

Escartin, J., Hirth, G. & Evans, B. 1997. Effects of serpentinization on the lithospheric strength and the style of normal faulting at slow-spreading ridges. *Earth and Planetary Science Letters,* **151**, 181-189.

Fitzgerald, P., Stump, E. & Redfield, T. 1993. Late Cenozoic uplift of the Denali, and its relation to relative plate motion and fault morphology. *Science,* **259**, 497-500.

Florensov, N. A. & Solonenko, V. P. 1967. *The Gobi-Altay earthquake*. Akademiya Nauk USSR, Moskow (in Russian; English translation by Israel Program for Scientific Translations, US Department of Commerce, Washington, DC, 1965).

Gao, J., Maosong, L., Xuchang, X., Yaoqing, T. & Guoqi, H. 1998. Paleozoic tectonic evolution of the Tainshan Orogen, northwestern China. *Tectonophysics,* **287**, 213-231.

Gao, S., Davis, P. M., Liu, H., Slack, P. D., Zorin, Y. A., Mordvinova, V. V., Kozhevnikov, V. M. & Meyer, R. P. 1994. Seismic anisotropy and mantle flow beneath the Baikal rift zone *Nature,* **371**, 149-151.

Gibsher, A. S., Izokh, A. E. & Khain, E. V. 1991. Pre-Middle Ordovician structure of the Tuva-Mongolian segment of the Central Asian fold belt [abs]. In: *Report no. 2, IGCP 283; Geodynamic evolution and main sutures of Palaeoasian Ocean: Abs. Pap. Int. Symp. on Evolution of Palaeoasian Ocean,* (edited by Xiao, X. & Li, J.) **2**, Shenyang, China, 25-28.

Graham, S. A., Hendrix, M. S., Johnson, C. L., Badamgarav, D., Badarch, G., Amory, J.

Y., Porte, M., Barsbold, R., Webb, L. E. & Hacker, B. R. 2001. Sedimentary record and tectonic implications of Mesozoic rifting in southern Mongolia. *Geological Society of America Bulletin,* **113**, 1560-1579.

Guo, Z. J., Ma, R. S., Guo, L. Z. & Shi, Y. S. 1993. A comparative study on three ophiolitic melange belts in Eastern Xinjiang. *Geol. Rev.,* **39**, 236-247.

Hartz, E. H. & Torsvik, T. H. 2002. Baltica upside down: a new plate tectonic model for Rodinia and the Iapetus Ocean. *Geology,* **30**, 255-258.

He, G. & Han, B. 1991. Paleozoic tectonic evolution of Altay orogenic belt in China. *IGCP 283 Geodynamic Evolution and Main Sutures of Paleoasian Ocean,* **Report 2**, 31-33.

Helo, C., Hegner, E., Kroner, A., Badarch, G., Tomurtogoo, O., Windley, B. F. & Dulski, P. 2006. Geochemical signature of Palaeozoic accretionary complexes of the central Asian orogenic Belt in South Mongolia: Constraints on arc environments and crustal growth. *Chemical Geology,* **227**, 236-257.

Hendrix, M. S., Graham, S. A., Amory, J. Y. & Badarch, G. 1996. Noyon Uul syncline, southern Mongolia: Lower Mesozoic sedimentary record of the tectonic amalgamation of central Asia. *GSA Bulletin,* **108**(10), 1256-1274.

Holdsworth, R. E., Butler, C. A. & Roberts, A. M. 1997. The recognition of reactivation during continental deformation. *Journal of the Geological Society, London,* **154** (1), 73-78.

Holdsworth, R. E., Hand, M., Miller, J. A. & Buick, I. S. 2001. Continental reactivation and reworking: an introduction. In: *Continental Reactivation and Reworking* (edited by Miller, J. A., Holdsworth, R. E., Buick, I. S. & Hand, M.) **184**. Geological Society of London, London, Special Publications, 1-12.

Jackson, J. & Molnar, P. 1990. Active faulting and block rotations in the western Transverse Ranges, California *Journal of Geophysical Research,* **95**, 22073-22087.

Jerzykiewicz, T. & Russell, D. A. 1991. Late Mesozoic stratigraphy and vertebrates of the Gobi Basin. *Cretaceous Research,* **12**, 345-377.

Johnson, C. L., Webb, L. E., Graham, S. A., Hendrix, M. S. & Badarch, G. 2001. Sedimentary and structural records of late Mesozoic high-strain extension and strain partitioning, East Gobi basin, southern Mongolia. In: *Paleozoic and Mesozoic tectonic evolution of central Asia: From continental assembly to*

intracontinental deformation (edited by Hendrix, M. S. & Davis, G. A.) **194**. Geological Society of America Memoir, Boulder, Colorado, 413-433.

Jolivet, M., Ritz, J.-F., Vassallo, R., Larroque, C., Braucher, R., Todbileg, M., Chauvet, A., Sue, C., Arnaud, N., Vicente, R. D., Arzhanikova, A. & Arzhanikov, S. 2007. Mongolian summits: An uplifted, flat, old but still preserved erosion surface *Geology,* **35**, 871-874.

Keller, E. A. & Pinter, N. 2002. *Active Tectonics*. Prentice Hall, Inc., Upper Saddle River, New Jersey, USA.

Kepezhinskas, P. K., Kepezhinskas, K. B. & Pukhtel, I. S. 1991. Lower Paleozoic oceanic crust in Mongolian Caledonides: Sm-Nd isotope and trace element data. *Geophysical Research Letters,* **18**, 1301-1304.

Khain, E. V., Bibikova, E. V., Salnikova, E. B., Kroner, A., Gibsher, A. S., Didenko, A. N., Degtyarev, K. E. & Fedotova, A. A. 2003. The Palaeo-Asian ocean in the Neoproterozoic and early Palaeozoic: new geochronological data and the palaeotectonic reconstructions. *Precambrian Research,* **122**, 329-358.

Kotov, A. B., Kozakov, I. K., Bibikova, E. V., Salnikova, E. B., Kirnozova, T. I. & Kovach, V. P. 1995. Duration of regional metamorphism epsiodes in the area of polycyclic development of endogenentic processes: Results of U-Pb geochronologic study,. *Petrology,* **3**, 622-631.

Kovach, V. P., Jian, P. & Yarmolyuk, V. V. 2005. Magmatism and geodynamics of early stages of the Paleoasian ocean formation: geochronological and geochemical data on ophiolites of the Bayan-Khongor zone. *Doklady Earth Sciences,* **404**, 1072-1077.

Kozakov, I. K. 1986. *Precambrian infrastructures of Palaeozoic complexes of Mongolia,*, Leningrad, Nauka Press.

Krassilov, V. A. & Makulbekov, N. M. 1996. Isoetalian megasporophylls with megaspores from the Upper Cretaceous of Mongolia. *Review of Palaeobotany and Palynology* **94**, 231-238.

Kurushin, R. A., Bayasgalan, A., Olziybat, M., Enhtuvshin, B., Molnar, P., Bayarsayhan, C., Hudnut, K. W. & Lin, J. 1997. *The Surface Rupture of the 1957 Gobi-Altay, Mongolia, Earthquake*. Geological Society of America.

Kvassnes, A. J. S., Strand, A. H., Moen-Eikeland, H. & Pedersen, R. B. 2004. The Lyngen Gabbro: the lower crust of an Orovician Incipient Arc. *Contrib. Mineral.*

Petrol, **148**, 358-379.

Lamb, M. A. & Badarch, G. 1997. Palaeozoic Sedimentary Basins and Volcanic-Arc Systems of Southern Mongolia: New Stratigraphic Constraints. *International Geology Review,* **39**, 542-576.

Lamb, M. A. & Badarch, G. 2001. Paleozoic sedimentary basins and volcanic arc systems of southern Mongolia: New Ggeochemical and petrographic constraints. In: *Paleozoic and Mesozoic tectonic evolution of central and eastern Asia: From continental assembly to intracontinental deformation:* (edited by Hendrix, M. S. & Davis, G. A.) **194**. Geological Society of America Memoir, Boulder, Colorado, 117-149.

Lamb, M. A. & Cox, D. 1998. New Ar-Ar age data for porphyry copper deposits and host rocks of Mongolia. *Economic Geology,* **93**, 524-526.

Lamb, M. A., Hanson, A. D., Graham, S. A., Badarch, G. & Webb, L. E. 1999. Left-lateral sense offset of Upper Proterozoic to Palaeozoic features across the Gobi Onon, Tostm and Zuunbayan faults in southern Mongolia and implications for other central Asian faults. *Earth and Planetary Science Letters,* **173**, 183-194.

Laurent-Charvet, S., Charvet, J., Shu, L., Ma, R. & Lu, H. 2002. Palaeozoic late collisional strike-slip deformations in Tainshan and Altay, Eastern Xinjiang, NW China. *Terra Nova,* **14**, 249-256.

Little, T. A., Cox, S., Vry, J. K. & Batt, G. 2005. Variations in exhumation level and uplift rate along the oblique-slip Alpine Fault, central Southern Alps, New Zealand. *Geological Society of America Bulletin,* **117**, 707-723.

Mann, P. 2007. Global catalogue, classification and tectonic origins of restraining- and releasing bends on active and ancient strike-slip fault systems. In: *Tectonics of Strike-Slip Restraining and Releasing Bends,* (edited by Cunningham, D. & Mann, P.) **290**. Geological Society, London, Special Publications.

Manning, C. E., Weston, P. E. & Mahon, K. I. 1996. Rapid high-temperature metamorphism of East Pacific Rise gabbros from Hess Deep. *Earth and Planetary Science Letters,* **144**, 123-132.

McClay, K. & Bonora, M. 2001. Analog models of restraining stepovers in strike-slip fault systems. *AAPG Bulletin,* **85**(2), 233-260.

Meert, J. G. & Lieberman, B. S. 2004. A palaeomagnetic and palaeogeographic perspective on latest Neoproterozoic and early Cambrian tectonic events. *Journal*

of the Geological Society, London, **161**, 477-486.

Meng, Q.-R. 2003. What drove late Mesozoic extension of the northern China-Mongolia tract? *Tectonophysics,* **369**, 155-174.

Meng, Q.-R., Hu, J.-M., Jin, J.-Q., Zhang, Y. & Xu, D.-F. 2003. Tectonics of the late Mesozoic wide extensional basin system in the China-Mongolia border region. *Basin Research* **15**, 397-415.

Miyashiro, A. 1961. Evolution of metamorphic belts. *Journal of Petrology*, **2**, 277-311.

Molnar, P. & Tapponier, P. 1975. Cenozoic Tectonics of Asia: Effects of a Continental Collision. *Science,* **189**(4201), 419-426.

Moody, J. B., Meyer, D. & Jenkins, J. E. 1983. Experimental characterization of the greenschist/amphibolite boundary in mafic systems. *American Journal of Science,* **283**, 48-92.

Morley, C. K. 2002. A tectonic model for the Tertiary evolution of strike-slip faults and rift basins in SE Asia. *Tectonophysics,* **347**, 195-215.

Muir, T. L. 2002. The Hemlo gold deposit, Ontario, Canada: principal deposit characteristics and constraints on mineralization *Ore Geology Reviews,* **21**(1), 1-66.

Murphy, J. B., Pisarevsky, S. A., Nance, R. D. & Keppie, J. D. 2004. Neoproterozoic-Early palaeozoic evolution of peri-Gondwana terranes: implications fro Laurentia-Gondwana connections. *International Journal of Earth Sciences,* **93**, 659-682.

Nicolas, A. & Mainprice, D. 2005. Burst of high-temperature seawater injection throughout accreting oceanic crust: a case study in Oman ophiolite. *Terra Nova,* **17**(4), 326-330.

Owen, L. A., Windley, B. F., Cunningham, D., Badamgarov, J. & Dorjnamjaa, D. 1997. Quaternary alluvial fans in the Gobi of southern Mongolia: evidence for neotectonics and climate change. *Journal of Quaternary Science,* **12**(3), 239-252.

Owen, L. A., Cunningham, D., Richards, B. W. M., Rhodes, E., Windley, B. F., Dorjnamjaa, D. & Badamgarov, J. 1999a. Timing of formation of forebergs in the northeastern Gobi Altai, Mongolia: implications for estimating mountain uplift rates and earthquake recurrence intervals. *Journal of the Geological Society, London,* **156**, 457-464.

Owen, L. A., Cunningham, D., Windley, B. F., Badamgarov, J. & Dorjnamjaa, D. 1999b. The landscape evolution of Nemegt Uul: a late Cenozoic transpressional uplift in

the Gobi Altai, southern Mongolia. In: *Uplift, Erosion and Stability: Perspectives on Longterm Landscape Development* (edited by Smith, B. J., Whalley, W. B. & Warke, P. A.) **162**. Geological Society, London, Special Publications, 201-218.

Ozacar, A. A. & Beck, S. L. 2004. The 2002 Denali Fault and 2001 Kunlun Fault Earthquakes: Complex Rupture Processes of Two Large Strike-Slip Events *Bulletin of the Seismological Society of America,* **94**(6B), 278-292.

Pearce, J. A. 1976. Statistical Analysis of Major Element Patterns in Basalts. *Journal of Petrology,* **17**(1), 15-43.

Pearce, J. A. 1983. Role of the sub-continental lithosphere in magma genesis at active continental margins. In: *Continental basalts and mantle xenoliths* (edited by Hawkesworth, C. J. & Norry, M. J.), Shiva, Nantwich, 230-249.

Pearce, J. A. & Cann, J. R. 1973. Tectonic setting of basic volcanic rocks determined using trace element analyses. *Earth and Planetary Science Letters*, **19**, 290-300.

Pearce, J. A. & Wanming, D. 1988. The ophiolites of the Tibetan Geotraverses, Lhasa to Golmund (1985) and Lhasa to Kathmandu (1986). *Philosophical Transactions of the Royal Society of London. Series A, Mathematical and Physical Sciences,* **327**, 215-238.

Pei, X., Li, Z., Liu, H., Li, G., Ding, S., Li, Y., Hu, B. & Guo, J. 2007. Geochemical characteristics and zircon U-Pb isotopic ages of island-arc basic igneous complexes from the Tianshui area in West Qinling. *Earth Sci. China,* **1**, 49-59.

Perello, J., Cox, D., Garamjav, D., Sanjdorj, S., Diakov, S., Schissel, D., Munkhbat, T. & Oyun, G. 2001. Oyu Tolgoi, Mongolia: Silurian-Devonian porphyry Cu-Au (Mo) and high-sulfidation epithermal Cu mineralization with a Cretaceous chalcocite blanket. *Economic Geology,* **96**, 1407-1428.

Peselnik, L., Nicolas, A. & Stevenson, P. R. 1977. Velocity anistropy in a mantle peridotite from the Ivrea zone: application to upper mantle anistropy. *Journal of Geophysical Research,* **79**, 1175-1182.

Pisarevsky, S. A., Wingate, M. T. D., Powell, C. M., Johnson, S. & Evans, D. A. D. 2003. Models of Rodinia assembly and fragmentation. In: *Proterozoic East Gondwana: Supercontinent Assembly and Breakup* (edited by Yoshida, M., Windley, B. F. & Dasgupta, S.) **206**. Geological Society, London, Special Publications, 35-55.

Popov, V., Kharamov, A. & Brachtadse, V. 2005. Palaeomagnetism, magnetic stratigraphy, and petromagnetism of the Upper Vendian sedimentary rocks in the

sections of the Zoloitsa River and in the Verkhotina Hole, Winter Coast of the White Sea, Russia. *Russian Journal of Earth Sciences,* **7**, 1-29.

Rippington, S., Cunningham, D. & England, R. 2008. Structure and petrology of the Altan Uul Ophiolite: new evidence for a Devonian-Carboniferous suture in the Gobi-Altai, southern Mongolia. *Journal of the Geological Society, London,* **in press**.

Robinson, P. T., Zhou, M.-F., Hu, X.-F., Reynolds, P., Wenji, B. & Yang, J. 1999. Geochemical constraints on the origin of the Hegenshan Ophiolite, Inner Mongolia, China. *Journal of Asian Earth Sciences,* **17**, 423-442.

Rollinson, H. R. 1993. *Using Geochemical Data: Evaluation, Presentation, Interpretation*. Longman Scientific and Technical.

Ruzhentsev, S. V. 1985. Geology of the Gobi Tienshan and aspects of the south Mongolian ocean. *Ivestiya VUZ. Geology i Razvedka 6,*, 12-19 in Russian.

Ruzhentsov, S. V. & Pospelov, I. I. 1992. The south Mongolian variscan fold system. *Geotectonics,* **26**, 383-395.

Saribudak, M., Sanver, M., Sengor, A. & Gorur, N. 1990. Paleomagnetic evidence for substantial rotation of the Almacik flake within the North Anatolian fault zone. *Geophysics Journal International,* **102**, 563-568.

Sibson, R. H. 1985. Stopping of earthquake ruptures at dilational jogs. *Nature,* **316**(248-251).

Senechal, G., Rondenay, S., Mareschal, M., Guilbert, J. & Poupinet, G. 1996. Seismic and electrical anistropies in the lithosphere across the Grenville Front, Canada. *Geophysical Research Letters,* **23**, 2255-2258.

Sengor, A. M. C., Natal'in, B. A. & Burtman, V. S. 1993. Evolution of the Altaid tectonic collage and Palaeozoic crustal growth in Eurasia. *Nature,* **364**, 299-307.

Shao, J., Mu, B. & Zhang, L. 2000. Deep geological process and its shallow response during Mesozoic transfer of tectonic framework in eastern North China. *Geological Review (in Chinese)* **46**, 32-40.

Shaw, B. 2006. Initiation propogation and termination of elastodynamic ruptures associated with segmentation of faults and shaking hazard. *Journal of Geophysical Research,* **111**(B08302).

Shu, L., Charvet, J., Lu, H. & Laurent-Charvet, S. 2002. Paleozoic accretion-collision events and kinematics of deformation in the eastern part of the Southern-Central

Tiansgan belt, China. *Acta Geologica Sinica,* **76**, 308-323.

Silver, P. G. 1996. Seismic Anisotropy Beneath the Continents: Probing the Depths of Geology. *Ann. Rev. Earth Planet. Sci.* **24**, 385-432.

Smethurst, M. A., Khramov, A. N. & Torsvik, T. H. 1998. The Neoproterozoic and palaeomagnetic data for the Siberian platform: from Rodinia to Pangea. *Earth-Science Reviews,* **43**, 1-24.

Spear, F. A. 1993. Metamorphic phase Equilibria and Pressure-Temperature-Time Paths. *Mineralogical Society of America Monograph*.

Storti, F., Holdsworth, R. E. & Salvini, F. 2003. Intraplate strike-slip deformation belts. In: *Intraplate Strike-Slip Deformation Belts* (edited by Storti, F., Holdsworth, R. E. & Salvini, F.) **210**. Geological Society, London, Special Publication, 1-14.

Tapponnier, P. & Molnar, P. 1979. Active faulting and Cenozoic tectonics of the Tien Shan, Mongolia, and Baykal regions. *Journal of Geophysical Research,* **84**, 3425-3459.

Tapponnier, P., Peltzer, G., Dain, A. Y. L., Armijo, R. & Cobbold, P. 1982. Propagating extrusion tectonics in Asia: New insights from simple experiments with plasticine. *Geology,* **10**, 611-616.

Tarney, J., Saunders, A. D., Mattey, D. P., Wood, D. A., Marsh, N. G., Roberts, D. & Stegena, L. 1981. Geochemical Aspects of Back-Arc Spreading in the Scotia Sea and Western Pacific *Philosophical Transactions of the Royal Society of London. Series A, Mathematical and Physical Sciences,* **300**(1454), 263-285.

Tarney, J. & Marsh, N. G. 1991. Major and trace element geochemistry of Holes CY-1 and CY-4 : Implications for petrogenetic models. In: *Initial Reports, Holes CY-1and CY-1A* (edited by Gibson, I. L., Malpas, J., Robinson, P. A. & Xenophotos, C.) **Paper 90-20**. Geological Survey of Canada.

Tommasi, A. 1995. Developpment de systemes de decrochements d'echelle continentale dans une lithosphere heterogene: Cas nuturales et modelisation numerique, University de Montpellier II, p83.

Tommasi, A. & Mainprice, D. 2000. Viscoplastic self-consistent and equilibrium-based modeling of olivine lattice preferred orientations: Implications for the upper mantle seismic anisotropy. *Journal of Geophysical Research,* **105**(B4), 7893-7908.

Tomurtogoo, O., Windley, B. F., Kroner, A., Badarch, G. & Liu, D. Y. 2005. Zircon age

and occurrence of the Adaatsag ophiolite and Muron shear zone, central Mongolia:constraints on the evolution of the Mongol-Okhotsk ocean, suture and orogen. *Journal of the Geological Society, London,* **162**, 125-134.

Traynor, J. J. & Sladen, C. 1995. Tectonic and stratigraphic evolution of the Mongolian People's Republic and its influence on hydrocarbon geology and potential. *Marine and Petroleum Geology,* **12**, 35-52.

Vassallo, R., Jolivet, M., Ritz, J.-F., Braucher, R., Arzhannikova, N., Arzhannikova, S., Chauvet, A., Larroque, C., Sue, C. & Todbileg, M. 2006. Chronology and uplift rates of the relief in the Altay and the Gobi-Altay mountain ranges (Mongolia). *Geophysical Research Abstracts,* **8**, 00573.

Vassallo, R., Jolivet, M., Ritz, J.-F., Braucher, R., Larroque, C., Sue, C., Todbileg, M. & Javkhlanbold, D. 2007. Uplift age and rates of the Gurvan Bogd system (Gobi-Altay) by apatite fission track analysis. *Earth and Planetary Science Letters,* **259**, 333-346.

Vauchez, A., Tommasi, A. & Barruol, G. 1998. Rheological heterogeneity, mechanical anisotropy and deformation of the continental lithosphere. *Tectonophysics,* **296**, 61-86.

Voznesenskaya, T. A. 1989. Sedimentation and volcanism in the axial zone of the southern Mongolian Variscides. *Lithology and Mineral Resources,* **23**, 426-437 (in Russian).

Wakabayashi, J., Hengesh, J. V. & Sawyer, T. L. 2004. Four-dimensional transform fault processes: porgressive evolution of step-overs and bends. *Tectonophysics,* **392**, 279-301.

Watson, M. P., Hayward, A. B., Parkinson, D. N. & Zhang, Z. M. 1987. Plate tectonic history, basin development and petroleum source rock deposition on shore China. *Marine and petroleum geology,* **4**, 205-255.

Westaway, R. 1995. Deformation around stepovers in strike-slip fault zones. *Journal of Structural Geology,* **17**(6), 831-846.

Wilcox, R. E., Harding, T. P. & Seely, D. R. 1973. Basin Wrench Tectonics. *The American Association of Petroleum Geologists Bulletin,* **57**(1), 74-96.

Winchester, J. A. & Floyd. P. A. 1977. Geochemical discrimination of different of different magma series and their differentiation products using immobile elements. *Chemical Geology*, **20**, 325-343.

Windley, B. F., Guo, J. & Zhang, C. 1994. Subdivisions and tectonic evolution of Chinese Altai. *Russian Geology and Geophysics,* **35**((7-8)), 116-117.

Windley, B. F., Alexeiev, D., Xiao, W., Kroner, A. & Badarch, G. 2007. Tectonic models for accretion of the Central Asian Orogenic Belt. *Journal of the Geological Society, London,* **164**, 31-47.

Xiao, W., Windley, B. F., Hao, J. & Zhai, M. 2003. Accretion leading to collisison and the Permian Solonker suture, Inner Mongolia, China: Termination of the central Asian orogenic belt. *Tectonics,* **22**(6), 1069.

Xiao, W., Windley, B. F., Badarch, G., Sun, S., Li, J., Qin, K. & Wang, Z. 2004a. Palaeozoic accretionary and convergent tectonics of the southern Altaids: implications for the growth of Central Asia. *Journal of the Geological Society, London,* **161**, 339-342.

Xiao, W., Zhang, C., Qin, K., Sun, S. & Li, J.-L. 2004b. Paleozoic accretionary and collisional tectonics of the Eastern Tianshan (China): Implications for the continental growth of central Asia. *American Journal of Science,* **304**, 370-395.

Yakubchuk, A., Seltmann, R., Shatov, V. & Cole, A. 2001. The Altaids: tectonic evolution and metallogeny. *Society of Economic Geologists, Newsletter,* **46**, 7-14.

Yardley, B. W. 1989. *An introduction to metamorphic petrology*. Pearson Education Limited, Harlow, England.

Zheng, Y., Zhang, Q., Wang, Y., Liu, R., Wang, S. G., Zuo, G., Wang, S. Z., Lkaasuren, B., Badarch, G. & Badamgarov, Z. 1996. Great Jurassic thrust sheets in Beishan (North Mountains) - Gobi areas of China and sourthern Mongolia. *Journal of Structural Geology,* **18**(9), 1111-1126.

Zhou, M.-F., Zhang, H.-F., Robinson, P. T. & Malpas, J. 2003. Comments on "Petrology of the Hegenshan ophiolite and its implication for the tectonic evolution of northern China" by T. Nozaka and Y. Liu [Earth Planet. Sci. Lett. 202 (2002) 89-104]. *Earth and Planetary Science Letters,* **217**, 207-210.

Zoback, M. L. 1992. First- and second-order patterns of stress in the lithosphere - The World Stress Map project. *Journal of Geophysical Research,* **97**(B8), 11703-11728.

Zonenshain, L. P., Kuzmin, M. I. & Natapov, L. M. 1990. Geology of the USSR: a Plate-Tectonic Synthesis. *American Geophysical Union, Geodynamic Series,* **21**.

Zorin, Y. A., Belichenko, V. G., Turutanov, E. K., Kozhevnikov, V. M., Ruzhentsev, S. V., Dergunov, A. B., Filippova, I. B., Tomurtogoo, O., Arvisbaatar, N., Bayasgalan, T., Biambaa, C. & Khosbayar, P. 1993. The South Siberia-Central Mongolia transect. *Tectonophysics,* **225**, 361-378.